

IEEE Signal Processing Magazine

Volume 33 | Number 2 | March 2016



ASSISTED LIVING TECHNOLOGIES

Signal Processing Inside

Discovering the Whole by the Coarse

Time Reversal for Future 5G Wireless

Ultrasound Imaging with Microbubbles

The JPEG XT Standard

New Fellows and Awardees



SIGNAL PROCESSING

The Science Behind Our Digital Life

Refer a Student or Colleague to Join SPS

Membership in the IEEE Signal Processing Society (SPS) can help you lay the foundation for many years of success ahead.

CONNECT with more than 19,000 signal processing professionals through SPS conferences, workshops, and local events hosted by more than 170 SPS Chapters worldwide.

SAVE with member discounts on conferences, publications, SigPort document archive, and access to travel grants.

ADVANCE with world-class educational resources, awards and recognition, and society-wide volunteer opportunities in publications, conferences, membership, and more.

signalprocessingsociety.org

Contents

Volume 33 | Number 2 | March 2016

SPECIAL SECTION

SIGNAL PROCESSING FOR ASSISTED LIVING

- 25 FROM THE GUEST EDITORS**
Fauzia Ahmad, A. Enis Cetin, K.C. (Dominic) Ho, and John Nelson
- 28 INERTIAL MEASUREMENT UNIT-BASED WEARABLE COMPUTERS FOR ASSISTED LIVING APPLICATIONS**
Terrell R. Bennett, Jian Wu, Nasser Kehtarnavaz, and Roozbeh Jafari
- 36 SENSORS IN ASSISTED LIVING**
Fatih Erden, Senem Velipasalar, Ali Ziya Alkar, and A. Enis Cetin



ON THE COVER

In this issue of *IEEE Signal Processing Magazine*, we provide a synopsis of the emerging area of signal processing for assisted living. Six special section articles discuss the most recent developments as well as interesting open problems at the forefront of the current research related to various sensing modalities in assisted living applications.

AGED MAN—@ISTOCKPHOTO.COM/KATARZYNABIALASIEWICZ
LOGOS—@ISTOCKPHOTO.COM/PIXTUM

- 45 DEVICE-FREE RADIO VISION FOR ASSISTED LIVING**
Stefano Savazzi, Stephan Sigg, Monica Nicoli, Vittorio Rampa, Sanaz Kianoush, and Umberto Spagnolini

- 59 HIGH-ACCURACY LOCALIZATION FOR ASSISTED LIVING**
Klaus Witrisal, Paul Meissner, Erik Leitinger, Yuan Shen, Carl Gustafson, Fredrik Tufvesson, Katsuyuki Haneda, Davide Dardari, Andreas F. Molisch, Andrea Conti, and Moe Z. Win

- 71 RADAR SIGNAL PROCESSING FOR ELDERLY FALL DETECTION**

Moeness G. Amin, Yimin D. Zhang, Fauzia Ahmad, and K.C. (Dominic) Ho

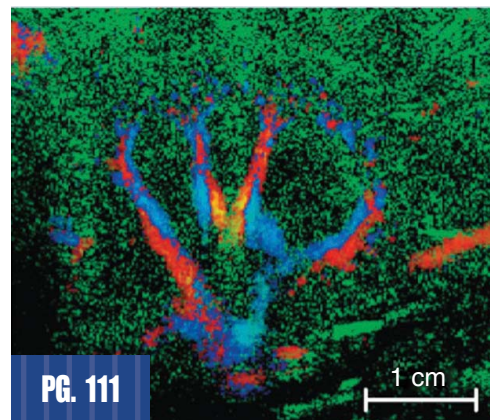
- 81 MONITORING ACTIVITIES OF DAILY LIVING IN SMART HOMES**

Christian Debes, Andreas Merentitis, Sergey Sukhanov, Maria Niessen, Nicolaos Frangiadakis, and Alexander Bauer

FEATURE

- 95 DISCOVERING THE WHOLE BY THE COARSE**

Hamid Krim, Thanos Gentimis, and Harish Chintakunta



IEEE SIGNAL PROCESSING MAGAZINE (ISSN 1053-5888) (ISPREG) is published bimonthly by the Institute of Electrical and Electronics Engineers, Inc., 3 Park Avenue, 17th Floor, New York, NY 10016-5997 USA (+1 212 419 7900). Responsibility for the contents rests upon the authors and not the IEEE, the Society, or its members. Annual member subscriptions included in Society fee. Nonmember subscriptions available upon request. **Individual copies:** IEEE Members US\$20.00 (first copy only), nonmembers US\$234.00 per copy. Copyright and Reprint Permissions: Abstracting is permitted with credit to the source. Libraries are permitted to photocopy beyond the limits of U.S. Copyright Law for private use of patrons: 1) those post-1977 articles that carry a code at the bottom of the first page, provided the per-copy fee indicated in the code is paid through the Copyright Clearance Center, 222 Rosewood Drive, Danvers, MA 01923 USA; 2) pre-1978 articles without fee. Instructors are permitted to photocopy isolated articles for noncommercial classroom use without fee. **For all other copying, reprint, or republication permission**, write to IEEE Service Center, 445 Hoes Lane, Piscataway, NJ 08854 USA. Copyright © 2016 by the Institute of Electrical and Electronics Engineers, Inc. All rights reserved. Periodicals postage paid at New York, NY, and at additional mailing offices. **Postmaster:** Send address changes to IEEE Signal Processing Magazine, IEEE, 445 Hoes Lane, Piscataway, NJ 08854 USA. Canadian GST #125634188 **Printed in the U.S.A.**

Digital Object Identifier 10.1109/MSP.2015.2510289

COLUMNS

- 3 From the Editor**
New Season, New Look
Min Wu
- 4 President's Message**
Your Work Powers Life
Rabab Ward
- 11 Reader's Choice**
Top Downloads in IEEE *Xplore*
- 13 Special Reports**
Signal Processing Powers a Sensor Revolution
John Edwards
- 17 Perspectives**
Why Time Reversal for Future 5G Wireless?
Yan Chen, Beibei Wang, Yi Han, Hung-Quoc Lai, Zoltan Safar, and K.J. Ray Liu
- 105 Applications Corner**
SPAM: Signal Processing to Analyze Malware
Lakshmanan Nataraj and B.S. Manjunath
- 111 Life Sciences**
Ultrasound Imaging with Microbubbles
Antonio Stanzola, Matthieu Toulemonde, Yesna O. Yildiz, Robert J. Eckersley, and Meng-Xing Tang
- 118 Standards in a Nutshell**
JPEG XT: A Compression Standard for HDR and WCG Images
Alessandro Artusi, Rafal K. Mantiuk, Thomas Richter, Pavel Korshunov, Philippe Hanhart, Touradj Ebrahimi, and Massimiliano Agostinelli

DEPARTMENTS

- 7 Society News**
SPS Fellows and Award Winners Recognized
- 128 Dates Ahead**



IEEE prohibits discrimination, harassment, and bullying.
For more information, visit
<http://www.ieee.org/web/aboutus/whatis/policies/p9-26.html>.

IEEE Signal Processing Magazine

EDITOR-IN-CHIEF

Min Wu—University of Maryland, College Park
United States

AREA EDITORS

Feature Articles

Shuguang Robert Cui—Texas A&M University,
United States

Special Issues

Wade Trappe—Rutgers University, United States

Columns and Forum

Gwenaël Doërr—Technicolor Inc., France
Kenneth Lam—Hong Kong Polytechnic University,
Hong Kong SAR of China

e-Newsletter

Christian Debes—TU Darmstadt and
AGT International, Germany

Social Media and Outreach

Andres Kwasinski—Rochester Institute
of Technology, United States

EDITORIAL BOARD

Mrityunjay Chakraborty—Indian Institute of
Technology, Kharagpur, India
George Chrisikos—Qualcomm, Inc.,
United States
Patrick Flandrin—ENS Lyon, France
Mounir Ghogho—University of Leeds,
United Kingdom
Lina Karam—Arizona State University,
United States
Hamid Krim—North Carolina State University,
United States
Sven Lončarić—University of Zagreb, Croatia
Brian Lovell—University of Queensland, Australia
Jian Lu—Qihoo 360, China
Henrique (Rico) Malvar—Microsoft Research,
United States
Stephen McLaughlin—Heriot-Watt University,
Scotland
Athina Petropulu—Rutgers University,
United States
Peter Ramadge—Princeton University,
United States
Shigeaki Sagayama—Meiji University, Japan
Erchin Serpedin—Texas A&M University,
United States
Shihab Shamma—University of Maryland,
United States
Hing Cheung So—City University of Hong Kong,
Hong Kong
Isabel Trancoso—INESC-ID/Instituto Superior
Técnico, Portugal
Pramod K. Varshney—Syracuse University,
United States
Z. Jane Wang—The University of British
Columbia, Canada
Gregory Wornell—Massachusetts Institute
of Technology, United States
Dapeng Wu—University of Florida, United States

ASSOCIATE EDITORS—COLUMNS AND FORUM
Ivan Bajic—Simon Fraser University, Canada
Rodrigo Capobianco Guido—
São Paulo State University, Brazil
Ching-Te Chiu—National Tsing Hua University,
Taiwan
Michael Gormish—Ricoh Innovations, Inc.
Xiaodong He—Microsoft Research

Danilo Mandic—Imperial College,
United Kingdom
Aleksandra Mojsilovic—
IBM T.J. Watson Research Center
Douglas O'Shaughnessy—INRS, Canada
Fatih Porikli—MERL
Shantanu Rane—PARC, United States
Saeid Sanei—University of Surrey, United
Kingdom
Roberto Togneri—The University of
Western Australia
Alessandro Vinciarelli—IDIAP-EPFL
Azadeh Vosoughi—University of Central Florida
Stefan Winkler—UIUC/ADSC, Singapore

ASSOCIATE EDITORS—e-NEWSLETTER

Csaba Benedek—Hungarian Academy
of Sciences, Hungary
Paolo Braca—NATO Science and Technology
Organization, Italy
Quan Ding—University of California,
San Francisco, United States
Pierluigi Failla—Compass Inc, New York,
United States
Marco Guerriero—General Electric Research,
United States
Yang Li—Harbin Institute of Technology, China
Yuhong Liu—Penn State University at Altoona,
United States
Andreas Merentitis—University of Athens, Greece
Michael Muma—TU Darmstadt, Germany
Xiaorong Zhang—San Francisco State University,
United States

ASSOCIATE EDITOR—SOCIAL MEDIA/OUTREACH

Guijin Wang—Tsinghua University, China

IEEE SIGNAL PROCESSING SOCIETY

Rabab Ward—President
Ali Sayed—President-Elect
Carlo S. Regazzoni—Vice President, Conferences
Konstantinos (Kostas) N. Plataniotis—
Vice President, Membership
Thrasylvoulos (Thrasos) N. Pappas—
Vice President, Publications
Walter Kellerman—Vice President,
Technical Directions

IEEE SIGNAL PROCESSING SOCIETY STAFF

Denise Hurley—Senior Manager of Conferences
and Publications
Rebecca Wollman—Publications Administrator

IEEE PERIODICALS MAGAZINES DEPARTMENT

Jessica Barragué, *Managing Editor*
Geraldine Krolin-Taylor, *Senior Managing Editor*
Mark David, *Senior Manager*
Advertising and Business Development
Felicia Spagnoli, *Advertising Production Manager*
Janet Dudar, *Senior Art Director*
Gail A. Schnitzer, Mark Morrissey,
Associate Art Directors
Theresa L. Smith, *Production Coordinator*
Dawn M. Melley, *Editorial Director*
Peter M. Tuohy, *Production Director*
Fran Zappulla, *Staff Director,*
Publishing Operations

Digital Object Identifier 10.1109/MSP.2015.2510290

SCOPE: IEEE Signal Processing Magazine publishes tutorial-style articles on signal processing research and applications as well as columns and forums on issues of interest. Its coverage ranges from fundamental principles to practical implementation, reflecting the multidimensional facets of interests and concerns of the community. Its mission is to bring up-to-date, emerging and active technical developments, issues, and events to the research, educational, and professional communities. It is also the main Society communication platform addressing important issues concerning all members.

FROM THE EDITOR

Min Wu | Editor-in-Chief | minwu@umd.edu

New Season, New Look

In many cultures, spring is a symbol of renewal. For the majority of our readers (who live in the Northern Hemisphere), it will be the start of spring when you receive this issue of *IEEE Signal Processing Magazine*. You will find a different look to the magazine from what you have become so familiar. Indeed, we are welcoming the new season with a new magazine design.

The design that we are replacing has served our members and readers for more than a decade. I still remember the refreshing look and feel of that change led by the then Editor-in-Chief K.J. Ray Liu—the font was updated, the graphics options were expanded, and, for the very first time, the magazine had a professional “perfect binding,” which allowed the topic name and volume number to be printed on the magazine’s spine for an easy at-a-glance view while on a bookshelf.

About a year ago, the IEEE Magazines Department brought to my attention that a redesign frequency of every three to five years is a common practice in the magazine world to keep the look and feel of a magazine up to date and stimulating. We were long overdue for a redesign by this standard. Although personally I was happy with many parts of the elegant design we had, I saw the need for more flexible templates to support appealing and informative visual content. Still, when Senior Art Director Janet Dudar told me the redesign would be a completely new design, including the cover’s iconic magazine title, I was a bit hesitant at first about the change.

Digital Object Identifier 10.1109/MSP.2016.2512339
Date of publication: 7 March 2016

Like many of you, the magazine’s title at the top of the front cover had been imprinted in my mind as a symbol of our magazine. But in the professional world of publishing, the decade-old font and design had begun to show some “age,” while other magazines within and beyond the IEEE have embraced more modern font families and designs. Even the Google logo had undergone various redesigns, with the latest update as recent as last fall. So came the journey for our magazine to explore different design options and critique and iterate the designs to reach a new balance.

Thanks to our hardworking Area Editors Gwenaël Doërr and Kenneth Lam and associate editors, we have also experimented with new columns to complement the existing ones. For example, the traditional platform for the magazine to highlight new books is to invite volunteers who have a strong expertise in related areas to read through a whole book and write a thoughtful review, which can be a relatively slow process. Given the magazine’s large readership with diverse interests, we piloted out a complementary “lightweight” version to the “Book Review” column to inform readers of more recently published books in a timely fashion. This new “Book Digest” column is intended to provide a visually appealing summary of the books that have been selected by a group of senior editors based on such criteria as timeliness of the topic, track record of the authors, training material for students, signal processing focus, and other considerations beneficial to readers. You may have seen the first “Book Digest” column in the January 2016 issue of the magazine.

Another example is a new column called “Perspectives.” Several influential

magazines from sister Societies routinely publish commentary sections that present analysis by technical experts or policy gurus on issues of interest to the readers. These commentaries complement the existing editorials by offering readers valuable perspectives on a broader range of issues. Inspired by the values of commentaries, we initiated this new column to highlight an area of recent exciting research and project its potential technological impact to our everyday life. You will find the first “Perspectives” column article on the prospects of time reversal techniques in the 5G wireless communications in this issue.

I would like to take this opportunity to thank the IEEE Magazines Department staff for their efforts during this redesign. Special appreciation is given to Senior Art Director Janet Dudar, Associate Art Director Gail A. Schnitzer, Managing Editor Jessica Barragué, and Senior Managing Editor Geri Krolin-Taylor—the redesign could not be completed so efficiently without their thoughtful insights!

As professionals advancing technologies, we constantly benefit from going out of the status quo and trying out different things or in different ways with an open mind. Innovations often start from that moment of willingness to try something different. We hope you feel refreshed from this new design of the magazine, and perhaps venture out from your comfort zone to explore something different in this new season. Happy reading!



SP

PRESIDENT'S MESSAGE

Rabab Ward | SPS President | rababw@ece.ubc.ca

Your Work Powers Life

I am honored to begin the position of president of our IEEE Signal Processing Society (SPS). I'd like to take this opportunity to tell you why.

As an SPS volunteer these past 20 years or so, I've had the pleasure of working with a large number of volunteers and collaborating closely with many of you on various committees and tasks. I have learned so much from acclaimed leaders in industry and academia, as well as young professionals and students. Your energy, creativity, and intelligence inspire me every day.

It's been a privilege to work closely with our past presidents—Alex Acero, Ray Liu, José Moura, Mostafa Kaveh, Alfred Hero, Fred Mintzer, and Richard Cox. These colleagues have been true statesmen with visionary long-term goals for the future well-being of our Society. Their selfless devotion has propelled the Society to higher ground, and I'm humbled to be counted as a member of such a league of extraordinary people.

Presently, and for the last couple of years, I have also worked with members of our past and present SPS Executive Committee: Mari Ostendorf, Kostas Plataniotis, Charlie Bouman, Thrassos Pappas, Alex Kot, Wan-Chi Siu, and Carlo Regazoni. These colleagues are extremely wise, energetic, and dedicated leaders in their fields, and it's always a pleasure to work with them.

*Digital Object Identifier 10.1109/MSP.2015.2512658
Date of publication: 7 March 2016*

I am grateful that, due to the hard work of our staff and volunteers, our Society is in top shape both financially and from a management perspective. I am proud of the work of all of our members. Our publications continue to have a high impact in our field, our conferences and workshops continue to thrive, and many of our Chapters are making great strides in industry and academia. In recent years, several new initiatives have proven successful. Alex Acero, SPS's past president, touched on some of these achievements in the previous issue of this magazine [1]. These include the IEEE Signal Processing Cup, the seasonal schools, the growing numbers of Chapters around the world, increased student memberships, and the various types of travel grants available.

There has also been the introduction of two new publications; two new conferences ChinaSip and GlobaSIP; the paper repository, SigPort and the video tutorial online library SigView; two public relations videos about signal processing; and the newly introduced awards for industry members. In 2014, our five-year Society review and five-year periodical review passed with stellar results—so much so that the review committee said they'd be passing our Society's best practices to other Societies. Three special interest groups (SIGs) have been introduced in the last three years; these SIG are provisional groups created to promptly address emerging technical areas. The three SIG are on big data, Internet of Things, and computational imaging.

All of these fabulous achievements owe their great success to the dedication of our Society volunteers. Your innovations and foresight have born the ideas, but the successful implementations of these ideas also required a lot of novelty, persistence, and devil-in-the-details hard work.

I am excited to be working with you during these interesting times, as we watch signal processing theories and applications grow and broaden. It's astounding to see the ever-increasing abstractions of the signal processing discipline and its applications to a vast number of fields and to technical and societal needs. You anticipate and tackle these demands and develop innovative solutions that have influenced the world. Ours is a highly dynamic, ever-evolving Society, as evidenced by the increased capacity and scope of our technical committees, that take leading roles in fostering the development of new technologies, as new fields and theories emerge. Signal processing has become a fundamental science. It not only deals with signals captured by instruments, it's also essential for processing a wide range of information and data. In many ways, it is the science behind our digital life. It is the science that powers essential aspects of everyday life.

While I see a bright future for our Society and I'm excited to take a leadership role, I am aware of the many current and future challenges we face. I will discuss that in my next president's message in the May issue of the magazine. But, first and

foremost, thank you to Alex Acero, our past president, for not only directing and managing the daily affairs of the Society, but also dedicating so much time to raising the visibility of our SPS among the numerous other IEEE Societies and at the IEEE level. I was recently asked by another IEEE Society president if I will continue the great work started by Alex Acero and Ray Liu, in IEEE financial affairs. Those are big shoes to fill, yet I will certainly do my best.

I extend a warm welcome to our incoming President-Elect Ali Sayed. Ali is a superb researcher and a highly acclaimed academic and educator who has contributed greatly to our Society in so

many ways, and at the highest levels with both our publications and our conferences.

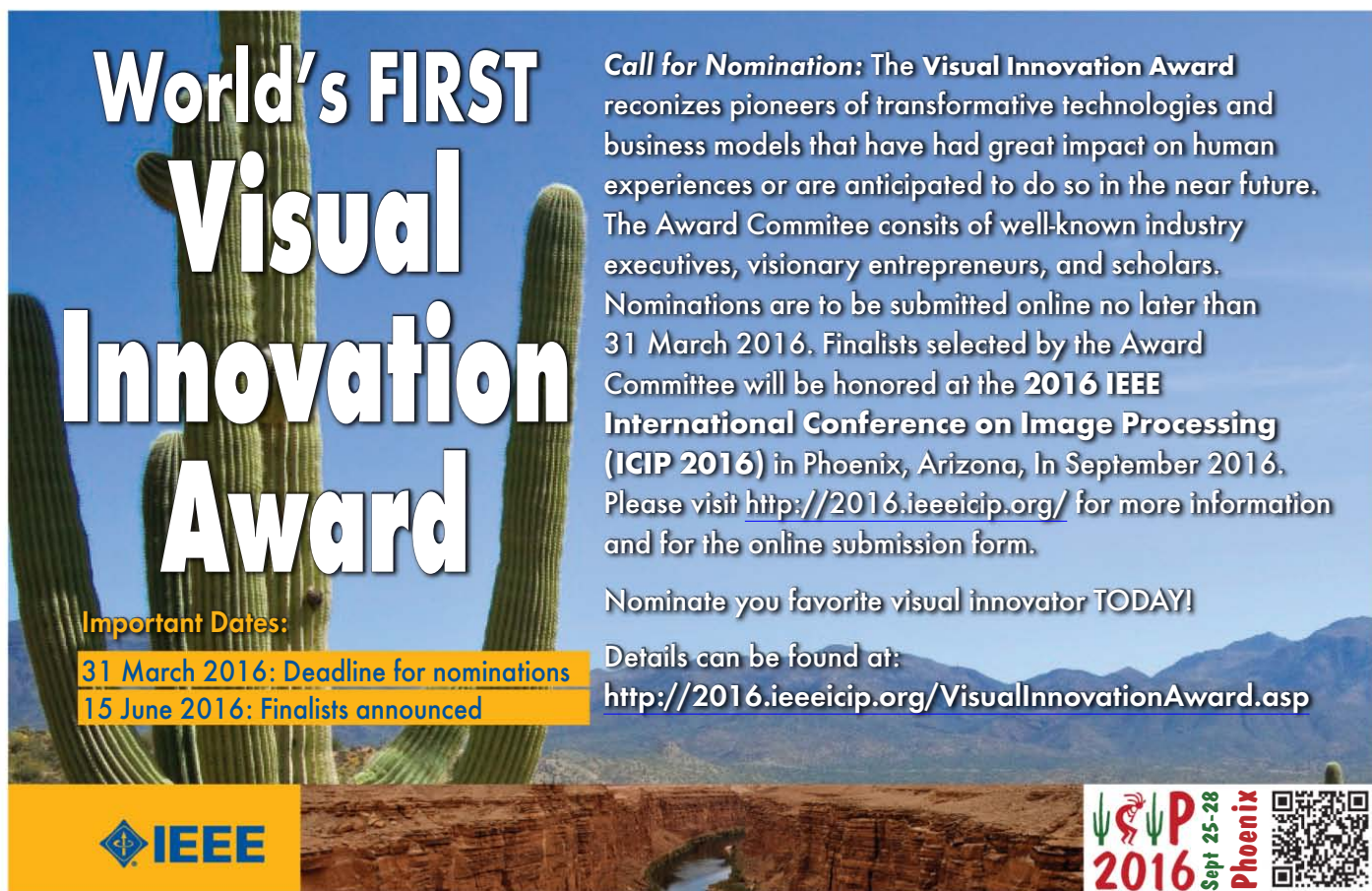
SPS's Vice President of Technical Directions Charlie Bouman ended his three-year term this past December. Charlie's brilliant mind and charisma will be missed, however, I am happy that Walter Kellerman has taken this position. I have worked closely with Walter over the last two years, and I have learned to pay close attention to his advice. John Apostolopoulos and Björn Ottersten will also be missed as they ended their terms on our Board of Governors in December 2015 while Robert Heath, Lina Karam, and Min Wu joined the board in January of this

year. I have a deep respect for every one of these people and feel fortunate to count them as colleagues.

I would love to hear from all of you, too. Your ingenuity and hard work power our Society. I welcome all feedback, comments, suggestions, and advice on any topic, big or small, that will help our Society thrive and continue growing and reaching for new heights. You can get in touch with me at rababw@ece.ubc.ca.



SP





World's FIRST Visual Innovation Award

Call for Nomination: The Visual Innovation Award recognizes pioneers of transformative technologies and business models that have had great impact on human experiences or are anticipated to do so in the near future. The Award Committee consists of well-known industry executives, visionary entrepreneurs, and scholars. Nominations are to be submitted online no later than 31 March 2016. Finalists selected by the Award Committee will be honored at the **2016 IEEE International Conference on Image Processing (ICIP 2016)** in Phoenix, Arizona, in September 2016. Please visit <http://2016.ieeeicip.org/> for more information and for the online submission form.

Nominate your favorite visual innovator TODAY!

Details can be found at:
<http://2016.ieeeicip.org/VisualInnovationAward.asp>

Important Dates:
31 March 2016: Deadline for nominations
15 June 2016: Finalists announced

Digital Object Identifier 10.1109/MSP.2016.2526278



Kiyoharu Aizawa



Ozgun B. Akan



Edward Baranoski



Kenneth Barner



Shannon Blunt



Tony Chan



Xilin Chen



Maria-Gabriella Di Benedetto



Frederic Dufaux



Faramarz Fekri



Dinei Florencio



Jessica Fridrich



Alan Hanjalic



Dimitrios Hatzinakos



Larry Heck



Wendi Rabiner Heinzelman



Jiwu Huang



Lance Kaplan



Hitoshi Kiya



Erik G. Larsson



Ta-Sung Lee

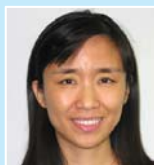


Weisi Lin



Fa-Long Luo

Congratulations!
*SPS Members Elected
IEEE Fellow Class 2016*



Xiaoli Ma



Dimitris Manolakis



Jonathan Manton



Farid Melgani



Lamine Mili



Hlaing Minn



Satoshi Nakamura



Antonio Napolitano



Fernando Perez-Gonzalez



Petar Popovski



Alexandros Potamianos



Sundeep Rangan



Kui Ren



Ivan Selesnick



Osvaldo Simeone



Sun Sumei



John Thompson



Qi Tian



Sennur Ulukus



Yue Wang



Zhengdao Wang



Zhongfeng Wang



Kaikit Wong



Chenyang Xu



Lie-Liang Yang



Mark Yeary



Jinhong Yuan



Bing Zeng



Jianzhong (Charlie) Zhang



IEEE

SPS Fellows and Award Winners Recognized

In this column of *IEEE Signal Processing Magazine*, 52 IEEE Signal Processing Society (SPS) members are recognized as Fellows, and award recipients are announced.

52 SPS members elevated to Fellow

Each year, the IEEE Board of Directors confers the grade of Fellow on up to one-tenth of 1% of the Members. To qualify for consideration, an individual must have been a Member, normally for five years or more, and a Senior Member at the time for nomination to Fellow. The grade of Fellow recognizes unusual distinction in IEEE's designated fields.

The SPS congratulates the following 52 SPS members who were recognized with the grade of Fellow as of 1 January 2016:

Kiyoharu Aizawa, Tokyo, Japan, for contributions to model-based coding and multimedia lifelogging.

Ozgur B. Akan, Istanbul, Turkey, for contributions to wireless sensor networks.

Edward Baranoski, McLean, Virginia, for leadership in knowledge-aided radar systems for indoor environments.

Kenneth Barner, Newark, Delaware, for contributions in nonlinear signal processing.

Shannon Blunt, Washington, D.C., for contributions to radar waveform diversity and design.

Tony Chan, Kowloon, Hong Kong, for contributions to computational models and algorithms for image processing.

Xilin Chen, Beijing, China, for contributions to machine vision for facial image analysis and sign language recognition.

Maria-Gabriella Di Benedetto, Rome, Italy, for contributions to impulse-radio ultrawideband and cognitive networks for wireless communications.

Frederic Dufaux, Paris, France, for contributions to visual information processing and coding.

Faramarz Fekri, Atlanta, Georgia, for contributions to coding theory and its applications.

Dinei Florencio, Redmond, Washington, for contributions to statistical and signal processing approaches to adversarial and security problems.

Jessica Fridrich, Binghamton, New York, for contributions to digital media forensics, steganography, and steganalysis.

Alan Hanjalic, Delft, The Netherlands, for contributions to multimedia information retrieval.

Dimitrios Hatzinakos, Toronto, Canada, for contributions to signal processing techniques for communications, multimedia and biometrics.

Larry Heck, Mountain View, California, for leadership in application of machine learning to spoken and text language processing.

Wendi Rabiner Heinzelman, Rochester, New York, for contributions to algorithms, protocols, and architectures for wireless sensor and mobile networks.

Jiwu Huang, Shenzhen, China, for contributions to multimedia data hiding and forensics.

Lance Kaplan, Adelphi, Maryland, for contributions to signal processing

and information fusion for situational awareness.

Hitoshi Kiya, Tokyo, Japan, for contributions to filter structure, data hiding, and multimedia security.

Erik Larsson, Linköping, Sweden, for contributions to the technology of multi-antenna wireless communications.

Ta-Sung Lee, Hsinchu, Taiwan, for leadership and contributions in communication systems and signal processing.

Weisi Lin, Singapore, Singapore, for contributions to perceptual modeling and processing of visual signals.

Fa-Long Luo, San Jose, California, for contributions to adaptive signal processing for hearing and multimedia applications.

Xiaoli Ma, Atlanta, Georgia, for contributions to block transmissions over wireless fading channels.

Dimitris Manolakis, Lexington, Massachusetts, for contributions to signal processing education, algorithms for adaptive filtering, and hyperspectral imaging.

Jonathan Manton, Parkville, Victoria, Australia, for contributions to geometric methods in signal processing and wireless communications.

Farid Melgani, Trento, Italy, for contributions to image analysis in remote sensing.

Lamine Mili, Falls Church, Virginia, for contributions to robust state estimation for power systems.

Hlaing Minn, Richardson, Texas, for contributions to synchronization and channel estimation in communication systems.

Satoshi Nakamura, Ikoma, Nara, Japan, for contributions to speech recognition and speech-to-speech translation.

Antonio Napolitano, Napoli, Italy, for contributions to the statistical theory of nonstationary signal processing.

Fernando Perez-Gonzalez, Vigo, Galicia, Spain, for contributions to multimedia security.

Petar Popovski, Aalborg, Denmark, for contributions to network coding and multiple access methods in wireless communications.

Alexandros Potamianos, Zografou, Attiki, Greece, for contributions to human-centered speech and multimodal signal analysis.

Sundeep Rangan, Brooklyn, New York, for contributions to orthogonal frequency division multiple access cellular communication systems.

Kui Ren, Buffalo, New York, for contributions to security and privacy in cloud computing and wireless networks.

Ivan Selesnick, Brooklyn, New York, for contributions to wavelet and sparsity based signal processing.

Oswaldo Simeone, Newark, New Jersey, for contributions to cooperative cellular systems and cognitive radio networks.

Sun Sumei, Singapore, Singapore, for leadership in design and standardization of wireless communication systems.

John Thompson, Edinburgh, United Kingdom, for contributions to multiple antenna and multihop wireless communications.

Qi Tian, San Antonio, Texas, for contributions to multimedia information retrieval.

Sennur Ulukus, College Park, Maryland, for contributions to characterizing performance limits of wireless networks.

Yue Wang, Arlington, Virginia, for contributions to genomic signal analytics and image-based tissue characterization.

Zhengdao Wang, Ames, Iowa, for contributions to multicarrier communications and performance analysis of wireless systems.

Zhongfeng Wang, Irvine, California, for contributions to very-large-scale integration design and implementation of forward error correction coding.

Kaikit Wong, London, United Kingdom, for contributions to multiuser communication systems.

Chenyang Xu, Berkeley, California, for contributions to medical imaging and image-guided interventions.

Lie-Liang Yang, Southampton, United Kingdom, for contributions to multi-carrier communications and wireless transceivers.

Mark Yeary, Norman, Oklahoma, for contributions to radar systems for meteorology.

Jinhong Yuan, Sydney, New South Wales, Australia, for contributions to multiantenna wireless communication technologies.

Bing Zeng, Chengdu, China, for contributions to image and video coding.

Jianzhong Zhang, Mountain View, California, for leadership in standardization of cellular systems.

The following individual was evaluated by the SPS, but is not an SPS member:

Yiu Chan, Kingston, Canada, for development of efficient localization and tracking algorithms.

Alan Gatherer, Plano, Texas, for contributions to systems-on-chip for 3G and 4G cellular systems.

2015 IEEE SPS Awards to be presented in Shanghai, China

The IEEE SPS congratulates the following SPS members who will receive the Society's prestigious awards during ICASSP 2016 in Shanghai, China.



The Society Award honors outstanding technical contributions in a field within the scope of the IEEE SPS and outstanding leadership within that field. The Society Award comprises a plaque, a certificate, and a monetary award of US\$2,500. It is the highest-level award bestowed by the IEEE SPS. This year's recipient is Alfred O. Hero, "for contributions to the field of statistical signal and image processing and for sustained service to the Society."

The Technical Achievement Award is presented this year to Li Deng "for



outstanding contributions to deep learning and to automatic speech recognition." The Technical Achievement Award honors a person who, over a period of years, has made outstanding technical contributions to theory and/or practice in technical areas within the scope of the Society, as demonstrated by publications, patents, or recognized impact on this field. The prize for the award is US\$1,500, a plaque, and a certificate.



The Meritorious Service Award honors volunteers whose dedication, effort, and contributions have benefited the Society significantly. This year's recipient is Min Wu, "for exemplary service to and leadership in the IEEE Signal Processing Society." The award comprises a plaque and a certificate.



The SPS Education Award honors educators who have made pioneering and significant contributions to signal processing education. The award comprises a plaque, a monetary award of US\$1,500 and a certificate. The recipient of the SPS Education Award is Ali H. Sayed "for the writing of scholarly and influential texts in the areas of adaptive systems and statistical signal processing."



The Industrial Leader Award recognizes an industry business or technical leader whose leadership has resulted in major and outstanding advances or new directions using signal processing technologies within the scope of the Society. This award is for executive leadership resulting in major advances and new directions using signal processing in a business area. The prize is US\$1,500, a plaque, and a certificate. The recipient of the Industrial Leader Award is John R.

Treichler “for sustained impact and leadership to the security and intelligence industry through signal processing innovations.”



The Industrial Innovation Award is presented this year to Gary Elko “for outstanding contributions toward industrial research and commercialization of innovative electroacoustic devices and microphone array signal processing.” The Industrial Innovation Award recognizes an individual or team at any level who were industry employees whose technical contributions have resulted in significant advances using signal processing technologies within the scope of the Society. The prize is US\$1,500 per awardee (up to a maximum of US\$4,500 per award) and a plaque and certificate.

Outstanding Publications Honored by SPS



A number of outstanding publications are honored by the Society. The Sustained Impact Paper Award honors the author(s) of a journal article of broad interest that has had sustained impact over many years on a subject related to the Society’s technical scope. The prize shall consist of US\$500 per author (up to a maximum of US\$1,500 per award) and a certificate. To be eligible for consideration, an article must have appeared in one of the IEEE Signal Processing Society transactions or *IEEE Journal of Selected Topics in Signal Processing*, in an issue predating the spring awards board meeting by at least ten years (typically held in conjunction with ICASSP). This year, the Sustained Impact Paper Award recipients are Ingemar J. Cox, Joe Kilian, F. Thomson Leighton, and Talal Shamoon for their paper “Secure Spread Spectrum Watermarking for Multimedia,” *IEEE Transactions on Image Processing*, vol. 6, no. 12, Dec. 1997.

The IEEE Signal Processing Magazine Best Paper Award honors the

author(s) of an article of exceptional merit and broad interest on a subject related to the Society’s technical scope and appearing in the Society’s magazine. The prize comprises US\$500 per author (up to a maximum of US\$1,500 per award) and a certificate. This year, the IEEE Signal Processing Magazine Best Paper Award recipients are Zhi-Quan Luo, Wing-Kin Ma, Anthony Man-Cho So, Yinyu Ye, and Shuzhong Zhang for their article “Semidefinite Relaxation of Quadratic Optimization Problems,” published in *IEEE Signal Processing Magazine*, vol. 27, no. 3, May 2010.

The IEEE Signal Processing Magazine Best Column Award honors the author(s) of a column of exceptional merit and broad interest on a subject related to the Society’s technical scope and appearing in the Society’s magazine. The prize shall consist of US\$500 per author (up to a maximum of US\$1,500 per award) and a certificate. In the event that there are more than three authors, the maximum prize shall be divided equally among all authors and each shall receive a certificate. This year, the IEEE Signal Processing Magazine Best Column Award recipients are Antonio Plaza, Javier Plaza, Abel Paz, and Sergio Sánchez for their article “Parallel Hyperspectral Image and Signal Processing,” published in *IEEE Signal Processing Magazine*, vol. 28, no. 3, May 2011.

The Overview Paper Award honors the author(s) of a journal article of broad interest that has had substantial impact over several years on a subject related to the Society’s technical scope. A paper considered for the award should present an overview of a method or theory with technical depth and application perspective. It should have a multiyear record of impact and also be relevant to current researchers and/or practitioners. The prize shall consist of US\$500 per author (up to a maximum of US\$1,500 per award) and a certificate. This year, the Overview Paper Award recipients are Beibei Wang and K.J. Ray Liu, for “Advances in Cognitive Radio Networks: A Survey,” *IEEE Journal of Selected Topics in Signal Processing*, vol. 5, no. 1, Feb. 2011.

Six Best Paper Awards were presented, honoring the author(s) of a paper of exceptional merit dealing with a subject related to the Society’s technical scope and appearing in one of the Society’s transactions, irrespective of the author’s age. The prize is US\$500 per author (up to a maximum of US\$1,500 per award) and a certificate. Eligibility is based on a five-year window preceding the year of election, and judging is based on general quality, originality, subject matter, and timeliness. This year, the awardees are:

- Mark A. Davenport, Petros T. Boufounos, Michael B. Wakin, and Richard G. Baraniuk, “Signal Processing with Compressive Measurements,” *IEEE Journal of Selected Topics in Signal Processing*, vol. 4, no. 2, Apr. 2010
- Moshe Mishali and Yonina C. Eldar, “From Theory to Practice: Sub-Nyquist Sampling of Sparse Wideband Analog Signals,” *IEEE Journal of Selected Topics in Signal Processing*, vol. 4, no. 2, Apr. 2010
- Xiaoyang Tan and Bill Triggs, “Enhanced Local Texture Feature Sets for Face Recognition Under Difficult Lighting Conditions,” *IEEE Transactions on Image Processing*, vol. 19, no. 6, June 2010
- Tomáš Pevný, Patrick Bas, and Jessica Fridrich, “Steganalysis by Subtractive Pixel Adjacency Matrix,” *IEEE Transactions on Information Forensics and Security*, vol. 5, no. 2, June 2010
- Junil Choi, David J. Love, and Patrick Bidigare, “Downlink Training Techniques for FDD Massive MIMO Systems: Open-Loop and Closed-Loop Training with Memory,” *IEEE Journal of Selected Topics in Signal Processing*, vol. 8, no. 5, Oct. 2014
- Chunming Li, Chenyang Xu, Changfeng Gui, and Martin D. Fox, “Distance Regularized Level Set Evolution and Its Application to Image Segmentation,” *IEEE Transactions on Image Processing*, vol. 19, no. 12, Dec. 2010.

The Young Author Best Paper Award honors the author(s) of an especially meritorious paper dealing with a subject

related to the Society's technical scope and appearing in one of the Society's transactions and who, upon date of submission of the paper, is under 30 years of age. The prize is US\$500 per author (up to a maximum of US\$1,500 per award) and a certificate. Eligibility is based on a three-year window preceding the year of election, and judging is based on general quality, originality, subject matter, and timeliness. Five Young Author Best Paper Awards are being presented this year:

- João F.C. Mota, for the paper co-authored with João M.F. Xavier, Pedro M.Q. Aguiar, and Markus Püschel, "Distributed Basis Pursuit," *IEEE Transactions on Signal Processing*, vol. 60, no. 4, Apr. 2012
- Dimitris S. Papaliopoulos, for the paper coauthored with Alexandros G. Dimakis, "Interference Alignment as a Rank Constrained Rank Minimization," *IEEE Transactions on Signal Processing*, vol. 60, no. 8, Aug. 2012
- Jingning Han, Ankur Saxena, Vinay Melkote, for the paper coauthored with Kenneth Rose, "Jointly Optimized Spatial Prediction and Block Transform for Video and Image Coding," *IEEE Transactions on Image Processing*, vol. 21, no. 4, Apr. 2012
- Yuhua Xu, for the paper co-authored with Jinlong Wang, Qihui Wu, Alagan Anpalagan, and Yu-Dong Yao, "Opportunistic Spectrum Access in Cognitive Radio Networks: Global Optimization Using Local Interaction Games," *IEEE Journal of Selected Topics in Signal Processing*, vol. 6, no. 2, Apr. 2012
- Peiran Song, for the paper coauthored with Gesualdo Scutari, Francisco Facchinei, Daniel P. Palomar, and Jong-Shi Pang, "Decomposition by Partial Linearization: Parallel Optimization of Multi-Agent Systems," *IEEE Transactions on Signal Processing*, vol. 62, no. 3, Feb. 2014

The IEEE Signal Processing Letters Best Paper Award honors the author(s) of a letter article of exceptional merit and broad interest on a subject related to the Society's technical scope and appearing in *IEEE Signal Processing Letters*.

The prize shall consist of US\$500 per author (up to a maximum of US\$1,500 per award) and a certificate. Judging is over a five-year window and is based on technical novelty, the research significance of the work, quality, and effectiveness in presenting subjects in an area of high impact to the Society's members. The recipients of the IEEE Signal Processing Letters Best Paper Award are Argyrios Zymnis, Stephen Boyd, and Emmanuel Candès, for "Compressed Sensing with Quantized Measurements," *IEEE Signal Processing Letters*, vol. 17, no. 2, Feb. 2010.

2015 Conference Best Paper Award for Industry

The Conference Best Paper Award for Industry recognizes author(s) of an International Conference on Image Processing (ICIP) and International Conference on Acoustics, Speech, and Signal Processing (ICASSP)/GlobalSIP paper of exceptional industrial merit and industrial impact dealing with a subject related to the Society's technical scope. To be eligible for consideration, the paper must have been submitted to ICIP or ICASSP/GlobalSIP.

The Conference Best Paper Award for Industry is being presented for the first time to Lingfei Meng and Kathrin Berkner for their ICIP 2015 paper "Parallax Rectification for Spectrally-Coded Plenoptic Cameras."

2015 Chapter of the Year Award

The IEEE Signal Processing Society Gujarat Chapter has been selected as the fifth recipient of the 2015 Chapter of the Year Award, which will be presented at the ICASSP 2016 Awards Ceremony in Shanghai, China. The award is presented annually to a Chapter that has provided its membership with the highest quality of programs, activities, and services. The SPS Gujarat Chapter will receive a certificate and a check in the amount of US\$1,000 to support local Chapter activities.

SPS members receive 2016 IEEE awards

The IEEE has announced the recipients of the 2016 IEEE medals. IEEE medals are the highest honor of awards presented

by the IEEE. The medals will be presented at the 2016 IEEE Honors Ceremony at ICASSP. Three SPS members were awarded with IEEE medals for 2016



The IEEE Jack S. Kilby Signal Processing Medal, awarded for outstanding achievements in signal processing, will be presented to Louis L. Scharf (Colorado State University, Fort Collins,) for "pioneering and sustained contributions to statistical signal processing and its practice."



The IEEE James H. Mulligan, Jr. Education Medal, distributed for a career of outstanding contributions to education in the fields of interest of IEEE, will be awarded to Simon S. Haykin (McMaster University, Hamilton, Ontario, Canada) for "contributions to engineering education in adaptive signal processing and communication."



The IEEE Dennis J. Picard Medal for Radar Technologies and Applications recognizes outstanding accomplishments in advancing the fields of radar technologies and their applications. The 2016 recipient is Nadav Levanon (Tel Aviv University, Israel) for "contributions to radar signal design and analysis, pulse compression, and signal processing."

In addition, as announced previously, five SPS members have received IEEE Technical Field Awards. They are: Takehiro Moriya (IEEE James L. Flanagan Speech and Audio Processing Technical Field Award), Bede Liu (IEEE Fourier Award for Signal Processing), K.J. Ray Liu (IEEE Leon K. Krichmayer Graduate Teaching Award), Yonina Eldar (IEEE Kiyo Tomiyasu Award), and P.P. Vaidyanathan (IEEE Gustav Robert Kirchhoff Award). Details can be found in the "Society News" column of the November 2015 issue of the magazine.

SP

READER'S CHOICE

Top Downloads in IEEE Xplore

The “Reader’s Choice” column has traditionally listed recent downloads from all publications of the IEEE Signal Processing Society (SPS). We decided to try some different things to increase the column’s utility to the reader. This month’s column focuses on articles in *IEEE Transactions on Image Processing*. Future issues will look at the top downloads from other SPS publications. We hope this will increase the number of different articles/papers we highlight, in part because we are guaranteed not to repeat from issue to issue, but also because journals with a focused readership will still have their top downloads highlighted.

IEEE Transactions on Image Processing includes image processing, imaging systems, image scanning, display, and printing. The “word cloud” image

seen in this article shows the concentration of topics used in the titles of the most downloaded papers over the past year weighted by the number of months the article was a top download. This journal considers theory, algorithms, and architectures for image coding, filtering, enhancement,

We decided to try some different things to increase the column’s utility to the reader. This month’s column focuses on articles in *IEEE Transactions on Image Processing*.

restoration, segmentation, and motion estimation; image formation in tomography, radar, sonar, geophysics, astronomy, microscopy, and crystallography; image scanning, digital half-toning and display, and color reproduction; and emerging topics related to image and video processing.

This issue’s “Reader’s Choice” lists the top ten papers most downloaded for the past year at the time of the print deadline. Download statistics can be found in the supplementary document on the SigPort repository (<http://sigport.org/256>), where we have included inset graphs to show the downloads for each month of the previous year and show if the article is a steady performer, a brilliant flash, a

past glory, or a rising star. Your suggestions and comments are welcome and should be sent to Associate Editor Michael Gormish (gormish@ieee.org).

Image Quality Assessment: From Error Visibility to Structural Similarity

Wang, Z.; Bovik, A.C.; Sheikh, H.R.; Simoncelli, E.P.

This paper introduces a framework for quality assessment based on the degradation of structural information. Within this framework a structure similarity index is developed and evaluated. MATLAB code available.

April 2004

New Challenges for Image Processing Research

Pappas, T.N.

The editor-in-chief of *IEEE Transactions on Image Processing* addresses the direction of the journal and image processing.

December 2011

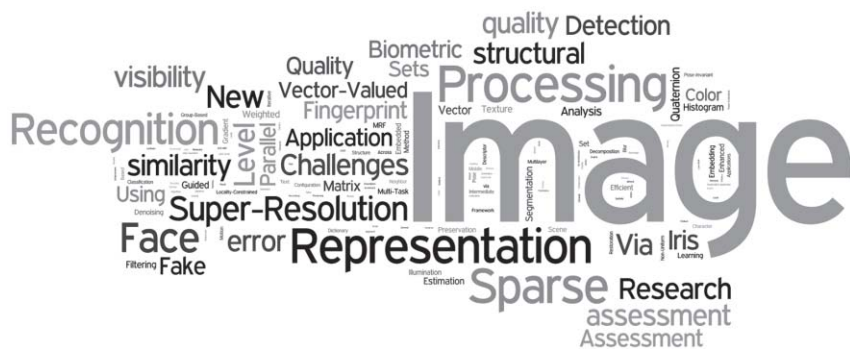


Image Super-Resolution Via Sparse Representation

Yang, J.; Wright, J.; Huang, T.S.; Ma, Y.
This paper presents an approach to single-image super-resolution based upon sparse signal representation of low- and high-resolution patches. Coefficients are determined for each patch of the low-resolution input, and then used to generate the high-resolution output.

November 2010

Vector Sparse Representation of Color Image Using Quaternion Matrix Analysis

Xu, Y.; Yu, L.; Xu, H.; Zhang H.; Nguyen, T.

The proposed model represents the color image as a quaternion matrix, where a quaternion-based dictionary learning algorithm is presented using the K-quaternion singular value decomposition (QSVD) (generalized K-means clustering for QSVD) method. It conducts the sparse basis selection in quaternion space, which uniformly transforms the channel images to an orthogonal color space. In this new color space, the inherent color structures can be completely preserved during vector reconstruction.

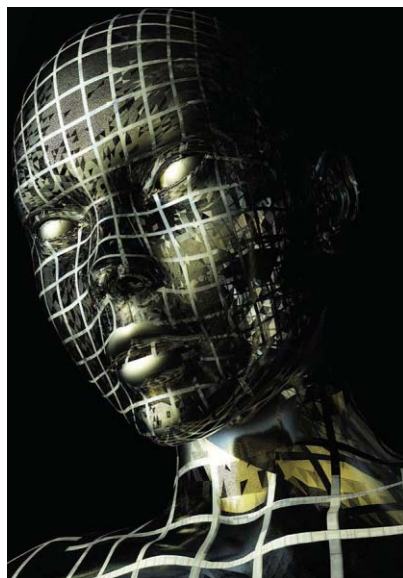
April 2015

Image Quality Assessment for Fake Biometric Detection: Application to Iris, Fingerprint, and Face Recognition

Galbally, J.; Marcel, S.; Fierrez J.

The proposed system attempts to enhance the security of biometric recognition frameworks by adding a liveness assessment in a fast, user-friendly, and nonintrusive manner. Twenty-five general image-quality features are extracted from the authentication image to distinguish between legitimate and imposter samples for fingerprint, iris, and two-dimensional face biometrics.

February 2014



HTTPS://WWW.GRAPHICSTOCK.COM/STOCK-IMAGE/DIGITAL-FEMALE-140220

Vector-Valued Image Processing by Parallel Level Sets

Ehrhardt, M.J.; Arridge, S.R.

This paper considers the components of an image as a vector based on the angle between the spatial gradients of their channels. By minimizing large angles parallel level sets are obtained and used for demosaicking.

January 2014

Face Recognition Across Non-Uniform Motion Blur, Illumination, and Pose

Punnappurath, A.; Rajagopalan, A.N.; Taheri, S.; Chellappa, R.; Seetharaman, G.

A methodology for face recognition in the presence of space-varying motion blur comprising of arbitrarily shaped kernels is presented. The authors model the blurred face as a convex combination of geometrically transformed instances of the focused gallery face and show that the set of all images obtained by nonuniformly blurring a given image forms a convex set. The framework is then extended to handle illumination varia-

tions by exploiting the fact that the set of all images obtained from a face image by nonuniform blurring and changing the illumination forms a biconvex set.

July 2015

Active Contours Without Edges

Chan, T.F.; Vese, L.A.

This paper presents a model to detect objects using curve evolution. Numerical comparisons show the advantage of a stopping criteria based on the segmentation rather than the gradient.

February 2001

Weighted Guided Image Filtering

Li, Z.; Zheng, J.; Zhu, Z.; Yao, W.; Wu, S.

The weighted guided image filter incorporates an edge-aware weighting into existing guided image filter to address the problem of halo artifacts. The filter is applied to detail enhancement, haze removal, and image fusion.

January 2015

Image Denoising Via Sparse and Redundant Representations over Learned Dictionaries

Elad, M.; Aharon, M.

This paper uses either a corrupted image itself or a high-quality image data base to learn dictionaries of small patches generated via the K-SVD algorithm. A global image prior is used to extend small patches to the entire image.

December 2006

SP

John Edwards

Signal Processing Powers a Sensor Revolution

We live on an increasingly sensor-driven planet. Sensors are virtually everywhere, feeding endless streams of data into a rapidly growing array of systems. The emerging Internet of Things (IoT) is poised to drive sensor deployments to an even higher level over the next several years, impacting business, government, and countless private lives in ways both known and not yet fully understood.

Connected smart devices that collect and exchange information with each other will form the IoT's heart. Market research firm Gartner forecasts that 4.9 billion connected "things" will be in use by the end of 2015, up 30% from 2014, and will reach 25 billion units by 2020. Without sensor end points, this progress would not be possible.

Signal processing is an enabling technology for a wide range of sensors and related devices. Researchers worldwide are currently implementing signal processing in various and frequently innovative ways to help create a new generation of powerful sensors that promise to improve lives and, in a number of cases, literally improve the world (or at least limit the destruction caused by human activities).

Assessing ocean dynamics

With the goal of advancing the measurement of oceanic dynamics that shape marine biology, climate patterns, and even military operations, engineers at the University of Nebraska and the U.S.

Naval Research Laboratory have turned to signal processing to help develop a next-generation temperature sensor.

"Temperature measurement is an important aspect of oceanography," says Ming Han, an associate professor of electrical and computer engineering at the University of Nebraska, Lincoln. Han notes that the new fiber-optic sensor he and his coresearchers created can register significantly smaller temperature changes at approximately 30 times the speed of existing commercial technologies. The high-speed sensor promises to help users gain a better understanding of a variety of ocean and ocean-related environments. "Currents, mixing events, large-scale circulation, air-sea exchange and, ultimately,

global climate change are a few obvious examples," he says.

Han and coresearcher postdoctoral researcher Guigen Liu developed the enhanced sensor by attaching a small silicon pillar to the tip of the fused silica glass typically used in fiber optics (Figure 1). The pair worked in collaboration with Weilin "Will" Hou, a Naval Research Laboratory oceanographer.

The optical density of silicon naturally changes whenever it is exposed to even slight temperature shifts, making it a sensitive material that's particularly suitable for thermometry, Han explains. The ease with which the silicon transfers heat, combined with its small size, enables the device to register changes at extremely fast rates. "We chose silicon

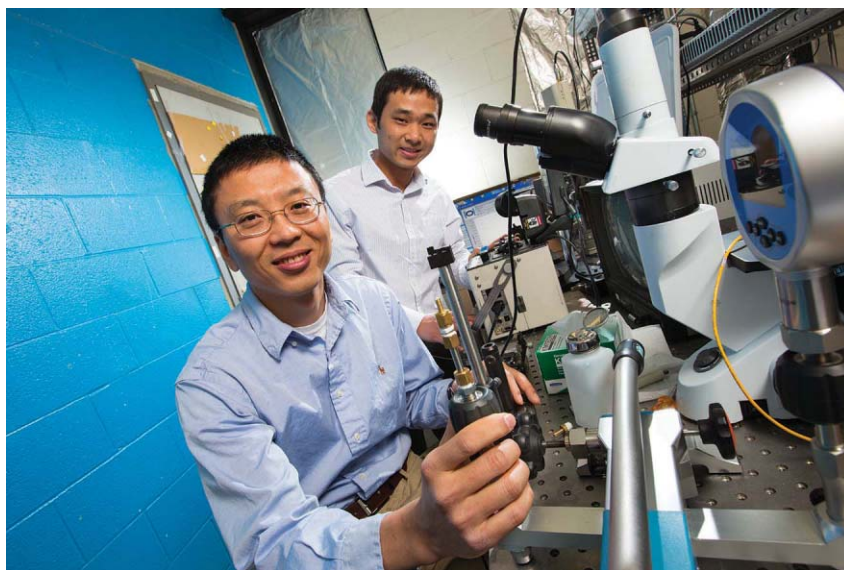


FIGURE 1. Ming Han, an associate professor of electrical and computer engineering at the University of Nebraska, Lincoln, and postdoctoral researcher Guigen Liu, developed an enhanced marine temperature sensor by attaching a small silicon pillar to the tip of the fused silica glass typically used in fiber optics.

Digital Object Identifier 10.1109/MSP.2015.2504562
Date of publication: 7 March 2016

as the sensing material for an optical Fabry–Perot cavity (a small light-trapping device, approximately a millionth of an inch wide, built out of small, half-silvered mirror), which forms the basis of the sensing scheme,” Han says.

The researchers also created a novel signal processing method that averages multiple wavelength peaks to help lower noise interference, which can introduce artificial temperature fluctuations that adversely affect sensor precision. “Compared to other fiber-optic thermometers that are mostly based on silica material, silicon not only provides us with higher sensitivity and faster response, but also a very high refractive index that endows the reflection spectrum from the Fabry–Perot cavity with many more wavelength peaks,” Han says.

Since each of the peak wavelengths can be used to monitor temperature change, and because they all have almost the same sensitivity, the average

wavelength is calculated as the ultimate signal. “Due to the independence of each peak wavelength, the random noise of the average wavelength has been substantially suppressed,” Han says. “We use curve fitting to find the peak wave-

lengths precisely, then we make an average to all the fitted wavelengths,” he notes, adding that the approach provides a relatively simple, yet very effective signal processing method for sensor noise reduction. “For each peak wavelength, we

used a Gaussian function to fit a set of discrete data of the spectrum to get the value more precisely,” Han says. In their experiments, the researchers were able to achieve an ultimate temperature resolution of less than 1×10^{-3} °C. “This high-resolution surveillance on temperature variation is a huge necessity for oceanography,” Han says.

With several sensor prototypes already successfully tested, the researchers are now working toward developing a field-deployable version designed to

operate in extreme conditions. “We are still working on improving the package and designing the graphical user interface for more convenient operation and smarter data processing,” Han says.

Han is also looking forward to developing versions of the sensors for other environmental measurement applications. “We have demonstrated that this sensor can also be explored for use as a fast response anemometer and temperature-compensated pressure sensor by using a laser to get the silicon optical cavity heated,” he remarks.

Sensitive sniffer

Chemical sensors used to detect hazardous gases and environmental pollutants are the focus of a growing number of research projects. At the Nanooptics and Plasmonics Laboratory of the Moscow Institute of Physics and Technology (MIPT), Dmitry Fedyanin and his doctoral student, Yury Stebunov, have created a small, highly sensitive nanomechanical sensor designed to analyze the chemical composition of various natural, man-made, and biological substances.

“The ultimate goal in chemical and biological sensing is detection and measurement of very low molecule concentration in air, blood, and other environments,” says Fedyanin, the project leader and a senior fellow at MIPT. “In order to achieve this goal, the sensor should be able to resolve a single molecule, which is bound to the sensor surface,” Fedyanin explains.

The new sensor contains no electronic circuits, yet can be produced through a standard complementary metal–oxide semiconductor process technology. The device consists of two parts: a photonic nanowaveguide to control the optical signal, and a cantilever (a rigid structure anchored at only one end) hanging over the waveguide (Figure 2). The cantilever, which measures 5 μm long, 1 μm wide, and 90 nm thick, is connected tightly to a chip.

Two optical signals travel through the waveguide during oscillations: a pump optical signal and a probe optical signal. Vibrations of the nanobeam cantilever are excited by the pump signal. “The pump signal propagates along the

With several sensor prototypes already successfully tested, the researchers are now working toward developing a field-deployable version designed to operate in extreme conditions.

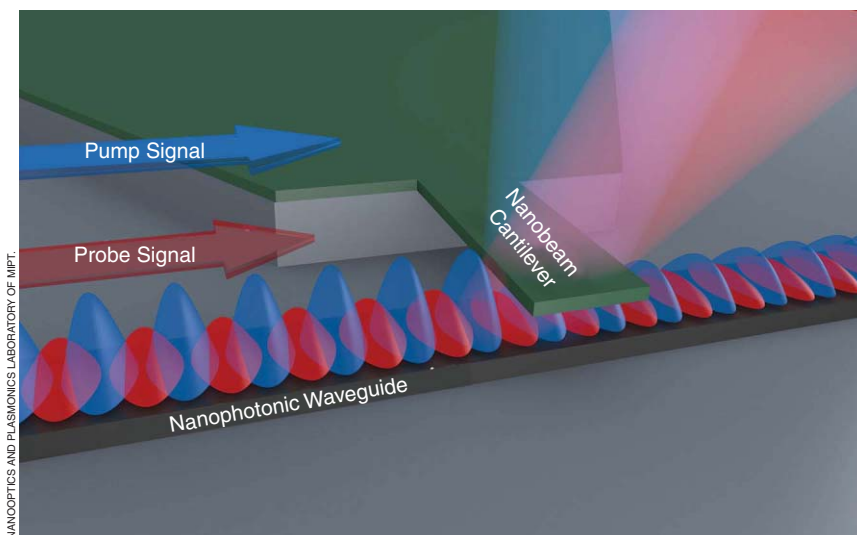


FIGURE 2. In the chemical and biological sensor developed by researchers at the Nanooptics and Plasmonics Laboratory of MIPT, a nanobeam cantilever is suspended above a photonic waveguide. A pump optical signal excited at a light wavelength and sinusoidally modulated at a frequency actuates the cantilever. Simultaneously, the power of the continuous wave probe signal excited at a light wavelength and propagating along the same waveguide is controlled by the vibrating nanobeam, providing the capability to gauge the amplitude of mechanical oscillations. By doing a scan of the modulation frequency, it is possible to measure the decrease in the resonant frequency of the cantilever and determine the mass of adsorbed molecules.

waveguide and the cantilever experiences a ponderomotive force (i.e., a nonlinear force that a charged particle experiences in an inhomogeneous oscillating electromagnetic field), which is proportional to the gradient of the squared electric field of the pump signal,” Fedyanin says. Since the pump signal is sinusoidally modulated, it produces a sinusoidal force on the cantilever. “This can be considered as a transduction process: the pump optical signal is converted to mechanical oscillations of the cantilever,” Fedyanin explains. “The amplitude of these oscillations depends on the resonant frequency of mechanical oscillations of the cantilever and the quality factor of the cantilever.”

The oscillating cantilever modulates the intensity of the probe optical signal at the frequency of the cantilever’s mechanical oscillations. “The probe signal transmitted through the waveguide section with the cantilever contains information about the cantilever’s vibrations and noise,” Fedyanin says. Thanks to the strong interaction between the highly confined optical mode and nanobeam cantilever, the laser noise is typically lower than the noise produced by the cantilever and does not limit the sensitivity of the sensor.” Finally, the probe signal is detected by a photodetector, which converts the optical signal into an electrical signal.

The cantilever’s oscillations make it possible to determine the chemical composition of the environment in which the chip is placed. That is because the frequency of mechanical vibrations depends not only on the materials’ dimensions and properties, but also on the mass of the oscillatory system, which changes during a chemical reaction between the cantilever and the environment. By placing different reagents on the cantilever, researchers can make it react with specific substances or even biological objects. “The sensor sensitivity is high enough to detect single proteins and DNA molecules,” Fedyanin says.

“To achieve ultimate sensitivity and single-molecule resolution, one needs to maximize the signal-to-noise ratio by reducing the effective electrical bandwidth of the photodetector and filtering out the noise, which can be done by

using advanced filtering,” Fedyanin says. “Such a low bandwidth can be achieved, for example, by embedding the actuation-transduction scheme in a phase-locked loop.” Under laboratory conditions, it is possible to efficiently perform measurements simply using a lock-in amplifier, Fedyanin notes.

Fedyanin says that the biggest challenge facing the researchers is getting the sensor to work reliably and accurately at room temperature, which has so far proved elusive. “Experimental studies and optimization are required for developing practical devices,” he says.

Although the research has already generated some commercial interest, Fedyanin says that the sensor itself remains several years away from production. “We expect that such a device can appear on the market in five to ten years,” Fedyanin predicts.

A “smart” fence

As the IoT gradually weaves its way into the fabric of everyday life, even property fences—such as types surrounding airports, nuclear power stations, industrial sites, and various other types of public

and private properties—are becoming Internet connected. A sensor technology developed by a team of experimental physicists led by Uwe Hartmann, a professor at Saarland University, aims to prevent unauthorized individuals from gaining access to secure sites by raising

an alert as soon as anyone attempts to climb over or cut through a fence.

The magnetic sensors are integrated into a thin cable that can be added to virtually any type of perimeter fence. The cable and fence are then connected via a

digital bus to a processing and analysis system that can rapidly calculate the precise location of any security breach. “Any tiny vibration of the fence due to intrusion can be detected by the magnetic field sensors in an accurate way through analyzing the data from all of the sensors,” says Saarland University physicist Haibin Gao, a research team member working on the project’s sensor technology. “Complex algorithms permit the discrimination of false alerts and identification of the intrusion category.”

The “smart” fence is designed to detect a wide range of tampering

Researchers worldwide are currently implementing signal processing in various and frequently innovative ways to help create a new generation of powerful sensors that promise to improve lives.



FIGURE 3. Fenced-in areas can be continuously, unobtrusively monitored with a sensor-powered “smart” fence technology developed by a team of experimental physicists, led by Prof. Uwe Hartmann (left) of Saarland University and coresearchers Uwe Schmitt (right) and Haibin Gao (front).

actions, including someone attempting to climb over it, or cut its links with bolt cutters. “The sensors can detect disturbances in the surrounding magnetic field, including the magnetic field above them, with a range extending several meters,” Gao states. The sensors can even detect a drone flying close overhead (as long as the drone contains metal, of course).

The cable, which contains the linearly arranged sensors, features a diameter comparable to a standard electrical cable. It allows the remote monitoring of many kilometers of perimeter fencing and can be attached to the fence, built into it, or even buried beneath it. The contactless sensors are not subject to wear, consume relatively little power, and are unaffected by rain or fog.

While using the fence to detect potential intrusions is relatively easy, preventing time-wasting false alerts is much more difficult. This is where signal processing becomes essential, improving the system’s ability to distinguish between real intrusion attempts and different types of natural phenomena. “There are various sources generating magnetic field changes that can be detected by magnetic sensors,” Gao explains. “The vibration of the fences can be caused by wind, passing animals, or real invasion events.”

Gao notes that signal processing, besides providing signal amplification and filtering, allows the fence to distinguish between various sources of induced magnetic field changes. “Signal processing is used to correct real-time data from all the magnetic sensors, which can be up to 1,000 devices, and to indicate the signal amplitude, frequency ranges and distributions, or to set up thresholds for signal amplitude and frequency,” he says. “Through the magnetic sensing technique, invasion events can be detected without influences from the environment such as temperature, weather, and animals.”

The researchers are currently refining the technology to enable the system to unambiguously assign a particular type of vibration or magnetic field change to a specific type of disturbance. To ensure both accuracy and reliability, the researchers are now simulating different types of disturbances on a series of test fences (Figure 3). The fences, installed on the Saarland University campus, are currently being subjected to long-term monitoring experiments in an effort to determine how the system is affected by various physical and environmental factors. Data collected by each fence is used by the researchers to model typical disturbance scenarios and to train the analysis system with complex mathematical methods. The

biggest remaining challenge, Gao says, is the development of a self-learning algorithm that will allow the system to work autonomously without continuous human interaction or supervision at airports and other fenced-in sites.

The researchers are currently collaborating with a number of companies to make the system more efficient and deployable and, most importantly, to lower the cost of producing the sensors to a price point where large-volume production becomes economically feasible.

Goa notes that the system’s ability to operate independently of environmental conditions gives the technology a significant advantage over many established surveillance techniques, particularly cameras, which are often hampered by rain and fog. Also, unlike cameras, the smart fence poses no threat to personal privacy. “The sensors simply report that a vibrational disturbance was caused by a human agent at a specific location,” Gao says, “No other information is gathered.”

Author

John Edwards (jedwards@johnedwardsmedia.com) is a technology writer based in the Phoenix, Arizona, area.

SP

Are You Moving?

Update your contact information
so you don't miss an issue of this magazine!

Change your address

E-MAIL: address-change@ieee.org

PHONE: +1 800 678 4333 in the United States

or +1 732 981 0060 outside the United States

If you require additional assistance regarding your IEEE mailings,
visit the IEEE Support Center at supportcenter.ieee.org.



IMAGE LICENSED BY INGRAM PUBLISHING


IEEE

Yan Chen, Beibei Wang, Yi Han, Hung-Quoc Lai,
Zoltan Safar, and K.J. Ray Liu

Why Time Reversal for Future 5G Wireless?

Editors' Note

Several influential magazines from sister Societies of the IEEE and other technical or scientific associations regularly publish commentary sections that present analysis by technical or policy experts on issues of interest to the readers. These commentaries complement existing editorials and offer readers valuable perspectives on a broader range of issues.

Inspired by the values of these commentaries, we are initiating a new column for *IEEE Signal Processing Magazine (SPM)* called "Perspectives," which highlights an area of recent exciting research and projects its potential technological impact to our everyday lives. Different from a feature article or other existing technical columns of *SPM*, this "Perspectives" column offers an outlook of an author or group of authors, as backed by technical evidences available thus far.

In this first "Perspectives" column article, Chen et al. present a brief overview and their technical opinions on

the prospects of time-reversal (TR) techniques in the fifth-generation (5G) wireless communications based on their survey of the literature as well as their firsthand, cutting-edge research that has been transferred into the early stages of practice.

It is possible that, after seeing the same technical evidences and perhaps having access to additional evidences, other experts may have different opinions. We welcome readers' feedback toward the "Perspectives" column articles, and we will be happy to share your comments with the authors. Your comments may be used to help us initiate future articles in this new column, organize forum discussions, or evolve into articles for the eNewsletters.

Gwenaël Doërr (gwenael.doerr@technicolor.com),
Kenneth Lam (enklam@poly.edu.hk),
and Min Wu (minwu@umd.edu)

As the demand for wireless voice and data services has continued to grow dramatically, operators struggle to satisfy this demand with acceptable quality of service. The main approach until now was to increase the system bandwidth and spectral efficiency. For instance, there was an almost tenfold increase for each new generation of cellular technology [the first generation (1G) technology can support up to 30 kHz, second generation (2G) around 200 kHz, third generation (3G) around 1.25–5 MHz, and fourth generation (4G) up to 20 MHz]. Meanwhile, technologists have begun seeking more innova-

tive and efficient communication technologies to meet the ever-increasing demand for data traffic with advanced signal processing capabilities for the 5G wireless communication systems. It is expected that 95% of data traffic will come from indoor locations in a few years [1]. Compared to outdoor propagation, wireless medium in an indoor environment often exhibits richer multipath propagation mostly without a strong line-of-sight (LOS) component, which makes the design of 5G indoor communication systems even more challenging.

Several key ideas have received attention as promising candidates for future 5G wireless communication systems in recent years. The first candidate solution is the massive multiple-input,

multiple-output (MIMO) technique [2]. The massive MIMO effect, in essence, makes the channels to different users quasiorthogonal with very simple spatial multiplexing/demultiplexing procedures and achieves large spectral efficiency gains [3]. A straightforward approach to implement this technique is to mount hundreds of antennas on the transmitter and/or the receiver. However, challenges such as pilot contamination, hardware implementation complexity, antenna correlation, and mutual coupling due to the large number of antennas have to be carefully addressed. In addition, the requirement of deploying a large number of antennas at the base station in massive MIMO systems may not be feasible in indoor scenarios.

Digital Object Identifier 10.1109/MSP.2015.2506347
Date of publication: 7 March 2016

The second candidate solution is network densification by more heterogeneous network deployment, such as the small cell technique and device-to-device (D2D) communication technique [4]. These techniques can improve the link efficiency by replacing longer links with shorter ones. However, coordination and interference management among the small cells (or D2D links) may become challenging. Ideally, the network should be easily scalable so that when additional cells/links are needed, little interference will be introduced, requiring only low-complexity interference management.

Another candidate solution is the cloud-based radio access networks (C-RAN) [5], where all the baseband processing is carried out through high-performance computing in a centralized structure, which transforms the evolution of the wireless networks from today's cell-centric architecture into a device-centric architecture [3]. Nevertheless, as with network densification, the limited fronthaul link capacity may prevent the C-RAN from fully utilizing the benefits made possible by concentrating the processing intelligence at the cloud.

Besides the aforementioned challenges of the candidate techniques, the operation of a large number of base stations and heterogeneous devices will consume a lot of energy. Therefore, the next-generation networks should focus on achieving better energy efficiency and reduce the complexity of user devices as much as possible.

From the aforementioned discussion, we can see that most of the existing solutions for 5G have their inherent limitations, which may make them either difficult to implement as a collectively cohesive solution or not as efficient as expected. Moreover, these solutions may not work well in indoor environments, where the vast majority of current and future data traffic will come from. In this article, we will show that TR communication possesses many outstanding characteristics to address most of the previously mentioned challenges and, therefore, is an ideal candidate platform for 5G indoor systems.

What is the TR phenomenon?

Time reversal (TR) is a fundamental physical phenomenon that takes advantage of an unavoidable but rich multipath radio propagation environment to create a spatial-temporal resonance effect, the so-called focusing effect. Let us imagine that there are two points A and B within the space of a metal box. When A emits a radio signal, its radio waves bounce back and forth within the box, some passing through B. After a certain time, the energy level reduces and is no longer observable. Meanwhile, B can record the multipath profile of the arriving waves as a distribution in time. Then, such a multipath profile is time reversed (and conjugated) by B and emitted accordingly, the last first and the first last. With channel reciprocity, all of the waves, following

the original paths, will arrive at A at the same particular time instant, adding up in a perfectly constructive way. This is called the *focusing effect*. In essence, it is a resonance effect taking place at A stimulated by B using the time-reversed multipath profile through the interaction with the box as demonstrated in Figure 1.

One can imagine that the larger the transmission power, the more bouncing back and forth of the electromagnetic (EM) waves in the box, and, therefore, the more observable multipaths. When the power is fixed, so is the maximum number of observable multipaths. Since radio waves travel at the speed of light, for one to see the multipath profile in detail, it needs high resolution in time, which implies very broad bandwidth in frequency. The larger the bandwidth, the better the time resolution, and, therefore, the more multipaths can be revealed. Essentially, multipaths are naturally existing degrees of freedom ready to be harvested via transmission power and bandwidth.

In a real environment, especially indoors, depending on the structure of the buildings, the number of observable multipaths is limited due to the power of the radio and its bandwidth. Still, one can observe around 15–30 significant multipaths with 150-MHz bandwidth—the entire Industrial Scientific Medical (ISM) band at 5.8 GHz. Such a large number of degrees of freedom that exist

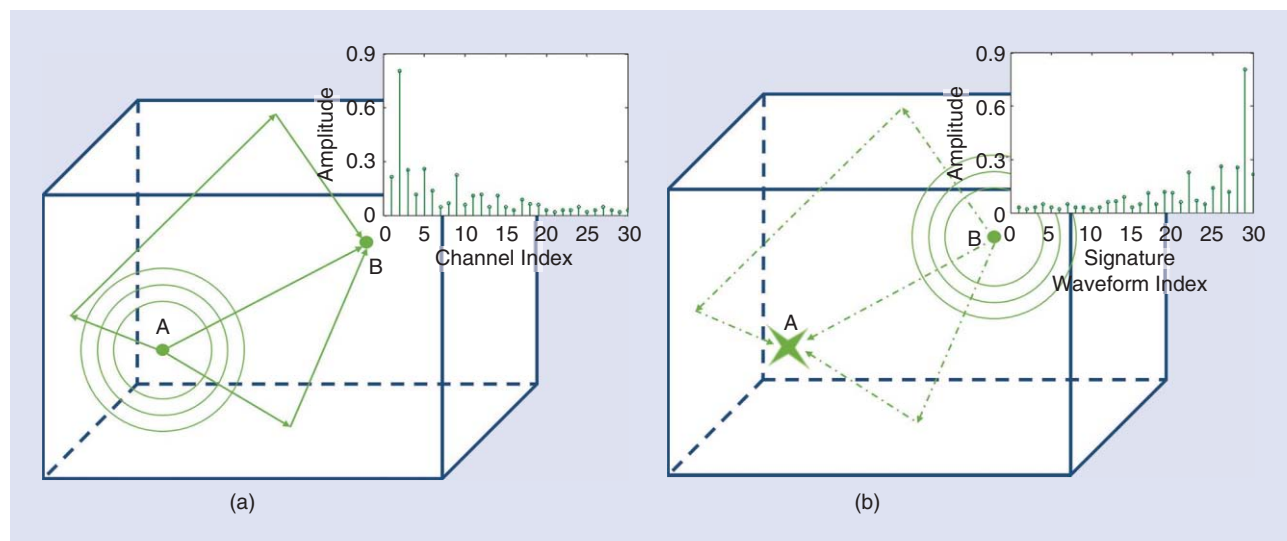


FIGURE 1. An illustration of TR: (a) the channel probing phase and (b) the data transmission and focusing phase.

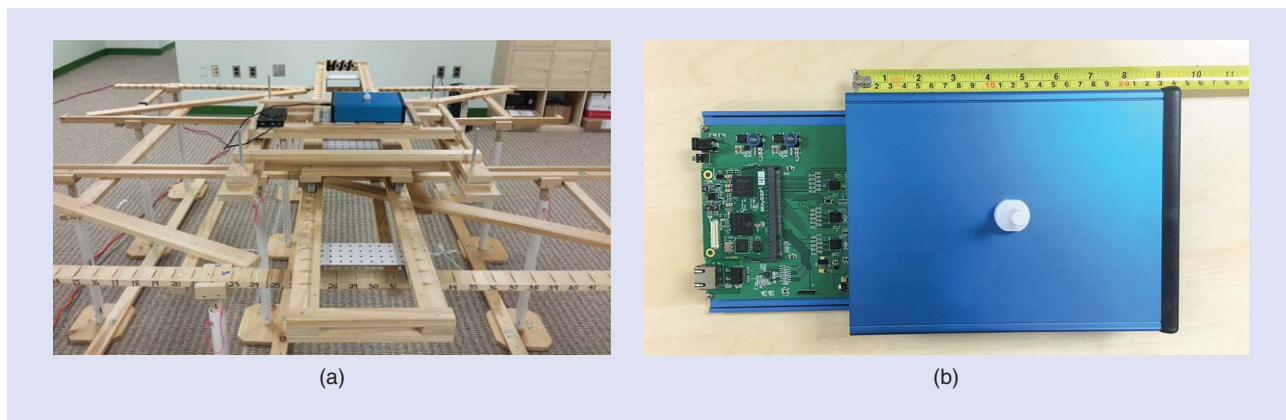


FIGURE 2. An example of the TR prototype: (a) three-dimensional (3-D) architecture for collecting measurements and (b) details of the prototype. (Figure courtesy of Origin Wireless, Inc.)

in nature can be harvested to enable engineering applications.

Brief history of TR

Mathematically, the TR effect is simply for the environment to serve as the computer to perform a perfect deconvolution; that is, the environment behaves like a matched filter! The research of TR dates back to the 1950s, where TR was utilized to compensate the phase-delay distortion that appears during long-distance transmissions of slow-speed pictures over telephone lines [6]. It has also been used to design noncausal recursive filters to equalize the ghosting artifacts of analog television signals caused by multipath propagation [7].

It was observed in a practical underwater propagation environment [8] that the energy of the TR acoustic waves from transmitters could be refocused only at the intended location with very high spatial resolution. The spatial and temporal focusing feature can also be used for radar imaging and acoustic communications. Note that the resolution of spatial and temporal focusing highly depends on the number of multipaths. To be able to harvest a large number of multipaths, large bandwidth and a high sampling rate is required, which was difficult or even impossible to achieve in the past. Fortunately, with the advance of semiconductor technologies, broadband wireless technology has

become available in recent years, and exploiting the TR effect has also become possible in wireless radio systems. Experimental validations of the TR technique with EM waves have been conducted [9], including the demonstration of channel reciprocity and spatial and temporal focusing properties. Combining the TR technique with ultrawideband (UWB) communications has been studied with the focus on the bit error rate (BER) performance through simulations [10]. A system-level theoretical investigation and comprehensive performance analysis of a TR-based multiuser communication system was conducted [11], where the concept of TR division multiple access was proposed. Also, a TR radio prototype was built to conduct TR research and development [12]. As shown in Figure 2, the TR prototype is a customized software-defined radio platform for designing and deploying TR-

based communication systems. The hardware architecture combines a specific designed radio-frequency (RF) board covering the ISM band with 125-MHz bandwidth, a high-speed Ethernet port, and an off-the-shelf user-programmable MityDSP-L138F module board (containing ARM9, floating point DSP, and Xilinx Spartan-6 FPGA). The size of the radio is $5\text{ cm} \times 17\text{ cm} \times 23\text{ cm}$, the weight is about 400 g, and the power consumption is 25 W. As a comparison, the size, weight, and power consumption of the massive MIMO prototype at Lund University in Sweden [13] is $0.8\text{ m} \times 1.2\text{ m} \times 1\text{ m}$, 300 kg, and 2.5 kW, respectively.

When applying the TR technique in wireless communications, if the transmitted symbol duration is larger than (or equal to) the channel delay spread, the time reversed waveform can guarantee the optimal BER performance by virtue of its maximum signal-to-noise ratio (SNR) property. However, if smaller, which is generally the case in high-speed wireless communication systems, the delayed versions of the transmitted waveforms will overlap and interfere with each other. Such intersymbol interference (ISI) can be notably severe and cause crucial performance degradation, especially when the symbol rate is very high. The problem becomes even more challenging in a multiuser transmission scenario, where the interuser

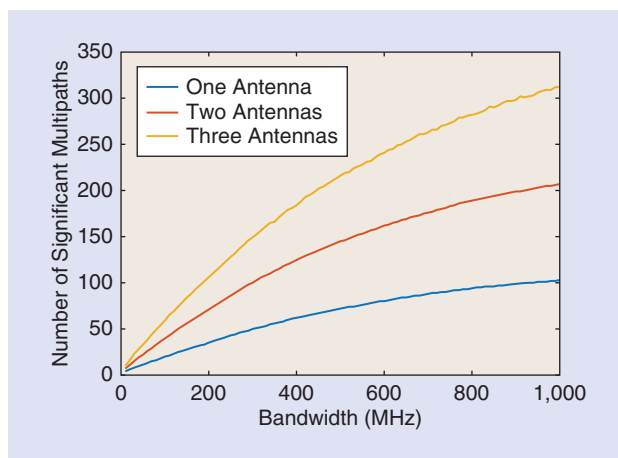


FIGURE 3. The number of significant multipaths at different bandwidths.

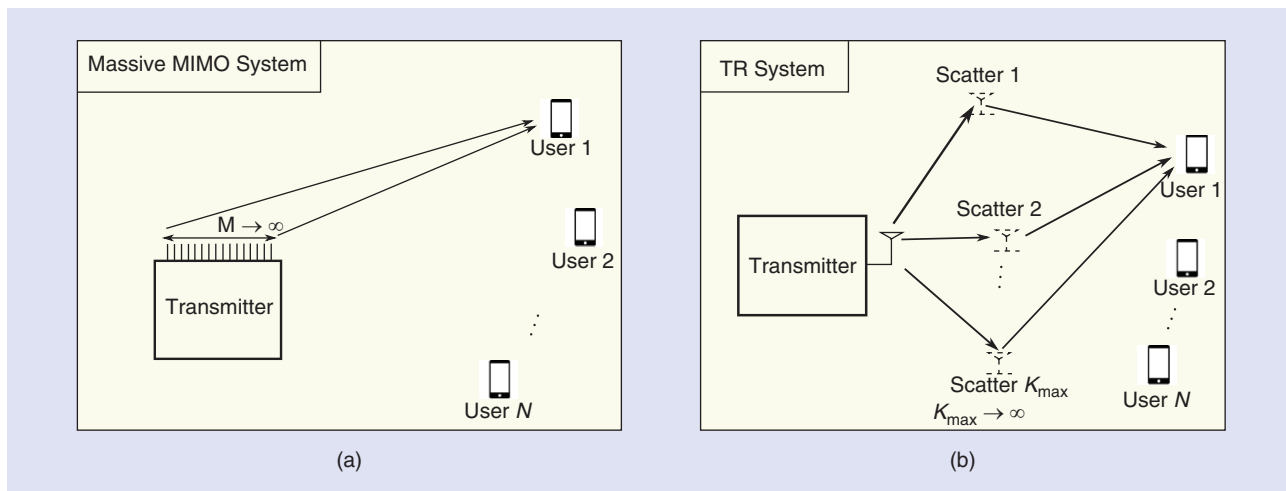


FIGURE 4. Two different ways of realizing a massive MIMO effect: (a) the multiantenna approach and (b) the TR approach.

interference (IUI) is introduced due to the nonorthogonality of the channel impulse responses among different users. To address this problem, one can utilize the degrees of freedom provided by the environment, i.e., the abundant multipaths, to combat the interference using signature waveform design techniques. The basic idea of signature waveform design is to carefully adjust the amplitude and phase of each tap of the signature waveform based on the channel information such that the signal at the receiver can retain most of the useful signal while suppressing the interference as much as possible. Moreover, with random scatterers, TR can achieve focusing that is far beyond the diffraction limit [14], which is a half wavelength.

TR effects

In this section, we argue that TR is an ideal platform for future 5G wireless communication systems because it can realize a massive MIMO-like effect using a single antenna and has low complexity, as the environment is serving as the computer. It is highly energy efficient, scalable for extreme network densification, and ideal for cloud-based radio access networks. It also offers, in a simple way, very high-resolution localization performance for indoor positioning systems, an essential property

for Internet of Things (IoT) applications. TR communication meets all the requirements one can envision for future 5G wireless!

A single-antenna realization of massive MIMO effect

In a typical indoor environment, the reflection, diffraction, and scattering in the wireless medium due to the various obstacles and reflectors—such as walls, windows, and furniture—often create a large number of multipath components. As new spectrum and larger bandwidth become available, more rich-scattering multipaths can be revealed. But how many multipaths can be harvested? To answer that, we used two universal software radio peripherals as channel sounders to probe the real channel in an office environment. Specifically, we

scanned the spectrum from 4.9 to 5.9 GHz to acquire the channel impulse response with a bandwidth of 10 MHz–1 GHz using transmission power of 100 mW. Based on these experiments, we show in Figure 3 the number of significant multipaths in an indoor environment versus the channel bandwidth. It can be seen that, with a single antenna, the number of multipaths can approach approximately 100 as the bandwidth increases to 1 GHz. Such degrees of freedom can be further scaled up by deploying more antennas.

Different from the way conventional techniques exploit the multipath propagation environment—e.g., orthogonal frequency-division multiplexing (OFDM) exploiting the multipath components as frequency diversity and code-division multiple access using the

Rake receiver to coherently combine the multipath components—the TR technique can take advantage of the multipath propagation without the need for deploying complicated receivers or a large number of antennas if sufficiently large bandwidth can be used. The larger the bandwidth, the better the resolution of individual multipath components. As shown in Figure 4(a) and (b), there are two ways to realize the massive MIMO effect. One is to use a large number of real antennas to straightforwardly

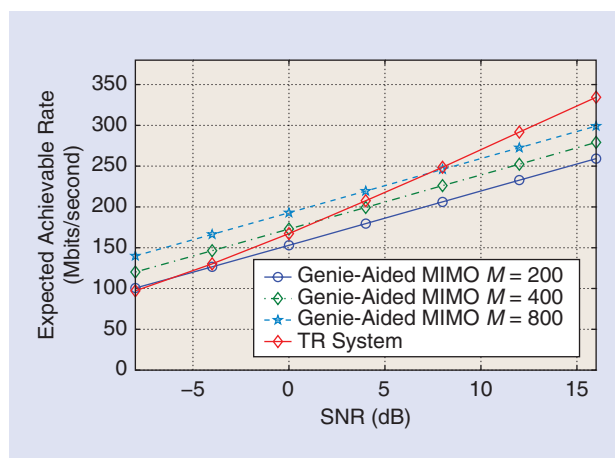


FIGURE 5. Expected achievable rate comparison between a massive MIMO system and the TR system.

build a massive antenna system. And the other is to leverage TR that inherently treats the multipaths in the environment as virtual antennas. Both can achieve the spatial-temporal resonance at a particular space and time that we now commonly term as the massive MIMO effect. Basically, it is a small focusing ball of energy that takes place due to the very high degree of freedom.

Therefore, by exploiting a large number of virtual antennas, a single-antenna TR system can achieve superior focusing effect in both time and spatial domains, resulting in similar promising performance as massive MIMO systems. In addition, the implementation complexity of a TR system is much lower since it utilizes the environment as a virtual antenna array and a computing resource. If cooperation of users, e.g., cooperative communications, is a distributed way of achieving the MIMO effect of high diversity, then TR is similarly a cooperation of virtual antennas to achieve the massive MIMO effect. The TR waveform is nothing but to control each multipath (virtual antenna). Of course, what cooperation pays for is the spectral efficiency due to the use of time for distributed processing, in return for the diversity effect.

In Figure 5, the performance comparison is shown in terms of the expected

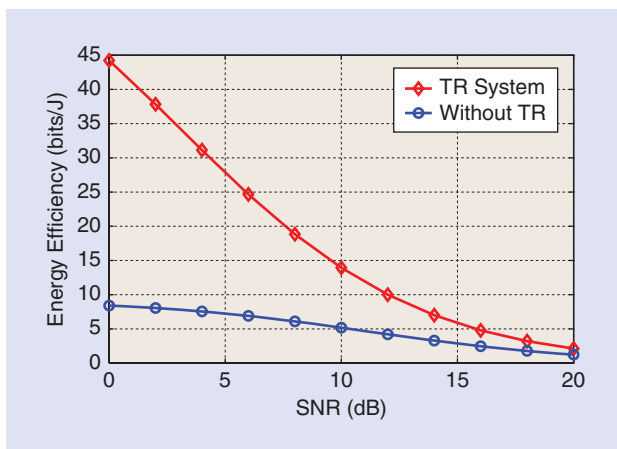


FIGURE 6. A comparison of energy efficiency between a TR system and direct transmission without TR.

achievable rate between a practical TR system and an ideal genie-aided massive MIMO system. The expected achievable rate is computed by averaging the achievable rate defined in [15] over different channel realizations. By genie aided, we mean an ideal condition that the interference and antenna coupling effects in the massive MIMO system can be completely eliminated with optimal beamforming. The genie-aided massive MIMO system has M transmit antennas with 20-MHz bandwidth where M is in the order of hundreds [13], while the TR system has a single transmit antenna with 1-GHz bandwidth. It is assumed that there are ten users in both systems, each equipped with a single antenna. In other words, the massive MIMO system we considered here is a multiuser MIMO (MU-MIMO) system [2]. The total transmit power is

set to be the same for both systems. The overhead of both systems mainly comes from the channel acquisition, and thus is similar. From Figure 5, it can be seen that, at the cost of a larger bandwidth, the TR system can achieve comparable if not better rates with the genie-aided massive MIMO system by using only a single antenna. This is achieved through exploiting a large number of virtual antennas that naturally exist in the environment. Note that the performance of the TR system was

obtained from real data, while that of massive MIMO is the best case scenario. Also note that the massive MIMO system requires a large number of antennas that is suited for high-power outdoor base stations, while the TR system leverages large bandwidth to harvest naturally existing multipaths, ideal for low-power indoor applications.

Energy efficiency

TR technology can take advantage of the multipath propagation and achieve good energy efficiency. The temporal focusing effect concentrates a large portion of the useful signal energy of each symbol within a short time interval, which effectively reduces the ISI for high-speed broadband communications. The spatial focusing effect allows the signal energy to be harvested at the

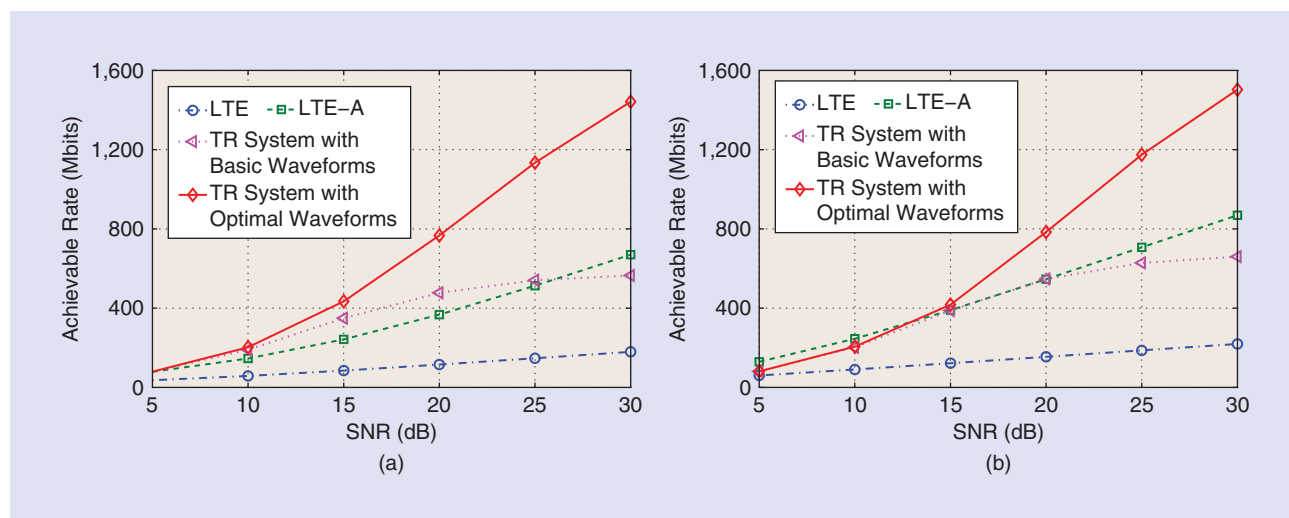


FIGURE 7. An achievable rate comparison: (a) one user case and (b) ten users case.

intended location and reduces leakage to other locations, leading to a reduction in both the required transmit power consumption and cochannel interference to other locations.

Defining energy efficiency (in bits/Joule) of a system as the spectral efficiency (sum-rate in bits/channel use) divided by the transmit power expended (in Joules/channel use), and using real-world channel measurements in a typical indoor environment, we compare the energy efficiency of a TR system with that of a direct transmission system without TR. The results are shown in Figure 6. It can be seen that with TR, the energy efficiency can be improved by up to 7 dB. Note that a wide bandwidth is generally required for a TR system to resolve the rich multipaths and fully harvest energy from the environment. As 5G technology is expected to be able to support larger bandwidth, the benefits and unique advantages of TR due to the temporal and spatial focusing effects in a rich-scattering environment promise a great potential for achieving high energy-efficiency in next-generation networks.

High capacity when bandwidth is available

By utilizing spatial focusing, a TR access point (AP) can communicate with multiple users simultaneously within the same spectrum, i.e., the spec-

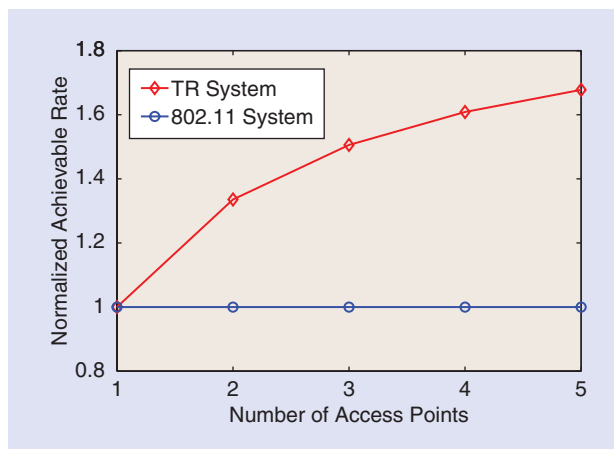


FIGURE 8. The normalized achievable rate comparison between the TR system and 802.11 system.

trum is fully reused by different users. Such a full spectrum reuse feature, together with wide bandwidth, have the potential to provide high capacity [15]. This is validated in Figure 7, where we show the performance comparison in terms of achievable rate between the TR system and two OFDM systems.

It can be seen that for the one-user case, even with basic TR waveform, the TR scheme can achieve much better performance than long-term evolution (LTE) in all SNR regions and better performance than LTE-advanced (LTE-A) in most SNR regions. With optimal waveform, the performance of the TR system can be further improved. When there are ten users, due to the selectivity among different users, the achievable rate of LTE and LTE-A can be enhanced, and LTE-A can achieve comparable and even slightly

better performance than the TR system with basic TR waveform. Nevertheless, with optimal waveform, the TR system can still outperform LTE and LTE-A in most SNR regions, which demonstrates that the TR system can achieve higher capacity than OFDM systems when the bandwidth is wide enough. Note that there is a large amount of spectrum at millimeter-wave frequencies [3] that can be utilized by TR.

Scalability for extreme network densification

With a high capacity, a single TR AP has the potential to serve many users while creating little interference to other wireless users. However, in some scenarios, the density of users may be so high that one single AP is insufficient to support all of them. We will show that the TR system is highly scalable and extra APs can be added with simple reconfiguration.

In conventional wireless communication systems, a mechanism is needed to prevent or alleviate the interference introduced by adding more APs due to the near-far effect. This near-far effect is solely the result of the distance between the AP and the users. In the TR system, however, different users have different resonances, which are the result of location-specific channel impulse responses instead of the distance only. With such a strong-weak focusing effect, there is no clear definition of

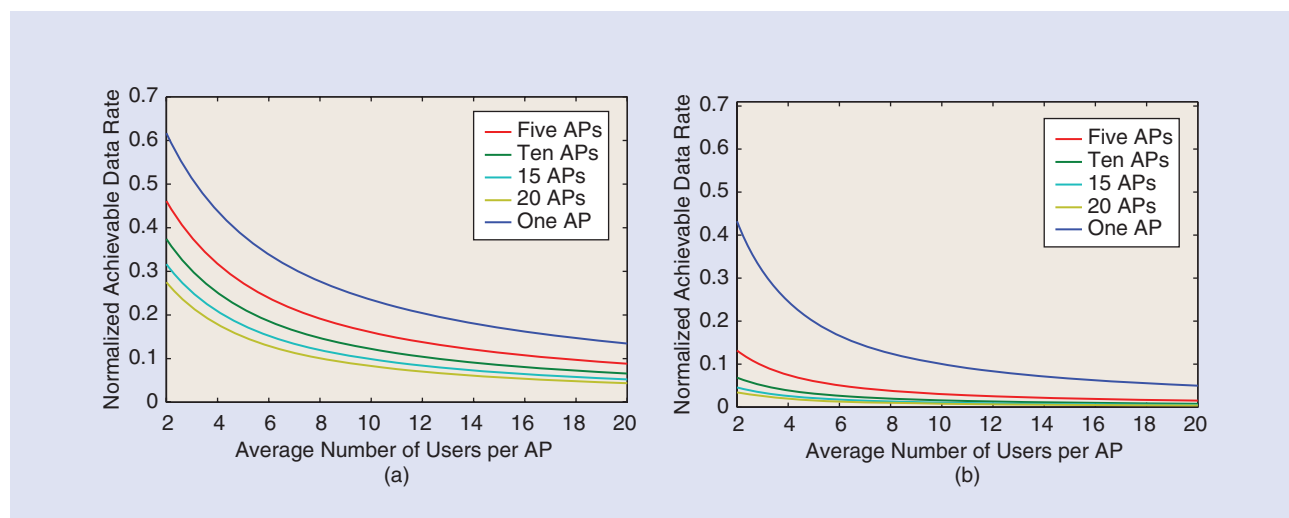


FIGURE 9. A comparison between the TR system and 802.11 system: (a) graceful performance degradation of TR and (b) performance degradation of 802.11.

cell boundaries. Thus, the TR system has a simple reconfiguration property, allowing the easy addition of new APs to the system. The newly added APs in the TR system help pick up users and reuse the same spectrum without incurring much interference, while in conventional systems, intercell radio resource management is needed to coordinate resource allocation between different cells and to limit the intercell interference. Such a self-configuring feature provides native support for machine-to-machine (M2M) and D2D communications where multiple pairs of machines/devices can coexist and share the spectrum without complicated transmission coordination strategies.

Figure 8 shows the performance comparison in terms of normalized achievable rate versus the number of APs, where the normalization is performed over the achievable rate of the single AP case. It can be seen that the normalized achievable rate of conventional systems remains unchanged regardless of the increase of the number of APs. This is because neighboring APs cannot use the same resource in conventional systems due to the interference. On

the other hand, with the TR system, by utilizing the spatial focusing effect, all APs use the same spectrum and thus the normalized achievable rate increases as the number of APs increases. Note that although different APs share the same spectrum, they are nearly orthogonal with each other. In traditional systems, such orthogonality can only be achieved by applying additional techniques, such as time, code, or frequency division multiplexing. In the TR system, this near-orthogonality is achieved naturally by utilizing the large number of multipath components in the wireless channel.

The performance degradation of each individual user is shown in Figure 9, where the normalization is over the point-to-point link capacity. It can be

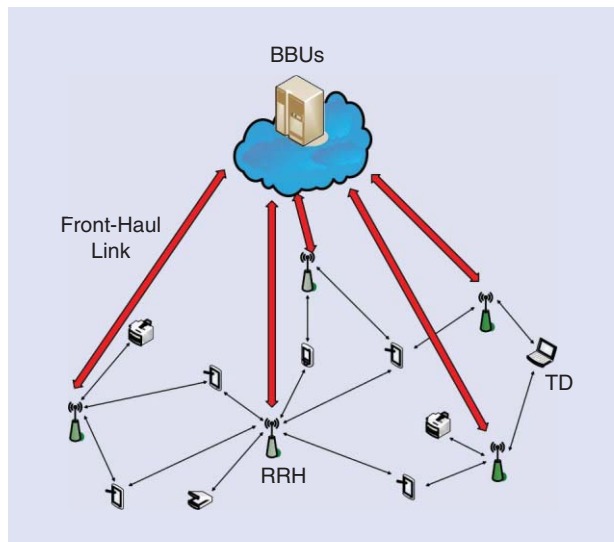


FIGURE 10. The C-RAN architecture.

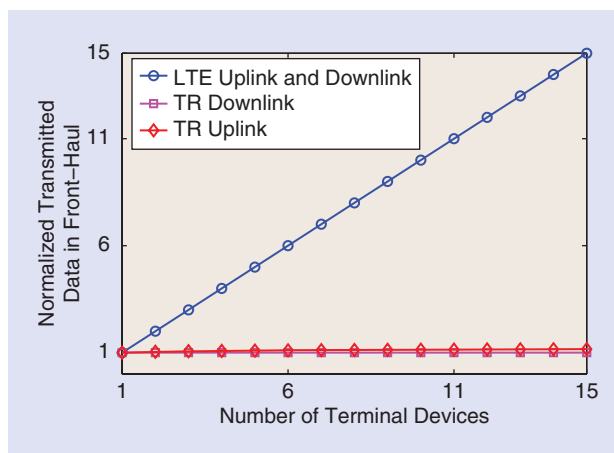


FIGURE 11. A comparison of the normalized total transmitted data in a fronthaul between TR-based and LTE-based C-RAN.

seen that the performance degradation of the IEEE 802.11 system is much more severe than the TR system. This is because each link in 802.11 requires an exclusive use of the channel, which is inefficient if there are many users/APs close to each other. On the contrary, the TR system can tolerate interference through the interference mitigation effect of TR so that multiple users/APs can share the same spectrum. Therefore, the performance degradation is more graceful, and each user is more robust against the interference from nearby users/APs.

Ideal for cloud-based networking

In most of the current C-RAN structures as shown in Figure 10, the fronthaul link capacity between the baseband units

(BBUs) and the distributed remote radio heads (RRHs) often becomes a bottleneck when there are a large number of users/terminal devices (TDs) in the network. Several solutions have been proposed to tackle this challenge, such as signal compression and sparse beamforming. However, in these schemes, the data transmitted in the fronthaul is proportional to the aggregated traffic of all TDs, and the fronthaul link capacity can still be a bottleneck in a very dense network.

On the other hand, if TR technology is used as the air interface in C-RAN, due to its unique spatial and temporal separation effects, all TDs are naturally separated by the location-specific signatures in both downlink and uplink, and the baseband signals for all TDs can be efficiently combined and transmitted. This unique feature of TR technology can be leveraged to create in essence a tunneling effect between the BBUs and the RRHs to alleviate the traffic load in the fronthaul link of C-RAN.

The data rate in the fronthaul connecting the BBUs and each RRH is only dependent on the system bandwidth and the

number of bits used for every symbol, thus serving more TDs will not increase the traffic on the fronthaul link. Figure 11 shows the performance comparison in terms of normalized total transmitted data versus the number of TDs, where the normalization is performed over the transmitted data of the single TD case. The normalized total transmitted data in the fronthaul in an LTE-based C-RAN increases linearly with the number of TDs, while that of a TR-based C-RAN almost keeps constant, showing that the TR tunneling effect can deliver more information in the C-RAN and alleviate the burden of the fronthaul caused by network densification, a feature essential to next-generation systems.

Low complexity

Since TR systems essentially treat the rich-multipath environment as a computing machine that facilitates matched filtering, the receiver can perform a simple one-tap detection and thus the complexity of TR systems can be significantly reduced—essentially, the environment is doing the analog signal processing! As discussed in [16], by convolving the signal sequences with the TR signature waveforms, a TR system can concentrate most of the computational complexity at the more powerful AP-side while keeping the complexity of TDs at a minimal level, i.e., the TR system exhibits a unique asymmetric architecture. This desirable feature can provide less complexity and thus lower the cost of the TDs, which is ideal for supporting IoT [16].

Additional features

Besides the features previously discussed, there are many additional features when operating TR systems in a rich-scattering environment. For example, the unique spatial focusing effect can be used to significantly improve the resolution of indoor positioning systems [12]. The idea is to utilize the location-specific characteristic of multipaths. That is, for each physical geographical location, there is a unique logical location in the multipath space. By matching the multipath profile with those in the database, the physical location can be identified. Real-world experiments show that the TR-based indoor positioning system can achieve perfect 1–2 cm localization accuracy with a single AP working in the ISM band with bandwidth 125 MHz under the non-LOS condition [12].

Moreover, the unique location-specific multipath profile can be exploited to enhance the system security at the physical layer, where the user at the intended location can receive better SINR than all other ineligible users at different locations. Another interesting and unique feature is the pinpoint beamforming effect, i.e., the spatial focusing can be a 3-D “ball” by utilizing the distributed virtual antennas that naturally exist at different geographic locations.

Conclusions and discussions

We have shown the major features of TR, including massive multipath effect, energy efficiency, high capacity, scalability for network densification, tunneling effect for cloud-based networking, low complexity, and some additional features such as improving the resolution of indoor positioning systems and providing physical layer security. Such features collectively address the major challenges of 5G indoor communications. Therefore, TR appears to be a promising platform for 5G indoor and offer great opportunities for the community to develop further.

However, some challenges deserve more consideration in the future:

- *Number of multipaths*: The performance of TR systems depends highly on the degrees of freedom in the environment, i.e., the number of multipaths. The larger the number of multipaths, the higher the TR focusing gain and thus the better the performance. When the number of multipaths varies from place to place, one may want to ensure the same performance.
- *Dynamic environment*: One implicit assumption of TR systems is that the channel is stationary. In a dynamic environment, the estimated channel in the channel probing phase may not be consistent with the real channel in the data transmission phase, due to which the focusing gain may be reduced causing performance degradation. Through real experiments, one can see that the channel is quite stable as long as there is no severe disturbance of the environment [9], [12]. When the environment is highly dynamic, one may need to probe the channel more frequently to sustain the operation.
- *Mobility*: The benefit from the focusing effect of TR relies on accurate channel estimation. If the transmitter and/or receiver become mobile, the channels are no longer reciprocal when the speed is faster than what the channel coherent time can handle, and the focusing gain may drop greatly due to outdated channel estimate. Therefore, the channel needs to be reprobated in mobile TR systems, and the reprobating will be more challenging if there are many TDs or the TDs are moving at a high speed.

- *Synchronization/timing*: Finding the right timing of the focusing peak is critical to facilitate the TR system operation. This can be resolved through oversampling and performing synchronization in the oversampled domain, which, however, will increase the cost of analog-to-digital converters and digital-to-analog converters.

Authors

Yan Chen (eecyan@uestc.edu.cn) is a principal technologist of Origin Wireless, Inc. He was also affiliated with the University of Maryland at the time of this writing. He is currently a professor with the School of Electronic Engineering, University of Electronic Science and Technology of China.

Beibei Wang (beibei.wang@originwireless.net) is a principal technologist of Origin Wireless, Inc. Her research interests include wireless communications and signal processing.

Yi Han (yhan1990@umd.edu) is currently a Ph.D. candidate in the Department of Electrical and Computer Engineering, University of Maryland, College Park. He is also affiliated with Origin Wireless, Inc.

Hung-Quoc Lai (quoc.lai@originwireless.net) is the vice president of engineering of Origin Wireless, Inc., which develops advanced time-reversal wireless technologies for use in a wide variety of positioning, recognition, security, communications, and power charging applications.

Zoltan Safar (zsafar@umd.edu) is a principal technologist of Origin Wireless, Inc. He is also with the Electrical and Computer Engineering Department at the University of Maryland, where he is the director of the Master's in Telecommunications Program.

K.J. Ray Liu (kjrliu@umd.edu) is the chief technology officer of Origin Wireless, Inc. He is also the Christine Kim Eminent Professor of Information Technology at the University of Maryland, College Park.

References

- [1] M. Paolini. (2011). Beyond data caps: An analysis of the uneven growth in data traffic. [Online]. Available: <http://www.senzafiliconsulting.com>

(continued on page 26)

FROM THE GUEST EDITORS

Fauzia Ahmad, A. Enis Cetin, K.C. (Dominic) Ho, and John Nelson

Signal Processing for Assisted Living: Developments and Open Problems

The old-age dependency ratio, which is defined as the ratio of the population age 65 and over to the population age between 15 and 64, has been rising in many countries all over the world. According to the United Nations estimates for the “more developed regions,” this ratio is anticipated to exceed 30% in 2020 and reach 40% by 2030, largely as a result of an accelerating increase in the aged population. This implies that those of working age, and, subsequently, the overall economy, will face a greater burden in supporting the aging population. In addition, the demand and trend are upward for continued independent living, in both more and less developed regions. As such, there is a growing interest in assisted living technologies that enable self-dependent living within homes and residences for the elderly, in particular those homes that will ensure an elderly person more years of life in good health.

Remote monitoring capabilities, such as fall risk assessment, fall detection, and detection of small changes from pre-defined baselines in health conditions and motor functional abilities of the elderly, will address the challenges associated with self-dependent living. All of the aforementioned capabilities are rooted in fundamental signal processing problems related to signal capturing, analysis, and interpretation. More specifically, these entail signal detection and enhancement in the presence of noise and interference; signal representation in a domain that is

conducive to capturing a rich set of features for vital signs estimation, human activity detection, localization, and health and well-being classification; the use of single and multiple sensors; centralized and distributed data fusion; and change or anomaly detection for risk assessments; to name but a few. Contributions in signal processing for assisted living technologies have not only been driven by recent developments in signal analysis and interpretation but also important revisits to “classical” approaches for exploiting the underlying phenomenology and the specificities of the problem at hand.

In this issue

This special issue of *IEEE Signal Processing Magazine (SPM)* provides a synopsis of the emerging area of signal processing for assisted living, including the most recent developments as well as interesting open problems at the forefront of the current research. The six articles demonstrate the role of signal processing in addressing key challenges and solving pressing problems encountered in assisted living applications related to various sensing modalities.

The first article by Bennett et al. provides an overview of wearable inertial measurement unit-based sensors for ubiquitous monitoring of movements and physical activities. It discusses associated signal processing techniques with a focus on enhancing accuracy, lowering computational complexity, reducing power consumption, and improving the unobtrusiveness of the wearable computers.

Erden et al. present a survey of signal processing methods employed with different types of sensors, including pyroelectric infrared and vibration sensors, accelerometers, cameras, depth sensors, and microphones. Their article demonstrates the need for a sensor network covering multiple modalities to achieve an intelligent home design that enables the elderly to live independently.

The article by Savazzi et al. investigates signal models and processing methodologies for exploiting the multitude of available wireless communication links to achieve device-free radio vision systems to address key challenges in assisted living applications.

Witrisal et al. provide insights into the potential of high-accuracy localization systems as a key component of assisted living technology, and their article demonstrates the ability of exploiting multipath and propagation environment knowledge to reduce the required infrastructure and enable robust localization.

Amin et al.'s contribution focuses on radar technology and discusses the non-stationary signal processing techniques that play a fundamental role in fall detection for elderly assisted living applications. It also reports on some of the challenges facing radar technology development for fall detection.

Finally, the article by Debes et al. covers state-of-the-art methods for monitoring activities of daily living to provide detection of deviations from previous patterns that can be crucial in identifying the early onset of geriatric dysfunctions.

Digital Object Identifier 10.1109/MSP.2016.2514718

Date of publication: 7 March 2016

Acknowledgments

We would like to express our deep gratitude to the many individuals who made this special issue of *SPM* possible. We thank all authors who submitted proposals and all reviewers whose recommendations significantly helped in improving the selected articles. We are grateful to Abdelhak Zoubir, *SPM*'s previous editor-in-chief, and the


previous special issues area editor, Fulvio Gini, for approving this special issue. We are also grateful to Min Wu, *SPM*'s current editor-in-chief, for her support. We are indebted to Wade Trappe, current special issues area editor, for his constant support and guidance throughout the reviewing process, as well as to Rebecca Wollman for her valuable administrative assistance.

About The Guest Editors

Fauzia Ahmad (fauzia.ahmad@villanova.edu) is with Villanova University, Villanova, PA, USA.

A. Enis Cetin (cetin@bilkent.edu.tr) is with Bilkent University, Ankara, Turkey.

K.C. (Dominic) Ho (HoD@missouri.edu) is with University of Missouri, Columbia, USA.

John Nelson (John.Nelson@ul.ie) is with University of Limerick, Limerick, Ireland. 

PERSPECTIVES (continued from page 24)

[2] F. Rusek, D. Persson, B. K. Lau, E. G. Larsson, T. L. Marzetta, O. Edfors, and F. Tufvesson, "Scaling up MIMO: Opportunities and challenges with very large arrays," *IEEE Signal Processing Mag.*, vol. 30, no. 1, pp. 40–60, Jan. 2013.

[3] F. Boccardi, R. Heath, A. Lozano, T. Marzetta, and P. Popovski, "Five disruptive technology directions for 5G," *IEEE Commun. Mag.*, vol. 52, no. 2, pp. 74–80, Feb. 2014.

[4] N. Bhushan, J. Li, D. Malladi, R. Gilmore, D. Brenner, A. Damnjanovic, R. Sukhavasi, C. Patel et al., "Network densification: The dominant theme for wireless evolution into 5G," *IEEE Commun. Mag.*, vol. 52, no. 2, pp. 82–89, Feb. 2014.

[5] C. I. C. Rowell, S. Han, Z. Xu, G. Li, and Z. Pan, "Toward green and soft: A 5G perspective," *IEEE Commun. Mag.*, vol. 52, no. 2, pp. 66–73, Feb. 2014.

[6] B. P. Bogert, "Demonstration of delay distortion correction by time-reversal techniques," *IRE*

Trans. Commun. Syst., vol. 5, no. 3, pp. 2–7, Dec. 1957.

[7] D. Harasty and A. Oppenheim, "Television signal dehosting by noncausal recursive filtering," in *Proc. Int. Conf. Acoustics, Speech, and Signal Processing*, Apr. 1988, no. 3, pp. 1778–1781.

[8] M. Fink, "Time reversal of ultrasonic fields. I. Basic principles," *IEEE Trans. Ultrason., Ferroelectr. Freq. Control*, vol. 39, no. 5, pp. 555–566, 1992.

[9] B. Wang, Y. Wu, F. Han, Y. H. Yang, and K. J. R. Liu, "Green wireless communications: A time-reversal paradigm," *IEEE J. Sel. Areas Commun.*, vol. 29, no. 8, pp. 1698–1710, Sept. 2011.

[10] N. Guo, B. M. Sadler, and R. C. Qiu, "Reduced-complexity UWB timereversal techniques and experimental results," *IEEE Trans. Wireless Commun.*, vol. 6, no. 12, pp. 4221–4226, Dec. 2007.

[11] F. Han, Y.-H. Yang, B. Wang, Y. Wu, and K. J. R. Liu, "Time-reversal division multiple access


over multi-path channels," *IEEE Trans. Commun.*, vol. 60, no. 7, pp. 1953–1965, July 2012.

[12] Z. H. Wu, Y. Han, Y. Chen, and K. J. R. Liu, "A time-reversal paradigm for indoor positioning system," *IEEE Trans. Veh. Technol.*, vol. 64, no. 4, pp. 1331–1339, Apr. 2015.

[13] J. Vieira et al., "A flexible 100-antenna testbed for massive MIMO," in *Proc. IEEE GLOBECOM*, 2014, pp. 287–293.

[14] G. Leroosey, J. de Rosny, A. Tourin, and M. Fink, "Focusing beyond the diffraction limit with far-field time reversal," *Science*, vol. 315, pp. 1120–1122, Feb. 2007.

[15] Y. Chen, Y. H. Yang, F. Han, and K. J. R. Liu, "Time-reversal wideband communications," *IEEE Signal Processing Lett.*, vol. 20, no. 12, pp. 1219–1222, Dec. 2013.

[16] Y. Chen et al., "Time-reversal wireless paradigm for green Internet of Things: An overview," *IEEE Internet Things J.*, vol. 1, no. 1, pp. 81–98, Feb. 2014. 

SigPort.org

Do you know? Your colleagues archived the slides of their signal processing work on IEEE SigPort.

The slides and posters you spent hours to make are highlights of your work. Aren't they "forgotten" soon after conference presentations or thesis defense?

IEEE Signal Processing Society's new SigPort repository helps extend the life of your slides and posters, and raise the visibility of your work by sharing these appealing summaries. Checkout the material from recent GlobalSIP, WIFS, ICIP and MLSP. Upload yours today!

- **Raise visibility:** Recent conference slides/posters posted on SigPort had an average of 25 downloads in a month, more than IEEE Xplore!
- **Easy to use:** Watch a short video tutorial and upload your work in less than 15 minutes; link slides to full papers on IEEE Xplore
- **Well indexed:** Each has a unique URL picked up by major search engines; plus additional highlights through the editor's picks



SigPort welcomes research drafts, white papers, theses, slides, posters, lecture notes, dataset descriptions, and more. Try out with promotion code **you14100** (expires 31 May 2016).

General Chairs

Zhi Tian
George Mason Univ.

Brian M. Sadler
Army Research Lab.

Technical Program Chairs

Phillip Regalia
NSF

Trac Tran
John Hopkins Univ.

Brian Mark
George Mason Univ.

Finance Chair

Jill Nelson
George Mason Univ.

Local Arrangements Chair

Nathalia Peixoto
George Mason Univ.

Publications Chair

Kathleen Wage
George Mason Univ.

Publicity Chairs

Piya Pal
Univ. MD, College Park

Seung-Jun Kim
Univ. MD, Baltimore Cty

Technical Workshop**Liaison Chair**

Min Wu
Univ. MD, College Park

Government Panel

Chairs
Joel Goodman
Naval Research Lab

Industrial Liaison Chairs

Kristine Bell
Metron Inc.

Hang Liu
Catholic Univ.

International Liaison Chairs

Chengyang Yang
BUAA, China

Mounir Ghogho
Univ. of Leeds, UK

Advisory Committee

Monson Hayes
George Mason Univ.

IEEE GlobalSIP**Fourth IEEE Global Conference on Signal and Information Processing**

December 7-9, 2016, Greater Washington D.C., USA

IEEE Signal Processing Society

<http://2016.ieeeglobalsip.org/>

Call for Papers

The fourth IEEE Global Conference on Signal and Information Processing (GlobalSIP) will be held in Washington, DC, USA on December 7-9, 2016. GlobalSIP has rapidly assumed flagship status within the IEEE Signal Processing Society. It focuses broadly on signal and information processing with an emphasis on up-and-coming signal processing themes. The conference aims to feature world-class plenary speeches and overview talks, tutorials, exhibits, oral and poster sessions, and government panel discussions on emerging topics and funding opportunities in Signal and Information Processing. GlobalSIP 2016 is comprised of co-located symposia selected based on responses to the Call for Symposium Proposals. Featured symposia include:

- Big data signal processing
- Signal and information processing over networks
- Distributed information processing, optimization and resource management over networks
- Machine learning, deep learning
- Signal processing in information secrecy, privacy and security
- Compressed sensing, sparsity analysis and applications
- Signal processing for 5G wireless networks
- Cognitive communications and radar
- Signal processing in energy and power systems
- Big data analytics in neuro-imaging
- Autonomous systems
- Emerging signal processing applications in industry

Prospective authors are invited to submit full-length papers, with up to four pages for technical content including figures and possible references, and with one additional optional 5th page containing only references. Manuscripts should be original (not submitted/published anywhere else) and written in accordance with the standard IEEE double-column paper template.

Note that IEEE Communications Society will hold its annual Globecom Conference at Washington DC in Dec. 4-8, 2016. Interested attendees may take advantage of the opportunity to attend both GlobalSIP and Globecom back to back in one trip.

For updated and detailed information about the technical symposia, please check online at <http://2016.ieeeglobalsip.org/>. For technical inquiries, please contact conference TPC Chairs at tpc-chairs@2016.ieeeglobalsip.org.

Conference Timeline:

- June 5, 2016 : Paper Submission Due
- August 5, 2016 : Final Acceptance decisions notifications sent to all authors
- September 5, 2016: Camera-ready papers due.



Terrell R. Bennett, Jian Wu,
Nasser Kehtarnavaz, and Roozbeh Jafari

Inertial Measurement Unit-Based Wearable Computers for Assisted Living Applications

A signal processing perspective

There has been a very rapid growth in wearable computers over the past few years. Assisted living applications leveraging wearable computers will enable a healthier lifestyle and independence in a variety of target populations, including those suffering from neurological disorders, patients in need of rehabilitation after surgical procedures or injury, the elderly, individuals who might be at high risk of emotional stress, and those who are looking for a healthier lifestyle. Application paradigms for assisted living include activities of daily living (ADLs) monitoring, indoor localization, emergency and fall detection, and rehabilitation. All of these applications require monitoring of movements and physical activities for individuals. Wearable inertial measurement unit (IMU)-based sensors can offer low-cost and ubiquitous monitoring solutions for physical activities. Signal processing techniques with a focus on enhancing accuracy, lowering computational complexity, reducing power consumption, and improving the unobtrusiveness of the wearable computers are of interest in this article, which constitutes the first attempt made at reviewing the literature of wearable IMU-based signal processing techniques for assisted living applications. Various signal processing techniques with the aforementioned performance metrics in mind are reviewed here.



IMAGE LICENSED BY INGRAM PUBLISHING.
WOMAN—©ISTOCKPHOTO.COM/SILVIAJENSEN

Introduction

Cisco predicts the number of wearable devices will increase from 22 million in 2013 to 177 million in 2018 [1]. Many innovative applications are under development for wearable devices. Assisted living is one of the application areas with major potential impact. There are two common approaches to implementing these monitoring systems: using vision or wearable sensors. Vision-based approaches are considered to be invasive to a user's privacy and suffer from line-of-sight issues for cameras. They may not be available everywhere, and signal processing techniques associated with vision sensors are typically computationally intensive, even though they may provide rich information for

Digital Object Identifier 10.1109/MSP.2015.2499314
Date of publication: 7 March 2016

certain applications. Wearable IMU-based sensors, however, can offer low-cost and ubiquitous monitoring solutions. Typical IMUs consist of a three-axis accelerometer that measures dynamic accelerations caused by motion and gravity and a three-axis gyroscope that measures angular velocities about the three axes. Some IMU sensors also include magnetometers that measure the Earth's magnetic field. These sensors are available as long as the user is wearing them. However, wearable sensors face their own challenges, such as reliability issues associated with wearing the sensors improperly. Moreover, users would only wear a few sensors, and, therefore the systems cannot sense the movements of every joint and limb. Power consumption is another challenge related to wearable sensors. Small form factor, long battery life, comfort, and wearability require low power consumption. Efficient signal processing techniques deliver solutions to address these challenges. Signal processing techniques with a focus on enhanced accuracy, lower computational complexity, and reduced power consumption of the wearable computers are of interest. Our survey article constitutes the first attempt at reviewing the literature of wearable IMU-based signal processing techniques for assisted living applications and reviews various signal processing techniques based on the given performance metrics.

A review of assisted living applications

As mentioned previously, assisted living applications can include ADLs, indoor localization, emergency and fall detection, and rehabilitation. Figure 1 shows the flow for IMU-based assisted living applications and topics. The following are applications that use IMU sensors to make an impact on everyday life.

Activities of daily living

Monitoring and classifying daily activities are keys to assessing the quality of life of various target populations. In this article, the ADLs tracked using IMUs are categorized into postural transitions (e.g., sit-to-stand and stand-to-sit), periodic movements (e.g., walking and running), eating, and sleeping habits. As people get older, performing daily tasks can become challenging. Due to the high cost of health-care centers and the need for the elderly to live independently in their homes, developing IMU-based monitoring systems for ADLs is becoming more important [2], [3]. This is not limited to assisting the aging population, it can also help many others. IMU-based wearables allow workers to function more efficiently and without distractions by providing information based on their current activity [4]. People can track their sleep patterns by wearing an IMU-based sensor on their wrist to detect and log the duration of their sleep/awake time [5]. Users are also able to automatically track their dietary activities by detecting the arm and trunk intake gestures, chewing,

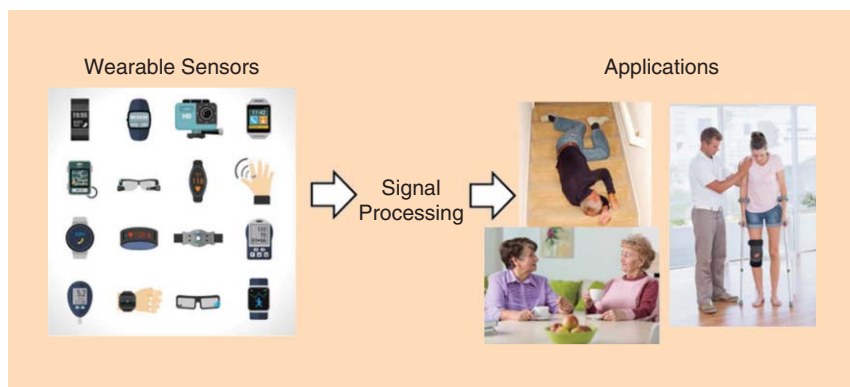


FIGURE 1. Data flow for IMU-based assisted living applications. (Wearable image copyright: Askold Romanov, elderly women copyright: KatarzynaBialasiewicz, fallen man copyright: AnnBaldwin, rehabilitation image copyright: Wavebreakmedia.)

and swallowing of food [6]. IMU-based wearables are a part of smart environments that monitor and recognize human gestures so that robots can assist them or the users can control things based on their hand gestures [7], [8]. These types of applications can influence the quality of life for those with disabilities. Several challenges need to be considered for monitoring and classifying ADLs using IMUs. These include sensor displacement, variations in the movements and environments, and the form factor of the sensors.

Indoor localization

People spend a considerable amount of their time indoors, so it can be very useful to have indoor localization systems. Human localization plays an important role in creating context-aware smart environments. IMU-based localization has been used in many applications such as location-aware computing [9], estimating energy expenditure in human walking [10], military operations [11], and finding specific locations in a building [12]. Assisted living technology can greatly benefit from IMU-based indoor localization. Some applications include locating users and providing directions to a desired place in a building and reducing the time necessary for first responders to find people in an emergency situation. It is necessary for such a system to be reliable and report the position accurately. A global positioning system (GPS) is mainly used for outdoor localization; due to obstacles and materials used in the buildings, it may not be available for indoor localization. A local positioning system (LPS) uses modalities such as received signal strength (RSS), vision, ultrasound, and inertial data to provide the location information within a specific coverage area. RSS and ultrasound approaches suffer from signal attenuation, while vision systems have line-of-sight issues. Pedestrian dead reckoning (PDR) is an alternative approach that estimates the user's movement by detecting steps, estimating stride lengths, and the direction of motion based on inertial data collected from body-worn sensors [13].

Emergency and fall detection

Elderly people are prone to falls, which may cause injury. This is a major area of concern in assisted living because these injuries can result in long-term hospitalization and medical costs.

Therefore, a fall detection system is necessary in assisted living. There are two major considerations for this application: 1) speed of detection and 2) accuracy of detection. The first is important because the nature of this application is to prevent injuries caused by falling if possible. For example, having a system that can detect falls before the user hits the ground becomes very promising if the system can activate a protective device (e.g., air bags attached to the user's hip). If no protective device is available, it is critical to get help to the user as soon as possible. The second consideration is necessary to ensure that falling events are properly detected and there are no false or missed detections. Several methods have been proposed using IMU sensors to detect falls before the target hits the ground [14], [15]. In these methodologies, detection speed is very important and challenging. Another approach reliably detects falls while also finding other common human activities that may share similar attributes (e.g., standing to lying in bed) [16]. Many elderly people cannot stand after falling due to injuries sustained, and an emergency message is needed to inform the hospital or care center [8].

Rehabilitation

There are many cases in which clinicians do not need to keep patients in the hospital to observe the recovery process after an operation or treatment. IMU-based systems can play an important role here and can allow patients to live independently in their homes while being monitored remotely by clinicians. The idea behind such systems is to provide general information about the effect of certain behavioral recommendations without having the patient admitted to a rehabilitation center or a laboratory for observation [17]. IMU sensors are able to measure the muscle strength and power by detecting high-frequency body sway [18] and the speed with which muscular forces produce movement of body segments [19]. Estimating knee joint flexion or extension angles can be used to infer activity type or intensity, muscle activity, and gait events [20]. Monitoring ADLs is also a key for evaluating changes in physical and behavioral profiles of the elderly and other patients, including obese people [21]. For example, increasing activity levels after surgery can be used to indicate overall improvement as well as efficacy of therapeutic procedures [22].

Signal processing techniques

Signal processing techniques translate the physical signals sensed from wearable IMU sensors into useful information required by target applications. In this article, our goal is to review the signal processing techniques from various perspectives, including preprocessing, feature extraction, feature selection, classification, and measurement models.

Preprocessing

For IMU-based assisted living applications, the raw sensor data usually gets preprocessed to remove noise from the signal and to determine the segments of interest. These tasks are called *filtering* and *segmentation*. Filtering techniques retain

the useful information in a signal while rejecting unwanted information based on the application. Segmentation techniques are used to determine the duration of the movements or events of interest.

Three different types of filters are used: low-pass filters, high-pass filters, and band-pass filters. A low-pass filter is used to remove high-frequency noise for a recognition task of five hand gestures [7] and for physical activity monitoring for assisted living [16]. A 17-Hz low-pass filter is used to reject electronic noise in gyroscope data for sit-to-stand and stand-to-sit measurements [8]. Based on the walking frequency of test subjects, a 3-Hz low-pass filter is applied to remove noise from walking signals [12]. A 6-Hz low-pass filter is applied for balance control measurements during sit-to-stand movements [18], while a low-pass filter with a cut-off frequency of 3 Hz is used to preprocess raw data for sit-to-stand parameter measurement [19]. The accelerometer measurement consists of gravitational acceleration and dynamic acceleration caused by motion. In some applications, only one part of the acceleration is used, and filtering techniques are applied to reject the other one. A 1-Hz low-pass filter is used to remove the dynamic acceleration, and thus the direction of the gravity vector is found during quasi-static activities [15]. A 1-Hz high-pass filter is used to reject the gravitational acceleration, which, in turn, removes the effect of the gross changes in the orientation of the body segment where the sensor is placed [23]. Some applications may only look at signals within a certain frequency range, and the band-pass filter can be used to preprocess the data. A 3–11-Hz band-pass filter is used to clean the accelerometer signal for detecting sleep and awakening phases [5]. For motor fluctuation monitoring in Parkinson's disease patients, a 3–8-Hz band-pass filter is used for the analysis of tremors, and a 1–3-Hz filter is applied for analysis of bradykinesia and dyskinesia [23]. The sliding window segmentation technique is simple and effective and is often used in the reviewed literature for segmentation [6], [7], [14], [17], [24], [25].

Feature extraction

Features are normally extracted from the sensor data depending on their effectiveness in a particular application. Feature extraction starts with the preprocessed sensor data and generates derived values that are intended to be informative and nonredundant while enabling subsequent learning and generalizing the data, which will lead to better human interpretation. The features are divided here into four categories: time domain features, frequency domain features, time–frequency domain features, and others. The time domain features are the general statistical measurements that can represent the generalization of the data. The frequency domain features analyze the frequency performance of the sensor signals, which is usually the periodicity of the signal over a long duration (i.e., periodicity of the walking). The time–frequency domain features refer to features that contain both time and frequency information simultaneously with different time–frequency representations (e.g., short-time Fourier transform, wavelets) that are useful for nonstationary signals (e.g., postural transitions). The other features refer to the features that have specific

meanings to specific applications (e.g., posture transition duration for fall detection and step length for gait analysis). Table 1 lists commonly used features of IMU sensors in assisted living applications.

The time domain features listed in Table 1 are primarily the general statistical features of a signal. Among those, signal vector magnitude and root mean square (RMS) look at the magnitude of the three-axis signal and do not contain directional information from the IMU sensor. These features usually play an essential role in movement classification and detection tasks if the most discriminative feature is not known. The frequency domain features are good at analyzing stationary signals that contain certain frequency patterns. For example, the fast Fourier transform (FFT) features for a certain long duration can be used to distinguish between walking, falling, and sitting down activities [2] and to distinguish between walking, running, standing, and going up stairs [27]. The principal frequency component can be considered to monitor the motor fluctuation of patients with Parkinson's disease [23]. The time–frequency domain feature listed captures the frequency features as well as the time at which the frequency component occurs. This information is important for analyzing nonstationary signals in which the frequency components change over time. This is true for all the transitional movements (e.g., sit-to-stand and sit-to-lie). This feature has been proven powerful for detecting daily activities of elderly subjects, which primarily consist of transitional movements [22]. It is also used to detect the postural transition time, which helps evaluate the fall risk of the elderly [8]. A comparison work shows that frequency domain features (FFT-based features) perform better than wavelet transform features in distinguishing continuously dynamic activities such as walking, walking upstairs, walking downstairs, running, and jogging [26].

The first three categories in the table generalize the signal based on statistics. The fourth category includes the features that are useful for certain applications. To extract these features, users are required to be knowledgeable about the application so that they know which features will best serve their purpose. Posture transition duration [3], [18], trunk tilt [3], and vertical velocity [15], [28] are among the features that can be used to detect and evaluate the sit-to-stand motion. Step

and stride length, velocity, cadence, swing, and stance are important in gait analysis [21]. Step length and heading are commonly used features for indoor localization [9], [11], [13].

Feature selection

In the previous section, we covered the extraction of various features from the IMU sensor data. Feature selection provides a way to select the most suitable feature subset for certain tasks from the available features. For example, to reduce over fitting and information redundancy, feature selection techniques can be applied to select the best feature subset for classification and detection tasks. It is useful when users do not know which features are useful and want to pick the best subset from a broad set of existing features. Here, feature selection also refers to the investigation that analyzes the sensitivity of different features for applications.

There are three different methods of feature selection: wrapper, filter, and embedded. Wrapper methods use a predictive model to score feature subsets. Each new subset is used to train a model that will be tested on the rest of the data set. Based on the prediction performance, each subset is assigned a score and the best subset will be chosen. Filter methods use general measurement metrics of a data set to score a feature subset instead of using the error rate of a predictive model. Some common measures are mutual information and inter/intra class distance. The embedded methods perform the feature subset selection in conjunction with the model construction. One example is the recursive feature elimination algorithm, which is commonly used with a support vector machine (SVM) to repeatedly construct a model and remove the features with low weights. The different feature selection techniques are stated next for assisted living applications.

A large set of features are extracted and a wrapper-based feature selection technique is applied to determine the best subset of the feature space in a preimpact fall detection application [14]. Each individual feature is assigned a ranking score based on its discriminative performance, and the best ranked features are selected to form a final feature vector and fit it to the classification algorithm. A framework is proposed to determine the best sensor locations and the most relevant sensor features for discriminating ADLs that can be important to assess physical and behavioral changes over time for the

Table 1. A list of features.

Feature Category	Feature List
Time domain	Mean, variance, signal vector magnitude, correlation coefficient, RMS, skewness, maximum magnitude change, slope of the fitting line, standard deviation of fitting error, standard deviation of difference, trapezoidal numerical integration, signal entropy, maximal acceleration, maximal jerk, maximal velocity, peak power, range of cross covariance between each of two axes [2], [3], [14], [16], [19], [22], [23], [26]
Frequency domain	FFT coefficients, principal frequency components, energy of 0.2-Hz window centered on the main frequency over the total FFT energy, logarithm of the magnitude-squared discrete Fourier transform coefficients [2], [23], [26], [27]
Time–frequency domain	Wavelet transform [8], [22]
Others	Posture transition duration, trunk tilt, vertical velocity, step length, step frequency, heading information, local energy of the trunk dynamics, postural transition smoothness, postural orientation, singular value decomposition, cadence, swing, stance [3], [9], [11], [12], [15], [16], [18], [21], [28]

elderly and patients with chronic diseases [24]. Three different feature selection algorithms are tested for 13 different features for five different groups of ADLs. Accelerometer based balance parameters are determined and compared during the sit-to-stand movement and the results show the area under the curve (AUC) and RMS are useful features and AUC appeared to be more sensitive than RMS [18].

Classification

Classification is widely used in applications of assisted living. Classification can be used to detect falls and prefalls, to distinguish between healthy and unhealthy motor function, and to detect ADLs. A variety of machine-learning and pattern recognition algorithms are explored in the area of the IMU-based assisted living. Table 2 shows some of the commonly used classification algorithms.

Thresholding-based decision making is a popular classification scheme in assisted living applications. This approach is straightforward to use and is often used for binary classification tasks. When the value of a feature is above a threshold, it is classified as one of the two states and when the value is below a threshold, it is recognized as the other. When the designer finds a feature that can discriminate between two possible states, the thresholding technique is a good candidate due to its simplicity and because it can be easily interpreted. The thresholding technique is applied to classify walking versus running [10]. If the variance of the accelerometer is below a defined threshold, the activity is recognized as walking, and recognized as running if the accelerometer variance is larger than a defined threshold. Based on this decision, an adaptive step length estimation algorithm is derived. A thresholding technique is applied to the inertial frame's vertical velocity magnitude to detect the occurrence of falls before impact [28]. To determine the posture transition time for sit-to-stand, a threshold is applied to determine the beginning and ending of the transition movement [8]. A threshold based on the maximum measured vertical velocity from ADLs and the minimum measured vertical velocity from falls is used to distinguish falls and normal activities [15]. Thresholding is used to distinguish tremor motions from nontremor motions in a movement

Feature selection provides a way to select the most suitable feature subset for certain tasks from the available features.

from the action research arm test, which is designed to test recovery of upper-limb function [29].

Instance-based learning methods classify an instance based on the similarity between the instance under test, and the labeled instances in the training data set. This method does not need to train a model in the training phase. However, it is computationally expensive in the testing phase because it needs to calculate the similarity between each testing instance and all of the instances in the training set. The k -nearest neighbors (kNN) algorithm is one example of an instance-based classification algorithm. It performs well in activity recognition tasks, and it is used to determine the different types of the ADLs [16], [24].

Neural networks are a family of statistical algorithms inspired by biological neural networks (i.e., the human brain). It consists of a large number of nodes acting as neurons in a network and the weighted connections between different neurons. With a large enough set of training data and parameter tuning, it can provide high classification performance. A very large data set is often required for training, and this is not usually available for IMU-based applications. Moreover, the trained model is not interpretable for users. In

IMU-based assisted living applications, the training data is usually small, and, in most cases, the user wants to understand the models. These two factors make neural networks less attractive in this area. The authors explored the classification performance of a neural network while varying the size of the training data set for a physical movement monitoring application [16]. Four transition movements were detected using the neural networks and kNN for an average accuracy of 84%.

SVM is one of the most popular discriminative classification algorithms in different areas in recent years. SVM tries to find the margins that will maximize the separation between different classes. In the training phase, the margins are determined and it is computationally efficient in the testing phase based on the trained model. It is similar to neural networks in that it will be difficult to interpret by users. However, it does not require a very thorough training or a very large training data set. A preimpact fall detection system is discussed based on the SVM classifier [14]. A SVM is applied for monitoring motor fluctuations in patients with Parkinson's disease and the optimal kernel is analyzed [23].

The HMM is a statistical Markov model in which the system is assumed to be a Markov process with unobserved states. HMM is well studied and is often used in temporal pattern recognition such as speech recognition and gesture recognition. It is widely used to recognize different activities based on IMU time series sensor data and is also good at recognizing a sequence of movements. Human intention recognition in smart assisted living systems is presented using a hierarchical HMM [7]. The HMM is first used to recognize the low-level hand gestures with a finger-worn inertial sensor

Table 2. Classification algorithms.

Classification Type	Classifier
Thresholding	[6], [8], [10], [15], [28], [29]
Instance based	KNN [16], [24]
Neural networks	Multilayer perceptron [16]
SVM	Linear kernel SVM [14], polynomial kernel SVM [23]
Hidden Markov models (HMMs)	Hierarchical HMM [7], continuous HMM [27], HMM [4], [17]

and, after that, a hierarchical HMM is applied to model the correlation and constraints between commands. A continuous HMM is proposed to jointly classify the pedestrian activity and gait phases with the assumption that state-conditional output density functions of the HMM to be a Gaussian mixture model [27]. This approach is robust to subject variability. It will still perform well when new subject data is tested without any training for this subject. In-home assembly task recognition is performed using a HMM on accelerometer data with fusion of the linear discriminant analysis (LDA) decision from sound data [4]. A method for spotting sporadically occurring gestures (e.g., handshake, drink, pick up the phone, etc.) in a continuous data stream from body-worn inertial sensors was designed using a HMM [17]. The method contains two stages. In the first stage, signal sections likely to contain specific motion events are selected using a similarity searching algorithm; and in the second stage, the HMM is applied to classify the activities.

Measurement models

In addition to classification algorithms, advanced measurement models are applied to fuse different modalities of IMU sensors (e.g., accelerometer, gyroscope, and magnetometer) to compensate for errors and drifts. This leads to robust measurements for different tasks in assisted living. Kalman filters and particle filters are among the most popular fusion techniques. The Kalman filter is an algorithm that uses a model and a series of noisy and possibly inaccurate measurements observed over time to produce estimates of unknown variables that tend to be more precise than those based on a single measurement alone. It is widely used in the navigation and control systems. A conventional Kalman filter is used to reduce the drift from inertial sensors in an indoor navigation system with foot-mounted strap-down inertial sensors [11]. The inertial navigation system calculates the position change at a high frequency rate, and the integration error from the inertial sensor will accumulate over time. The GPS is also a part of the system and when GPS data is available, the GPS derived positions are compared with the positions derived from the inertial navigation system. The differences are fed into a Kalman filter that estimates the errors from the inertial navigation system and compensates the measurements so that the errors remain small. A Kalman filter is used to combine the acceleration, angular velocity and biomechanical constraints to generate robust estimation of the knee joint flexion/extension angles [20]. The gyroscope noise and the accelerometer noise are modeled by the Kalman filter. The proposed system works effectively for both walking and running for five minutes when compared to a camera-based motion tracking system.

Unlike the Kalman filter, the adaptive filter is a system with a linear filter that has a transfer function controlled by variable parameters that are adaptively updated according to

certain optimization criterion. An adaptive filter is designed to fuse all of the sensor information and pseudo-measurements to provide a self-contained pedestrian tracking system during normal walking [9]. In the cases that the systems are nonlinear and the noise is non-Gaussian, a particle filter, which is more complex, will usually perform better than a Kalman filter. A particle filter is used to fuse the step length and heading information from inertial sensors to provide an indoor localization system [12].

Performance analysis

The performance and efficiency of assisted living technologies can be evaluated using many metrics. The goal for this section is to compare recent signal processing advances with respect to accuracy, power consumption, and computational complexity of the sensors and algorithms.

Accuracy

The accuracy of IMU-based signal processing techniques is a key aspect for assisted living applications. The cost of faults can be significant, especially when the techniques are used to assist the elderly, individuals who are vulnerable, and those that are in need of care.

Signal processing techniques are proposed to reliably detect the human postural transition and ADLs, recognize gestures, and track the users' sleeping patterns and diet. FFT was used to extract information from IMU sensor data to recognize and distinguish falling, sitting, and walking activities [2]. Using FFT on data from a wrist-worn sensor with a 10-Hz sampling rate was unable to accurately discern

between falling and sitting down. A method of physical activity monitoring to detect activities such as sitting, standing, and lying has sensitivities and specificities of 90.2% and 93.4% for sitting, 92.2% and 92.1% for standing+walking, and, 98.4% and 99.7% for lying with a sternum-mounted sensor sampling at 40 Hz [22]. Overall, the detection errors were 3.9% for standing + walking, 4.1% for sitting, and 0.3% for lying. Finally, the overall symmetric mean average errors were 12% for standing + walking, 8.2% for sitting, and 1.3% for lying. A model to fuse data from hand movements and audio sampled at 2 kHz from a wood workshop to recognize workers' activities is presented [4]. Different methods were used to improve the classification and it is shown that in isolation, the accuracy of activity detection is 98%, 87%, and 95% for the user-dependent, user-independent, and user-adapted detection, respectively. A data set was created from a wrist-worn IMU sensor, and a method to detect sleep and wake states was proposed [5]. The algorithm was compared with traditional algorithms using total sleep time (TST) and sleep efficiency (SE) as the comparison parameter. The proposed method achieves an overall median accuracy of 79% for detecting sleep and wake intervals.

Several accurate human localization techniques are proposed, leveraging IMU-based wearable solutions. An adaptive

Classification can be used to detect falls and prefalls, to distinguish between healthy and unhealthy motor function, and to detect ADLs.

step-length estimation algorithm for the pedestrian navigation system (PNS) has an accuracy of 95% in the worst case [10]. Two PDF algorithms including Weiberg and zero velocity updates (ZVU) for stride-length estimation are tested at three different walking speeds (slow, normal, and fast) [13]. The authors show that the Weiberg algorithm performs better than ZVU at all walking speeds. An IMU-based self-contained pedestrian tracking method is proposed that uses ZVU and the step length estimation as a control variable to correct the acceleration drift. This method improves the tracking accuracy by decreasing the final position error for different scenarios such as short and long distance walking and reduces the final position error up to 66% when compared to other algorithms [9]. A method using IMU sensors attached on soldiers' boots is compared to the implementation of ZVU with and without magnetic heading information [11]. Using ZVUs along with magnetic heading information can be accurate for the soldiers when they are operating an attack in a building. This method stayed within 2 m of the true path over a path of more than 90 m. A method using phone inertial sensors with a default rate of 50 Hz is proposed, i.e., infrastructure-free, phone position independent, user adaptive, and easy to deploy [12]. The step-length estimation is used as a personal model for a user and this model is updated each time the system collects data. The users are put into different groups based on their personal models. The step-detection error for the cellphone in hand and in pocket cases for different algorithms were compared and error rates from 1.6% to 24.5% (in hand) and 1.1% to 25.6% (in pocket) were reported. An investigation using IMU sensors sampling at 1 kHz detects preimpact falls using trunk vertical velocity [15]. Falls can be distinguished from normal ADLs, with 100% accuracy and with an average detection speed of 323 milliseconds prior to trunk impact and 140 milliseconds prior to knee impact, in their subject group. Sensor locations

and sampling can impact accuracy. This information for the reviewed papers is given in Table 3.

Power consumption/computational complexity

Power-aware IMU-based sensors can potentially reduce the size of batteries, enhance sensor lifetime, and enable long-term monitoring. Signal processing algorithms with lower computational complexity make it possible to analyze the collected data more quickly and provide faster feedback. Exploring the lowest sampling rate for activity detection using FFT features can save power [2]. The results show that 10 Hz is able to distinguish between walking and sitting, but does not do well distinguishing falling with a wrist-worn accelerometer. A granular decision-making module is proposed to reduce the power consumption significantly for a wearable IMU-based movement monitoring system [30]. Movements that are of no interest are removed as early as possible from the signal processing chain, deactivating all of the remaining modules in the signal processing chain as well as the microprocessor. The bit resolution, the key factor that affects the system power consumption, is only increased as the target movement is detected. Similarly, a low-power programmable signal processing architecture for dynamic and periodic activity monitoring applications saves power by performing signal processing in a tiered fashion by removing irrelevant data as soon as possible [25]. Using wavelet decomposition 75.7% power savings are achieved while maintaining 96.9% sensitivity detection of target actions.

Conclusions

The growth of wearable IMU sensors has created many opportunities to improve people's health and lives through the development of innovative applications. This article has provided an overview of signal processing techniques and their performance for assisted living applications. Many of the applications reviewed are the subject of ongoing research and there many opportunities for improvement still remain. A variety of signal processing techniques are being used, but for an actual working system, the accuracy and power concerns must be taken into consideration on a case by case basis noting that applications and related hardware have different needs. Applications using wearable IMU sensors will continue to improve and provide valuable information to help people to have healthier lifestyles with greater independence.

Authors

Terrell R. Bennett (tbennett@utdallas.edu) received his S.B. degree in electrical engineering and computer science from the Massachusetts Institute of Technology in 2002 and his M.S. degree in electrical engineering from the University of Texas at Dallas in 2007. His research is focused on signal processing and algorithm design for synchronization of cyber-physical systems and the Internet of Things as well as working with data from wearable sensors to detect activities, estimate motion, and improve the quality of the sensor data.

Jian Wu (jian.wu@tamu.edu) received his M.S. degree in communication and information systems in 2012 from

Table 3. Sensor sampling rate and location.

Sensor Sampling Rates	Sensor Locations
100 Hz [4]–[6], [9]–[11], [13], [17], [20], [23]	Wrist/Hand [2], [4]–[7], [12], [17], [23], [24], [26], [29]
50 Hz [7], [12], [19], [24], [29]	Hip/Waist [14], [19], [24], [25], [28]
40 Hz [3], [8], [22]	Thigh [14], [20], [21], [23], [26]
Below 10 Hz [2], 25 Hz [25], 32Hz [21]	Sternum/Trunk [3], [7], [8], [15], [16], [18], [21], [22], [24], [27]
47 Hz [14]	Lower Leg/Calf [20], [23]
57 Hz [28]	Ankle/Foot [7], [9]–[11], [13], [21], [25], [26]
64 Hz [26]	Upper Arm [4], [6], [17], [24], [29]
Above 128 Hz [18], 250 Hz [27], 1 kHz [15]	Other Ear [24], pocket [12], knees [25]

Huazhong University of Science and Technology, Wuhan, China. He is currently working toward his Ph.D. degree in computer engineering at Texas A&M University. His research interests include signal processing algorithm development for inertial measurement unit-based movement monitoring and activity recognition.

Nasser Kehtarnavaz (kehtar@utdallas.edu) received his Ph.D. degree in electrical and computer engineering from Rice University, Houston, Texas, in 1987. He is a professor of electrical engineering and director of the Signal and Image Processing Laboratory at the University of Texas at Dallas. His current research interests include signal and image processing, real-time implementation on embedded processors, biomedical image analysis, and pattern recognition. He has authored or coauthored nine books and more than 300 journal papers, conference papers, patents, industry manuals, and editorials in these areas. He is currently the editor-in-chief of *Journal of Real-Time Image Processing*. He is a Fellow of the IEEE and the SPIE, and he is a licensed professional engineer.

Roozbeh Jafari (rjafari@tamu.edu) received his Ph.D. degree in computer science from the University of California, Los Angeles, and completed a postdoctoral fellowship at the University of California, Berkeley. He is an associate professor in biomedical engineering, computer science and engineering, and electrical and computer engineering at Texas A&M University. His research interest lies in the area of wearable computer design and signal processing. He is the recipient of the National Science Foundation CAREER Award in 2012, the IEEE Real-Time and Embedded Technology and Applications Symposium (RTAS) Best Paper Award in 2011, and the Andrew P. Sage Best Transactions Paper Award from the IEEE Systems, Man, and Cybernetics Society in 2014. He is an associate editor of *IEEE Sensors Journal*, *IEEE Internet of Things Journal*, and *IEEE Journal of Biomedical and Health Informatics*. He is an associate editor of *IEEE Sensors Journal*, *IEEE Internet of Things Journal*, *IEEE Journal of Biomedical and Health Informatics*, and *IEEE Transactions on Biomedical Circuits and Systems*.

References

- [1] "Cisco visual networking index: Global mobile data traffic forecast update, 2014–2019," Cisco, White Paper, Feb. 2015.
- [2] S. D. Bersch, C. M. Chislett, D. Azzi, R. Khusainov, and J. S. Briggs, "Activity detection using frequency analysis and off-the-shelf devices: Fall detection from accelerometer data," in *Proc. 5th IEEE Int. Conf. Pervasive Computing Technologies for Healthcare (PervasiveHealth)*, IEEE, 2011, pp. 362–365.
- [3] R. Ganea, A. Paraschiv-Ionescu, C. Büla, S. Roachat, and K. Aminian, "Multi-parametric evaluation of sit-to-stand and stand-to-sit transitions in elderly people," *Med. Eng. Phys.*, vol. 33, no. 9, pp. 1086–1093, 2011.
- [4] J. A. Ward, P. Lukowicz, G. Tröster, and T. E. Starner, "Activity recognition of assembly tasks using body-worn microphones and accelerometers," *IEEE Trans. Pattern Anal. Mach. Intell.*, vol. 28, no. 10, pp. 1553–1567, 2006.
- [5] M. Borazio, E. Berlin, N. Kucukyildiz, P. Scholl, and K. Van Laerhoven, "Towards benchmarked sleep detection with wrist-worn sensing units," in *Proc. IEEE Int. Conf. Healthcare Informatics (ICHI)*, 2014, pp. 125–134.
- [6] O. Amft and G. Tröster, "Recognition of dietary activity events using on-body sensors," *Artif. Intell. Med.*, vol. 42, no. 2, pp. 121–136, 2008.
- [7] C. Zhu, Q. Cheng, and W. Sheng, "Human intention recognition in smart assisted living systems using a hierarchical hidden Markov model," in *Proc. IEEE Int. Conf. Automation Science and Engineering (CASE)*, 2008, pp. 253–258.
- [8] B. Najafi, K. Aminian, F. Loew, Y. Blanc, and P. A. Robert, "Measurement of stand-sit and sit-stand transitions using a miniature gyroscope and its application in fall risk evaluation in the elderly," *IEEE Trans. Biomed. Eng.*, vol. 49, no. 8, pp. 843–851, 2002.
- [9] X. Meng, Z.-Q. Zhang, J.-K. Wu, W.-C. Wong, and H. Yu, "Self-contained pedestrian tracking during normal walking using an inertial/magnetic sensor module," *IEEE Trans. Biomed. Eng.*, vol. 61, no. 3, pp. 892–899, 2014.
- [10] S. Shin, C. Park, J. Kim, H. Hong, and J. Lee, "Adaptive step length estimation algorithm using low-cost MEMS inertial sensors," in *Proc. IEEE Sensors Applications Symp.*, 2007, pp. 1–5.
- [11] J. Bird and D. Arden, "Indoor navigation with foot-mounted strapdown inertial navigation and magnetic sensors [emerging opportunities for localization and tracking]," *IEEE Wireless Commun.*, vol. 18, no. 2, pp. 28–35, 2011.
- [12] F. Li, C. Zhao, G. Ding, J. Gong, C. Liu, and F. Zhao, "A reliable and accurate indoor localization method using phone inertial sensors," in *Proc. ACM Conf. Ubiquitous Computing*, 2012, pp. 421–430.
- [13] A. R. Jimenez, F. Seco, C. Prieto, and J. Guevara, "A comparison of pedestrian dead-reckoning algorithms using a low-cost MEMS IMU," in *Proc. IEEE Int. Symp. Intelligent Signal Processing*, 2009, pp. 37–42.
- [14] M. Nyan, F. E. Tay, and E. Murugasu, "A wearable system for pre-impact fall detection," *J. Biomech.*, vol. 41, no. 16, pp. 3475–3481, 2008.
- [15] A. Bourke, K. O'Donovan, and G. O'Laughlin, "The identification of vertical velocity profiles using an inertial sensor to investigate pre-impact detection of falls," *Med. Eng. Phys.*, vol. 30, no. 7, pp. 937–946, 2008.
- [16] R. Jafari, W. Li, R. Bajcsy, S. Glaser, and S. Sastry, "Physical activity monitoring for assisted living at home," in *Proc. 4th Int. Workshop on Wearable and Implantable Body Sensor Networks*, 2007, pp. 213–219.
- [17] H. Junker, O. Amft, P. Lukowicz, and G. Tröster, "Gesture spotting with body-worn inertial sensors to detect user activities," *Pattern Recognit.*, vol. 41, no. 6, pp. 2010–2024, 2008.
- [18] W. Janssen, D. G. Kulcu, H. Horemans, H. J. Stam, and J. Bussmann, "Sensitivity of accelerometry to assess balance control during sit-to-stand movement," *IEEE Trans. Neural Syst. Rehabil. Eng.*, vol. 16, no. 5, pp. 479–484, 2008.
- [19] G. R. H. Regterschot, M. Folkersma, W. Zhang, H. Baldus, M. Stevens, and W. Zijlstra, "Sensitivity of sensor-based sit-to-stand peak power to the effects of training leg strength, leg power and balance in older adults," *Gait Posture*, vol. 39, no. 1, pp. 303–307, 2014.
- [20] G. Cooper, I. Sheret, L. McMillian, K. Silverdis, N. Sha, D. Hodgins, L. Kenney, and D. Howard, "Inertial sensor-based knee flexion/extension angle estimation," *J. Biomech.*, vol. 42, no. 16, pp. 2678–2685, 2009.
- [21] M. Benedetti, A. Di Gioia, L. Conti, L. Berti, D. Esposti, G. Tarrini, N. Melchionda, and S. Giannini, "Physical activity monitoring in obese people in the real life environment," *J. Neuroeng. Rehabil.*, vol. 6, no. 1, 2009. [Online]. Available: <http://link.springer.com/article/10.1186%2F1743-0003-6-47>
- [22] B. Najafi, K. Aminian, A. Paraschiv-Ionescu, F. Loew, C. J. Bula, and P. Robert, "Ambulatory system for human motion analysis using a kinematic sensor: Monitoring of daily physical activity in the elderly," *IEEE Trans. Biomed. Eng.*, vol. 50, no. 6, pp. 711–723, 2003.
- [23] S. Patel, K. Lorincz, R. Hughes, N. Huggins, J. Growdon, D. Standaert, M. Akay, J. Dy et al., "Monitoring motor fluctuations in patients with Parkinson's disease using wearable sensors," *IEEE Trans. Inf. Technol. Biomed.*, vol. 13, no. 6, pp. 864–873, 2009.
- [24] L. Atallah, B. Lo, R. King, and G.-Z. Yang, "Sensor positioning for activity recognition using wearable accelerometers," *IEEE Trans. Biomed. Circuits Syst.*, vol. 5, no. 4, pp. 320–329, 2011.
- [25] M.-M. Bidmeshki and R. Jafari, "Low power programmable architecture for periodic activity monitoring," in *Proc. ACM/IEEE 4th Int. Conf. Cyber-Physical Systems*, 2013, pp. 81–88.
- [26] S. J. Preece, J. Y. Goulermas, L. P. Kenney, and D. Howard, "A comparison of feature extraction methods for the classification of dynamic activities from accelerometer data," *IEEE Trans. Biomed. Eng.*, vol. 56, no. 3, pp. 871–879, 2009.
- [27] G. Panahandeh, N. Mohammadiha, A. Leijon, and P. Handel, "Continuous hidden Markov model for pedestrian activity classification and gait analysis," *IEEE Trans. Instrum. Meas.*, vol. 62, no. 5, pp. 1073–1083, 2013.
- [28] G. Wu and S. Xue, "Portable preimpact fall detector with inertial sensors," *IEEE Trans. Neural Syst. Rehabil. Eng.*, vol. 16, no. 2, pp. 178–183, 2008.
- [29] J. Lim, T. Lee, X. Pang, and S. Sane'i, "Investigation of wireless rehabilitative assessment data using singular spectrum analysis," in *Proc. 13th IEEE Int. Conf. Control Automation Robotics and Vision (ICARCV)*, 2014, pp. 669–674.
- [30] H. Ghasemzadeh and R. Jafari, "Ultra low power granular decision making using cross correlation: Optimizing bit resolution for template matching," in *Proc. 17th IEEE Real-Time and Embedded Technology and Applications Symp. (RTAS)*, 2011, pp. 137–146.

Fatih Erden, Senem Velipasalar,
Ali Ziya Alkar, and A. Enis Cetin

Sensors in Assisted Living

A survey of signal and image processing methods

Our society will face a notable demographic shift in the near future. According to a United Nations report, the ratio of the elderly population (aged 60 years or older) to the overall population increased from 9.2% in 1990 to 11.7% in 2013 and is expected to reach 21.1% by 2050 [1]. According to the same report, 40% of older people live independently in their own homes. This ratio is about 75% in the

developed countries. These facts will result in many societal challenges as well as changes in the health-care system,

such as an increase in diseases and health-care costs, a shortage of caregivers, and a rise in the number of individuals unable to live independently [2].

Thus, it is imperative to develop ambient intelligence-based assisted living (AL) tools that help elderly people live independently in their homes. The recent developments in sensor technology and decreasing sensor costs have made the deployment of various sensors in various combinations viable, including static setups as well as wearable sensors. This article presents a survey that concentrates on the signal processing methods employed with different types of sensors. The types of sensors covered are pyro-electric infrared (PIR) and vibration sensors, accelerometers, cameras, depth sensors, and microphones.

Introduction

AL systems basically aim to provide more safety and autonomy and improve wellness and health conditions of older people while allowing them to live independently, as well as relieving the workload of caregivers and health providers.

A fundamental component of the AL systems is the use of different types of sensors to monitor the activities of the residents. These sensors can be broadly categorized into two groups: 1) static sensors at fixed locations, e.g., PIR sensors, vibration sensors, pressure sensors, cameras, and microphones, and 2) mobile and wearable sensors, e.g., accelerometers, thermal sensors, and pulse oximeters. There are several choices of specific sensors or sensor combinations—currently there are many AL

IMAGE LICENSED BY INGRAM PUBLISHING
WOMAN—©ISTOCKPHOTO.COM/SILVIANSEN



Digital Object Identifier 10.1109/MSP.2015.2489978
Date of publication: 7 March 2016

systems implementing various tasks, such as fall detection [3]–[5], mobile emergency response [6], video surveillance [7], automation [8], monitoring activities of daily living [9], and respiratory monitoring [10]. Falls among the elderly are a major concern for both families and medical professionals. Falls are considered to be the eighth leading cause of death in the United States [11] and fall injuries can result in serious complications [12], [13]. Autonomous fall detection systems for AL can reduce the severity of falls by informing other people to deliver help and reduce the amount of time people remain on the floor. These systems can increase safety and independence of the elderly.

To truly assist elderly people, an AL system should satisfy some basic requirements [14]:

- *Low-cost*: Almost 90% of the older adults prefer to stay in the comfort of their own homes. Therefore, an AL system should be affordable by the average elderly person or couple.
- *High accuracy*: Since the aim is to enhance the wellness and the life quality of elderly people, a tolerable error rate should be achieved.
- *User acceptance*: The AL systems should be compatible with the ordinary activities of people so that they can interact with the system easily, i.e., by speaking naturally, using simple gestures, etc. Also, users do not find wearable systems or those that need to be carried practical. Thus, contact-free and remotely controllable systems are desired.
- *Privacy*: The AL systems should be non-visual and share minimal private data with the monitoring call center regarding the daily living activities of individuals.

Despite the presence of surveys [2], [15], [16] and proliferation of different types of sensors in the AL field, a comprehensive study concentrating on the utilized sensor signal processing methods is not available. This article aims to provide an overview of most recent research trends in the AL field by focusing on PIR sensors, vibration sensors, accelerometers, cameras, depth sensors, and microphones and the related signal processing methods, which together meet most of the aforementioned requirements. Ambient information monitoring sensors are used in home safety [17]–[19], home automation [8], [20]–[23], activity monitoring [14], [24]–[27], fall detection [28]–[34], localization and tracking [35]–[37], and monitoring the health status indicators of elderly and chronically diseased people outside hospitals [38]–[44].

Human activity recognition using various sensor modalities

The most important signal processing problem in AL systems is the recognition of human activity from signals generated by various sensors including vibration sensors, PIR sensors, and wearable accelerometers. Obviously, each sensor generates different kinds of time-series data. Therefore, signal-processing

and machine-learning algorithms tailored for each specific sensor need to be developed.

PIR sensor signal processing

PIR sensors are low-cost devices designed to detect the presence of moving bodies from stationary objects. They are easy to use and can even work in the dark, unlike ordinary vision-based systems, because they image infrared light. A PIR sensor functions by measuring the difference in infrared radiation between the two pyro-electric elements inside of it. This difference occurs due to the motion of bodies in the viewing range of the sensor. When the two pyro-electric elements are subject to the same infrared radiation level, they generate a zero-output signal by canceling each other out. Therefore, the analog circuitry of a PIR sensor can reject false detections very accurately.

PIR sensors are widely used in the context of AL. In [38], eight PIR sensors are installed in the ceiling of hospital rooms to assess the daily activities of elderly patients. The activities are classified in 24 different categories by checking the number of sensors activated and recording the time interval for which they remain activated. Barger et al. [24] introduce a system of distributed PIR sensors to monitor a person's in-home activity. The activity level of the person is defined as the number of sensor firings in a room per time spent in the room. Mixture models are applied to the sensor data in the training set to develop a probabilistic

model of event types. These models are then used to identify the type of event associated with each observation in the test set. In [27], a PIR sensor installed in a corner of a living room is employed to detect the abnormalities in daily activities of an elderly person. The PIR sensor sends the value “1” to the controller if there are activities from the person and the value “0” otherwise. Hidden Markov models (MMs), forward algorithms, and Viterbi algorithms are used to analyze the obtained data sequence. If a certain deviation from the constituted models is detected, the caregiver receives an alert. In [26] a wireless sensor network including PIR, chair, bed, toilet, and couch sensors is suggested to determine the wellness of the elderly. Time-stamped sensor activities are recorded and fed to predefined wellness functions.

In [25], PIR and contact sensors are used to assess neurologic function in cognitively impaired elders. The contact sensor is responsible for tracking the presence or the absence of the resident and recording the time spent in the home and out of the home. PIR sensors are utilized for the estimation of walking speed and daily activity. The walking speed of the resident is estimated from the time of PIR sensor firings that are placed sequentially along a hall. The amount of daily activity is decided based on the number of sensor firings per minute when the subject is in the home.

The most important signal processing problem in AL systems is the recognition of human activity from signals generated by various sensors including vibration sensors, PIR sensors, and wearable accelerometers.

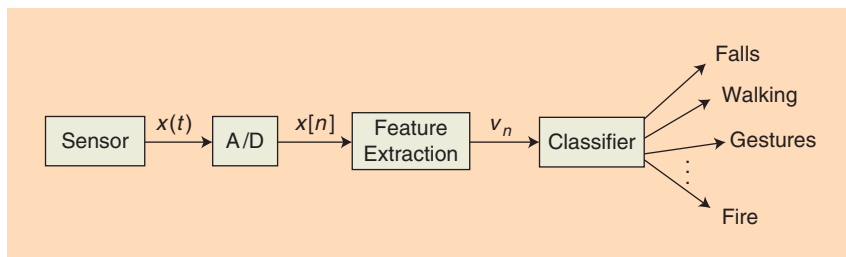


FIGURE 1. A block diagram of an intelligent PIR sensor signal processing system.

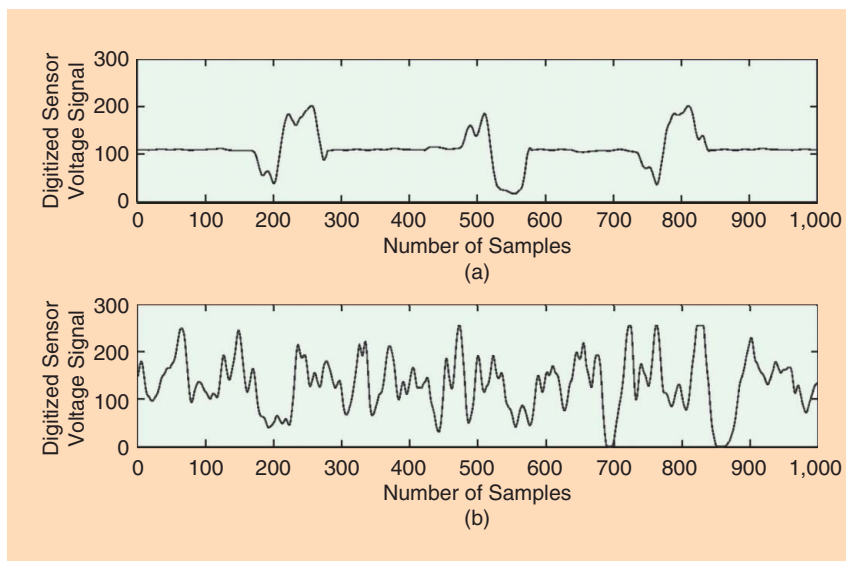


FIGURE 2. A PIR sensor raw output signal recorded at a distance of 5 m (a) for a person walking and (b) for a flame of an uncontrolled fire.

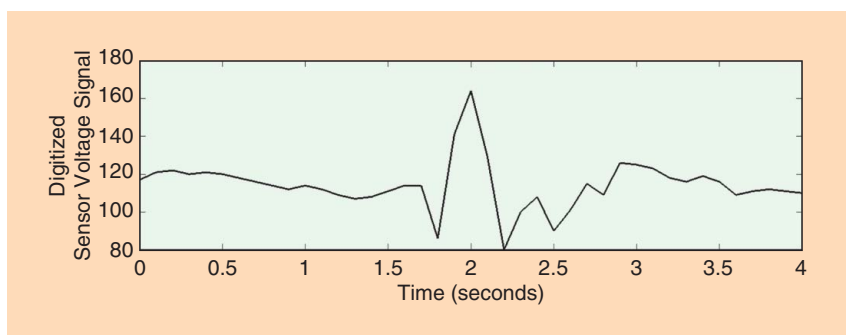


FIGURE 3. A time-domain PIR sensor signal record due to a person falling.

In [35], a system to actively assist in the resident's life such as housework, rest, sleep, etc. is described. The system is formed by an array of PIR sensors and locates a resident with a reasonable accuracy by combining the overlapping detection areas of adjacent sensors. In [17], an intruder detection system based on PIR sensors is developed. Mrazovac et al. [8] use a microphone array and a three-dimensional (3-D) camera in addition to PIR sensors for home automation, i.e., to detect the presence of and localize the users for smart audio/video playback control.

The aforementioned studies all use the binary outputs produced by the analog PIR motion detector circuits. However, it is possible to capture a continuous-time analog signal corresponding to the amplitude of the voltage signal of the PIR sensor that represents the transient behavior of the sensor circuit. By processing these analog signals, more complicated tasks, as opposed to just the on/off type operations, can be accomplished. The block diagram of an intelligent PIR sensor signal processing system is shown in Figure 1. The original output of the sensor signal $x(t)$ is first digitized using an analog-to-digital converter. Feature vectors v_n are then extracted from the digitized signal $x[n]$. It is possible to extract a feature vector for each signal sample. However, it is computationally more efficient to extract a feature vector for a frame of data, as in speech processing systems. Finally, these feature vectors are fed to a classifier to detect the events of interest such as walking, falls, uncontrolled fires etc. The classifier is usually trained using past and/or simulated data.

A PIR sensor-based system for human activity detection is described in [19], [33], and [45]. The system is capable of detecting accidental falls and the flames of a fire. Instead of the binary signal produced by the comparator structure in the PIR sensor circuit, an analog output signal is captured and transferred to a digital signal processor for further processing. As shown in Figure 2(a), a walking event is almost periodic when the person walks across the viewing range of the sensor. On the other hand, a person falling produces a clearly distinct signature as shown in Figure 3, and uncontrolled flames lead to a signal with high-frequency content. Since flames of an uncontrolled fire flicker up to a frequency of 13 Hz, a sampling frequency of 50 Hz, which is well above

the Nyquist rate, is chosen. The goal is to recognize falls, uncontrolled fire events, and a person's daily activities. In practice, PIR signals are not as clearly distinguishable as the ones shown in Figures 2 and 3. For example, the person may walk toward the sensor and the periodic behavior is no longer clearly visible.

Wavelet transform is used for feature extraction from the PIR sensor signal. In the training stage, wavelet coefficients corresponding to each event class signals are computed and concatenated. Three, three-state MMs are designed to recognize the three classes. The characteristics of the

transitions between the three states of the MMs are different for each event class. The wavelet coefficient sequence corresponding to the current time window of two seconds is fed to the three MMs, and the MM producing the highest frequency determines the activity within the window. Uncontrolled flames are very accurately detected, since the sensor signal for a flickering flame exhibit high frequency activity that no person can produce by moving his or her body as shown in Figure 2(b).

It is not possible to distinguish a fall from sitting on the floor or a couch using only a single PIR sensor. In [33] and [45], multisensor systems are developed for fall detection. Sound, PIR, and vibration sensors are placed in a home. MMs are used as classifiers in these multisensor systems. They are trained for regular activities and falls of an elderly person using PIR, sound, and vibration sensor signals. Vibration and sound sensor data processing will be described in the next two sections. Decision results of MMs are fused by using a logical “and” operator to reach a final decision.

In [21], a remote control system is developed based on a PIR sensor array and a camera for home automation. The system recognizes hand gestures. The camera is responsible to detect the hands of the user. Once a hand is detected, simple hand gestures such as left-to-right, right-to-left, and clockwise and counterclockwise hand movements are recognized by the PIR sensor signal analysis to remotely interact with an electrical device. The system includes three PIR sensors, each of which is located at a corner of a triangle. Signals received from each PIR sensor are transformed into wavelet domain and then concatenated according to a predefined order. In this case, the distinctive property of the resulting wavelet features for different hand gestures is not the oscillation characteristics, but the order of the appearances of the peaks in the wavelet sequence. Therefore, the winner-take-all (WTA) hashing, which is an ordinal measure, is used for further feature extraction and classification instead of MMs. Wavelet sequences are converted to binary codes using the WTA hash method, and Jaccard distances are calculated between the trained and test binary codes. The model yielding the smallest distance is determined as the class of the current test signal. The system described in [21] produces higher recognition results than the system in [22], which uses only the binary outputs of the analog PIR sensor circuitry for the same task.

In [41], a method for the detection of breathing movement using PIR sensors is proposed. PIR sensors are placed near a person's bed. Sensor signals, corresponding to body movements due to breathing activity, are recorded. Short-time Fourier analysis of the PIR sensors' signals is carried out. The recorded signals are divided into windows, and the existence of sleep apnea within each window is detected by analyzing the spectrum. If there are no peaks in a window, that is an indicator of a sleep apnea. It may also be possible to measure the respiratory rate of a person who is sleeping using PIR sensor signals.

Vibration and acoustic sensor signal processing

Accelerometers designed to measure vibration are either based on the piezoelectric effect or electromechanical energy conversion. They are transducers for measuring the dynamic acceleration of a physical device. All of the commercially available wearable fall detection systems are based on accelerometers. They convert vibrations into electrical signals depending on the intensity of the vibration waves in the axis of the vibration sensor. Vibration sensors can be categorized into two groups based on the number of their axes: one-axis and three-axes sensor types.

As mentioned previously, vibration sensors can be wearable or they can be installed on intelligent homes with the aim of sensing the vibrations on the floor. In this section, we first review the stationary systems.

Regular daily activities, such as walking, running, sitting on a chair, or objects falling on the floor cause measurable vibrations on the floor. Human falls also cause vibrations, which are transmitted through the floor. Therefore, a vibration sensor installed in each room of a house or an apartment can pick up the vibrations on the floor, and it may be possible to detect a human's fall by continuously analyzing the sensor signal. In Figure 4, a ten-second-long vibration sensor signal generated by a person walking is shown. It is clearly different from the human fall signal shown in Figure 5. This signal was recorded on a concrete floor and the fall took place 3 m away from the sensor. Human falls usually take about two seconds and create strong vibration signals because a typical human is more than 100 lb heavier than most of the objects that can

fall on the floor in a house. Machine-learning techniques can be used to classify the vibration signals.

In [33], a multisensor AL system consisting of PIR sensors and vibration sensors is developed. Vibration sensor signals are sampled with a rate of 500 Hz. As shown in Figure 5, there is very little signal energy above 125 Hz on a concrete floor. Since vibrations and acoustic and sound waves are related to each other, it is natural to use the feature extraction techniques utilized in speech processing to analyze the vibration signals. Various wavelet and frequency domain feature extraction schemes are employed every two seconds to extract feature vectors from the signals. Wavelet and different frequency analysis methods are studied and compared to each other. Discrete Fourier transform (DFT) subband energy values, MFCCs, discrete wavelet transform (DWT), and dual-tree complex wavelet transform (DT-CWT)-based feature extraction methods are studied for feature extraction [33]. These feature vectors are classified using a support vector machine (SVM) for fall detection. They can also be used to estimate a person's daily activity and can provide feedback to him or her.

In [33], the data set contains 2,048-sample-long signals corresponding to 100 falls, 1,419 walking/running incidents, 30 sitting cases on the floor, 30 slammed door cases, and 65 cases of

Even though several user-activated commercial devices are available for fall detection, they have limited benefits, especially in situations where the user loses consciousness.

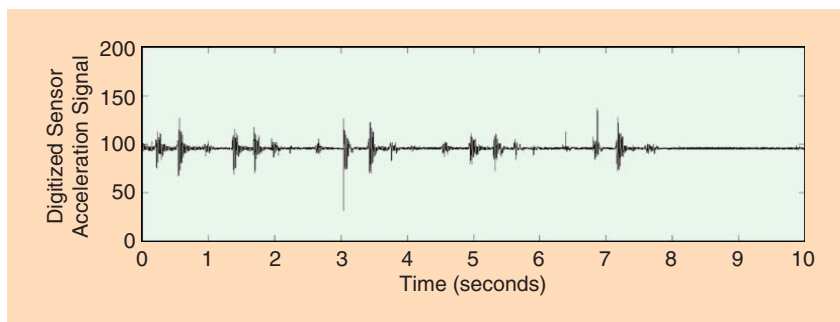


FIGURE 4. A ten-second-long vibration sensor signal generated by a person walking.

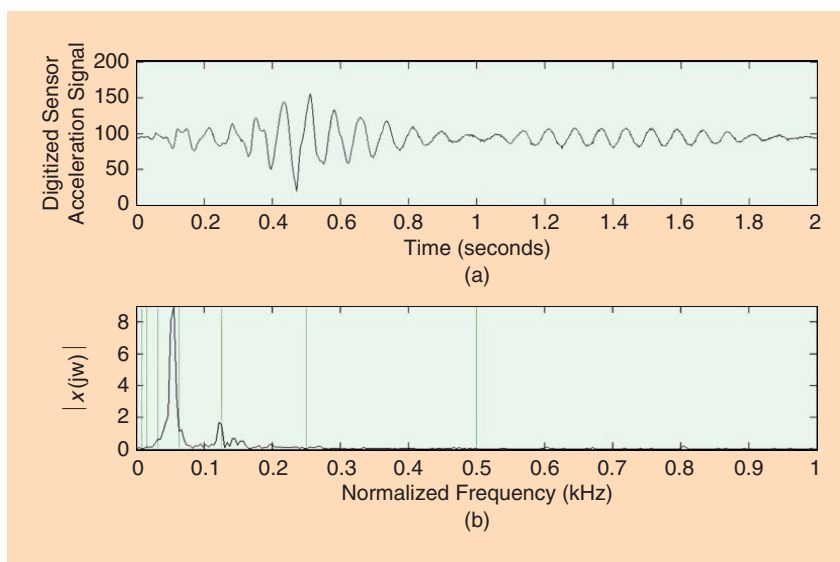


FIGURE 5. (a) A two-second-long human fall record. (b) The Fourier transform magnitude. The Fourier transform domain is divided into eight nonuniform bands, and subband energy values are used as a feature set representing the time-domain vibration signal together with wavelet coefficients and Mel-frequency cepstral coefficients (MFCCs).

fallen items. Eight MFCCs, eight DFT coefficients, eight wavelet coefficients, and eight CWT coefficients are extracted for each record. About 40% of falling and walking/running records are used for training the SVM classifier. About one-third of sitting, slammed door, and fallen object records are also used for training. Remaining records are used as the test data set. The data set is available to the public. Best recognition results are obtained when complex wavelet transform based features and modified mel-frequency cepstrum coefficients are used. When combined with PIR sensors the multisensor AL system becomes very reliable. The AL system has the capability to place a phone call to a call center whenever a fall is detected.

In [46], acoustic sensors are used instead of vibration sensors for fall detection. The acoustic sensor is placed like a stethoscope on the floor. In a practical system, it is desirable to

have a single vibration sensor unit installed on each floor of a house; however, there are some challenges. This unit has to be robust against variations on the type of the floor and the weight of the person as well as the distance between the sensor and the fall. The distance problem can be solved by installing two or more sensors, but this increases the cost. To cover all possibilities, extensive studies have to be implemented. In addition, the overall multisensor system described in [62] turns out to be a little bit too costly for a typical house and the network infrastructure. We hope that the Internet of Things (IoT) will be widespread in the near future, which will make the entire system feasible.

AL systems may provide safety and autonomy for elderly people while allowing them to live independently, as well as relieve the workload of caregivers and health providers.

Wearable accelerometer sensor signal processing

Even though several user-activated commercial devices are available for fall detection, they have limited benefits, especially

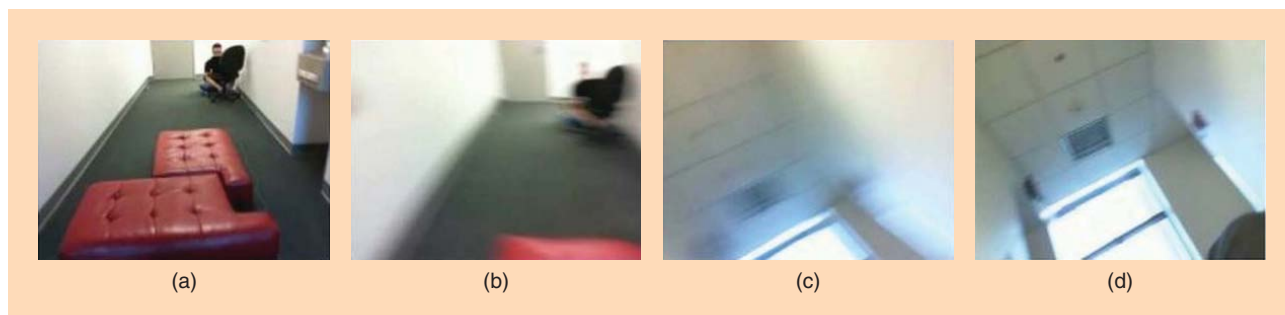


FIGURE 6. Example frames captured during a fall from a standing position.

in situations where the user loses consciousness. As previously mentioned, all commercially available autonomous fall detection systems are based on wearable accelerometers. Such systems can also provide information about an individual's functional ability and lifestyle. Wearable devices also use tilt sensors to automatically detect a fall event. One drawback is that the individual has to wear the device continuously day and night. On the other hand, monitoring is not limited to confined areas, where the static sensors are installed, and can be extended wherever the subject may travel.

Dai et al. [47] developed a fall detection system using the accelerometers of a mobile phone. The app is capable of detecting falls when the phone is placed in a shirt pocket, on a belt, or in a pants pocket. When the average magnitude of the 3-D acceleration vector and the average value of the vertical acceleration in a short-time window exceed predefined thresholds a fall is reported. In [48] and [49], adaptive thresholds are developed. In [48], the threshold is determined using the body mass index of the user. Currently, mobile phone apps are not widely used by elderly people. In addition, methods based on using thresholds cannot be as reliable as systems that use machine-learning techniques, since threshold-based methods are more prone to producing frequent false alarms.

In [50], artificial neural networks (ANNs) are used for human-activity recognition. A single triaxial accelerometer is attached to the subject's chest. Acceleration signals are modeled using autoregressive (AR) modeling. AR model coefficients along with the signal-magnitude area and the tilt angle form an augmented feature vector. The resulting feature vector is further processed by the linear-discriminant analysis and ANNs to recognize various human activities.

Camera sensor-based methods

In recent years, one of the key aspects of elderly care has been intensive activity monitoring, and it is very important that any such activity monitoring be also autonomous. An ideal autonomous activity monitoring system should be able to classify activities into critical events, such as falling, and noncritical events, such as sitting and lying down. While fast and precise detection of falls is critical in providing immediate medical attention, other noncritical activities like walking, sitting, and lying down can provide valuable information in the study of chronic diseases and functional ability monitoring [51], [52] and

for early diagnosis of potential health problems. Furthermore, the system should be able to smartly expend its resources for providing quick and accurate real-time response to critical events versus performing computationally intensive operations for noncritical events.

There has been a lot of work on activity monitoring by vision-based sensors [28], [53]–[61]. However, in all of these methods, cameras are static at fixed locations watching the subjects, thus introducing the issue of confining the monitoring environment to the region where the cameras are installed. The images acquired from the cameras are usually offloaded to a dedicated central processor. Also, 3-D model-based techniques require initializations and are not always robust. Another major practical issue is that the subjects who are being monitored often raise privacy concerns [54], as they feel they are being watched all the time.

In contrast to static camera-based methods, Ozcan et al. [5] take a different approach, introducing an autonomous fall detection and activity classification system by using wearable embedded smart cameras. Since the camera is worn by the subject, the monitoring is not limited to confined areas and extends to wherever the subject may travel, as opposed to static sensors installed in certain rooms. In addition, since the images captured will not be of the subject, as opposed to static cameras watching the subject, privacy issues for the subjects is alleviated. Moreover, captured images are processed locally on the device, and they are not saved or transmitted anywhere. Only when a fall occurs can an appropriate message be wirelessly sent to emergency response personnel, optionally including an image from the subject's camera. This image of the surroundings can be helpful in locating the subject. Also, the captured images carry an abundance of information about the surroundings that other types of sensors cannot provide. A recent study about privacy behaviors of lifeloggers using wearable cameras discusses privacy of bystanders and ways to mitigate concerns [62]. It is also expected that wearable cameras will be employed more to understand lifestyle behaviors for health purposes [63].

The proposed approach [5] is based on the oriented image gradients. Different from the original histograms of oriented gradients (HOG), separate histograms for gradient strength and gradient orientations are constructed, and the correlation between them is found. The gradient orientation range is between 0–180°, and it is equally divided into nine bins. The



FIGURE 7. An Android smartphone attached to the waist.

gradient strength histogram contains 18 bins. Moreover, instead of using a constant number of cells in a block, the cells that do not contain significant edge information are adaptively and autonomously determined and excluded from the descriptor in this proposed modified HOG algorithm. In [5], it is shown that the proposed method is more robust compared to using fixed number of cells in detecting falls. In addition to detecting falls, the proposed algorithm provides the ability to classify events of sitting and lying down using optical flow. The method is composed of two stages. The first stage involves detection of an event. An event can be one of the following: falling, sitting, or lying down. Once an event is detected, the next stage is the classification of this event. An example set of captured frames for falling from standing up position is presented in Figure 6.

As reported in [5], the fall detection part of the algorithm was implemented on the CITRIC embedded camera platform [64], which is a small, stand-alone, battery-operated unit. It features a 624-MHz fixed-point microprocessor, 64 MB synchronous dynamic random access memory, and 16 MB NOR FLASH memory. The wireless transmission of data is performed by a Crossbow TelosB mote. The images are processed locally onboard, and then dropped, thus, they are not transferred anywhere. For the falls starting from a standing position, an average detection rate of 87.84% has been achieved with prerecorded videos. With the embedded camera implementation, the fall detection rate is 86.66%. Moreover, the correct classification rates for the events of sitting and lying down are 86.8% and 82.7%, respectively.

More recently, we have implemented the fall detection part of this algorithm on a Samsung Galaxy S4 phone with Android OS and performed experiments with ten subjects carrying this phone. The experimental setup can be seen in Figure 7. We have also implemented a method to fuse two sensor modalities: the accelerometer and camera data. The average sensitivity rates for fall detection are 65.66%, 74.33%, and 91%, when we use only accelerometer data, only camera data, and camera data together with accelerometer data, respectively.

Vibration sensors can be categorized into two groups based on the number of their axes: one-axis and three-axes sensor types.

Zhan et al. [65] propose an activity recognition method that uses a front-facing camera embedded in a user's eyeglasses. Optical flow is used as the feature extraction method. Three classification approaches—k-nearest neighbor, logitBoost, and SVM—are employed. Further smoothing with hidden MMs provide an accuracy of 68.5–82.1% for a four-class classification problem, including drinking, walking, going upstairs, and going downstairs, on recorded videos.

Moghimi et al. [66] use an RGB-D camera mounted on a helmet to detect the users' activities. They use compact and global image descriptors, including GIST, and a skin segmentation-based histogram descriptor. For activity classification, learning-based methods such as bag of scale invariant feature transform words, convolutional neural networks, and SVMs were explored.

Ishimaru et al. [67] propose an activity recognition method using eye blink frequency and head motion patterns acquired from Google glass. An infrared proximity sensor is used for blink detection. The average variance of a 3-D-accelerometer is calculated to construct the head motion model. In the classification framework, four features (variance value of accelerometer, mean value of blink frequency, and

the x-center and y-center of mass value of the blink frequency histogram) have been used to classify five different activities (watching, reading, solving, sawing, and talking) on eight participants with overall accuracy of 82%.

Conclusions

AL systems may provide safety and autonomy for elderly people while allowing them to live independently as well as relieve the workload of caregivers and health providers. However, to find widespread use, these systems should be robust and reliable. Current commercially available autonomous systems, which are not user activated, employ simple threshold-based algorithms for sensor data processing. As a result, they are prone to producing too many false alarms. Advanced signal processing techniques have to be developed to take full advantage of the recent developments in sensor technologies and provide robustness against variations in real-life conditions and the environment. Moreover, fusing multiple sensor modalities provides promising results with higher accuracy. Computational problems can be solved with the help of the IoT, which refers to wireless systems connecting industrial, medical, automotive, and consumer devices to the Internet. The IoT will allow objects and people to be sensed over existing Internet infrastructure. Vibration and PIR sensors, acoustic sensors and microphones, and cameras can be connected to form a network for an intelligent home designed for elderly people. The data and decision results that the sensors produce can be processed and fused over a cloud or a fog. We expect that the IoT will lead to remote health monitoring and emergency notification AL systems that will operate autonomously, without requiring user intervention.

Acknowledgement

This work has been funded in part by the National Science Foundation (NSF) under CAREER grant CNS-1206291 and NSF grant CNS-1302559.

Authors

Fatih Erden (fatih.erden@atilim.edu.tr) received his B.S. and M.S. degrees in electrical and electronics engineering with high honors from Bilkent University, Ankara, Turkey, in 2007 and 2009, respectively, and his Ph.D. degree in electrical and electronics engineering from Hacettepe University, Ankara, Turkey, in 2015. He is currently a faculty member of the Department of Electrical and Electronics Engineering at Atılım University, Ankara, Turkey. His research interests include sensor signal processing, infrared sensors, sensor fusion, multimodal surveillance systems, and pattern recognition. He received the Best Paper Award in the Fourth International Conference on Progress in Cultural Heritage Preservation organized by UNESCO and Cyprus Presidency of the European Union.

Senem Velipasalar (svelipas@syrr.edu) received her B.S. degree in electrical and electronic engineering with high honors from Bogazici University, Istanbul, Turkey, in 1999; her M.S. degree in electrical sciences and computer engineering from Brown University, Providence, Rhode Island, in 2001; and her M.A. and Ph.D. degrees in electrical engineering from Princeton University, New Jersey, in 2004 and 2007, respectively. She is currently an associate professor in the Department of Electrical Engineering and Computer Science at Syracuse University, New York. Her research has focused on mobile camera applications, wireless embedded smart cameras, and multicamera tracking and surveillance systems. She received a Faculty Early Career Development Award from the National Science Foundation in 2011. She is the recipient of the Excellence in Graduate Education Faculty Recognition Award. She is a Senior Member of the IEEE.

Ali Ziya Alkar (alkar@hacettepe.edu.tr) received his M.S. and Ph.D. degrees in electrical and computer engineering from the University of Colorado at Boulder, in 1991 and 1995, respectively. He is currently an associate professor in the Department of Electrical and Electronics Engineering at Hacettepe University, Ankara, Turkey. He has worked as a consultant at several companies and has supervised several government and internationally funded projects. His research interests include image processing, networking, and video analytics in embedded systems. His awards include the Best Thesis Award from the Technology Development Foundation of Turkey and the Ihsan Dogramaci High Success Award. He is a Member of the IEEE.

A. Enis Cetin (cetin@bilkent.edu.tr) studied electrical engineering at Middle East Technical University, Ankara, Turkey. He received his M.S. and Ph.D. degrees from the University of Pennsylvania. Currently, he is a full professor at Bilkent University, Ankara, Turkey. He was previously an assistant professor at the University of Toronto, Canada. He is the editor-in-chief of *Signal, Image, and Video Processing* (Springer), and a member of the editorial boards of *IEEE Transactions on*

Circuits and Systems for Video Technology and *IEEE Signal Processing Magazine*. He holds four U.S. patents and is a Fellow of the IEEE.

References

- [1] "World Population Ageing 2013," United Nations Department of Economic and Social Affairs, Population Division, Report ST/ESA/SER.A/348, 2013.
- [2] P. Rashidi and A. Mihailidis, "A survey on ambient-assisted living tools for older adults," *IEEE J. Biomed. Health Inform.*, vol. 17, no. 3, pp. 579–590, May 2013.
- [3] F. Ahmad, B. Jokanovic, M. G. Amin, and Y. D. Zhang, "Multi-window time-frequency signature reconstruction from undersampled continuous-wave radar measurements for fall detection," *IET Radar Sonar Navig.*, vol. 9, no. 2, pp. 173–183, Feb. 2015.
- [4] M. Popescu, Y. Li, M. Skubic, and M. Rantz, "An acoustic fall detector system that uses sound height information to reduce the false alarm rate," in *Proc. Annu. Int. Conf. IEEE Engineering in Medicine and Biology Society*, 2008, pp. 4628–4631.
- [5] K. Ozcan, A. K. Mahabalagiri, M. Casares, and S. Velipasalar, "Automatic fall detection and activity classification by a wearable embedded smart camera," *IEEE J. Emerg. Sel. Top. Circuits Syst.*, vol. 3, no. 2, pp. 125–136, 2013.
- [6] B. Silva, J. Rodrigues, T. Simoes, S. Sendra, and J. Lloret, "An ambient assisted living framework for mobile environments," in *Proc. IEEE-EMBS Int. Conf. Biomedical Health Informatics (BHI)*, 2014, pp. 448–451.
- [7] Z. Zhou, X. Chen, Y. C. Chung, Z. He, T. X. Man, and J. M. Keller, "Activity analysis, summarization, and visualization for indoor human activity monitoring," *IEEE Trans. Circuits Syst. Video Technol.*, vol. 18, no. 11, pp. 1489–1498, Nov. 2008.
- [8] B. Mrazovac, M. Z. Bjelica, I. Papp, and N. Teslic, "Smart audio/video playback control based on presence detection and user localization in home environment," in *Proc. 2nd Eastern European Regional Conf. Engineering Computer Based Systems*, 2011, pp. 44–53.
- [9] A. K. Bourke, S. Prescher, F. Koehler, V. Cionca, C. Tavares, S. Gomis, V. Garcia, and J. Nelson, "Embedded fall and activity monitoring for a wearable ambient assisted living solution for older adults," in *Proc. Annu. Int. Conf. IEEE Engineering in Medicine and Biology Society*, 2012, pp. 248–251.
- [10] M. Uenoyama, T. Matsui, K. Yamada, S. Suzuki, B. Takase, S. Suzuki, M. Ishihara, and M. Kawaki, "Non-contact respiratory monitoring system using a ceiling-attached microwave antenna," *Med. Biol. Eng. Comput.*, vol. 44, no. 9, pp. 835–840, 2006.
- [11] M. Heron, "Deaths: Leading causes for 2007," *Nat. Vital Stat. Rep.*, vol. 59, no. 8, pp. 1–95, 2011.
- [12] J. Sheller, D. Zapala, and L. Lundy, "Fall risk, vestibular schwannoma, and anticoagulation therapy," *J. Am. Acad. Audiol.*, vol. 19, no. 3, pp. 237–245, 2008.
- [13] R. C. O. Voshhaar, S. Banerjee, M. Horan, R. Baldwin, N. Pendleton, R. Proctor, N. Tarrier, Y. Woodward et al., "Predictors of incident depression after hip fracture surgery," *Am. J. Geriatr. Psychiatry*, vol. 15, no. 9, pp. 807–814, 2007.
- [14] S. Chernbumroong, S. Cang, A. Atkins, and H. Yu, "Elderly activities recognition and classification for applications in assisted living," *Expert Syst. Appl.*, vol. 40, no. 5, pp. 1662–1674, 2013.
- [15] F. Cardinaux, D. Bhowmik, C. Abhayaretne, and S. Mark, "Video based technology for ambient assisted living: A review of the literature," *J. Ambient Intell. Smart Environ.*, vol. 3, no. 3, pp. 253–269, 2011.
- [16] A. A. A. Chaaaroui, P. Climent-Perez, F. Florez-Revuelta, P. Climent-Pérez, and F. Flórez-Revuelta, "A review on vision techniques applied to human behaviour analysis for ambient-assisted living," *Expert Syst. Appl.*, vol. 39, no. 12, pp. 10873–10888, 2012.
- [17] M. Moghavvemi and L. C. S. L. C. Seng, "Pyroelectric infrared sensor for intruder detection," in *Proc. IEEE Region 10 Conf. TENCN*, 2004, vol. D, pp. 656–659.
- [18] F. Erden, E. B. Soyer, B. U. Toreyin, A. E. Çetin, and A. C. Enis, "VOC gas leak detection using pyro-electric infrared sensors," in *Proc. IEEE Int. Conf. Acoustics, Speech and Signal Processing (ICASSP)*, 2010, pp. 1682–1685.
- [19] F. Erden, B. U. Toreyin, E. B. Soyer, I. Inac, O. Gunay, K. Kose, and A. E. Cetin, "Wavelet based flickering flame detector using differential PIR sensors," *Fire Saf. J.*, vol. 53, pp. 13–18, Oct. 2012.
- [20] M. A. Sehili, D. Istrate, B. Dorizzi, and J. Boudy, "Daily sound recognition using a combination of GMM and SVM for home automation," in *Proc. European Signal Processing Conf. (EUSIPCO)*, 2012, pp. 1673–1677.
- [21] F. Erden and A. E. Cetin, "Hand gesture based remote control system using infrared sensors and a camera," *IEEE Trans. Consum. Electron.*, vol. 60, no. 4, pp. 675–680, Nov. 2014.
- [22] P. Wojtczuk, A. Armitage, T. Binnie, and T. Chamberlain, "PIR sensor array for hand motion recognition," in *Proc. SENSORDEVICES 2011: The 2nd Int. Conf. Sensor Device Technologies and Applications*, pp. 99–102.

- [23] M. Vacher, D. Istrate, F. Portet, T. Joubert, T. Chevalier, S. Smidtas, B. Meillon, B. Lecouteux et al., "The SWEET-HOME project: Audio technology in smart homes to improve well-being and reliance," in *Proc. Annu. Int. Conf. IEEE Engineering in Medicine and Biology Society*, 2011, pp. 5291–5294.
- [24] T. S. Barger, D. E. Brown, and M. Alwan, "Health-status monitoring through analysis of behavioral patterns," *IEEE Trans. Syst. Man Cybern. Part A Syst. Hum.*, vol. 35, no. 1, pp. 22–27, Jan. 2005.
- [25] T. L. Hayes, F. Abendroth, A. Adami, M. Pavel, T. A. Zitzelberger, and J. A. Kaye, "Unobtrusive assessment of activity patterns associated with mild cognitive impairment," *Alzheimers Dement.*, vol. 4, no. 6, pp. 395–405, Nov. 2008.
- [26] N. K. Suryadevara and S. C. Mukhopadhyay, "Determining wellness through an ambient assisted living environment," *IEEE Intell. Syst.*, vol. 29, no. 3, pp. 30–37, 2014.
- [27] G. Yin and D. Bruckner, "Daily activity learning from motion detector data for ambient assisted living," in *Proc. 3rd Int. Conf. Human System Interaction*, 2010, pp. 89–94.
- [28] A. N. Belbachir, S. Schraml, and A. Nowakowska, "Event-driven stereo vision for fall detection," in *Proc. IEEE Computer Society Conf. Computer Vision Pattern Recognition Workshops*, 2011, pp. 78–83.
- [29] R. Cucchiara, A. Prati, and R. Vezzani, "A multi-camera vision system for fall detection and alarm generation," *Expert Syst.*, vol. 24, no. 5, pp. 334–345, 2007.
- [30] L. Palmerini, F. Bagalà, A. Zanetti, J. Klenk, C. Becker, and A. Cappello, "A wavelet-based approach to fall detection," *Sensors*, vol. 15, no. 5, pp. 11575–11586, 2015.
- [31] M. Van Wieringen and J. Eklund, "Real-time signal processing of accelerometer data for wearable medical patient monitoring devices," in *Proc. Annu. Int. Conf. IEEE Engineering in Medicine and Biology Society*, 2008, pp. 2397–2400.
- [32] J. J. Villacorta, M. I. Jiménez, L. del Val, and A. Izquierdo, "A configurable sensor network applied to ambient assisted living," *Sensors*, vol. 11, no. 11, pp. 10724–10737, 2011.
- [33] A. Yazar, F. Keskin, B. U. Töreyn, and A. E. Çetin, "Fall detection using single-tree complex wavelet transform," *Pattern Recognit. Lett.*, vol. 34, no. 15, pp. 1945–1952, 2013.
- [34] B. U. Töreyn, Y. Dedeoglu, and A. E. Cetin, "HMM based falling person detection using both audio and video," in *Computer Vision in Human-Computer Interaction*, vol. 3766. Springer Berlin Heidelberg, 2005, pp. 211–220.
- [35] S. Lee, K. N. Ha, and K. C. Lee, "A pyroelectric infrared sensor-based indoor location-aware system for the smart home," *IEEE Trans. Consum. Electron.*, vol. 52, no. 4, pp. 1311–1317, Nov. 2006.
- [36] M. A. Stelios, A. D. Nick, M. T. Effie, K. M. Dimitris, and S. C. A. Thomopoulos, "An indoor localization platform for ambient assisted living using UWB," in *Proc. 6th Int. Conf. Advances in Mobile Computing and Multimedia*, 2008, p. 178.
- [37] A. Rajgarhia, F. Stann, and J. Heidemann, "Privacy-sensitive monitoring with a mix of IR sensors and cameras," in *Proc. Second Int. Workshop on Sensor and Actor Network Protocols and Applications*, 2004, pp. 21–29.
- [38] S. Banerjee, F. Steenkeste, P. Couturier, M. Debray, and A. Franco, "Telesurveillance of elderly patients by use of passive infra-red sensors in a 'smart' room," *J. Telem. Telecare*, vol. 9, no. 1, pp. 23–29, Feb. 2003.
- [39] T. L. T. Hayes, M. Pavel, N. Larimer, I. A. I. Tsay, J. Nutt, and A. G. Adami, "Simultaneous assessment of multiple individuals," *IEEE Pervasive Comput.*, vol. 6, no. 1, pp. 36–43, 2007.
- [40] A. Hein, M. Eichelberg, O. Nee, A. Schulz, A. Helmer, and M. Lipprandt, "A service oriented platform for health services and ambient assisted living," in *Proc. Int. Conf. Advanced Information Networking and Applications Workshops*, 2009, pp. 531–537.
- [41] V. Hers, D. Corbugy, I. Joslet, P. Hermant, J. Demarteau, B. Delhougne, G. Vandermoten, and J. P. Hermant, "New concept using passive infrared (PIR) technology for a contactless detection of breathing movement: A pilot study involving a cohort of 169 adult patients," *J. Clin. Monit. Comput.*, vol. 27, no. 5, pp. 521–529, Apr. 2013.
- [42] A. Jin, B. Yin, G. Morren, H. Duric, and R. M. Aarts, "Performance evaluation of a tri-axial accelerometry-based respiration monitoring for ambient assisted living," in *Proc. Annu. Int. Conf. IEEE Engineering in Medicine and Biology Society*, 2009, pp. 5677–5680.
- [43] S. Pasler and W.-J. Fischer, "Acoustical method for objective food intake monitoring using a wearable sensor system," in *Proc. 5th Int. Conf. Pervasive Computing Technologies for Healthcare Workshops*, 2011, pp. 266–269.
- [44] J. Sachs, M. Helbig, R. Herrmann, M. Kmec, K. Schilling, and E. Zaikov, "Remote vital sign detection for rescue, security, and medical care by ultra-wide-band pseudo-noise radar," *Ad Hoc Netw.*, vol. 13, part A, pp. 42–53, 2014.
- [45] B. U. Töreyn, E. B. Soyer, I. Onaran, and E. E. Cetin, "Falling person detection using multisensor signal processing," *EURASIP J. Adv. Signal Process.*, vol. 2008, Jan. 2008.
- [46] E. Principi, P. Olivetti, S. Squartini, R. Bonfigli, and F. Piazza, "A floor acoustic sensor for fall classification," in *Proc. 138th Audio Engineering Soc. Convention*, 2015, pp. 949–958.
- [47] J. D. J. Dai, X. B. X. Bai, Z. Y. Z. Yang, Z. S. Z. Shen, and D. X. D. Xuan, "PerFallD: A pervasive fall detection system using mobile phones," in *Proc. 8th IEEE Int. Conf. Pervasive Computing and Communications Workshops (PERCOM Workshops)*, 2010, pp. 292–297.
- [48] Y. Cao, Y. Yang, and W. H. Liu, "E-FallID: A fall detection system using android-based smartphone," in *Proc. 9th Int. Conf. Fuzzy Systems and Knowledge Discovery*, 2012, pp. 1509–1513.
- [49] G. A. Koshmak, M. Linden, and A. Loutfi, "Evaluation of the android-based fall detection system with physiological data monitoring," in *Proc. Annu. Int. Conf. IEEE Engineering in Medicine and Biology Society*, 2013, pp. 1164–1168.
- [50] A. M. Khan, Y. K. Lee, S. Y. Lee, and T. S. Kim, "A triaxial accelerometer-based physical-activity recognition via augmented-signal features and a hierarchical recognizer," *IEEE Trans. Inf. Technol. Biomed.*, vol. 14, no. 5, pp. 1166–1172, 2010.
- [51] D. W. Kang, J. S. Choi, J. W. Lee, S. C. Chung, S. J. Park, and G. R. Tack, "Real-time elderly activity monitoring system based on a tri-axial accelerometer," *Disabil. Rehabil. Assist. Technol.*, vol. 5, no. 4, pp. 247–253, 2010.
- [52] D. M. Karantonis, M. R. Narayanan, M. Mathie, N. H. Lovell, and B. G. Celler, "Implementation of a real-time human movement classifier using a triaxial accelerometer for ambulatory monitoring," *IEEE Trans. Inf. Technol. Biomed.*, vol. 10, no. 1, pp. 156–167, 2006.
- [53] M. Yu, A. Rhuma, S. M. Naqvi, L. Wang, and J. Chambers, "A posture recognition-based fall detection system for monitoring an elderly person in a smart home environment," *IEEE Trans. Inf. Technol. Biomed.*, vol. 16, no. 6, pp. 1274–1286, 2012.
- [54] N. Noury, A. Galay, J. Pasquier, and M. Ballussaud, "Preliminary investigation into the use of autonomous fall detectors," in *Proc. Annu. Int. Conf. IEEE Engineering in Medicine and Biology Society*, 2008, pp. 2828–2831.
- [55] G. Wu, "Distinguishing fall activities from normal activities by velocity characteristics," *J. Biomech.*, vol. 33, no. 11, pp. 1497–1500, 2000.
- [56] C. Rougier, J. Meunier, A. St-Arnaud, and J. Rousseau, "Fall detection from human shape and motion history using video surveillance," in *Proc. 21st Int. Conf. Advanced Information Networking and Applications Workshops (AINAW)*, 2007, vol. 2, pp. 875–880.
- [57] A. N. Belbachir, A. Nowakowska, S. Schraml, G. Wiesmann, and R. Sablatnig, "Event-driven feature analysis in a 4-D spatiotemporal representation for ambient assisted living," in *Proc. IEEE Int. Conf. Computer Vision*, 2011, pp. 1570–1577.
- [58] H. Foroughi, A. Naseri, A. Saberi, and H. S. Yazdi, "An eigenspace-based approach for human fall detection using integrated time motion image and neural network," in *Proc. 9th Int. Conf. Signal Processing*, 2008, pp. 1499–1503.
- [59] S. G. Miaoou, P. H. Sung, and C. Y. Huang, "A customized human fall detection system using omni-camera images and personal information," in *Proc. 1st Transdisciplinary Conf. Distributed Diagnosis and Home Healthcare*, 2006, vol. 2006, pp. 39–42.
- [60] B. Jansen and R. Deklerck, "Context aware inactivity recognition for visual fall detection," in *Proc. Pervasive Health Conf. and Workshops*, 2007, pp. 1–4.
- [61] A. N. Belbachir, M. Litzberger, S. Schraml, M. Hofstatter, D. Bauer, P. Schon, M. Humenberger, C. Sulzbachner et al., "CARE: A dynamic stereo vision sensor system for fall detection," in *Proc. IEEE Int. Symp. Circuits and Systems*, 2012, pp. 731–734.
- [62] R. Hoyle, R. Templeman, S. Armes, D. Anthony, D. Crandall, and A. Kapadia, "Privacy behaviors of lifeloggers using wearable cameras," in *Proc. ACM Int. Joint Conf. Pervasive and Ubiquitous Computing*, 2014, pp. 571–582.
- [63] A. R. Doherty, S. E. Hodges, A. C. King, A. F. Smeaton, E. Berry, C. J. A. Moulin, S. E. Lindley, P. Kelly et al., "Wearable cameras in health: The state of the art and future possibilities," *Am. J. Prev. Med.*, vol. 44, no. 3, pp. 320–323, Mar. 2013.
- [64] P. Chen, P. Ahammad, C. Boyer, S. I. Huang, L. Lin, E. Lobaton, M. Meingast, S. Oh et al., "Citric: A low-bandwidth wireless camera network platform," in *Proc. 2nd ACM/IEEE Int. Conf. Distributed Smart Cameras*, 2008, pp. 110.
- [65] K. Zhan, F. Ramos, and S. Faux, "Activity recognition from a wearable camera," in *Proc. 12th Int. Conf. Control Automation Robotics Vision*, Dec. 2012, vol. 2012, pp. 365–370.
- [66] M. Moghimi, P. Azagra, L. Montesano, A. C. Murillo, S. Belongie, D. Ia, C. Tech, and N. York, "Experiments on an RGB-D Wearable Vision System for Egocentric Activity Recognition," in *Proc. IEEE Conf. Computer Vision and Pattern Recognition Workshops*, 2014, pp. 611–617.
- [67] S. Ishimaru, K. Kunze, and K. Kise, "In the Blink of an Eye – Combining Head Motion and Eye Blink Frequency for Activity Recognition with Google Glass," in *Proc. 5th Augmented Human Int. Conf.*, 2014, pp. 15:1–15:4

Stefano Savazzi, Stephan Sigg, Monica Nicoli,
Vittorio Rampa, Sanaz Kianoush, and Umberto Spagnolini

Device-Free Radio Vision for Assisted Living

Leveraging wireless channel quality information for human sensing

Wireless propagation is conventionally considered as the enabling tool for transporting information in digital communications. However, recent research has shown that the perturbations of the same electromagnetic (EM) fields that are adopted for data transmission can be used as a powerful sensing tool for device-free radio vision. Applications range from human body motion detection and localization to passive gesture recognition. In line with the current evolution of mobile

phone sensing [1], radio terminals are not only ubiquitous communication interfaces, but they also incorporate novel or augmented sensing potential, capable of acquiring an accurate human-scale understanding of space and motion. This article shows how radio-frequency (RF) signals can be employed to provide a device-free environmental vision and investigates the detection and tracking capabilities for potential benefits in daily life.

It's not difficult. Every time I lift my arm, it distorts a small electromagnetic field that is maintained continuously across the room. Slightly different positions of my hand and fingers produce different distortions and my robots can interpret these distortions as orders. I only use it for simple orders: Come here! Bring tea! and so on.

—Isaac Asimov,
The Robots of Dawn, 1983.

Introduction

Device-free radio vision is an augmented functionality provided by radio transceivers—typically heterogeneous, densely distributed, and networked—that monitor the fluctuations of the EM field across the space. These monitoring devices may be pre-existing, deployed at arbitrary (or optimized) locations for communication purposes in the area of interest, and exchange digital information by any wireless communication protocol. Radio vision systems leverage diffraction, reflection, and scattering phenomena that affect RF propagation for ubiquitous sensing. RF signals can be either narrowband or wideband, in licensed or unlicensed frequency bands, with carrier frequencies ranging from MHz to GHz and higher. The presence, position, and motion of a human body in the network area affect the EM field in a

IMAGE LICENSED BY INGRAM PUBLISHING
WOMAN—©ISTOCKPHOTO.COM/SILVIAHANSEN



Digital Object Identifier 10.1109/MSP.2015.2496324
Date of publication: 7 March 2016

predictable way, making it possible to estimate and track its activity without the need to deploy and calibrate any additional wearable sensor (sensor-free detection), nor to ask for specific user actions (noncooperative detection). This passive sensing approach has been experimented with in heterogeneous networks, but it is also appropriate for most of the emerging low-power wireless standards, and for personal and device-to-device (D2D) communications [2], including Wi-Fi, Bluetooth low energy (BLE), ZigBee, and D2D-enabled long-term evolution (LTE Advanced) [3].

Tracking and recognition of human motions and activities are done through real-time processing of the wireless channel quality information (CQI). In this article, leading-edge research and developments are discussed with a special focus on assisted living applications [4].

Leveraging RF signals for sensing: Device-free vision

Personal sensing is the current scale at which these technologies are being studied by the research community: they are designed for sensing a single (or a limited number of) individual(s) based on real-time analysis of CQI. As depicted in Figure 1, radio-based vision systems track RF field perturbations by dense networks of air-interacting wireless devices and process CQI data for the purpose of human sensing. To support “vision” functions, three key distinctive technological features are incorporated:

A crucial problem for quantitative evaluation of radio vision system performance is the availability of a simple but realistic model to describe human body-induced shadowing.

- *Sensorless interaction and anonymous tracking.* Gesture-based interactions of the user with the environment are detected without instrumenting the human body (device-free) or deploying sensors calibrated for each user (sensorless). Subjects are anonymously tracked and localized, in contrast to privacy-intrusive video cameras, inferring the EM perturbations from CQI.
- *Ubiquitous monitoring.* Unlike existing infrared (IR) recognition platforms [4], device-free radio vision systems support ubiquitous user detection in complex non-line-of-sight (NLOS) indoor spaces [5], using both fixed (e.g., Wi-Fi access points, ZigBee/Bluetooth devices) and nomadic (e.g., smartphones, tablets) radio devices (see Figure 1) that are interacting over mixed line-of-sight (LOS) and NLOS, or through-the-wall links [6]. RF signals with wavelengths that are long enough to penetrate dense objects, such as doors or walls, can be exploited to recognize human motion and gestures even if these gestures are visually in shadow or in a different room adjacent to the one where the RF device itself is operating.
- *Scalable CQI (big-data) analytics.* The technology typically requires information aggregation, processing, and computation of massive amounts of CQI data generated from, and delivered to, highly distributed and heterogeneous wireless devices. CQI data for real-time processing are often produced at high

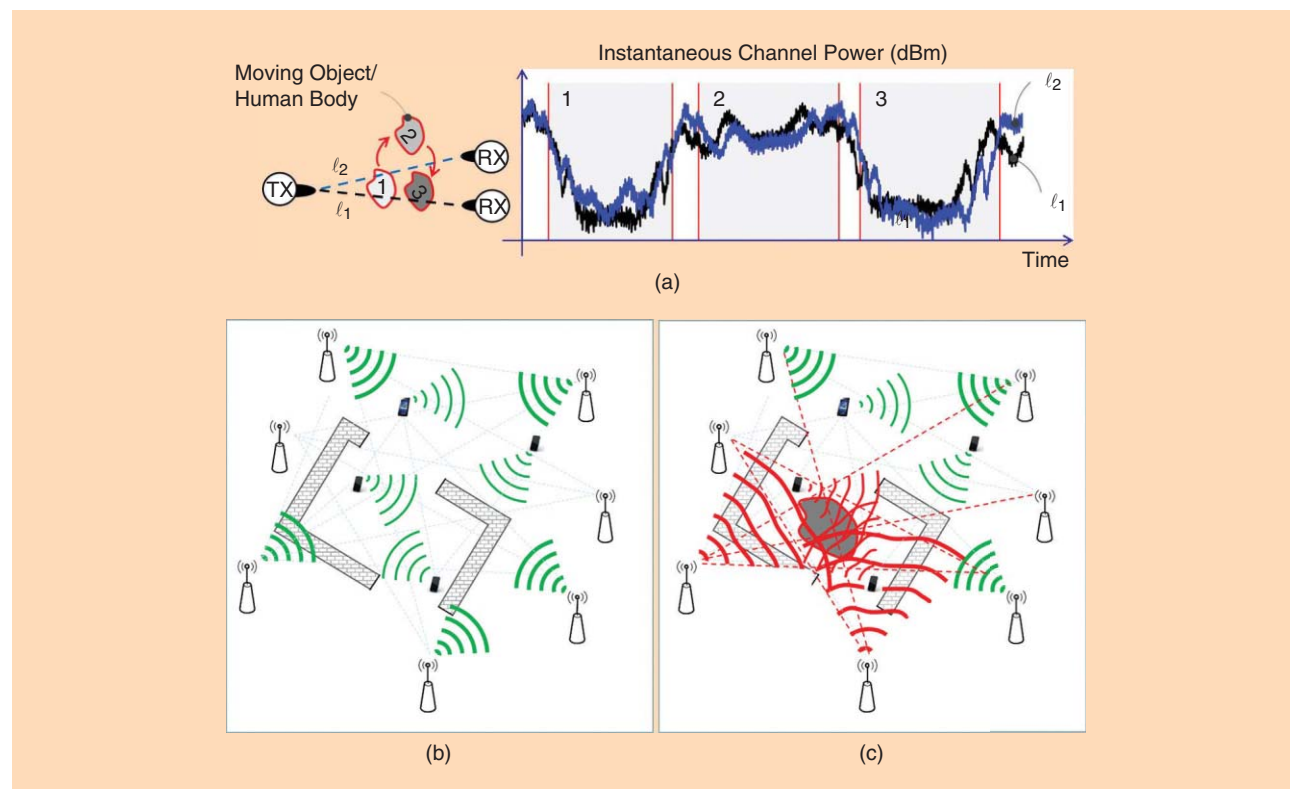


FIGURE 1. Device-free radio vision is based on tracking the perturbations of the RF field sensed by dense networks of radio-interacting wireless devices.

rates, in the order of tens of thousands of observations per second, to cover large spaces. Learning and running analytics from these large volumes of data requires the use of signal processing tools designed to efficiently work on high-dimensional and often incomplete data sets [7] (e.g., due to random power cycling of devices or communication failures).

Active and passive configurations

Device-free radio vision systems can be based on active or passive configurations, as illustrated in Figure 2. The distinction between active and passive systems differentiates systems in which the active part (the transmitter) is under the control of the system from those where it is not [8]. Passive systems capitalize on a pre-existing network infrastructure where densely air-interacting devices are exposed to some EM fields (e.g., FM radio [8], Wi-Fi [5], [9]), and capture those ambient RF signals. CQI processing might be carried out distributedly or centrally. Active systems exploit dense communications with fixed/nomadic transmitters acting as interconnected mobile probes. These systems typically rely on a decentralized architecture where user data are propagated in direct mode instead of through a remote service provider (e.g., cellular base stations, Wi-Fi access points), even if providers might trigger the first device connection, for logging, uplink/downlink (UL/DL) synchronization, etc. This concept is in line with the current trend [3] of enabling small/femto-cell deployments with smartphones that are able to discover other phones in proximity and overhear RF signals from D2D links.

Modeling of RF signals for radio vision

In radio vision systems, CQI measurements used for recognition can be either in the form of physical (PHY) layer values, e.g., the baseband radio channel state information (CSI) sampled at symbol level, or received signal strength (RSS) data extracted at upper layers.

Let us consider a wireless transmission organized into periodic frames consisting of groups of adjacent symbols, and a human body, located at position \mathbf{x} inside the wireless link area,

performing an activity δ defined as an ensemble of nonrigid body motions [10]. The user state $\Theta = [\mathbf{x}, \delta]$ defines a generic combination of user location and activity. The effects of the user state Θ on the channel response are observed over a set $\mathcal{J} = \{1, \dots, T\}$ of consecutive received symbols (or frames). For a static environment where the human body does not obstruct the link (i.e., human-free state $\Theta = \emptyset$), the equivalent baseband channel response $h(\tau|\emptyset) = \sum_{k=0}^N \alpha_k g_{\tau-\tau_k} e^{-j\phi_k}$ can be modeled as multipath with a combination of N delayed paths: α_k and ϕ_k are the amplitude and the phase shift of the k th ray, respectively, and $g_{\tau-\tau_k}$ models the received pulse waveform with delay τ_k . A human in state Θ modifies the channel response at symbol time $t \in \mathcal{J}$ as

$$h_t(\tau|\Theta) = \sum_{k=0}^N \alpha_k(t|\Theta) g_{\tau-\tau_k(t|\Theta)} e^{-j\phi_k(t|\Theta)}, \quad (1)$$

where the amplitude $\alpha_k(t|\Theta) = \alpha_k + \Delta\alpha_k(t|\Theta)$, the phase shift $\phi_k(t|\Theta) = \phi_k + \Delta\phi_k(t|\Theta)$, and the augmented delay $\tau_k(t|\Theta) = \tau_k + \Delta\tau_k(t|\Theta)$ of the k th ray highlight the human-induced perturbations compared to the human-free state $\Theta = \emptyset$. Amplitude $\alpha_k(t|\Theta)$ and phase shift $\phi_k(t|\Theta)$ incorporate human-induced micro-Doppler effects.

In what follows, the effect of human body motion on CQI is experimentally evaluated, either for single and multicarrier digital communication systems. An introductory case study is shown in Figure 3, where detection of human motion is based on RSS [Figure 3(a)], and CSI measurements extracted from an orthogonal frequency-division multiplexing (OFDM) implementation [Figure 3(b)].

RSS

The RSS is a practical metric to assess CQI at frame level, and it is commonly adopted for transmitter (TX)–receiver (RX) link adaptation and link-layer transmission scheduling tasks. Power estimators, or peak detectors, are commonly used to acquire information about signal strength as depicted

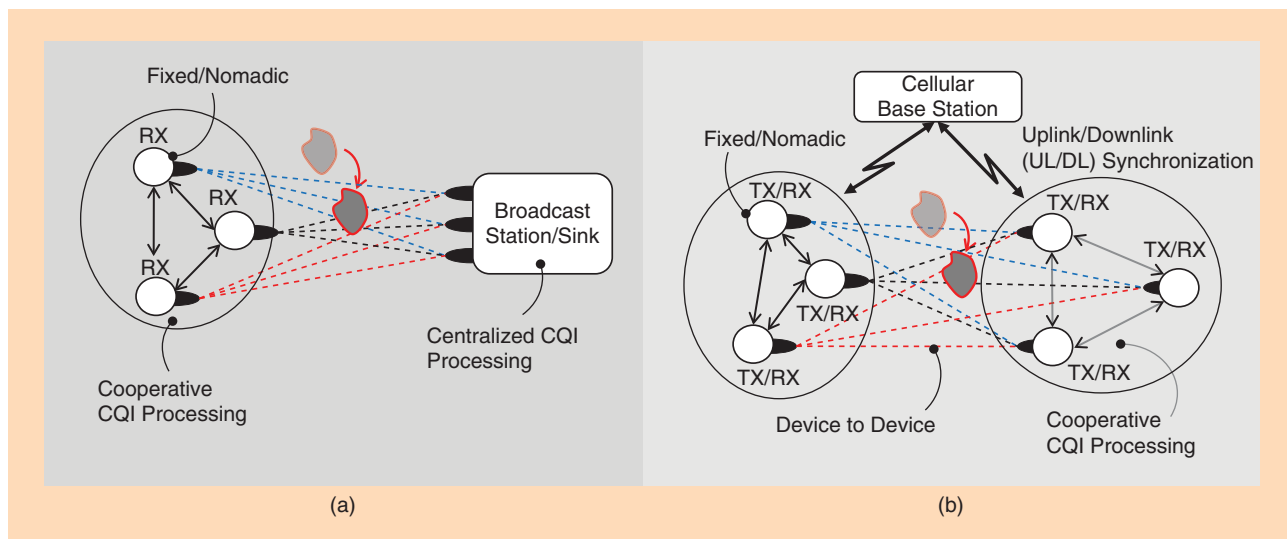


FIGURE 2. Active/passive network configurations for device-free radio vision. (a) Passive: capturing ambient radio signals. (b) Active: D2D communications.

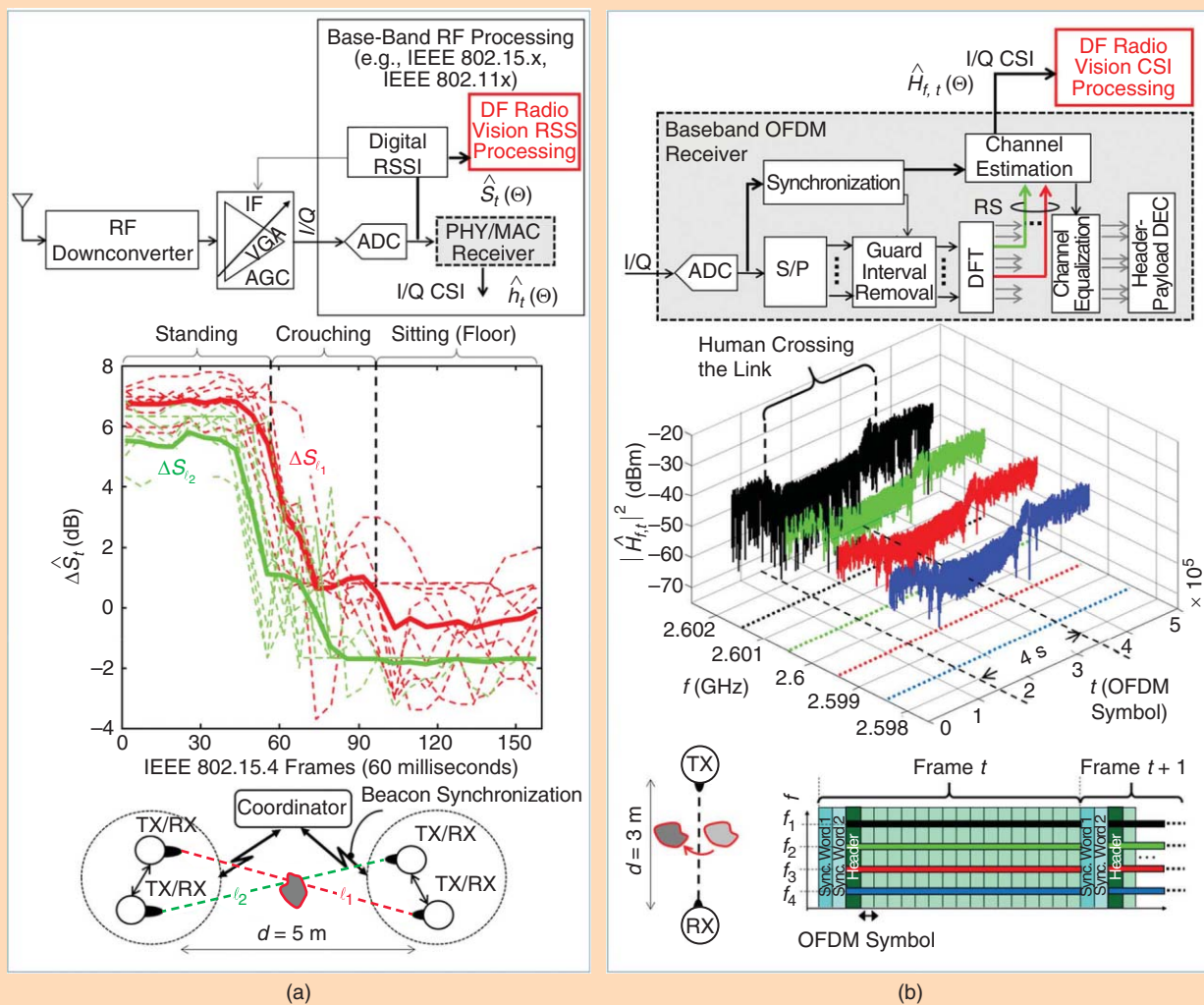


FIGURE 3. CQI: RSS and baseband CSI. (a) RSS information extraction: example. RSS processing for device-free radio vision: (top) digital/analog RSSI extraction, (bottom) RSSI data (dashed curves)—and corresponding average profiles (solid curves)—for a human standing, crouching, and sitting on the floor ($T = 160$ IEEE 802.15.4 frames). Active configuration is considered with two IEEE 802.15.4 links. (b) CSI extraction in multicarrier (OFDM) modulation. Baseband processing example for OFDM modulation: (top) CSI extraction, (bottom) CSI power footprints over $K=4$ OFDM pilot subcarriers ($T = 223,000$ symbols) corresponding to the human body crossing the link in four seconds. OFDM implementation: 2.6 GHz, 64 subcarriers, cyclic prefix 16 samples, baseband sampling 5MHz with 16 payload symbols/frame.

in Figure 3(a): the automatic gain control (AGC) loop exploits RSS information to adapt the dynamic range before analog to digital conversion. At frame time t , the RSS s_t can be modeled in logarithmic (dB) scale as

$$s_t(\Theta) = s(\emptyset) + \Delta s_t(\Theta), \quad (2)$$

where the additive deviation $\Delta s_t(\Theta)$ from $\Theta = \emptyset$ models the body-induced perturbation and $s(\emptyset) = \mathbb{E}[s_t(\Theta = \emptyset)]$ is the (average) RSS observed in the human-free state. The sequence $\mathbf{s}(\Theta) = [s_t(\Theta)]_{t \in \mathcal{J}} \in \mathbb{R}^{T \times 1}$ collects the human-induced RSS footprint observed over T frames. Likewise, the RSS profile is the deviation with respect to $\Theta = \emptyset$: $\Delta \mathbf{s}(\Theta) = [s_t(\Theta) - s(\emptyset)]_{t \in \mathcal{J}} \in \mathbb{R}^{T \times 1}$. In IEEE 802.15.4 standard-compliant devices, the digital RSS indicator (RSSI) \hat{s}_t can be used as

estimator of the RSS with 8-bit resolution. Other radios also implement the link quality indicator (LQI) that correlates with packet reception rate (see [11] and references therein), and provides an indirect estimate of RSS values. In Wi-Fi standards, RSS estimation can be obtained from the received channel power indicator (RCPI). In LTE, the reference signal received power (RSRP) measures the power over the reference signals.

Recognition of human activity can be also based on multi-link processing. Figure 3(a) (bottom) shows the profiles $\Delta \mathbf{s}_\ell(\Theta) \in \mathbb{R}^{T \times 1}$ over two IEEE 802.15.4 links $\ell \in \{l_1, l_2\}$, for $T = 160$ frames, based on 20 RSSI independent measurements $\hat{\mathbf{s}}_\ell(\Theta) = [\hat{s}_{\ell,t}(\Theta)]_{t \in \mathcal{J}} \in \mathbb{R}^{T \times 1}$ featuring a human body standing in the surroundings of both links (located at 0.5 m above the ground), then crouching and sitting on the floor. Since the human torso causes more attenuation than the waist

and ankles, when a person is standing, there is a larger RSS attenuation with respect to the same body lying on the floor. The profiles $\Delta s_t(\Theta)$, superimposed in solid lines, average out noise and time-warping effects. Detection of the human state can be based on matching (e.g., using simple time-domain features) the observed entries $\hat{s}_t(\Theta)$, or the estimated deviations $\Delta \hat{s}_t(\Theta)$, with the corresponding RSS profiles learned during a training procedure. Human-state estimation possibly entails denoising, time warping, and reconstruction of missing RSSI observations (i.e., by interpolation methods) [12], [13]. Missing or incomplete data can be represented as $\wp_\Omega[\hat{s}_t(\Theta)]$ over the set of $t \in \Omega \subseteq \mathcal{J}$ received frames, where $\wp_\Omega(\cdot)$ is the sampling operator nulling the entries of $\hat{s}_t(\Theta)$ not in Ω [7].

Baseband modeling of CSI

Baseband CSI measures the channel response at symbol level: CSI estimation is typically obtained from training/reference signals (RSs) multiplexed with information symbols and periodically placed in every frame. Therefore, in contrast to RSS, processing of CSI for the purpose of radio vision can leverage on multiple independent measurements at frame level and can be used to capture fast human body movements and gestures. Assuming frequency-flat channel as for narrowband communication but time-varying for dynamic multipath environments, the received RSs $r_t = h_t(\Theta)\omega_t + n_t$ at symbol time $t \in \mathcal{J}$ (with ω_t and n_t the transmitted RSs and the noise term, respectively), captures the moving body in state Θ through the corresponding complex channel envelope adopted from (1)

$$h_t(\Theta) = \sum_{k=0}^N \alpha_k(t|\Theta) e^{-j\phi_k(t|\Theta)} = h(\varnothing) + \Delta h_t(\Theta). \quad (3)$$

Human body effects on the channel response are now embedded into a characteristic footprint of channel variations over T received symbols $\mathbf{h}(\Theta) \in \mathbb{C}^{T \times 1} = [h_t(\Theta)]_{t \in \mathcal{J}}$. The CSI profile set is $\Delta \mathbf{h}(\Theta) \in \mathbb{C}^{T \times 1} = [\Delta h_t(\Theta) = h_t(\Theta) - h(\varnothing)]_{t \in \mathcal{J}}$, with $h(\varnothing) = \mathbb{E}[h_t(\Theta) = \varnothing]$ being the average response for the human-free state. Noisy profiles $\Delta \hat{\mathbf{h}}(\Theta) = [\hat{h}_t(\Theta) - \hat{h}(\varnothing)]_{t \in \Omega}$ with estimated channels $\hat{h}_t(\Theta)$ and human-free response $\hat{h}(\varnothing)$ are typically observed over a subset of times (or symbol indexes) $\Omega \subseteq \mathcal{J}$ accounting for the training/data multiplexing, and missing symbols.

The use of multicarrier (OFDM) modulation enables multi-dimensional processing of CSI over the time-frequency grid and allows a fine-grained classification of human motion [12]. As depicted in Figure 3(b), the CSI estimation is carried out by periodic transmission of RSs over standard defined time-frequency patterns [3]. The received RSs \mathbf{r}_t over the K pilot subcarriers $\{f_1, \dots, f_K\}$ inside OFDM symbol t can be written as $\mathbf{r}_t = \text{diag}[\omega_t] \cdot \mathbf{h}_t(\Theta) + \mathbf{n}_t$ with vector ω_t collecting the transmitted RSs, and baseband channel vector $\mathbf{h}_t(\Theta) = [H_{f,t}(\Theta)]_{f=f_1}^{f_K}$ containing the Fourier transform $\mathcal{F}(\cdot)$ of channel $h_t(\tau|\Theta)$

$$H_{f,t}(\Theta) = H_f(\varnothing) + \underbrace{\mathcal{F}(\Delta h_t(\tau|\Theta))}_{\Delta H_{f,t}(\Theta)}|_f. \quad (4)$$

The CSI footprint is the matrix $\mathbf{H}(\Theta) \in \mathbb{C}^{K \times T} = [\mathbf{h}_1(\Theta), \dots, \mathbf{h}_T(\Theta)]_{t \in \mathcal{J}}$ with human-induced profile $\Delta \mathbf{H}(\Theta) = [\mathbf{H}(\Theta) - \mathbf{H}(\varnothing)]$. The estimate $\hat{\mathbf{H}}(\Theta)$ is evaluated over the time-frequency set Ω now accounting for framing structure and irregular time-frequency RSs spacing. In Figure 3(b) (bottom), an OFDM transmission over 2.6 GHz is implemented in-lab using software-defined radio (SDR) devices: a person is crossing the link and standing for four seconds, causing an average attenuation of 5 dB. The CSI power footprint estimates $|\hat{H}_{f,t}(\Theta)|^2$ are shown for $K = 4$ pilots and $T = 223,000$ symbols.

A crucial problem for quantitative evaluation of radio vision system performance is the availability of a simple but realistic model to describe human body-induced shadowing. Ray-tracing [14], EM/stochastic [15], [16], and geometric-based (see [2] for a review) models have been investigated to predict the correlation between the human body position \mathbf{x} and the corresponding channel perturbations. EM methods that exploit geometric/uniform theory of diffraction (GTD/UTD), as well as ray-tracing algorithms, can be employed for their ability to accurately evaluate the EM field at the receiver, but they are usually very complex, time consuming and, above all, require perfect knowledge of the shape, composition, and properties of the obstacle. In “Diffraction-Based Modeling of Human Body Shadowing,” we consider a simplified but effective framework based on the Fresnel-Kirchoff diffraction theory as shown in Figure 4(a).

Research on radio vision: A survey

There has recently been an increasing interest in research on wireless human tracking via RF devices. This broadly defined domain encompasses different research areas such as signal processing, computer vision, communication networks, and human-machine interfaces. The first experimental activity dates back to the works [17], [18] showing that body motions leave a characteristic footprint on RSS patterns [17], while RSS fluctuations can be effectively used for body localization [18].

Focusing on device-free human body localization, the radio tomography imaging (RTI) proposed in [6], [19], and [20] adopts computed tomography methods to reconstruct an image of the object(s) inside the network area. The technology has been now transferred to a commercial product (i.e., Xandem system) targeting assisted living applications. The methods introduced in [5], [9], and [11] allow the explicit tracking of the target’s (or targets’) position using a Bayesian approach that jointly process the RSS mean and standard deviations [11]. More recently, device-free systems based on Bayesian tracking of RSS profiles have been also designed for obstacle/object two-dimensional (2-D) mapping [21], detection of human breathing [13], [22], and fall detection [23], [24]. Human gesture recognition and body motion detection have been addressed in recent research projects (SenseWaves, E-eyes, WiSee, and Wi-Vi) targeting both RSS [25] and baseband CSI analytics using radio devices operating at 900 MHz [8], [26], 2.4 GHz with 20-MHz

DIFFRACTION-BASED MODELING OF HUMAN BODY SHADOWING

Here we consider the framework proposed in [16] and summarized according to the link scenario of Figure 4(a) (top), where the human body is sketched as a three-dimensional (3-D) homogeneous cylinder, having height $2a_z$ and an elliptical base with semi-axes a_{yv} and a_{yv} . The cylinder rotates along the vertical axis x_φ with azimuth φ , thus modeling a human body standing in a specific position but possibly changing its posture. As a tradeoff between model simplicity and accuracy, the 3-D cylinder is reduced to an equivalent 2-D rectangular knife-edge absorbing surface [11], [16] that is modeled according to the Fresnel–Kirchhoff diffraction theory. The obstacle has the same height $2a_z$ but variable traversal semisize $a_y(\varphi)$ with $a_{yv} \leq a_y(\varphi) \leq a_{yv}$ while its barycenter B is placed in a specific position $\mathbf{x} = [x_1 = x, x_2 = y]$. If the obstacle location \mathbf{x} is near the LOS path, and if multipath body-induced effects are neglected, by exploiting the paraxial approximation, the attenuation term in decibel scale

$$\Delta E_{\text{dB}}^2(\mathbf{x}; \varphi) = -10 \log_{10} |E(\mathbf{x}; \varphi) / E_0|^2 \quad (S1)$$

due to the obstacle is derived analytically in [16]. $\Delta E_{\text{dB}}^2(\mathbf{x}; \varphi)$ depends on the received electric field $E(\mathbf{x}; \varphi)$

and the free-space case E_0 . Focusing on body localization, attenuation can be considered as random due to the varying orientations φ of the obstruction body. Figure 4(a) shows the mean $\Delta\mu(\mathbf{x}) = \mathbb{E}_\varphi[\Delta E_{\text{dB}}^2(\mathbf{x}; \varphi)]$ and the standard deviation $\Delta\sigma(\mathbf{x}) = \sqrt{\mathbb{E}_\varphi[(\Delta E_{\text{dB}}^2(\mathbf{x}; \varphi) - \Delta\mu(\mathbf{x}))^2]}$ perturbation maps of the RF attenuation for the link of length d as a function of the obstacle position \mathbf{x} after averaging with respect to azimuth ($d = 5$ m, carrier frequency 2.48 GHz, with $a_z = 90$ cm, $a_{yv} = 27.5$ cm, $a_{yv} = 12$ cm). With the given geometrical constants, the sensitivity area \mathcal{X} due to the obstacle has a maximum width of about 0.7 m around the LOS path. The model (S1) neglects the true shape, complex composition, and EM properties of the obstacle (e.g., polarization, permittivity, and conductivity), but it is accurate enough to model human-induced attenuation effects. Figure 4(b) shows the comparison of the average channel power perturbation $\mathbb{E}_\varphi[(|E(\mathbf{x}; \varphi) / E_0|^2)_{\text{dB}}]$ induced by a person against the values predicted by the model (S1) and the ones obtained by simulating the obstacle as a perfect conductor, having the same size of the person, placed over a concrete floor. As expected, the impact of the target presence is higher along the LOS path and close to the transmitting/receiving devices.

band Wi-Fi-compliant RF front ends [12], [27], and 5.8 GHz [28]. Signal processing methodologies for these systems, most recent developments, and open issues will be discussed in the following sections.

Device-free localization and motion tracking

In the context of assisted living, knowledge of the user location [5] is important for a number of services ranging from monitoring daily activities, forecasting user tendencies, to remote control of appliances (e.g., lights, doors, windows, air-conditioners). RSS-based device-free localization (DF-L) [11], [18], [19] has emerged in the last few years for passive localization of people movements in areas covered by pre-existing wireless mesh networks. Considering a single target at location $\mathbf{x} = [x_1, x_2]^T$ in the network area, if s_ℓ is the RSS of the link ℓ at a given time instant, the objective of DF-L is the estimation of \mathbf{x} from the RSS set $\mathbf{s} = [s_1, \dots, s_L]^T$. As shown in Figure 5, RSS is approximated as a Gaussian variable in the logarithmic domain (i.e., as log-normal shadowing [11])

$$s_\ell = \begin{cases} \mu_{0,\ell} + w_{0,\ell}, & \mathbf{x} \notin \mathcal{X}_\ell \\ \mu_{1,\ell}(\mathbf{x}) + w_{1,\ell}, & \mathbf{x} \in \mathcal{X}_\ell \end{cases} \quad (5)$$

for a target outside ($\mathbf{x} \notin \mathcal{X}_\ell$) or inside ($\mathbf{x} \in \mathcal{X}_\ell$) the sensitivity area of the link ℓ , respectively. In the first case (empty scenario), the RSS has a deterministic mean $\mu_{0,\ell}$ that accounts for path-loss and other static effects due to fixed obstructions or scattering objects, while the random term $w_{0,\ell} \sim \mathcal{N}(0, \sigma_{0,\ell}^2)$ accounts for RSS measurement errors due to the hardware (i.e., for noisy RSSI) as well as for small power fluctuations due to variations in the surrounding environment. The mean RSS for

$\mathbf{x} \in \mathcal{X}_\ell$ is $\mu_{1,\ell}(\mathbf{x}) = \mu_{0,\ell} + \Delta\mu_\ell(\mathbf{x})$ (with $\Delta\mu_\ell(\mathbf{x}) \leq 0$), while the random shadowing is modeled as $w_{1,\ell} \sim \mathcal{N}(0, \sigma_{1,\ell}^2(\mathbf{x}))$ with $\sigma_{1,\ell}(\mathbf{x}) = \sigma_{0,\ell} + \Delta\sigma_\ell(\mathbf{x})$ (and $\Delta\sigma_\ell(\mathbf{x}) \geq 0$). An experimental evidence for model (5) is depicted in Figure 5 (top): a measurement campaign was conducted to evaluate experimental RSS distributions to be compared with model (5) for target moving in the surrounding of location \mathbf{x} , both outside (blue) and inside (red) the sensitivity area of two selected links. Although better fits can be provided using other parametric distributions

(e.g., Weibull, Nakagami distributions [29]), the approximation is reasonable to design estimation methods and infer performance bounds of practical interest (see “Accuracy Bounds for DF-L”). As shown in several experimental studies [6], [11], [20], both average $\Delta\mu_\ell(\mathbf{x})$ and standard deviation $\Delta\sigma_\ell(\mathbf{x})$ maps of the RSS perturbations (i.e., perturbation maps) are strongly related to the target position relative to the

Gesture-based interactions of the user with the environment are detected without instrumenting the human body (device-free) or deploying sensors calibrated for each user (sensorless).

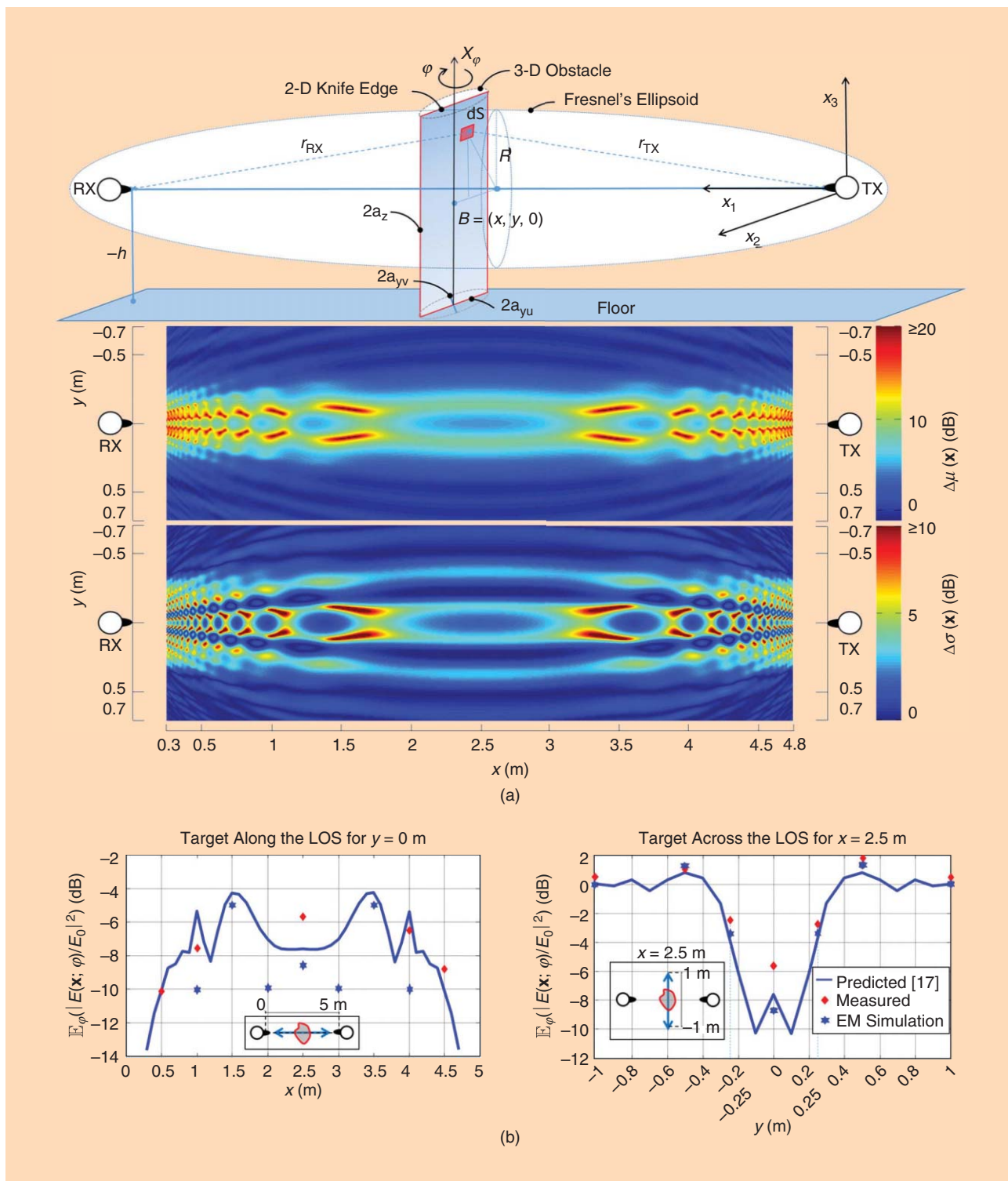


FIGURE 4. (a) Link layout (top) and perturbation maps (bottom) of RF attenuation for mean and standard deviation. (b) Predicted versus measured- and EM-simulated average channel power perturbations (along and across the LOS path). Measurements are obtained with a person standing in $\mathbf{x} = [x, y]^T$ with varying posture. Predicted values are obtained for a rotating cylinder moving inside a 10×10 -cm bin centered in \mathbf{x} .

link. This can be further appreciated in Figure 5, where 2-D experimental RSS profiles are shown at bottom for a subset of links. Based on the RSS measurements collected by a network of 14 nodes deployed in indoor and outdoor scenarios, the maps are evaluated for a human body moving over the positions \mathbf{x}

within a $4 \text{ m} \times 3 \text{ m}$ -area. The sensitivity area X_ℓ for each link ℓ is centered on the LOS path (highlighted in green) and it is larger in indoor than in outdoor due to multipath effects.

For position estimation, knowledge of the reference parameters $\{\mu_{0,\ell}, \sigma_{0,\ell}\}$ (for the human-free case) is required for all

ACCURACY BOUNDS FOR DF-L

The Cramer–Rao bound (CRB) provides a useful benchmark for assessing DF-L performances. The covariance matrix for any unbiased estimator $\hat{\mathbf{x}}$ of the target position \mathbf{x} is lower bounded as $\text{Cov}(\hat{\mathbf{x}}) = \mathbb{E}[(\mathbf{x} - \hat{\mathbf{x}})(\mathbf{x} - \hat{\mathbf{x}})^T] \geq \mathbf{F}^{-1}(\mathbf{x})$, where $\mathbf{F}(\mathbf{x})$ is the 2×2 Fisher information matrix (FIM). According to the Gaussian model $\mathbf{s} \sim \mathcal{N}(\boldsymbol{\mu}(\mathbf{x}), \mathbf{Q}(\mathbf{x}))$ in (5), the FIM term (i, j) with $i, j \in \{1, 2\}$, is

$$F_{i,j} = [\mathbf{F}(\mathbf{x})]_{i,j} = \sum_{\ell=1}^L \frac{1}{\sigma_{\ell}^2(\mathbf{x})} \left[\frac{\partial \mu_{\ell}(\mathbf{x})}{\partial x_i} \frac{\partial \mu_{\ell}(\mathbf{x})}{\partial x_j} + 2 \frac{\partial \sigma_{\ell}(\mathbf{x})}{\partial x_i} \frac{\partial \sigma_{\ell}(\mathbf{x})}{\partial x_j} \right], \quad (\text{S2})$$

where the gradient functions $\partial \mu_{\ell}(\mathbf{x}) / \partial x_i = \partial \Delta \mu_{\ell}(\mathbf{x}) / \partial x_i$ and $\partial \sigma_{\ell}(\mathbf{x}) / \partial x_i = \partial \Delta \sigma_{\ell}(\mathbf{x}) / \partial x_i$, $i \in \{1, 2\}$, embody the information on the target location provided by the perturbation maps of

attenuation $\Delta \mu_{\ell}(\mathbf{x})$, and standard deviation $\Delta \sigma_{\ell}(\mathbf{x})$, respectively [11]. According to the diffraction model (5), and the related analytical maps $\Delta \mu_{\ell}(\mathbf{x}) = \mathbb{E}_{\varphi}[\Delta E_{\text{dB}}^2(\mathbf{x}; \ell; \varphi)]$ and $\Delta \sigma_{\ell}(\mathbf{x}) = \sqrt{\mathbb{E}_{\varphi}[(\Delta E_{\text{dB}}^2(\mathbf{x}; \ell; \varphi) - \Delta \mu_{\ell}(\mathbf{x}))^2]}$ obtained as in “Diffraction-Based Modeling of Human Body Shadowing,” by computing all derivative terms of (S2), it is possible to obtain the $\mathbf{F}(\mathbf{x})$ matrix and, finally, the CRB for the complete L -link network. To demonstrate the effects of multiple links on the localization accuracy, the maps shown in Figure 6(b) show the lower bound to the root mean square error of the location estimate $\text{RMSE} = \sqrt{\mathbb{E}[\|\hat{\mathbf{x}} - \mathbf{x}\|^2]} \geq \sqrt{\text{tr}[\mathbf{F}^{-1}(\mathbf{x})]}$ for $L = 1, 8, 16, 24$ links. As expected, the localization accuracy is higher for a target near the terminals and along the LOS paths. For targets located in-between, the reduced sensitivity could be counterbalanced by increasing the number of links [11].

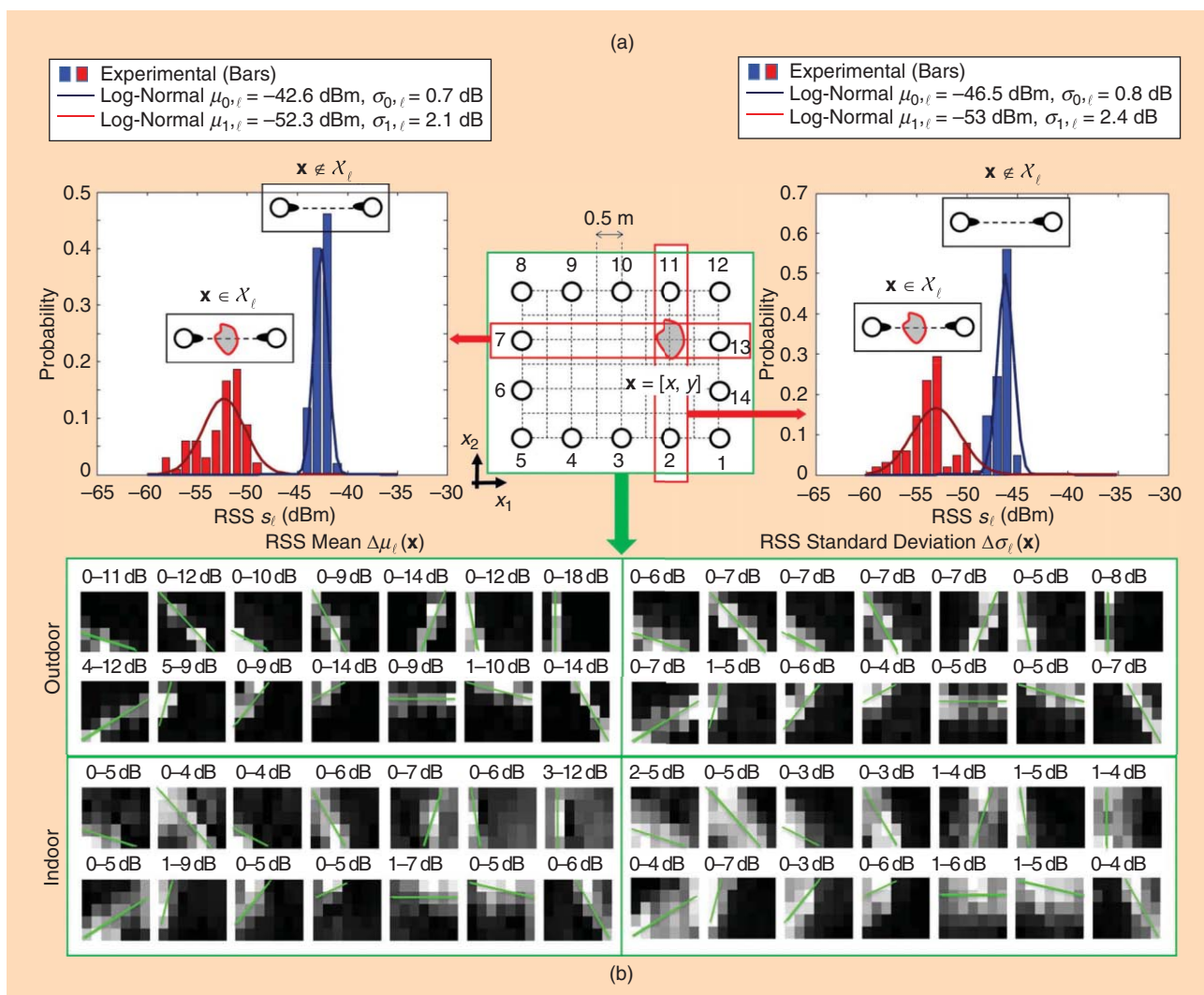


FIGURE 5. (a) Log-normal RSS modeling for two links (top left and top right) and for target inside (red) and outside (blue) the sensitivity area \mathcal{X}_{ℓ} for link ℓ . (b) Experimental RSS mean and standard deviation maps versus the target location \mathbf{x} for the highlighted network layout (top center) and some links in indoor and outdoor scenarios.

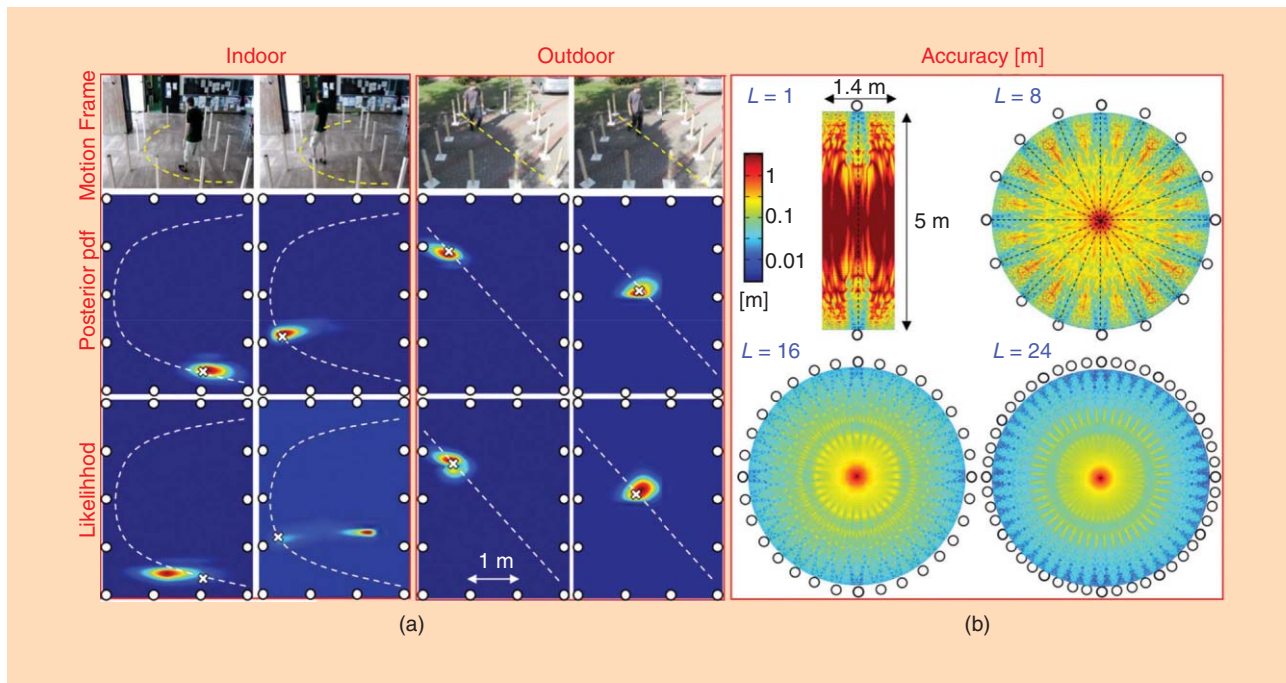


FIGURE 6. (a) DF-L: belief images of the target location for two frames of the user trajectories in 4-m x 3-m indoor and outdoor scenarios. (b) CRB limit to the DF-L accuracy considering L=1, 8, 16, 24 RF links of 5-m length.

links $\ell = 1, \dots, L$, together with the information about the perturbation maps $\{\Delta\mu_\ell(\mathbf{x}), \Delta\sigma_\ell(\mathbf{x})\}$ for all position values $\mathbf{x} \in \mathcal{X}_\ell$. While $\{\mu_{0,\ell}, \sigma_{0,\ell}\}$ can be easily precalibrated when no target is moving in the network area, the evaluation of profiles $\{\Delta\mu_\ell(\mathbf{x}), \Delta\sigma_\ell(\mathbf{x})\}$ is more critical as it requires extensive fingerprinting campaigns [9], [11], [19] or ray-tracing simulations [14]. Analytical modeling, when viable, has to be preferred as it allows to simplify the calibration to few model parameters and/or to evaluate predeployment performance. In [19] and [20], a simple single-parameter model is considered where $\Delta\mu_\ell(\mathbf{x})$, and $\Delta\sigma_\ell(\mathbf{x})$ are assumed to be constant and inversely proportional to the square root of the link distance for $\mathbf{x} \in \mathcal{X}_\ell$ with \mathcal{X}_ℓ modeled as an ellipsoid with foci at the two nodes. Parametric models for shadowing effects can be also found in [2], while diffraction-based models are considered in [16]. Once the perturbation maps are available, the target position \mathbf{x} can be estimated from (5) using inference methods. The weighted least squares (WLS) criterion is $\hat{\mathbf{x}} = \arg\min_{\mathbf{x}} \|\mathbf{s} - \boldsymbol{\mu}(\mathbf{x})\|_{\mathbf{C}^{-1}(\mathbf{x})}$, with $\|\mathbf{s} - \boldsymbol{\mu}(\mathbf{x})\|_{\mathbf{C}^{-1}(\mathbf{x})} = [\mathbf{s} - \boldsymbol{\mu}(\mathbf{x})]^T \mathbf{C}^{-1}(\mathbf{x}) [\mathbf{s} - \boldsymbol{\mu}(\mathbf{x})]$, $\boldsymbol{\mu}(\mathbf{x}) = [\mu_1(\mathbf{x}) \dots \mu_L(\mathbf{x})]^T$, and covariance $\mathbf{C}(\mathbf{x}) = \text{diag}[\sigma_1^2(\mathbf{x}), \dots, \sigma_L^2(\mathbf{x})]$ as weighting factor. Assuming the RSS fluctuations as independent over the links, the maximum likelihood (ML) criterion also applies as $\hat{\mathbf{x}} = \arg\max_{\mathbf{x}} \mathcal{L}(\mathbf{s} | \mathbf{x})$, with the log-likelihood function $\mathcal{L}(\mathbf{s} | \mathbf{x}) = -\ln(\det[\mathbf{C}(\mathbf{x})]) - \|\mathbf{s} - \boldsymbol{\mu}(\mathbf{x})\|_{\mathbf{C}^{-1}(\mathbf{x})}^2$ (irrelevant constant terms are neglected) and $\det[\cdot]$ the determinant operator. The information provided by instantaneous measurements \mathbf{s} can also be augmented with prior information about the target motion, using sequential Bayesian filtering such as Kalman filtering (KF), grid-based filtering (GF), or particle filtering (PF) [11].

Another DF-L approach is the radio tomographic imaging (RTI) [19], where the DF-L problem is formulated as the estimation of a motion image of the area, capturing any variation with respect to the human-free scenario observed during the calibration phase. In RTI, the area is divided into M voxels, $m = 1, \dots, M$, the image to be estimated is $\mathbf{v} = [v_1 \dots v_M]^T$ where $0 \leq v_m \leq 1$ measures the target occupancy (i.e., in terms of “probability” metric) of voxel m . For sparse motion, RSS is approximated as the sum of the contributions generated by all occupied voxels

$$s_\ell = \sum_{m=1}^M \Delta\mu_\ell(m) v_m + \mu_{0,\ell} + w_\ell, \quad (6)$$

where $\Delta\mu_\ell(m)$ is now the attenuation contribution due to target in voxel m and $w_\ell \sim \mathcal{N}(0, \sigma_\ell^2)$ the RSS fluctuation. Considering all links, it is $\mathbf{s} = \Delta\boldsymbol{\mu} \cdot \mathbf{v} + \boldsymbol{\mu}_0 + \mathbf{w}$, with matrix $\Delta\boldsymbol{\mu} \in \mathbb{R}^{L \times M} = [\Delta\mu_\ell(m)]$ that collects the perturbations for all links and voxels, $\boldsymbol{\mu}_0 = [\mu_{0,1} \dots \mu_{0,L}]^T$ the human-free reference vector, and $\mathbf{w} = [w_1 \dots w_L]^T \sim \mathcal{N}(\mathbf{0}, \mathbf{Q})$ the shadowing term. LS estimation has been proposed for imaging solution, as $\hat{\mathbf{v}} = (\Delta\boldsymbol{\mu}^T \Delta\boldsymbol{\mu} + \boldsymbol{\Gamma}_{x_1}^T \boldsymbol{\Gamma}_{x_1} + \boldsymbol{\Gamma}_{x_2}^T \boldsymbol{\Gamma}_{x_2})^{-1} \Delta\boldsymbol{\mu}^T \mathbf{s}$ with $\boldsymbol{\Gamma}_{x_i}$ accounting for regularization along each direction [19]. The target position corresponds to the voxel associated with the maximum image value: $\hat{m} = \arg\max_m \hat{v}_m$. In [20], RTI has been also applied to RSS variances modeled as linearly increasing with the number of occupied voxels $\sigma_\ell^2 = \sigma_{\ell}^2(\mathbf{v}) = \sigma_{0,\ell}^2 + \sum_{m=1}^M \Delta\sigma_\ell^2(m) v_m$: the same LS approach is then adopted for image evaluation.

Examples of DF-L results based on both mean and variance measurements are given in Figure 6(a), for indoor (left) and outdoor (right) scenarios, where a human target moves according to

the highlighted trajectory. The snapshot likelihood $\mathcal{L}(\mathbf{s} | \mathbf{x})$ and the posterior pdf $p(\mathbf{x} | \mathbf{s})$ are evaluated by GF Bayesian filtering and serve as location belief images. It can be seen that filtering is especially useful in indoor environments as it allows to solve ambiguities due to multipath.

Human activity and gesture recognition

Focusing on device-free activity recognition (DF-AR), active and passive systems (Figure 2) can be further differentiated into systems exploiting baseband signal processing (e.g., using SDR devices) or RSS-related metrics for the prediction of surrounding activities. With respect to DF-L, DF-AR systems typically require a higher sampling frequency. Typical recommendations for optimal sampling frequencies in activity recognition are above 6 Hz but higher sampling potentially fosters good recognition accuracy [8], [25] (see Figure 7).

Methods such as RTI and fingerprinting are too slow and thus not employed. Instead, either systems conditioned on characteristic signal patterns or machine learning techniques are frequently applied. Apart from RSS, movement-indicating

features/profiles in frequency-domain (for instance Doppler shift) are exploited.

The main classes considered for DF-AR are the detection of basic whole-body activities, whole/half body gestures and human breathing detection. The achievable recognition accuracy for DF-AR is limited by the system class (active or passive), the CQI (baseband CSI or RSS), the radio technology, the sampling rate (6+ Hz) and time/frequency domain features. For basic activities such as walking (at different speeds), crawling or standing, the recognition

accuracies reached from CSI-based systems match those achievable with body-worn accelerometers [8]. Highly accurate, fine-grained part- and whole-body motions can be

This article shows how radio-frequency (RF) signals can be employed to provide a device-free environmental vision and investigates the detection and tracking capabilities for potential benefits in daily life.

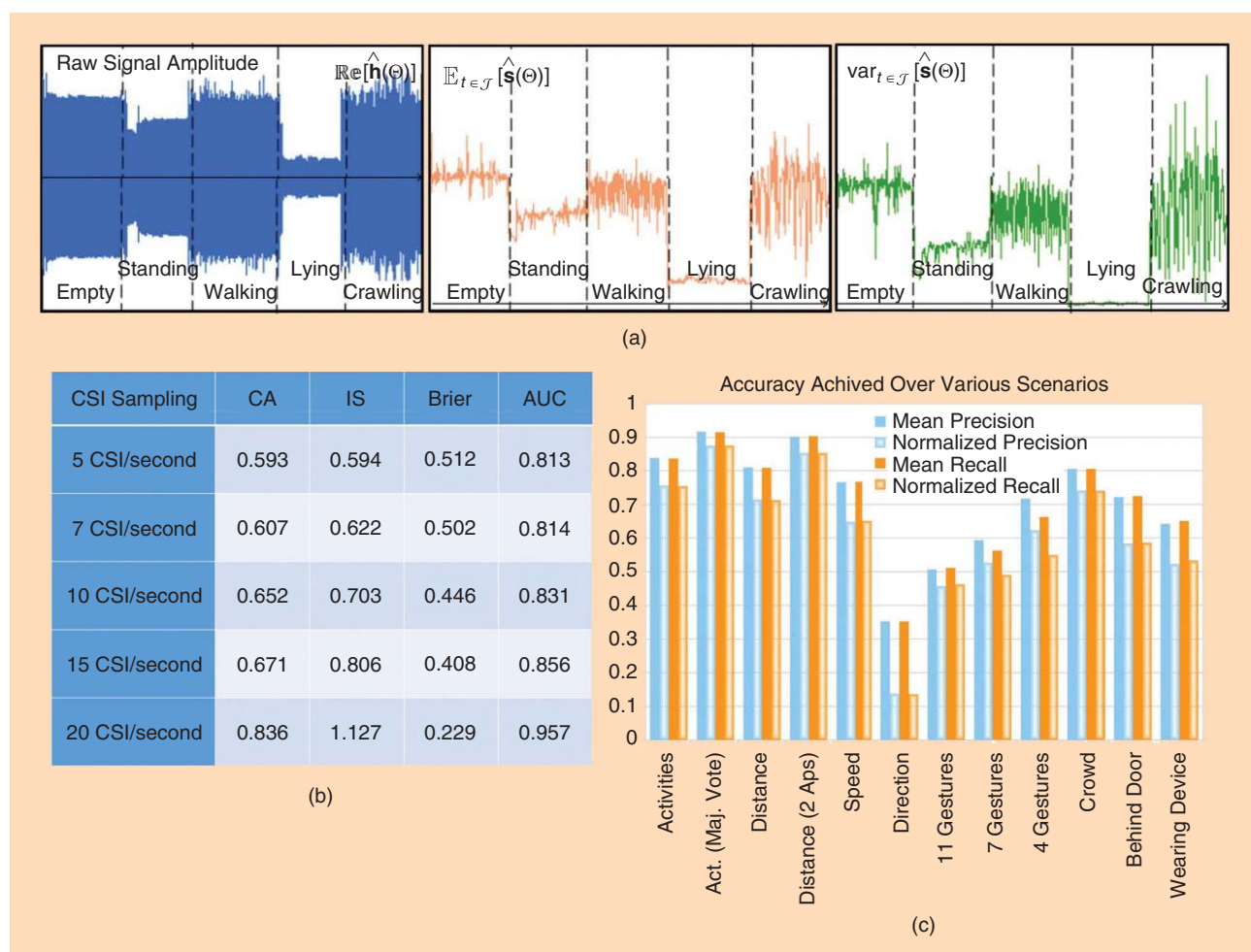


FIGURE 7. (a) The impact of human body movements/activities: CSI power footprints for human standing, walking, lying, and crawling with time-domain features. (b) The impact of different CSI sampling rates (CSI/second) on the performance of a k -nearest neighbor classifier [8]. (c) Classification accuracy from RSSI for movement in proximity, distance to receiver, walking speed, gestures (standing, walking, lying, and crawling), and crowd size. In this example, RSSI from environmental 802.11 access points was captured by a single receiver (a smartphone) [25].

CQI-BASED HUMAN ACTIVITY RECOGNITION

Baseband CSI based

CSI processing enables accurate activity recognition thanks to fine-grained frequency- and high time-resolution. Standard machine-learning techniques (e.g., k -nearest neighbor, decision trees, support vector machines) can be applied to time-domain CSI features such as mean $\mathbb{E}_{t \in \mathcal{J}}[\hat{\mathbf{s}}]$, variance $\text{var}_{t \in \mathcal{J}}[\hat{\mathbf{s}}]$ (Figure 7), or CSI power footprint $\hat{\mathbf{s}} \in \mathbb{R}^{T \times 1} = \left[\|\hat{h}_t(\Theta)\|^2 \right]_{t \in \mathcal{J}}$. Elementary activities such as phone calls, opened/closed doors, or a human body standing, walking at different speeds [8], lying, and crawling can be distinguished. These activities (or combination of) have to be trained separately by machine-learning methods beforehand. For recognition of fine-grained activities or gestures, frequency-domain features, e.g., micro-Doppler fluctuations, are required [28]. However, Doppler shifts caused by human motion are several magnitudes smaller than the signal bandwidth. Focusing on MIMO OFDM modulations, analysis of such fluctuations is possible after

transforming the received symbols into narrowband pulses. Then, patterns from falling/rising signal edges of Doppler fluctuations can be exploited for gesture and activity recognition.

RSS based

RSS-based passive systems measure noisy link-layer RSSI. In such settings, human activity can be detected using simple time-domain features [see Figure 3(a)], including denoising [13] and dynamic time warping [12]. Although RSS samples are often bursty, a weak distinction between simple human activity classes is feasible [25] with about ten RSS observations/second while best accuracy is achieved with 40–80 RSS/second, where a precision and recall rate in the order of 90% for simple activities and 70% for gestures is possible. Further improvement is achieved by filtering noise, and focusing on the falling and rising edges of the composition of the signal features.

recognized via frequency-domain features like Doppler shifts from OFDM sub-channels (micro-Doppler fluctuation) [28]. However, as highlighted in the tutorial “CQI-Based Human Activity Recognition” and also depicted in Figure 7, RSS-based systems are further limited in their achievable accuracy and recognized classes; thus, they qualify for applications in ambient assisted living but not, e.g., for highly reliable systems.

Basic whole-body activities

Machine-learning approaches can be applied to extract information about the environmental situation from RSS fluctuations. Radio devices at frequencies between 900 MHz up to 5 GHz with arbitrary node deployments are typically utilized. Simple time-domain features are employed, such as root mean square (RMS), average magnitude squared (AMS), signal-to-noise ratio (SNR), signal amplitude, signal peaks, and the number of large delta in successive peaks. The E-eyes system [12] combines Wi-Fi 2.4-GHz links from different devices (e.g., access points, thermostats, laptops) and collects fine-grained CSI measurements as location-activity profiles. In [8], recognition accuracy has been improved by exploiting frequency domain features. Furthermore, the authors have compared DF-AR performance with accelerometer-based recognition, showing comparable accuracy, in the order of 90–95% for indoor scenarios. Signals from nearby broadcasting FM radio stations also qualify for the detection of activities [26].

Gestures

Utilizing a multiple-input, multiple-output (MIMO)-OFDM receiver, the WiSee system [28] can distinguish nine pre-defined gestures from different people simultaneously with an accuracy of 94%. Simultaneous detection of gestures from multiple individuals can be obtained by utilizing multi-antenna nodes and leveraging micro-Doppler fluctuations. In a related system (WiVi [27]), a single antenna receiver is used, while a preamble transmission stage is designed to isolate the time-varying reflections induced by the human body and null direct and wall-reflected disturbance. The

system tracks the direction of the moving object using inverse synthetic aperture radar: consecutive CSI measurements are collected over time to emulate an antenna array at the receiver. Gestures can be also detected by monitoring RSS at link-layer. In [25], simple classes of hand gestures can be recognized using off-the-shelf smartphone devices (observing more than ten RSS samples/second). Although the achievable accuracy is lower than for the active systems previously discussed, a clear distinction of up to 11 hand gestures performed in proximity of the phone is possible.

In radio vision systems, CQI measurements used for recognition can be either in the form of physical (PHY) layer values, e.g., baseband radio channel state information (CSI), or received signal strength (RSS) extracted at upper layers.

Recognition of breathing

Contact-free RF respiration monitoring systems can detect the breathing rate of a single individual. Detection of breathing can be based on monitoring the RSS fluctuations from a pre-existing IEEE 802.15.4 network surrounding the subject [22]. Using ML estimation, an error of 0.3 breaths/minute is

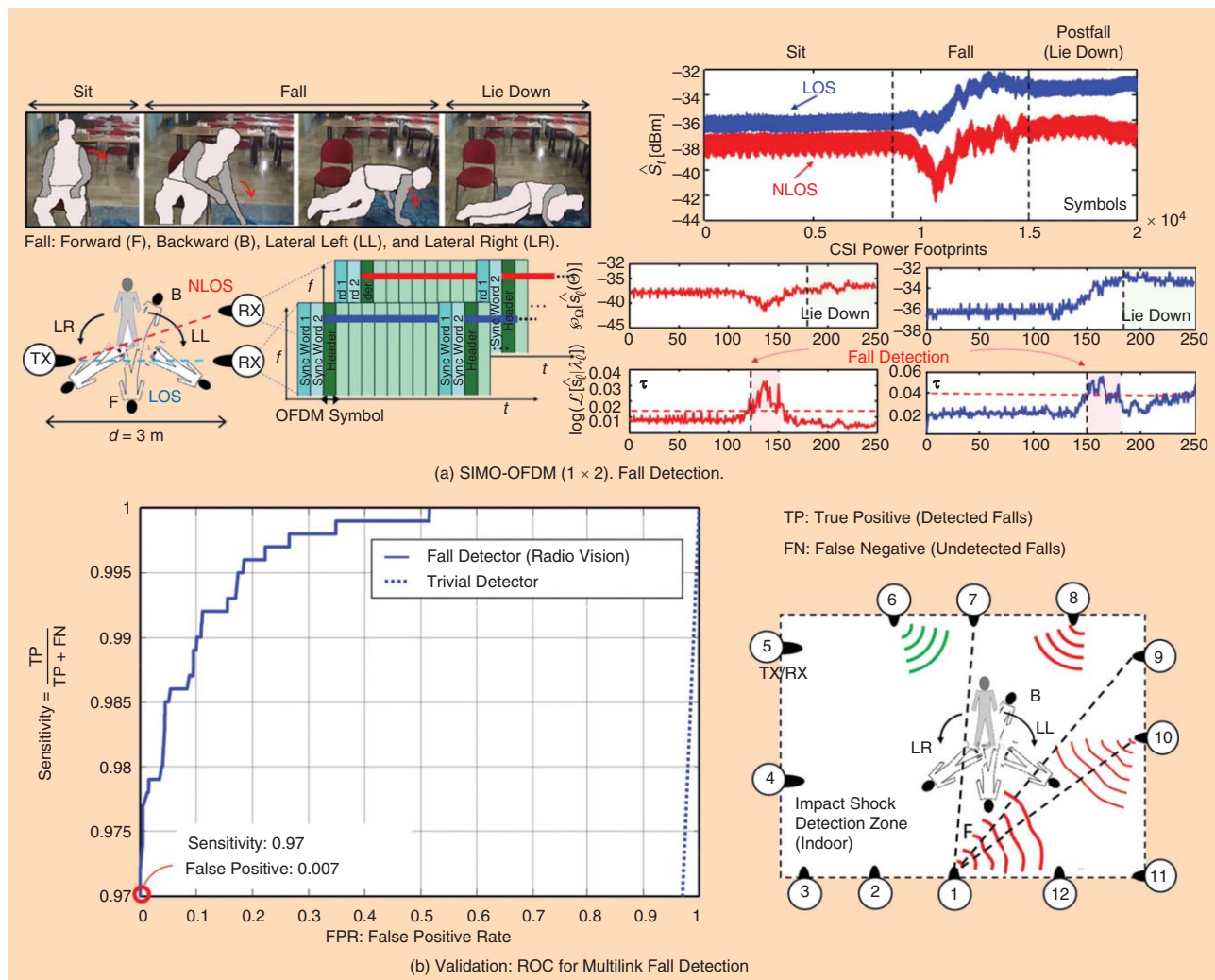


FIGURE 8. (a) HMM-based fall detection using SDR devices. SIMO-OFDM, (two RX antennas, single RS subcarrier). (b) Impact shock detector based on CQI data (ROC curve).

shown as achievable. The nodes transmitted every 240 milliseconds at 2.48 GHz. Prediction is taken after a 10–60-second measurement period. The UbiBreathe system [13] uses off-the-shelf Wi-Fi devices and provides a reasonable breathing estimation accuracy even using a single point-to-point link. Other systems are based on microwave Doppler radars and ultrawideband (UWB) (see [13] and references therein): they provide high accuracy but limited range and require an ad-hoc design and PHY layer optimization.

Monitoring a human’s fall: A case study

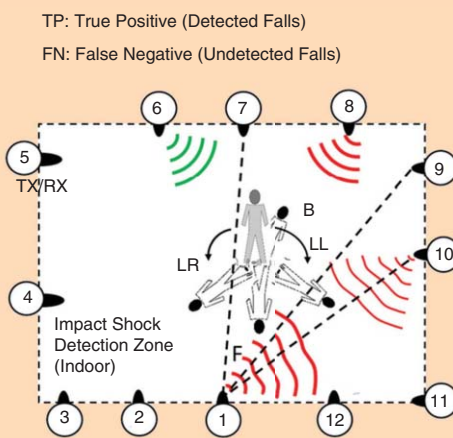
The adoption of a device-free wireless fall detection technology is highly attractive in the context of assisted living, as a person who has fallen might not only be unable to activate a personal emergency response system but may have also forgotten how to use it. Today’s

commercially available products already use a broad range of active devices (e.g., necklaces with emergency buttons, fall sensors in mobile phones, etc.). However, these devices are often too difficult for elderly people to operate and are thus useless in emergencies [30]. Body-worn sensing devices also require cooperation from the monitored subjects and might hinder daily activities. Systems based on cameras, video, or acoustic sources are also effective but penalized by privacy concerns. However, the proliferation of in-home wireless connected devices as part of the Internet of Things paradigm is acting as a boost to the development of new radio-based vision technologies. The possibility of monitoring human well-being by leveraging pre-existing indoor network infrastructures is

Future research on radio vision systems is expected to combine the use of localized RF signal inspection with large-scale and big-data processing.

becoming attractive in several applications.

Here, we highlight an experimental case study specifically focused on real-time processing of CQI for detection of



the impact shock during a body's fall. The in-lab system of Figure 8(a) consists of a deployment of wireless devices exchanging data over 2.6-GHz bands using an OFDM radio front end. A single-antenna OFDM transmitter communicates with a receiver employing two antennas (with spacing of 24 cm). The receiver extracts and processes two, possibly incomplete, CSI power footprints $\wp_{\ell_0}[\hat{s}_\ell]$ from the corresponding links (LOS and NLOS) $\ell \in \{\ell_1, \ell_2\}$. Body falling is monitored over a predefined position (\mathbf{x}): localization can be obtained by DF-L methods.

The observed sequences \hat{s}_ℓ are modeled by a hidden Markov model (HMM) [23], [24] with state space $\mathbf{Q}_\ell(\Theta) \in \mathbb{R}^{Q \times 1} = [q_i]_{i=1}^Q$ containing Q -selected values from the CQI profiles $\Delta s_\ell(\Theta)$ learned during training for falling-state estimation. HMM parameters, $\lambda_\ell(\Theta) = [\mathbf{A}_\ell, \mathbf{B}_\ell, \pi_\ell]$, include probabilities of state transition $[\mathbf{A}_\ell]_{i,j} = p[q_t = q_i | q_{t-1} = q_j]$, observation $[\mathbf{B}_\ell]_{i,j} = p[\hat{s}_{\ell,t} = s_i | q_t = q_j]$, and initial state $[\pi_\ell]_i = p[q_0 = q_i]$. The HMM parameters are learned by the expectation maximization algorithm (e.g., Baum–Welch algorithm) and trained separately for each link [23]. Other methods [24] can be adopted to leverage space-time profiles correlation over collocated links. A decision about a human fall is based on the model likelihood

$$\mathcal{L}[\hat{s}_\ell | \lambda_\ell(\Theta)] = \sum_{\mathbf{q} \in \mathbf{Q}_\ell(\Theta)} p[\hat{s}_\ell, \mathbf{q} | \lambda_\ell(\Theta)] \quad (7)$$

with state sequence $\mathbf{q} = [q_1, \dots, q_T]$ and joint probability $p[\hat{s}_\ell, \mathbf{q} | \lambda_\ell(\Theta)] = \prod_{t=1}^T p[\hat{s}_{\ell,t} | q_t] \cdot p[q_t | q_{t-1}]$. Functions $\mathcal{L}[\hat{s}_\ell | \lambda_\ell]$ are continuously evaluated for both links [Figure 8(a) on the right].

Fall detection can be based on a hard decision with respect to precalibrated threshold τ such that $\mathcal{L}[\hat{s}_\ell | \lambda_\ell(\Theta)] / \mathcal{L}[\hat{s}_\ell | \lambda_\ell(\emptyset)] > \tau$. Likelihood $\mathcal{L}[\hat{s}_\ell | \lambda_\ell(\emptyset)]$ is obtained for HMM $\lambda_\ell(\emptyset)$ that considers arbitrary (but safe) body movements in the same position. After the impact shock is detected, a simple change detector can be applied to the observed CQI sequences for tracking any postfall event and, in turn, detect possibly long lie conditions, corresponding to negligible RF fluctuations.

Impact shock detection

In the complete case study highlighted in Figure 8(b), the human fall detector is now based on an optimized subset of pre-existing links [23] deployed around the subject of interest and selected during a calibration procedure (noninformative links are purged). A decision about the fall/nonfall event is based on majority voting over the optimized link subset.

The analysis of detector performance is crucial: undetected falls might have a dramatic impact—on the other hand, an excessive number of false activations might cause the detector to be perceived as useless. Validation of detector accuracy is thus illustrated in Figure 8(b) where the receiver operating characteristic (ROC) curve relates

The adoption of a device-free wireless fall detection technology is highly attractive in the context of assisted living, as a person who has fallen might not only be unable to activate a personal emergency response system but may have also forgotten how to use it.

sensitivity versus false positive rate. A sensitivity of 0.97 and false positive rate of 0.007 compares well with performances of existing device-based systems [30].

Concluding remarks and future directions

This article focuses on device-free radio vision systems acting as a flexible sensing tool and addressing key challenges in assisted living applications. The goal of this emerging research field is to develop models and processing methodologies for exploiting the inherent (but currently unused) sensing capabilities of the multi-

tude of available wireless communication links, opening also to investigate new radio technologies and unexplored bands. Future research on radio vision systems is expected to combine the use of localized RF signal inspection with large-scale and big-data processing. Running real-time analytics from massive volumes of RF data will pose new signal processing relevant problems, as well as the redesign of conventional statistical learning tools applied to unprecedented high-dimensional data structures.

Authors

Stefano Savazzi (stefano.savazzi@ieiit.cnr.it) is a researcher at the Institute of Electronics, Computer, and Telecommunication Engineering of Consiglio Nazionale delle Ricerche, Italy. He received the Ph.D. degree (with honors) in information technology from Politecnico di Milano, in 2008. He was a researcher at Uppsala University in 2005, the University of California San Diego in 2008, and Forschungszentrum Telekommunikation Wien in 2010. His main research interests include cooperative and cognitive wireless networks, industrial Internet of Things, and device-free methods for radio-frequency vision and localization.

Stephan Sigg (stephan.sigg@aalto.fi) is an assistant professor in the Department of Communications and Networking at Aalto University, Finland. He was previously with the Computer Networks group of Georg-August-University of Göttingen and a researcher at TU Braunschweig. As an academic guest, he has cooperated with the Wearable Computer Lab at ETH-Zurich, the Nodes Laboratory at the University of Helsinki, and the National Institute of Informatics in the information systems architecture research division. He obtained his Ph.D. degree (with honors) from the University of Kassel, Germany. His research interests include the design, analysis, and optimization of algorithms for ubiquitous systems, in particular for device-free passive activity recognition.

Monica Nicoli (monica.nicoli@polimi.it) is an assistant professor in the Dipartimento di Elettronica, Informazione e Bioingegneria, Politecnico di Milano, Italy. She received her Ph.D. degree in communication engineering from Politecnico di Milano in 2002. She was visiting researcher at Uppsala University, Sweden, in 2001. Her research interests are in the

area of signal processing with an emphasis on wireless communications, distributed and cooperative systems, radio localization, and intelligent transportation systems.

Vittorio Rampa (vittorio.rampa@ieit.cnr.it) is a senior researcher at the Institute of Electronics, Computer, and Telecommunication Engineering of Consiglio Nazionale delle Ricerche, Italy. From 1999 to 2015, he has been an adjunct professor at the Politecnico di Milano, Italy, where he taught courses on software radio and radio localization systems. His main research interests are signal processing algorithms and architectures for wireless communications, virtual instrumentation techniques for test and verification of wireless systems, radio vision algorithms, and architectures for wireless sensor networks.

Sanaz Kianoush (sanaz@kianoush@ieit.cnr.it) received her Ph.D. degree in electronic engineering from the University of Pavia, Italy, in 2014. She is a postdoctoral researcher at the Institute of Electronics, Computer, and Telecommunication Engineering of Consiglio Nazionale delle Ricerche, Italy. Her research interests include localization in wireless sensor and cognitive radio networks and context-aware activity recognition.

Umberto Spagnolini (umberto.spagnolini@polimi.it) is a professor at the Politecnico di Milano, Italy. He is the author of more than 250 peer-reviewed papers and some patents. His areas of experience include channel estimation and space-time processing for wireless communication systems, cooperative and distributed systems, parameter estimation/tracking and wavefield interpolation for ultrawideband radar, oil exploration, and remote sensing. His interests are in statistical signal processing for communication systems and remote sensing.

References

- [1] N. D. Lane, E. Miluzzo, H. Lu, D. Peebles, T. Choudhury, and A. T. Campbell, "A survey of mobile phone sensing," *IEEE Commun. Mag.*, vol. 48, no. 9, pp. 140–150, Sept. 2010.
- [2] R. M. Buehrer, C. R. Anderson, R. K. Martin, N. Patwari, and M. G. Rabbat, "Introduction to the special issue on non-cooperative localization networks," *IEEE J. Sel. Top. Signal Processing*, vol. 8, no. 1, pp. 2–4, Feb. 2014.
- [3] A. Laya, W. Kun, A. A. Widaa, J. Alonso-Zarate, J. Markendahl, and L. Alonso, "Device-to-device communications and small cells: Enabling spectrum reuse for dense networks," *IEEE Wireless Commun.*, vol. 21, no. 4, pp. 98–105, Aug. 2014.
- [4] J. Lloret, A. Canovas, S. Sendra, and L. Parra, "A smart communication architecture for ambient assisted living," *IEEE Commun. Mag.*, vol. 53, no. 1, pp. 26–33, Jan. 2015.
- [5] M. Seifeldin, A. Saeed, A. E. Kosba, A. El-Keyi, and M. Youssef, "Nuzzer: A large-scale device-free passive localization system for wireless environments," *IEEE Trans. Mobile Comput.*, vol. 12, no. 7, pp. 1321–1334, July 2013.
- [6] N. Patwari and J. Wilson, "RF sensor networks for device-free localization: Measurements, models and algorithms," *Proc. IEEE*, vol. 98, no. 11, pp. 1961–1973, Nov. 2010.
- [7] K. Slavakis, G. B. Giannakis, and G. Mateos, "Modeling and optimization for Big Data analytics," *IEEE Signal Processing Mag.*, vol. 31, no. 5, pp. 18–31, Sept. 2014.
- [8] S. Sigg, M. Scholz, S. Shuyu, J. Yusheng, and M. Beigl, "RF-sensing of activities from non-cooperative subjects in device-free recognition systems using ambient and local signals," *IEEE Trans. Mobile Comput.*, vol. 13, no. 4, pp. 907–920, Apr. 2014.
- [9] A. Saeed, A. E. Kosba, and M. Youssef, "Ichnaea: A low-overhead robust WLAN device-free passive localization system," *IEEE J. Sel. Top. Signal Processing*, vol. 8, no. 1, pp. 5–15, Feb. 2014.
- [10] K. Youngwook and L. Hao, "Human activity classification based on micro-Doppler signatures using a support vector machine," *IEEE Trans. Geosci. Remote Sens.*, vol. 47, no. 5, pp. 1328–1337, May 2009.
- [11] S. Savazzi, M. Nicoli, F. Carminati, and M. Riva, "A Bayesian approach to device-free localization: Modelling and experimental assessment," *IEEE J. Sel. Top. Signal Processing*, vol. 8, no. 1, pp. 16–29, Feb. 2014.
- [12] Y. Wang, J. Liu, Y. Chen, M. Gruteser, J. Yang, and H. Liu, "E-eyes: Device-free location-oriented activity identification using fine-grained WiFi signatures," in *Proc. ACM Int. Conf. Mobile Computing and Networking*, 2014, pp. 617–628.
- [13] H. Abdelnasser, K. Harras, and M. Youssef, "UbiBreathe: A ubiquitous non-invasive WiFi-based breathing estimator," in *Proc. MobiHoc*, Hangzhou, China, 22–25 June 2015, pp. 277–286.
- [14] M. Scholz, L. Kohout, M. Horne, M. Budde, M. Beigl, and M. A. Youssef, "Device-free radio-based low overhead identification of subject classes," in *Proc. ACM Workshop on Physical Analytics*, Florence, Italy, 2015, pp. 1–6.
- [15] D. B. Smith, D. Miniutti, T. A. Lamaheewa, and L. W. Hanlen, "Propagation models for body-area networks: A survey and new outlook," *IEEE Antennas Propag. Mag.*, vol. 55, no. 5, pp. 97–117, Oct. 2013.
- [16] V. Rampa, S. Savazzi, M. Nicoli, and M. D'Amico, "Physical modeling and performance bounds for device-free localization systems," *IEEE Signal Processing Lett.*, vol. 22, no. 11, pp. 1864–1868, Nov. 2015.
- [17] K. Woyach, D. Puccinelli, and M. Haenggi, "Sensorless sensing in wireless networks: Implementation and measurements," in *Proc. 4th Int. Symp. Modeling and Optimization in Mobile, Ad Hoc and Wireless Networks*, 3–6 Apr. 2006, pp. 1–8.
- [18] M. Youssef, M. Mah, and A. Agrawala, "Challenges: Device-free passive localization for wireless environments," in *Proc. ACM Int. Conf. Mobile Computing and Networking*, 2007, pp. 222–229.
- [19] J. Wilson and N. Patwari, "Radio tomographic imaging with wireless networks," *IEEE Trans. Mobile Comput.*, vol. 9, no. 5, pp. 621–632, 2010.
- [20] J. Wilson and N. Patwari, "See-through walls: Motion tracking using variance-based radio tomography networks," *IEEE Trans. Mobile Comput.*, vol. 10, no. 5, pp. 612–621, May 2011.
- [21] Y. Mostofi, "Cooperative wireless-based obstacle/object mapping and see-through capabilities in robotic networks," *IEEE Trans. Mobile Comput.*, vol. 12, no. 5, pp. 817–829, May 2013.
- [22] N. Patwari, L. Brewer, Q. Tate, O. Kaltiokallio, and M. Bocca, "Breathfinding: A wireless network that monitors and locates breathing in a home," *IEEE J. Sel. Top. Signal Processing*, vol. 8, no. 1, pp. 30–42, Feb. 2014.
- [23] S. Kianoush, S. Savazzi, F. Vicentini, V. Rampa, and M. Giussani, "Leveraging RF signals for human sensing: Fall detection and localization in human-machine shared workspaces," in *Proc. IEEE Int. Conf. Industrial Informatics*, Cambridge, U.K., July 2015, pp. 1456–1462.
- [24] B. Mager, N. Patwari, and M. Bocca, "Fall detection using RF sensor networks," in *Proc. IEEE 24th Int. Symp. Personal Indoor and Mobile Radio Communications*, Sept. 2013, pp. 3472–3476.
- [25] S. Sigg, S. U. Blanke, and G. Troster, "The telepathic phone: Frictionless activity recognition from WiFi-RSSI," in *Proc. IEEE Int. Conf. Pervasive Computing*, Mar. 2014, pp. 148–155.
- [26] S. Shi, S. Sigg, and Y. Ji, "Monitoring of attention from ambient FM-radio signals," *IEEE Pervasive Comput.*, vol. 13, no. 1, pp. 30–36, Jan.–Mar. 2014.
- [27] F. Adib and D. Katabi, "See through walls with WiFi!" in *Proc. ACM SIGCOMM Conf. Applications, Technologies, Architectures and Protocols for Computer Communication*, Hong Kong, Aug. 2013, pp. 75–86.
- [28] Q. Pu, S. Gupta, S. Gollakota, and S. Patel, "Whole-home gesture recognition using wireless signals," in *Proc. ACM Int. Conf. Mobile Computing and Networking*, Miami, FL, Sept. 2013, pp. 27–38.
- [29] H. Hashemi, M. McGuire, T. Vlasschaert, and D. Tholl, "Measurements and modeling of temporal variations of the indoor radio propagation channel," *IEEE Trans. Veh. Technol.*, vol. 43, no. 3, pp. 733–737, Aug. 1994.
- [30] R. Igual, C. Medrano, and I. Plaza, "Challenges, issues and trends in fall detection systems," *Biomed. Eng. Online*, vol. 12, no. 66, pp. 1–66, 2013.

Klaus Witrisal, Paul Meissner, Erik Leitinger, Yuan Shen,
Carl Gustafson, Fredrik Tufvesson, Katsuyuki Haneda, Davide Dardari,
Andreas F. Molisch, Andrea Conti, and Moe Z. Win

High-Accuracy Localization for Assisted Living

5G systems will turn multipath channels from foe to friend

Asisted living (AL) technologies, enabled by technical advances such as the advent of the Internet of Things, are increasingly gaining importance in our aging society. This article discusses the potential of future high-accuracy localization systems as a key component of AL applications. Accurate location information can be tremendously useful to realize, e.g., behavioral monitoring, fall detection, and real-time assistance. Such services are expected to provide older adults and people with disabilities with more independence and thus to reduce the cost of caretaking. Total cost of ownership and ease of installation are paramount to make sensor systems for AL viable. In case of a radio-based indoor localization system, this implies that a conventional solution is unlikely to gain widespread adoption because of its requirement to install multiple fixed nodes (anchors) in each room. This article therefore places its focus on 1) discussing radiolocalization methods that reduce the required infrastructure by exploiting information from reflected multipath components (MPCs) and 2) showing that knowledge about the propagation environment enables localization with high accuracy and robustness. It is demonstrated that new millimeter-wave (mm-wave) technology, under investigation for 5G communications systems, will be able to provide centimeter (cm)-accuracy indoor localization in a robust manner, ideally suited for AL.

Such services are expected to provide older adults and people with disabilities with more independence and thus to reduce the cost of caretaking. Total cost of ownership and ease of installation are paramount to make sensor systems for AL viable. In case of a radio-based indoor localization system, this implies that a conventional solution is unlikely to gain widespread adoption because of its requirement to install multiple fixed nodes (anchors) in each room. This article therefore places its focus on 1) discussing radiolocalization methods that reduce the required infrastructure by exploiting information from reflected multipath components (MPCs) and 2) showing that knowledge about the propagation environment enables localization with high accuracy and robustness. It is demonstrated that new millimeter-wave (mm-wave) technology, under investigation for 5G communications systems, will be able to provide centimeter (cm)-accuracy indoor localization in a robust manner, ideally suited for AL.

Introduction

The robust provisioning of accurate location information is a key enabler for AL systems. A recent survey on ambient intelligence in health care [1] illustrates the wide range of applications that could be supported by a cm-accuracy indoor positioning system alone: activity recognition, behavioral pattern discovery, anomaly detection, and decision support methods can all be based on such a sensor modality. Application examples include behavioral monitoring to assess the physical and mental health of individuals, emergency (fall) detection to alert caretakers or emergency services, real-time assistance to provide context awareness to medication management systems (as a reminder—for instance—to take medications

IMAGE LICENSED BY INGRAM PUBLISHING
WOMAN—©ISTOCKPHOTO.COM/SILVIAHANSEN



Digital Object Identifier 10.1109/MSP.2015.2504328
Date of publication: 7 March 2016

before/during/after meals) or as an orthotic and rehabilitation tool for individuals suffering from cognitive decline, geofencing for people with dementia, and even as a navigation aid for visually impaired (see [1] and the references therein).

However, as of today, the technologies for indoor localization have not converged toward a unique winning approach, hence, the topic is still a subject of research and competitions [2]. Among the many location sensing methods proposed [3]–[9], active or passive radiolocalization are most promising, because radio transceivers can be integrated in existing devices like smartphones and built at small form factors with low power consumption. In active localization, devices to be localized are equipped with a radio device participating in the communication, which is not the case in passive localization [10]. Video cameras and microphones [11]–[13], for example, suffer from occlusions and a lack of acceptance because of privacy concerns. But the influence of the dense multipath radio channel in indoor environments still makes accurate and robust radiolocalization a challenging task. Ultrawideband (UWB) signals have been shown to deliver excellent accuracy, since they allow for a separation of the MPCs [14]–[17]. On the one hand, the direct signal path can be isolated from interfering MPCs; on the other hand, position-related information in later-arriving MPCs becomes accessible as well and turned into an advantage [18].

Unfortunately, dedicated technology is required to implement traditional UWB systems operating in the microwave band (at 3.1–10.6 GHz). With the advent of mm-wave communications in the 60-GHz band [19]–[21], a UWB localization system could operate synergetically with an existing communication system, e.g., using the IEEE 802.11ad standard [22]. Furthermore, 60-GHz regulations allow much higher transmit power compared to microwave UWB systems. Beamforming technologies proposed for these systems [19] perfectly complement the needs of the localization system and vice versa: also, the beamforming

algorithms will benefit from the location information and from environmental radio maps, i.e., spatial characterizations of the propagation channel that can be estimated and tracked in real time. Location awareness is created, which is beneficial for different layers of the protocol stack of a communications system [23].

The reduction of the required infrastructure is of key importance for a viable localization system for AL. At the same time, localization with high accuracy and robustness is needed. This article discusses a range of multipath-assisted localization approaches that actively take environmental propagation information into account to cope with these seemingly conflicting requirements. Even with only a single anchor node within each room, highly accurate and robust location estimates can be obtained [18], [24], [25]. As a side effect, this method also reduces the amount of electromagnetic radiation, possibly increasing its acceptance by users. High accuracy and robustness are more easily achieved with active systems [18], [24] where the user has to wear, e.g., a bracelet as illustrated in Figure 1, while passive systems [25], [26] prevent the risk of lacking user compliance.

The following issues are highlighted in this article:

- A model of the received signal using a geometry-based stochastic channel model and the concept of virtual sources/anchors. This leads to an environment model that describes the localization capability in a specific environment.
- Performance limits for indoor localization employing multipath propagation, showing the relevance of geometrically modeled MPCs.
- Algorithms for multipath-assisted localization and tracking: maximum likelihood localization, tracking filters with data association, algorithms for passive localization, and multitarget identification.
- Experimental and numerical results demonstrating the localization accuracy and robustness using a current experimental microwave-band system and the potential performance of a mm-wave system.
- Discussions and conclusions, evaluating the usefulness of the presented concepts for accurate and robust localization as a key component of an AL system.

Creating the proposed infrastructure, developing the appropriate distributed processing algorithms, and validating the applications in challenging AL environments will require significant multidisciplinary work over the coming years.

Signal models and performance bounds

A suitable signal model supporting the analysis of a multipath-assisted localization system requires a description of the geometry to address the position dependence of signal features and stochastic elements to represent signal impairments and noise. We use a geometry-based stochastic channel model to describe the signal transmitted from a mobile agent node to a fixed anchor node (or the other way around, from anchor to agent).

In addition to localization and tracking, radio signals may be used for the reconstruction of a three-dimensional map of the surrounding environment, e.g., to assist people with impaired vision capabilities.

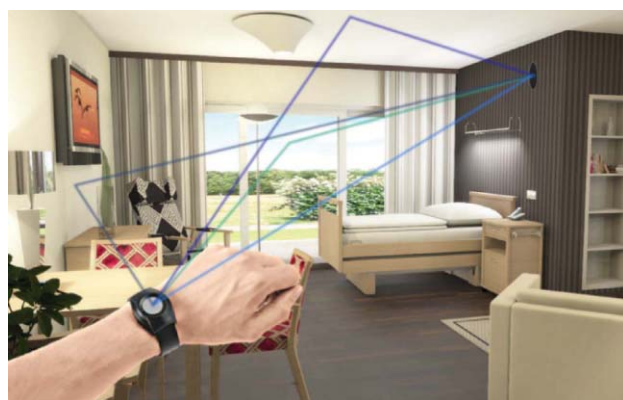


FIGURE 1. An illustration of a high-accuracy, multipath-enabled indoor localization system for AL applications. Information from reflected signals (such as the exemplary rays depicted) can be exploited if the geometry of the environment is taken into account. (Images used with permission; rendering: www.lauenstein-planungen.de; photo: www.aktivwelt.de.)

The received signal is modeled as a convolution of a UWB transmit pulse $s(t)$ with the channel

$$r(t) = \sum_{k=1}^K \alpha_k s(t - \tau_k) + s(t) * \nu(t) + w(t), \quad (1)$$

where the sum accounts for K -deterministic MPCs with complex amplitudes $\{\alpha_k\}$ whose delays $\{\tau_k\}$ yield useful position-related information, while the stochastic process $\nu(t)$ represents diffuse multipath (DM), which is interference to these useful components. The signal $w(t)$ denotes white Gaussian measurement noise at power spectral density (PSD) N_0 . We assume a unit-energy pulse $s(t)$, such that the energy of the k th MPC is given as $|\alpha_k|^2$. DM is everything that is not or cannot be described by the deterministic components. It is modeled as a (Gaussian) random process with autocovariance $E\{\nu(t)\nu^*(\tau)\} = S_\nu(\tau)\delta(t - \tau)$, where $S_\nu(\tau)$ is a power delay profile (PDP) accounting for the nonstationary variance of the DM in the delay domain [27].

We assume that the result of a possible linear beamformer is already incorporated in $r(t)$. Beamforming will have an impact on the energies $|\alpha_k|^2$ and the DM, but, for simplicity, we do not indicate these dependencies in our equations.

To describe the localization environment, we propose a model for the signal-to-interference-plus-noise ratios (SINRs) of MPCs along with their propagation delays. The delays are deterministically related to the geometry at hand. We model the delay τ_k of the k th MPC using a virtual anchor (VA) [28], [18] at position \mathbf{a}_k , yielding $\tau_k = 1/c\|\mathbf{p} - \mathbf{a}_k\|$, where \mathbf{p} is the position to be determined and c is the speed of light. For reflections at plane surfaces, the positions of the VAs can be computed straightforwardly: physical anchors are simply mirrored with respect to the planes; iterated mirroring operations account for higher-order reflections [27].

The SINR of the k th component is defined as

$$\text{SINR}_k = \frac{|\alpha_k|^2}{N_0 + T_p S_\nu(\tau_k)}, \quad (2)$$

relating the useful MPC energy $|\alpha_k|^2$ to the combined effects of the noise and the interfering DM. The latter is characterized by its PDP at the corresponding delay. The influence of the DM scales with the effective pulse duration T_p , i.e., with the inverse of the bandwidth of the measurement signal.

The model for the received signal in (1) enables the derivation of a Cramér–Rao lower bound (CRLB) on the position estimation error. (The derivation is briefly discussed in “Derivation of the PEB.”) Using the information inequality, we obtain a bound for the position error as $E_{\mathbf{r}|\mathbf{p}}\{\|\hat{\mathbf{p}} - \mathbf{p}\|^2\} \geq \text{tr}\{\mathbf{J}_p^{-1}\}$, where the square root of the right-hand side is defined as the position error bound (PEB), $\hat{\mathbf{p}}$ is the estimated position, and \mathbf{J}_p is the equivalent Fisher information matrix (EFIM) [29]–[32]. The EFIM can be written under the assumption of resolvable, “nonoverlapping” MPCs in the form [27]

$$\mathbf{J}_p = \frac{8\pi^2\beta^2}{c^2} \sum_{k=1}^K \text{SINR}_k \mathbf{J}_r(\phi_k), \quad (3)$$

where β denotes the effective (root mean square) bandwidth of the measurement signal and $\mathbf{J}_r(\phi_k)$ is a rank-one matrix with an eigenvector pointing along the angle of arrival (AoA) ϕ_k of the k th MPC. This simple, canonical form of the EFIM allows for important conclusions regarding localization:

- Each geometrically modeled (deterministic) MPC yields additional position-related information that is quantified by its SINR value. In fact, the range \hat{d}_k estimated from the k th MPC has an error variance bounded as $\text{var}\{\hat{d}_k\} \geq c^2/(8\pi^2\beta^2\text{SINR}_k)$; i.e., the SINRs indicate the uncertainties of the MPC ranges.
- The equations relate to the system parameters (e.g., bandwidth expressed by β and T_p), the environment model (the SINR values), and the geometry (the AoAs) and, thus, indicate the expected performance in a specific scenario.

Figure 2 shows an evaluation of the PEB according to (3) for a single fixed anchor for SINR values estimated from measured channel impulse response data [33]. The evaluation takes into account the visibility of the VAs across the floor plan, but it assumes a “global” model of SINRs for the entire room shown. To create a more detailed picture, one could estimate individual SINR-sets for different parts of a room or even estimate the SINR values online [34]. Two-dimensional (2-D) positioning is considered here; the measurement data have been acquired over a bandwidth of 2 GHz at a 7 GHz carrier [33]. According to this result, the expected precision lies between 1–10 cm for most of the area.

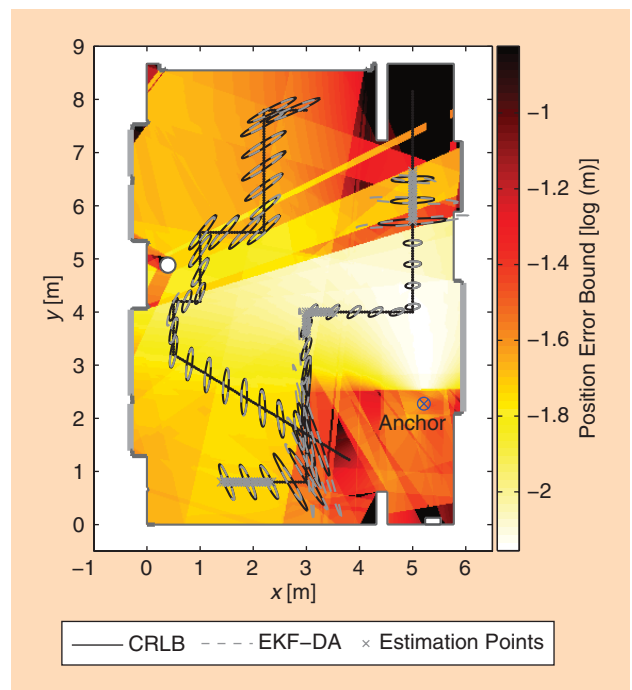


FIGURE 2. The PEB and tracking results for $T_p = 0.5$ ns, $f_c = 7$ GHz, and a single fixed anchor. The PEB (3) has been computed from estimated SINRs (2); gray crosses are 60 positions used for this SINR estimation [18]. Solid and dashed ellipses denote the standard deviation ellipses corresponding to the CRLB and to the error covariance matrices of an extended Kalman tracking filter, respectively, at several points along two trajectories. These ellipses are enlarged by a factor of 20 for better visibility.

Derivation of the PEB

The CRLB is a lower bound on the error variance of a parameter estimator. It is obtained from the second derivative of the log of the measurement likelihood function with respect to (w.r.t.) the estimation parameters, quantifying the curvature of this likelihood function. For an unbiased estimator, this curvature relates to the potential measurement precision [48]. Assuming zero-mean complex Gaussian noise processes, a likelihood function derived from a discrete-time version of the signal model (1) can be written as

$$f(\mathbf{r}|\boldsymbol{\phi}) \propto \exp\{-\mathbf{r} - \mathbf{S}\boldsymbol{\alpha}\}^H \mathbf{C}_n^{-1} (\mathbf{r} - \mathbf{S}\boldsymbol{\alpha}), \quad (S1)$$

where \mathbf{r} is the received signal sampled at rate $1/T_s$, the parameter vector $\boldsymbol{\phi} = [\boldsymbol{\alpha}^T, \boldsymbol{\tau}^T]^T$ stacks the complex amplitudes $\{\alpha_k\}$ and delays $\{\tau_k\}$, $\mathbf{S} = [s_{\tau_1}, \dots, s_{\tau_K}] \in \mathbb{R}^{N \times K}$ is the signal matrix containing delayed versions $s_{\tau_k} = [s(-\tau_k), s(T_s - \tau_k), \dots, s((N-1)T_s - \tau_k)]^T$ of the sampled transmit pulse, and the matrix $\mathbf{C}_n = \sigma_n^2 \mathbf{I}_N + \mathbf{C}_c \in \mathbb{R}^{N \times N}$ denotes the covariance matrix of the noise processes. The elements of the DM covariance matrix are given by $[\mathbf{C}_c]_{n,m} = T_s \sum_{i=0}^{N-1} S_v(iT_s) s(nT_s - iT_s) s(mT_s - iT_s)$; the AWGN samples have variance $\sigma_n^2 = N_0/T_s$.

A number of analytical manipulations are needed to obtain the insightful expressions (2) and (3) for the CRLB. First of all, it can be intuitively argued that (S1) satisfies the regularity condition required for the CRLB derivation [48] for all points within the room: considering a correct geometry and a sufficiently large signal bandwidth, the likelihood has a maximum at the true position whose spatial extent is small w.r.t. the room dimensions. It can be shown that the regularity condition is satisfied even without these assumptions, but this is out of the scope of this article. The difficulty in the derivation of the CRLB lies in finding the inverse of the covariance matrix \mathbf{C}_n . Under the assumption that the useful components in (1) are nonoverlapping, it is fair to

assume that each of these components can be observed independently. The DM process is then treated as stationary for each MPC at a variance defined by the PDP at the MPC's corresponding excess delay, $S_v(\tau_k)$. We can then use the Fourier transform to compute the inverse and obtain for the Fisher information of the k th delay estimate the expression [27]

$$\mathbb{E}_{\mathbf{r}|\boldsymbol{\phi}} \left\{ -\frac{\partial^2 \ln f(\mathbf{r}|\boldsymbol{\phi})}{\partial \tau_k \partial \tau_k} \right\} \approx 8\pi^2 |\alpha_k|^2 \int_f f^2 \frac{|S(f)|^2}{N_0 + S_v(\tau_k) |S(f)|^2} df$$

$$\stackrel{\text{(BS)}}{=} 8\pi^2 \beta^2 \text{SINR}_k, \quad (S2)$$

where $\beta^2 = \int_f f^2 |S(f)|^2 df$ is the mean square bandwidth of the Fourier transform $S(f)$ of pulse $s(t)$, $\text{SINR}_k = |\alpha_k|^2 / (N_0 + T_p S_v(\tau_k))$ is the SINR of the k th MPC. The second line only holds for a block spectrum (BS) $|S(f)|^2 = T_p$ for $|f| \leq 1/(2T_p)$; a generalized version of this equation has been derived in [27].

To compute the EFIM for the position vector from the Fisher information matrix of the parameter vector $\boldsymbol{\phi}$, we evoke the matrix inversion lemma to account for the nuisance parameters $\{\alpha_k\}$ and a parameter transformation to convert the delays $\{\tau_k\}$ to the position vector \mathbf{p} [30]. The latter requires the computation of the Jacobian $\mathbf{H} = \partial \boldsymbol{\tau} / \partial \mathbf{p}$, the derivative of the delays $\{\tau_k\}$ w.r.t. position \mathbf{p} . It describes the variation of the delays w.r.t. the position and can assume different, scenario-dependent forms, depending on the roles of anchors and agents. General expressions for these spatial delay gradients have been derived in [27]. For an MPC arriving from direction ϕ_k we get $\partial \tau_k / \partial \mathbf{p} = \mathbf{e}(\phi_k)$ with unit-norm vector $\mathbf{e}(\phi_k)$ pointing in direction ϕ_k , which leads to the matrices $\mathbf{J}_r(\phi_k) = \mathbf{e}(\phi_k) \mathbf{e}^T(\phi_k)$ in (3).

Figure 2 provides a prediction of the spatial distribution of the achievable performance. It can be considered as an indication for the robustness of the localization system for a specific environment. As mentioned in the section “Signal Models and Performance Bounds,” the set of VAs and the quantification of their relevance as given by the SINR model represents an environment model that reflects the potential localization accuracy. Using (2) and (3), the influence of system parameters, such as the signal bandwidth, can be quantified.

Algorithms for multipath-assisted environment-aware localization

For the practical application of a multipath-assisted positioning and tracking system, two core challenges need to be tackled:

- Algorithms are needed that can properly exploit the position-related information provided by each MPC.
- Algorithms are needed that can estimate the required side information, i.e., the environment model.

Efficient solutions must be able to capture the relevant information from measurements at a reasonable computational complexity.

Multipath-assisted localization and tracking

Figure 3 shows the block diagram of a multipath-assisted tracking scheme that is based on a Bayesian tracking filter [18], [33]. A core component of this scheme is the data association block. It associates, at each timestep n , the arrival times of a number of MPCs to the predicted delays. The

arrival times (collected in the set \mathcal{Z}_n) are estimated from the received signal $r_n(t)$ by a high-resolution maximum-likelihood channel estimation (MLE) algorithm; the predicted delays are computed from the VA positions $\{\mathbf{a}_k\}$ (collected in the set \mathcal{A}_n) and the predicted agent position $\hat{\mathbf{p}}_n^-$. The data association is needed to identify the potential (virtual) signal sources, to discard false detections due to DM, and to ignore missing arrival-time measurements. It has been accomplished in [18] and [33] using a constrained optimal subpattern assignment approach [35]. This means that the predicted and estimated MPC delays are matched using combinatorial optimization with the constraint that associations at a distance larger than a so-called cut-off distance are discarded. The output of the data association block, i.e., the positions of the associated VAs $\mathcal{A}_{n, \text{ass}}$ and corresponding MPC delays $\mathcal{Z}_{n, \text{ass}}$, are fed into the tracking algorithm as measurement inputs.

In the upper branch of the block diagram, the SINR model is updated, which reflects the reliability of the range measurements: the SINRs are estimated using past measurements of the MPC amplitudes [34]. The SINRs can also be estimated from offline training data [18]. Using this side information, the tracking filter can perform an appropriate measurement weighting of the extracted delays [18]. Furthermore, the SINRs allow for relevance determination: the overall set of VAs \mathcal{A}_n can be reduced to a set of relevant VAs $\tilde{\mathcal{A}}_n$. Also geometric considerations, like the visibilities of certain VAs, can be incorporated at this stage [33].

Figure 4 illustrates the efficiency of this approach based on experimental data in the microwave-UWB at a bandwidth of 2 GHz [18], [33]. It compares the CDFs of the position errors for algorithms having different levels of environment models available. The data have been obtained on 25 measurement trajectories with two fixed anchors. Trajec-

tory points were spaced by 5 cm, while the different trajectories were obtained by shifting the entire tracks in 1-cm steps. An algorithm that exploits SINR information (red curves) obtains excellent robustness and accuracy: all 25 runs have similar performance with 90% of the errors below 4 cm. Without SINR information (black and gray), ten of 25 runs diverge. This occurs mostly in a short part of the trajectory where the line-of-sight (LOS) to one of the anchors is lost, being a strong indication of a reduced robustness. The overall CDF for the 15 nondiverging runs is shown by the black bold dashed line; 90% of the errors are within 7 cm. Tracking results are also observable in Figure 2, showing two example trajectories and the performance using only a single anchor. The standard deviation ellipses of the tracking filter match those corresponding to the CRLB and indicate the relevance of position information available in different directions.

Figure 4 also shows the influence of a correction of the VA positions, which has been done to refine the environment model in comparison to a VA model computed from the floor plan. A maximum a posteriori (MAP) estimator has been used for this refinement, employing a set of training data at known locations. The performance without this MAP refinement is indicated by the blue dash-dotted curve. It shows a similar robustness but a reduced accuracy. We see this result as an evidence that the SINR model improves the robustness, while the VA-position refinement is needed to optimize the accuracy.

The environment model, e.g., the SINR information, is the key to obtaining efficient tracking algorithms; not only in terms of achieving optimal performance, but also in terms of complexity. The set of relevant VAs in a scenario is significantly smaller than the overall set of VAs that would be taken into account by visibility considerations [18] (usually, the number

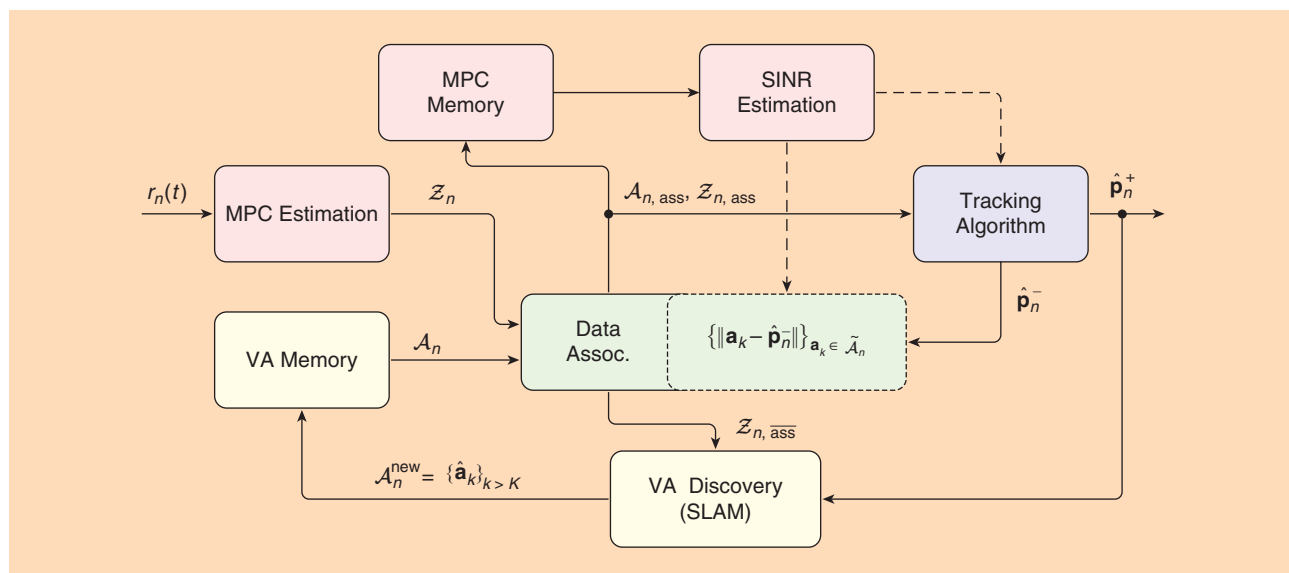


FIGURE 3. A block diagram of state space tracking and data association scheme using MPC range estimates. The input is the received signal $r_n(t)$, the overall output is the estimated agent position $\hat{\mathbf{p}}_n^+$ at time step n . The estimation is performed using the environment model represented by the memory blocks.

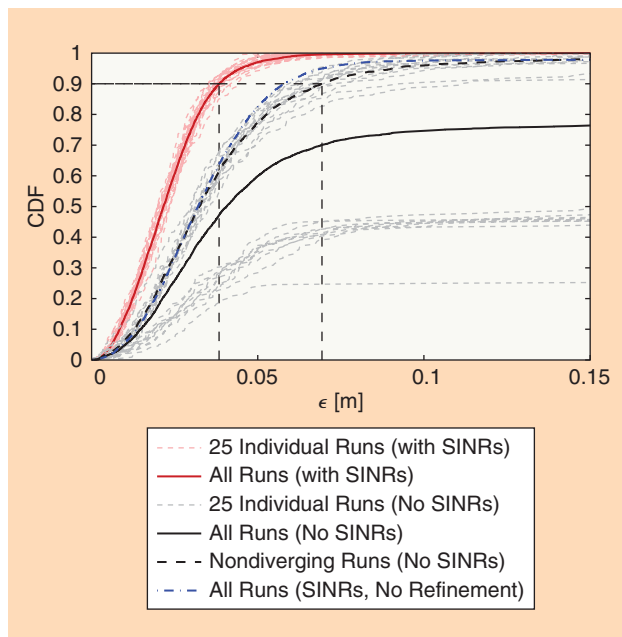


FIGURE 4. CDFs of the position error $\epsilon = \|\hat{\mathbf{p}}_n^+ - \mathbf{p}_{\text{true}}\|$ for $T_p = 0.5$ ns and $f_c = 7$ GHz. Thin dashed lines show the individual 25 runs over the trajectories. Red and gray indicate the performance of the EKFs with and without estimated SINRs. Bold lines denote the total performance for all runs, the dashed line indicates the performance without SINRs on all nondiverging runs (15 out of 25).

of MPCs carrying relevant information is on the order of five to ten per radio link for the scenarios considered). By also considering the uncertainty of the VA positions in the environment model, i.e., including the VAs to the state space, the position refinement can be done online at low complexity [34], eliminating the need for training measurements. Processing steps such as environment model tracking and relevance determination are potential features of a cognitive localization system. Cognition is aimed at understanding the surrounding world as found, for instance, in human visual perception (cf. [36] and [37]).

The presented tracking approach naturally makes use of the position estimate obtained in the previous time step. Hence, an initialization strategy is also needed, i.e., a localization algorithm. Reference [24] proposes a maximum likelihood estimation algorithm based on (SI). The important role of DM is taken into account by directly estimating the corresponding PDP $S_V(\tau)$ from the sampled received signals. No data association is necessary, since the entire received signal is used. In this way, a similar performance is achieved as in Figure 4. Examples of the likelihood as a function of position \mathbf{p} are shown in the section “Analysis of mm-Wave Localization Systems for Assisted Living” for mm-wave measurements.

This maximum likelihood approach can also be used in a tracking manner, resulting in particle-filter-based implementations of the scheme in Figure 3. Although such algorithms have increased computational complexity, they provide enhanced robustness because the particles can represent multiple position hypotheses. This helps to avoid cases where Kalman filter-based schemes diverge.

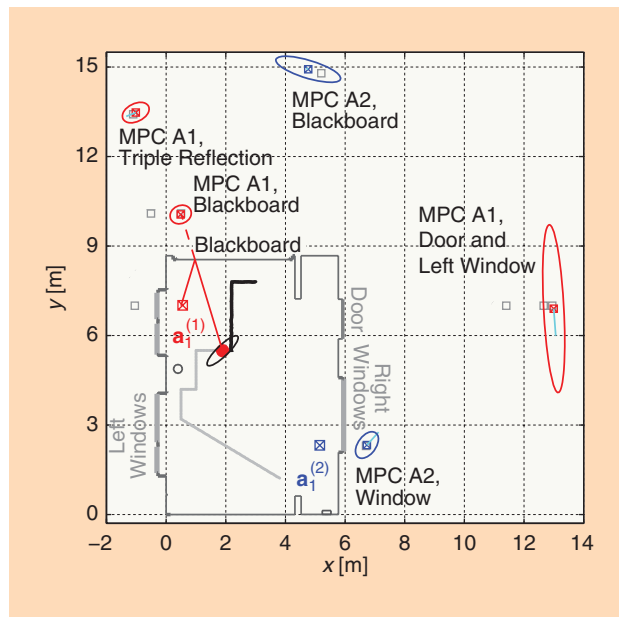


FIGURE 5. An illustration of the environment map obtained by a simultaneous localization and mapping (SLAM) algorithm. Two anchors at $\mathbf{a}_1^{(1)}$ and $\mathbf{a}_1^{(2)}$ represent the infrastructure. The agent position as well as the floor plan (represented by VAs) are estimated using specular multipath, for which one example path is shown. Gray squares indicate geometrically expected VAs, blue and red square-cross markers with uncertainty ellipses (30-fold) represent discovered VAs. An agent tracking result is shown in black with an error ellipse (100-fold).

Simultaneous localization and mapping using multipath channel information

How the environment model information can be obtained in practice remains a problem. In particular, in AL scenarios, plug-and-play installation is of prime importance. That is, ideally, the environment model has to be acquired “online” while the system is in operation. Simultaneous localization and mapping (SLAM) is a well-known approach to learn a map of the environment with a mobile agent and, at the same time, localize the agent within this map [38]. Its application to multipath-assisted indoor localization is discussed in [34]. In this case, the learned map contains the data of the environment model, the VA positions, and the SINR values; i.e., the requirement of plug-and-play installation is fulfilled. In [39], a structure-from-motion approach has been proposed to also estimate the agent and (virtual) anchor locations simultaneously from a set of UWB measurements.

The SLAM algorithm presented in [34] includes map features (the VA positions) within a joint state-space of a tracking filter with the agent and thus updates the VAs whenever new data are available. Again, a data association is needed for this purpose, which has been accomplished by a similar subpattern assignment approach as previously discussed. Sets of associated past measurements are then used to estimate the current SINR values. Nonassociated measurements $\mathcal{Z}_{n, \text{ass}}$, on the other hand, are grouped by their delays and used to compute candidate VAs that will be included in the environment model, if observed for a sufficiently long time. These new VAs are described by the set $\mathcal{A}_n^{\text{new}}$ shown in Figure 3.

Reference [34] demonstrated that a 2-D-map can be constructed with no prior information about the scenario other than the absolute positions of two fixed anchors. Figure 5 shows an illustrative example of this SLAM approach, which has been obtained from the same measurement data as the CDFs in Figure 4. Gray squares indicate the positions of some expected VAs computed from the floor plan. Discovered VAs are shown by red (Anchor 1) and blue (Anchor 2) square-cross markers; their marginal position covariance matrices are indicated by standard deviation ellipses, enlarged by a factor of 30 for better visibility. The corresponding true agent trajectory is indicated in gray. The current estimated agent position is shown by the red dot; its standard deviation ellipse is in black (enlarged by a factor of 100).

As shown in the figure—after 68 time steps—a number of relevant VAs have been identified that match very well with the geometrically computed VAs. Some of these VAs have only been associated for a few time steps, corresponding to rather large variances due to large geometric dilution of precision and/or low SINR values (e.g., MPC “A1 door and left window”). On the other hand, some VAs already have converged accurately to their true location (e.g., MPC “A1 blackboard”). Falsely discovered VAs often show a very large variance of their associated amplitudes, corresponding to a low SINR. Thus, their influence on the tracking process remains limited. The overall tracking performance almost matches up the performance of the approach discussed in Figure 4, and 90% of the errors are within 4.4 cm. Assuming the availability of side information, e.g., from an inertial measurement unit, we expect that the robustness of this SLAM algorithm against divergence gets even higher.

Passive localization exploiting multipath

As mentioned previously, passive localization has the great advantage that no specific user compliance is necessary—in other words, the person to be helped does not need to remember to carry a specific device. At the same time, the passive principle makes it more challenging to handle multipath. While in an active system, localization can be achieved based on the triangulation with LOS paths, in passive localization we have to base it on “direct paths” that go from the transmitter, via reflection at the target, to the receiver. Furthermore, these “direct paths” are embedded in background paths—paths that propagate from transmitter to receiver without participation of the target—and the delay of the background paths can be larger or smaller than those of the direct path. Second, there are also indirect paths, which involve reflection at both target and additional objects. And analogously to active localization, where the LOS path might be shadowed off, the direct path might be blocked. This overall makes target localization much more difficult.

Despite these difficulties, passive vital sign monitoring has a long history (the main motivation used to be in a military/surveillance context, but the principles can be applied to AL as well). Narrowband Doppler radar was already being used to detect the presence of breathing beginning in the 1970s.

However, this does not allow the localization of the breathing person and is of somewhat limited utility for AL applications. A more promising approach seems to be the use of wideband multiple-input, multiple-output (MIMO) radar. Reference [40] demonstrated a prototype that could precisely localize a person and track the small-scale movement of the chest that occurs during breathing from a distance of several meters away. This was enabled with a sounding waveform extending over 7-GHz bandwidth (within the UWB band from 3 to 10 GHz), combined with an eight-element transmit array and high-resolution (iterative maximum-likelihood estimation) evaluation. Most noteworthy, the localization can be achieved without a direct path, as long as the environment (location of walls, etc.) is known. The figures in [40] demonstrate the relative location of the echo reflected from the head and chest when the target is breathing in/out.

The situation is more difficult when more than one possible target is present. In contrast to active devices that send out unique signatures and allow identification of all associated signals, it is difficult (and often impossible) to distinguish between the MPCs belonging to different targets. Such multitarget localization is another difficult but important problem—obviously, in many AL situations (e.g., eldercare homes), multiple targets might be present simultaneously, and if they are moving, their trajectories might intersect. From an algorithmic point of view, we have to distinguish the cases where transmitter and receiver have multiple antenna elements (and can resolve directions of the echoes), versus the (much more difficult) case of distributed single-antenna transceivers (e.g., [41]).

In addition to localization and tracking, radio signals may be used for the reconstruction of a three-dimensional map of the surrounding environment, e.g., to assist people with impaired vision capabilities. This is, of course, strongly related to the mapping task of the SLAM approach. The passive reflections of the radio waves from the environment are exploited together with additional reflections from targets and walls. A single sensor through-the-wall radar with data association is discussed in [25], multipath-assisted through-the-wall imaging in [26]. The suitability of UWB radars for mapping, imaging, and also breathing detection was shown in [42]. Recently, the concept of personal radar has been proposed as a smartphone-centric low-cost solution for the navigation and mapping problem [43]. Personal radar could be an additional feature offered by 5G smartphones, exploiting mm-wave massive antenna arrays with electronic pencil-beam steering capability and high ranging accuracy. The small wavelength of mm-wave technology permits the packing of a massive antenna array in pocket-size space [44]. In fact, mm-wave technologies could provide a most suitable platform for the purpose of high-accuracy localization for AL, as discussed next.

Analysis of mm-wave localization systems for assisted living

Insights gained so far show the promising features of a multipath-assisted indoor localization system. However, the

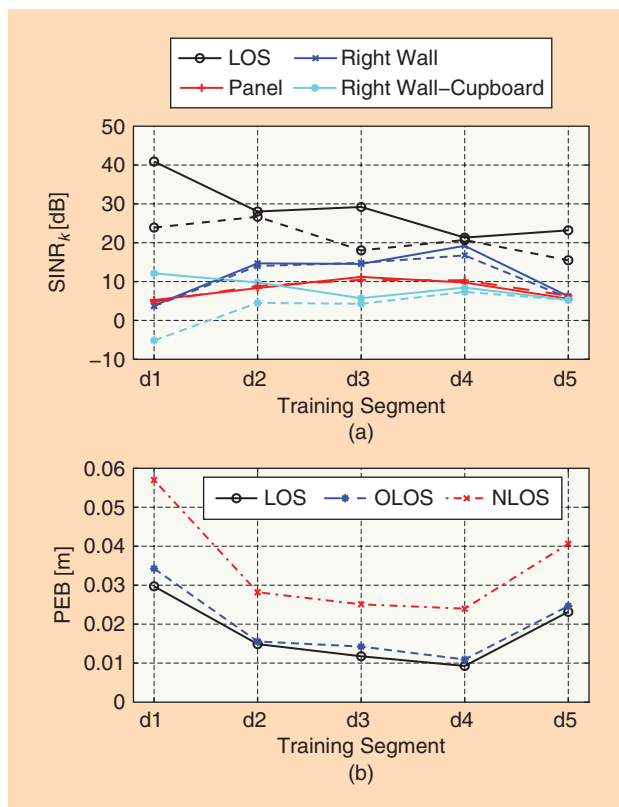


FIGURE 6. (a) Estimated SINRs of selected reflections using $T_p = 0.5$ ns and $f_c = 63$ GHz and (b) PEB for LOS, OLOS, and NLOS (complete lack of the LOS component) scenarios. Solid lines indicate LOS measurements; while dashed and dash-dotted lines correspond to OLOS and NLOS measurements, respectively. The x-axis labeling refers to the measurement sets acquired at different positions d_1, d_2, \dots, d_5 as reported in [19] and [20].

price to pay is a very large signal bandwidth to enable the separation of MPCs at sufficiently high SINRs. Microwave-band UWB systems can fulfill this promise, but their mass-market adoption seems unlikely [9] given the recent developments of indoor wireless systems. For conventional wireless systems, it would also be possible to utilize the phase evolution of the MPCs for precise localization and tracking [45]. This technique, however, requires large arrays for separating the MPCs at moderate bandwidths and might not be relevant in an AL context. On the other hand, 5G wireless systems will include UWB radios in the mm-wave frequency band. The IEEE 802.11ad standard [22], for example, already defines an air-interface for a 2-GHz bandwidth system in the 60-GHz frequency band. Beamforming and tracking of MPCs are key elements of such systems. Despite the promising features of mm-wave systems for localization, only few papers address this aspect so far, and even fewer discuss measurement data and realistic channel models [46], [47].

This section highlights the great potential of mm-wave technologies for realizing multipath-assisted indoor localization. We analyze, for this purpose, exemplary measurement

data discussed in [19] and [20] that mimic the intended AL application scenario. It is shown that a single access point provides enough position-related information to enable high accuracy localization. A properly parameterized environment model is a key ingredient to achieve this.

Measurement scenario and setup

The mm-wave channel measurements of [19] and [20] are MIMO measurements with 7×7 locations on both transmitter (TX) and receiver (RX) sides obtained by a vector network analyzer. In the intended application, one array assumes the role of the agent to be localized, while the other corresponds to the anchor, i.e., the fixed infrastructure. The measurement grid on the agent side was moved to 22 different locations in the room. Both LOS and obstructed LOS (OLOS) situations have been measured; the latter were obtained using a laptop screen to shadow the direct link to the anchor. These measurements have been conducted at a center frequency of 63 GHz. To mimic the IEEE 802.11ad standard [22], we selected a subband of 2 GHz from the total measured bandwidth of 4 GHz using a raised cosine filter (cf. [33]).

Measurement results

We first analyze the SINRs of the MPCs as defined in (2), i.e., the ratio of the useful energies of the deterministic MPCs to the interference by DM and additive white Gaussian noise (AWGN). The SINRs are estimated using the technique of [18] and [33], a method of moments estimator operating directly on the MPC amplitudes. In this way, the PDP $S_\nu(\tau)$ does not explicitly have to be estimated. We use the array positions on the anchor side to provide the required signal ensemble. The array at the agent side is used to show the potential of beamforming. In a practical setup, it may be advantageous to implement the beamforming at the anchor side, i.e., at the infrastructure, where the array has a known orientation, while at the agent side, low-complexity terminals may be used that have only one or a few fixed antennas. We reverse these roles here, since the horizontal array geometry at the agent side was better suited for a proof of principle.

The estimated SINRs in Figure 6(a) show the relevance of selected MPCs in this environment for several agent positions. The LOS is the MPC providing most position-related information. Besides the fact that it is usually the strongest component of a radio channel, this significance is due to the relatively low impact of DM on the LOS component at a bandwidth of 2 GHz [33]. Interestingly, in some cases, the SINR of the LOS component drops only slightly in the OLOS situation, although its energy drops significantly (the average LOS K-factor over the estimation positions decreases from 8.9 dB to -7.4 dB). This implies that the component is still exploitable for localization. The reflected components also show significant SINRs over the estimation points but there is a considerable amount of location-dependence of the SINRs. It is more pronounced than

The reduction of the required infrastructure is of key importance for a viable localization system for AL.

for microwave band UWB measurements [33], highlighting the need for online estimation (tracking) of the environment model, as explained in the section “Simultaneous Localization and Mapping Using Multipath Channel Information” and [34].

Figure 6(b) shows the PEB corresponding to the estimated SINRs of Figure 6(a). The PEB is a measure of the potentially achievable localization accuracy, hence, highly accurate single-anchor localization is possible in this scenario. The PEB increases only slightly in the OLOS situations due to the still significant SINR of the LOS component. Even if the LOS component is not taken into account at all, (NLOS; the red dash-dotted line), the agent is still localizable at centimeter level, easily satisfying requirements of most AL applications. A proper operation in total absence of an LOS indicates the “good” robustness of the discussed techniques.

Figure 7 shows the likelihood (S_1) for a sampled received signal $r(t)$ as a function of position \mathbf{p} , evaluated over the floor plan. Figure 7(a) compares LOS and (b) OLOS conditions with (c) OLOS with the use of beamforming. The bold black lines indicate the directions to the anchor, thin black lines the directions to first-order VAs, and black dashed lines the directions to second-order VAs. The black diamonds mark the estimated positions of the agent. Using a maximum likelihood positioning algorithm as in [24], an error in the centimeter level is achieved (2 cm for the LOS and 3 cm for the OLOS situations). Only a small degradation results in the OLOS case, as anticipated from the analysis of the SINR values.

The potential use of beamforming shows a different great advantage: the multimodality of the likelihood function is reduced, which reduces the risk of converging to a wrong local maximum. Large modes at locations farther away from the true agent position are suppressed due to the angular resolution of the array antenna. Note, however, that MPC delays are still responsible for providing a high accuracy in a direction orthogonal to the LOS path. Without the processing of multipath, we would see a smooth maximum (along the circle) instead of a sharp peak. The likelihood function in Figure 7(c)

has been computed by using a phased-array beamformer for each exploited MPC. This is achieved by coherently adding the signals at the agent-side array positions, taking into account the relative phase shifts that correspond to the known arrival angles of the MPCs. The figure exemplarily shows that such a processing, envisioned for 5G mm-wave communication systems, can greatly improve the robustness of the localization, since many local maxima can be ruled out.

Discussion and conclusions

This article envisions accurate and robust indoor localization as a key sensing modality of an AL system. It has been shown that awareness to the signal propagation conditions enables the robustness and allows to reduce the needed infrastructure. Experimental, measurement-based results support the discussion of theoretical findings.

A geometry-based stochastic model of the received signal allows the derivation of theoretical PEBs and thus provides the theoretical background for a number of multipath-assisted localization and tracking algorithms. More specifically, an environment model, consisting of a geometrical model (based on VA positions) and a measurement uncertainty model (based on the SINR of MPCs), yields insight in the potential location information that can be acquired at a certain position, in a certain environment. Several algorithms have been discussed that exploit such information: maximum likelihood localization, tracking filters with data association, and algorithms for passive localization. The benefit of using this environmental information has been shown.

Future 5G mm-wave communication systems could be an ideal platform for achieving high-accuracy indoor localization with this concept. In addition to a large signal bandwidth, beamforming capabilities are envisioned for such systems, which can be exploited to make the localization and tracking more robust and efficient. It becomes feasible to obtain accurate and robust indoor localization with only a single anchor node in a

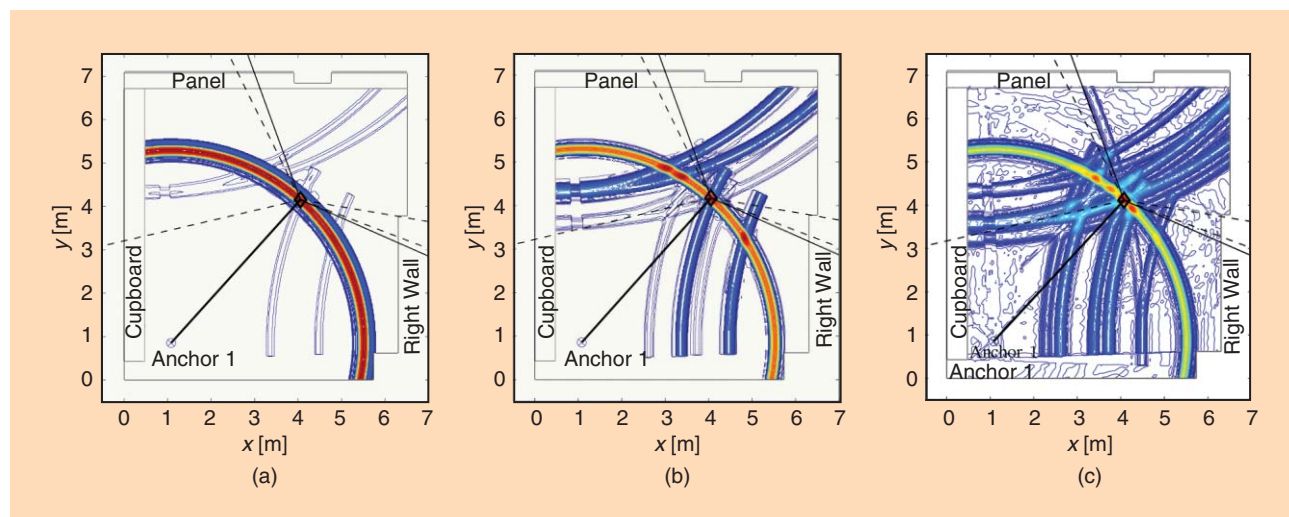


FIGURE 7. The likelihood function over the floor plan for (a) LOS, (b) OLOS situation, and (c) OLOS situation with phased-array beamforming. The position error of the MLE is 2 cm and 3 cm for LOS and OLOS situations, respectively. Bold black lines show the directions to the anchors, thin black line the directions to first-order VAs, and black dashed lines the directions to second-order VAs. The black diamonds mark the estimated positions of the agent.

room, with a system that also serves as a standard-compliant access point for 5G communications.

Note that, vice versa, the environment model can be exploited by the communications system. “Location awareness” is created by providing a site-specific propagation model that can be used to improve the robustness of the radio air-interface. For example, the arrival and departure angles of the most significant radio paths are encoded in the environment model, which will be useful for efficient beamsteering algorithms for communications in highly dynamic environments, extending the scope of the proposed concepts well beyond AL scenarios.

Acknowledgments

The work of K. Witrisal, P. Meissner, and E. Leitinger was partly supported by the Austrian Research Promotion Agency (FFG) within the project REFLEX (project number 845630) and within the Austrian COMET Competence Center FTW. The work of D. Dardari and A. Conti was supported in part by the Italian MIUR project GRETA under grant 2010WHY5PR. The work of Y. Shen and M.Z. Win was supported in part by the Office of Naval Research under grant N00014-11-1-0397. The work of A.F. Molisch was supported by ONR, NSF, and KACST.

Authors

Klaus Witrisal (witrisal@tugraz.at) received his Dipl.-Ing. degree from Graz University of Technology, Austria, in 1997, his Ph.D. degree from Delft University of Technology, The Netherlands, in 2002; and the Habilitation from Graz University of Technology, Austria, in 2009, where he is currently an associate professor. He was an associate editor of *IEEE Communications Letters*, a cochair of the TWG “Indoor” of the COST Action IC1004, a leading chair of the IEEE Workshop on Advances in Network Localization and Navigation, and TPC cochair of the Workshop on Positioning, Navigation, and Communication. His research interests are in signal processing for wireless communications, propagation channel modeling, and positioning. He is a Member of the IEEE.

Paul Meissner (paul.meissner@ieee.org) received the B.Sc. degree and Dipl.-Ing. degree (with distinction) in information and computer engineering from Graz University of Technology, Austria, in 2006 and 2009, respectively. He received the Ph.D. degree in electrical engineering (with distinction) from the same university in 2014. In 2015, he received the award of the Association of German Engineers for his Ph.D. thesis. He is currently a postdoctoral researcher at the Signal Processing and Speech Communication Laboratory of Graz University of Technology. His research topics include statistical signal processing, localization, estimation theory, and channel modeling. He is a Member of the IEEE.

Erik Leitinger (erik.leitinger@tugraz.at) received his B.Sc. degree (with distinction) in electrical engineering from Graz

Creating the proposed infrastructure, developing the appropriate distributed processing algorithms, and validating the applications in challenging AL environments will require significant multidisciplinary work over the coming years.

University of Technology, Austria, in 2009, and his Dipl.-Ing. degree (with distinction) in electrical engineering from Graz University of Technology, Austria, in 2012. He is currently pursuing his Ph.D. degree at the Signal Processing and Speech Communication Laboratory of Graz University of Technology. His research interests are in ultrawideband wireless communication, indoor positioning, estimation theory, Bayesian inference, and statistical signal processing. He is a Student Member of the IEEE.

Yuan Shen (shenyuan_ee@mail.tsinghua.edu.cn) received his B.E. degree (with highest honors) in electrical engineering from Tsinghua University, Beijing, China, in 2005, and his S.M. and Ph.D. degrees in electrical engineering and computer science from the Massachusetts Institute of Technology in 2008 and 2014, respectively. He is currently an associate professor with the Electrical Engineering Department at Tsinghua University. His research focuses on network localization and navigation, inference techniques, resource allocation, and intrinsic wireless secrecy. He is the elected secretary (2015–2017) for the IEEE ComSoc Radio Communications Committee. He is an editor of *IEEE Communications Letters* and a guest editor of *International Journal of Distributed Sensor Networks* (2015).

Carl Gustafson (carl.gustafson@eit.lth.se) received the Ph.D. degree in radio systems and M.Sc. degree in electrical engineering from the Department of Electrical and Information Technology, Lund University, Sweden, where he currently works as a postdoctoral researcher. His main research interests include channel measurements and modeling for mm-wave wireless systems, cellular systems operating above 6 GHz, and vehicular wireless communication systems. Other research interests include massive multiple-input, multiple-output, antenna array processing, statistical estimation, and electromagnetic wave propagation.

Fredrik Tufvesson (fredrik.tufvesson@eit.lth.se) received his Ph.D. degree in 2000 from Lund University, Sweden. After two years at a start-up company, he joined the Department of Electrical and Information Technology at Lund University, where he is now professor of radio systems and heads the department’s Wireless Propagation group. His main research interests are channel modeling, measurements and characterization for wireless communication, with applications in various areas such as massive multiple-input, multiple-output, ultrawideband, mm-wave communication, distributed antenna systems, vehicular communication systems, and radio-based positioning. He has authored/coauthored approximately 50 journal papers and 120 conference papers. He is a Senior Member of the IEEE.

Katsuyuki Haneda (katsuyuki.haneda@aalto.fi) received the Doctor of Engineering from the Tokyo Institute of Technology, Japan, in 2007. He is currently an assistant professor in the Aalto University School of Electrical Engineering, Finland. He was the recipient of the best paper awards in VTC2013-Spring and

EuCAP2013. He has served as an associate editor of *IEEE Transactions on Antennas and Propagation* since 2012 and as an editor of *IEEE Transactions on Wireless Communications* since 2013. His current research activity includes millimeter-wave radios, wireless for medical and postdisaster scenarios, radio wave propagation prediction, and in-band full-duplex radio technologies. He is a Member of the IEEE.

Davide Dardari (davide.dardari@unibo.it) received the Laurea degree in electronic engineering (*summa cum laude*) and the Ph.D. degree in electronic engineering and computer science from the University of Bologna, Italy, in 1993 and 1998, respectively, where he is now an associate professor. Since 2005, he has been a research affiliate at the Massachusetts Institute of Technology. His interests are on wireless communications, localization techniques, and distributed signal processing. He received the IEEE Aerospace and Electronic Systems Society's M. Barry Carlton Award (2011) and the IEEE Communications Society Fred W. Ellersick Prize (2012). He is a Senior Member of the IEEE, where he was the chair for the Radio Communications Committee of the IEEE Communication Society. He served as an editor of *IEEE Transactions on Wireless Communications* from 2006 to 2012.

Andreas F. Molisch (andreas.molisch@ieee.org) received the Dipl.-Ing., Dr. techn., and habilitation degrees from the Technical University Vienna, Austria, in 1990, 1994, and 1999, respectively. He is now a professor of electrical engineering at the University of Southern California, where he is also currently the director of the Communication Sciences Institute. His research interest is wireless communications, with an emphasis on wireless propagation channels, multiantenna systems, ultrawideband signaling and localization, novel cellular architectures, and cooperative communications. He is the author of four books, 16 book chapters, more than 420 journal and conference papers, as well as 70 patents. He is a Fellow of the American Association for the Advancement of Science, the Institution of Engineering and Technology, and the National Academy of Inventors; a member of the the Austrian Academy of Sciences; and a recipient of numerous awards.

Andrea Conti (a.conti@ieee.org) received the Laurea degree (*summa cum laude*) in telecommunications engineering and the Ph.D. degree in electronic engineering and computer science from the University of Bologna, Italy, in 1997 and 2001, respectively. He is an associate professor at the University of Ferrara, Italy. His research interests involve theory and experimentation of wireless systems and networks including network localization, adaptive diversity communications, cooperative relaying techniques, and network secrecy. He has been elected as chair of the IEEE Communications Society Radio Communications Committee and is an IEEE Distinguished Lecturer. He received the HTE Puskás Tivadar Medal, the IEEE Fred W. Ellersick Prize, and the IEEE Stephen O. Rice Prize in the Field of Communications Theory. He is a Senior Member of the IEEE.

Moe Z. Win (moewin@mit.edu) received the B.S. degree (*magna cum laude*) in electrical engineering from Texas A&M University in 1987, the M.S. degree in electrical engineering at

the University of Southern California (USC) in 1989, the M.S. degree in applied mathematics as a presidential fellow, and the Ph.D. degree in electrical engineering, both in 1998 at USC. He is a professor at the Massachusetts Institute of Technology (MIT) and the founding director of the Wireless Communication and Network Sciences Laboratory. Prior to joining MIT, he was with AT&T Research Laboratories for five years and with the Jet Propulsion Laboratory for seven years. His current research topics include network localization and navigation, network interference exploitation, intrinsic wireless secrecy, adaptive diversity techniques, and ultrawideband systems. He is an elected Fellow of the IEEE, the American Association for the Advancement of Science, and the Institution of Engineering and Technology, and was an IEEE Distinguished Lecturer.

References

- [1] G. Acampora, D. Cook, P. Rashidi, and A. Vasilakos, "A survey on ambient intelligence in healthcare," *Proc. IEEE*, vol. 101, no. 12, pp. 2470–2494, Dec. 2013.
- [2] P. Barsocchi, S. Chessa, F. Furfari, and F. Potorti, "Evaluating ambient assisted living solutions: The localization competition," *IEEE Pervasive Comput.*, vol. 12, no. 4, pp. 72–79, Oct. 2013.
- [3] P. Rashidi and A. Mihailidis, "A survey on ambient-assisted living tools for older adults," *IEEE J. Biomed. Health Inform.*, vol. 17, no. 3, pp. 579–590, May 2013.
- [4] M. Z. Win, A. Conti, S. Mazuelas, Y. Shen, W. M. Gifford, D. Dardari, and M. Chiani, "Network localization and navigation via cooperation," *IEEE Commun. Mag.*, vol. 49, no. 5, pp. 56–62, May 2011.
- [5] S. Gezici, Z. Tian, G. B. Giannakis, H. Kobayashi, A. F. Molisch, H. V. Poor, and Z. Sahinoglu, "Localization via ultra-wideband radios: A look at positioning aspects for future sensor networks," *IEEE Signal Processing Mag.*, vol. 22, no. 4, pp. 70–84, July 2005.
- [6] S. Bartoletti, W. Dai, A. Conti, and M. Z. Win, "A mathematical model for wideband ranging," *IEEE J. Sel. Top. Signal Processing*, vol. 9, no. 2, pp. 216–228, Mar. 2015.
- [7] D. Dardari, A. Conti, U. J. Ferner, A. Giorgetti, and M. Z. Win, "Ranging with ultrawide bandwidth signals in multipath environments," *Proc. IEEE*, vol. 97, no. 2, pp. 404–426, Feb. 2009.
- [8] H. Wymeersch, J. Lien, and M. Z. Win, "Cooperative localization in wireless networks," *Proc. IEEE*, vol. 97, no. 2, pp. 427–450, 2009.
- [9] A. Conti, M. Guerra, D. Dardari, N. Decarli, and M. Win, "Network experimentation for cooperative localization," *IEEE J. Sel. Areas Commun.*, vol. 30, no. 2, pp. 467–475, 2012.
- [10] S. Bartoletti, A. Giorgetti, M. Z. Win, and A. Conti, "Blind selection of representative observations for sensor radar networks," *IEEE Trans. Veh. Technol.*, vol. 64, no. 4, pp. 1388–1400, Apr. 2015.
- [11] B. U. Töreyn, Y. Dedeoğlu, and A. Çetin, "HMM based falling person detection using both audio and video," in *Computer Vision in Human-Computer Interaction* (Lecture Notes in Computer Science), N. Sebe, M. Lew, and T. Huang, Eds. Berlin; Heidelberg, Germany: Springer, 2005, vol. 3766, pp. 211–220.
- [12] D. Weinland, R. Ronfard, and E. Boyer. (2011). A survey of vision-based methods for action representation, segmentation and recognition. *Comput. Vis. Image Underst.* [Online]. 115(2), pp. 224–241. Available: <http://www.sciencedirect.com/science/article/pii/S1077314210002171>
- [13] Y. Li, K. Ho, and M. Popescu, "A microphone array system for automatic fall detection," *IEEE Trans. Biomed. Eng.*, vol. 59, no. 5, pp. 1291–1301, May 2012.

- [14] M. Z. Win and R. A. Scholtz, "Impulse radio: How it works," *IEEE Commun. Lett.*, vol. 2, no. 2, pp. 36–38, Feb. 1998.
- [15] M. Z. Win and R. A. Scholtz, "Ultra-wide bandwidth time-hopping spread-spectrum impulse adio for wireless multiple-access communications," *IEEE Trans. Commun.*, vol. 48, no. 4, pp. 679–691, Apr. 2000.
- [16] M. Z. Win and R. A. Scholtz, "Characterization of ultra-wide bandwidth wireless indoor communications channel: A communication-theoretic view," *IEEE J. Sel. Areas Commun.*, vol. 20, no. 9, pp. 1613–1627, Dec. 2002.
- [17] A. F. Molisch, D. Cassioli, C.-C. Chong, S. Emami, A. Fort, B. Kannan, J. Karedal, J. Kunisch et al., "A comprehensive standardized model for ultrawideband propagation channels," *IEEE Trans. Antennas Propag.*, vol. 54, no. 11, pp. 3151–3166, Nov. 2006.
- [18] P. Meissner, E. Leitinger, and K. Witrisal, "UWB for robust indoor tracking: Weighting of multipath components for efficient estimation," *IEEE Wireless Commun. Lett.*, vol. 3, no. 5, pp. 501–504, Oct. 2014.
- [19] S. Wyne, K. Haneda, S. Ranvier, F. Tufvesson, and A. Molisch, "Beamforming effects on measured mm-wave channel characteristics," *IEEE Trans. Wireless Commun.*, vol. 10, no. 11, pp. 3553–3559, Nov. 2011.
- [20] C. Gustafson, K. Haneda, S. Wyne, and F. Tufvesson, "On mm-wave multipath clustering and channel modeling," *IEEE Trans. Antennas Propag.*, vol. 62, no. 3, pp. 1445–1455, Mar. 2014.
- [21] A. Molisch and F. Tufvesson, "Propagation channel models for next-generation wireless communications systems," *IEICE Trans. Commun.*, vol. E97B, no. 10, pp. 2022–2034, 2014.
- [22] *ISO/IEC/IEEE International Standard for Information Technology—Telecommunications and information exchange between systems—Local and metropolitan area networks—Specific requirements—Part 11: Wireless LAN Medium Access Control (MAC) and Physical Layer (PHY) Specifications Amendment 3: Enhancements for Very High Throughput in the 60 GHz Band (adoption of IEEE Std 802.11ad-2012)*, ISO/IEC/IEEE Std. 8802-11:2012/Amd.3:2014(E), 2014.
- [23] R. Di Taranto, S. Muppirisetty, R. Raulefs, D. Slock, T. Svensson, and H. Wymeersch, "Location-aware communications for 5G networks: How location information can improve scalability, latency, and robustness of 5G," *IEEE Signal Processing Mag.*, vol. 31, no. 6, pp. 102–112, Nov. 2014.
- [24] E. Leitinger, M. Froehle, P. Meissner, and K. Witrisal, "Multipath-assisted maximum-likelihood indoor positioning using UWB signals," in *Proc. IEEE ICC Workshop on Advances in Network Localization and Navigation (ANLN)*, 2014, pp. 170–175.
- [25] P. Setlur, G. Smith, F. Ahmad, and M. Amin, "Target localization with a single sensor via multipath exploitation," *IEEE Trans. Aerosp. Electron. Syst.*, vol. 48, no. 3, pp. 1996–2014, July 2012.
- [26] M. Leigsnering, M. Amin, F. Ahmad, and A. Zoubir, "Multipath exploitation and suppression for SAR imaging of building interiors: An overview of recent advances," *IEEE Signal Processing Mag.*, vol. 31, no. 4, pp. 110–119, 2014.
- [27] E. Leitinger, P. Meissner, C. Ruedisser, G. Dumphart, and K. Witrisal, "Evaluation of position-related information in multipath components for indoor positioning," *IEEE J. Sel. Areas Commun.*, vol. 33, no. 11, pp. 2313–2328, Nov. 2015.
- [28] Y. Shen and M. Win, "On the use of multipath geometry for wideband cooperative localization," in *Proc. IEEE Global Telecommunications Conf. (GLOBECOM)*, 2009, pp. 1–6.
- [29] D. B. Jourdan, D. Dardari, and M. Z. Win, "Position error bound for UWB localization in dense cluttered environments," *IEEE Trans. Aerosp. Electron. Syst.*, vol. 44, no. 2, pp. 613–628, Apr. 2008.
- [30] Y. Shen and M. Win, "Fundamental limits of wideband localization—Part I: A general framework," *IEEE Trans. Inform. Theory*, vol. 56, no. 10, pp. 4956–4980, 2010.
- [31] Y. Shen, H. Wymeersch, and M. Win, "Fundamental limits of wideband localization—Part II: Cooperative networks," *IEEE Trans. Inform. Theory*, vol. 56, no. 10, pp. 4981–5000, 2010.
- [32] Y. Qi, H. Kobayashi, and H. Suda, "Analysis of wireless geolocation in a non-line-of-sight environment," *IEEE Trans. Wireless Commun.*, vol. 5, no. 3, pp. 672–681, 2006.
- [33] P. Meissner, "Multipath-assisted indoor positioning," Ph.D. dissertation, Faculty of Electrical and Information Engineering, Graz Univ. of Technology, 2014.
- [34] E. Leitinger, P. Meissner, M. Lafer, and K. Witrisal, "Simultaneous localization and mapping using multipath channel information," in *Proc. IEEE ICC Workshop on Advances in Network Localization and Navigation (ANLN)*, June 2015, pp. 754–760.
- [35] D. Schuhmacher, B.-T. Vo, and B.-N. Vo, "A consistent metric for performance evaluation of multi-object filters," *IEEE Trans. Signal Processing*, vol. 56, no. 8, pp. 3447–3457, 2008.
- [36] S. Haykin, "Cognitive radar: A way of the future," *IEEE Signal Processing Mag.*, vol. 23, no. 1, pp. 30–40, Jan. 2006.
- [37] K. Witrisal, E. Leitinger, P. Meissner, and D. Arnitz, "Cognitive radar for the localization of RFID transponders in dense multipath environments," in *Proc. IEEE Radar Conf.*, Ottawa, Canada, Apr. 2013, pp. 1–6.
- [38] H. Durrant-Whyte and T. Bailey, "Simultaneous localization and mapping: Part I," *IEEE Robot. Autom. Mag.*, vol. 13, no. 2, pp. 99–110, June 2006.
- [39] Y. Kuang, K. Astrom, and F. Tufvesson, "Single antenna anchor-free UWB positioning based on multipath propagation," in *Proc. IEEE Int. Conf. Communications (ICC)*, June 2013, pp. 5814–5818.
- [40] J. Salmi and A. F. Molisch, "Propagation parameter estimation, modeling and measurements for ultrawideband MIMO radar," *IEEE Trans. Antennas Propag.*, vol. 59, no. 11, pp. 4257–4267, 2011.
- [41] J. Shen and A. Molisch, "Estimating multiple target locations in multi-path environments," *IEEE Trans. Wireless Commun.*, vol. 13, no. 8, pp. 4547–4559, 2014.
- [42] R. Zetik, J. Sachs, and R. Thoma, "UWB short-range radar sensing - The architecture of a baseband, pseudo-noise UWB radar sensor," *IEEE Instrum. Meas. Mag.*, vol. 10, no. 2, pp. 39–45, Apr. 2007.
- [43] F. Guidi, A. Guerra, and D. Dardari, "Personal mobile radars with millimeter-wave massive arrays for indoor mapping," *IEEE Trans. Mobile Comput.*, vol. PP, no. 99, pp. 1–1, 2015.
- [44] W. Hong, K.-H. Baek, Y. Lee, Y. Kim, and S.-T. Ko, "Study and prototyping of practically large-scale mmWave antenna systems for 5G cellular devices," *IEEE Commun. Mag.*, vol. 52, no. 9, pp. 63–69, Sept. 2014.
- [45] M. Zhu, J. Vieira, Y. Kuang, K. Astrom, A. F. Molisch, and F. Tufvesson, "Tracking and positioning using phase information from estimated multi-path components," in *Proc. IEEE ICC Workshop on Advances in Network Localization and Navigation (ANLN)*, London, UK, June 2015, pp. 712–717.
- [46] H. El-Sayed, G. Athanasiou, and C. Fischione, "Evaluation of localization methods in millimeter-wave wireless systems," in *Proc. IEEE 19th Int. Workshop on Computer Aided Modeling and Design of Communication Links and Networks (CAMAD)*, Dec. 2014, pp. 345–349.
- [47] A. Guerra, F. Guidi, and D. Dardari, "Position and orientation error bound for wideband massive antenna arrays," in *Proc. IEEE ICC Workshop on Advances in Network Localization and Navigation (ANLN)*, 2015, pp. 853–858.
- [48] S. Kay, *Fundamentals of Statistical Signal Processing: Estimation Theory* (Prentice Hall Signal Processing Series, vol. 1). Upper Saddle River, NJ: Prentice Hall, 1993.

Moeness G. Amin, Yimin D. Zhang,
Fauzia Ahmad, and K.C. (Dominic) Ho

Radar Signal Processing for Elderly Fall Detection

The future for in-home monitoring

Radar is considered an important technology for health monitoring and fall detection in elderly assisted living due to a number of attributes not shared by other sensing modalities. In this article, we describe the signal processing algorithms and techniques involved in elderly fall detection using radar. A human's radar signal returns differ in their Doppler characteristics, depending on the nature of the human gross motor activities. These signals are nonstationary in nature, inviting time-frequency analysis in both its linear and bilinear aspects, to play a fundamental role in motion identification, including fall features determination and classification. This article employs real fall data to demonstrate the success of existing detection algorithms as well as to report on some of the challenges facing technology developments for fall detection.

Introduction

The elderly population aged 65 years or older is growing, and their ratio to the population aged 20–64 will reach 35% in 2030 [1]. The worldwide population over 65 is projected to increase to one billion in 2030. An overwhelming majority of elders exercise self-care within their own homes most of the time. One out of three elderly people over the age of 65 will fall every year, and the percentage rises for the elderly living in long-term care institutions. The fall can result in injuries and reduced quality of life and, unfortunately, it represents one of the leading causes of death in the elderly population. Eventually, the elderly who are at high risk of falling will have to move to institutionalized care, which can cost approximately US\$3,500 per month. Most seniors are unable to get up by themselves after a fall, and it was reported that, even without direct injuries, half of those who experienced an extended period of lying on the floor (more than an hour) died within six months after the incident. Therefore, prompt fall detection saves lives, leads to timely interventions and most effective treatments, and reduces medical expenses. Furthermore, it avoids placing major burdens on the elderly's family. Driven by a pressing need to detect and attend to a fall, elderly fall detection has

IMAGE LICENSED BY INGRAM PUBLISHING
WOMAN—©ISTOCKPHOTO.COM/SILVIAJENSEN



Digital Object Identifier 10.1109/MSP.2015.2502784
Date of publication: 7 March 2016

become an active area of research and development and is identified as a major innovation opportunity to allow seniors to live independently [2]. There are competing technologies for fall detection, of which wearable devices, like accelerometers and “push buttons,” are most common. The shortcomings of these devices are that they are intrusive, easily broken, and must be worn or carried. In addition, push-button devices are less suited for cognitively impaired users.

Although in-home radar monitoring of the elderly for fall detection is still in its early stage of development, it carries great potential to be one of the leading technologies in the near future. The attractive attributes of radar, related to its proven technology, nonobstructive illumination, nonintrusive sensing, insensitivity to lighting conditions, privacy preservation, and safety, have brought electromagnetic waves to the forefront of indoor monitoring modalities in competition with cameras and wearable devices [3]. Radar backscatters from humans in motion generate changes in the radar frequencies referred to as *Doppler effects*. The Doppler signatures determine the prominent features that underlie different human motions and gross motor activities. Recently, enhanced detection and classification techniques of radar signals associated with micro- and macromotions have been developed to identify falls from standing, sitting, kneeling, and other motion articulations [4]–[10]. Reference [4] explored the dynamic nature of a fall signal and used the Mel-frequency cepstral coefficients (MFCCs) in conjunction with machine-learning approaches to differentiate radar echo behaviors between falls and nonfalls. This differentiation was achieved in [4], [6], [7], and [9] using features extracted from time-frequency signal representations. Radar fall signals were analyzed using wavelet transform (WT) in [8] and [10] and features extracted in the joint time-scale domain were used for fall classification.

A Doppler radar obtains target Doppler information by observing the phase variation of the return signal from the targets corresponding to repetitively transmitted signals. An important property of Doppler radar is its ability to effectively suppress clutter, represented by strong scatterings of the electromagnetic waves from a room’s furniture, floors, ceiling, or from interior walls. Radars also have the capability to separate motions of animate and inanimate targets, like fans and pendulums [11]. Radar units in homes can be low cost, low power, small in size, and can be mounted on walls and ceilings in different rooms, depending on operational requirements and logistic needs as well as the required signal strength.

The role of radars in assisted living predicates on its ability to perform detection, classification, and localization. Successful detection of a fall as well as locating its occurrence to at least room accuracy, and classifying its type (see Figure 1) with low false alarm and high classification rates would provide key information to first responders on the scene. On the other hand, distinguishing between a fall due to a heart attack and one due to tripping can certainly aid in mobilizing the necessary care and treatment.

The emerging area of fall detection using radar builds on three foundations:

- 1) *Information Technology*: via the development of signal processing algorithms and the corresponding software for elderly fall detection, localization, and classification.
 - 2) *Human Factors and Behavior Science*: via the understanding of human normal gross motor activities and those affected by medications and physically impairing illnesses.
 - 3) *System Engineering and Engineering Design*: via efficient integrations of hardware and software modules to produce a cost-effective, reliable, and smart system that realizes the full potential of fall detection algorithms.
- In this article, we discuss only the first foundation, though the other two foundations are essential for the development of an overall system for fall monitoring. The main challenges in fall detection using radar are:
- High false-alarm rates stemming from confusion of falls with similar motions, like sitting and kneeling
 - Presence of scatterers caused by interior walls that create clutter and ghost targets
 - Occlusion of the fall due to large stationary items, e.g., filing cabinets
 - Weak Doppler signatures stemming from orthogonality of motion direction to the radar line-of-sight
 - Reliability of fall detection irrespective of the immediate preceding motion articulations
 - Similar Doppler signatures of pets jumping off tables and chairs to those of a human falling
 - The presence of multiple persons in the radar field of view.
- Although it is important to develop superior fall detection algorithms, some of the aforementioned challenges can be addressed through logistics and increased system resources. In [5], multiple Doppler sensors are exploited to raise the precision of fall detection by covering the target movement from multiple directions and to combat occlusions. The fusion of data is performed by feature combination or selection. Although more complex to implement, the combination method is shown to outperform the selection method for different fall and nonfall motion classifications. When using multiple radars, a change in the carrier frequency is recommended to avoid mutual interference. The radar operational frequencies should not, in general, intervene with other services, such as terrestrial TV, cellular phones, global positioning system, and Wi-Fi, and should adhere to the frequency allocations guidelines.
- In [4]–[6], [8], and [9], a fall is isolated from a preceding motion by prescreening that involves identifying the beginning and the end of a possible fall event. The fall micro-Doppler features are then extracted within the identified time interval. An ultrawideband range-Doppler radar with 2.5-GHz bandwidth is used in [13] to provide range information for target localization. Range-Doppler radars are also used in [14] to detect physiological (heartbeat, respiration) and motion parameters to identify a fallen person. Characteristics corresponding to the detected heartbeat, respiration, and motion, or combinations thereof, are proposed to differentiate between an animal present in the room and the fallen person. A range-Doppler radar can also resolve targets and thereby permits the radar to handle more than one person in the field of view (e.g., [15]). In this case, both the intended elderly and other person(s) in the room will be monitored. When used in a

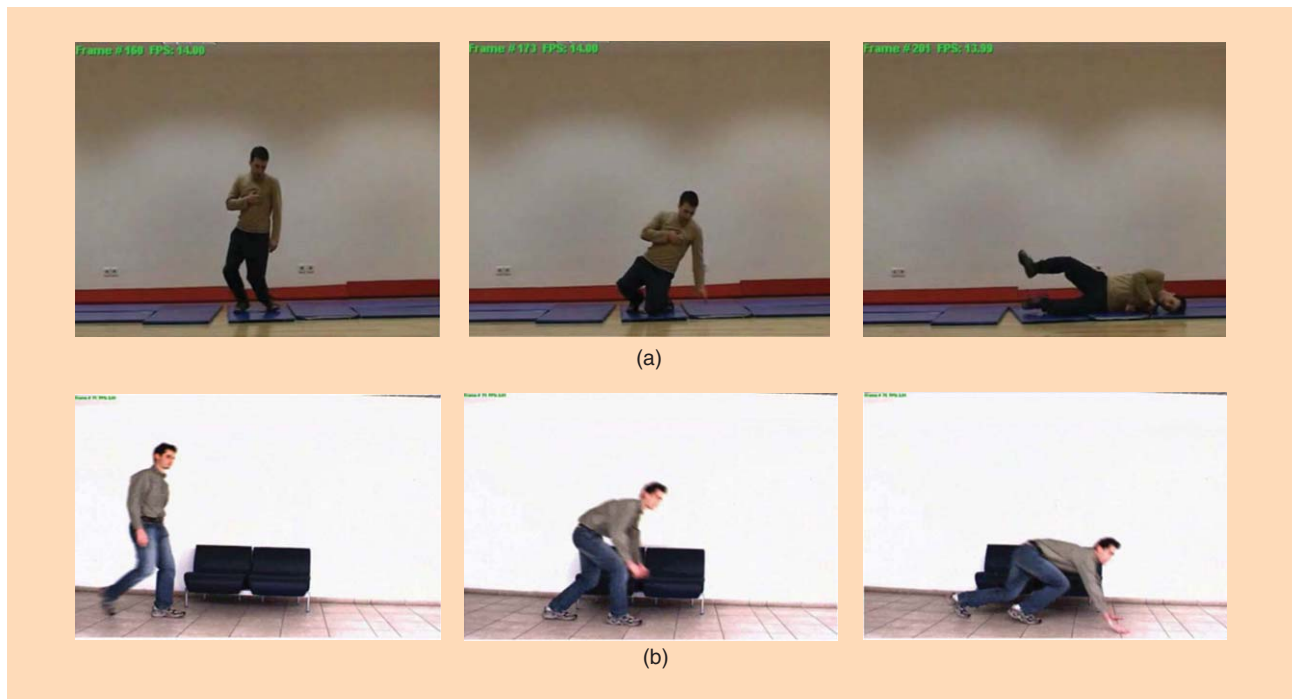


FIGURE 1. Types of falls from (a) a heart attack and (b) tripping. (Figure used with permission of [12].)

multiunit system, the range information localizes the target, through trilateration, and as such, can eliminate ghosts [5].

Signal model

Consider a monostatic continuous-wave (CW) radar that transmits a sinusoidal signal with frequency f_c over the sensing period. The transmitted signal is expressed as $s(t) = \exp(j2\pi f_c t)$. Consider a point target located at a distance of R_0 from the radar at time $t = 0$, and that moves with a velocity $v(t)$ in a direction forming an angle θ with the radar line-of-sight. As such, the distance between the radar and the target at time instant t is given by

$$R(t) = R_0 + \int_0^t v(u) \cos(\theta) du. \quad (1)$$

The radar return scattered from the target can be expressed as

$$x_a(t) = \rho \exp\left(j2\pi f_c \left(t - \frac{2R(t)}{c}\right)\right), \quad (2)$$

where ρ is the target reflection coefficient and c is the velocity of the electromagnetic wave propagation in free space. The Doppler frequency corresponding to $x_a(t)$ is given by $f_D(t) = 2v(t) \cos(\theta) / \lambda_c$, where $\lambda_c = c/f_c$ is the wavelength. A spatially extended target, such as a human, can be considered as a collection of point scatterers. Therefore, the corresponding radar return is the integration over the target region Ω and is expressed as

$$x(t) = \int_{\Omega} x_a(t) da. \quad (3)$$

In this case, the Doppler signature is the superposition of all component Doppler frequencies. Torso and limb motions generally generate time-varying Doppler frequencies, and the nature of this variation defines the Doppler signature associated with each human gross motor activity, including a fall. The exact Doppler signatures depend on the target shape and motion patterns.

Appropriate signal analysis domains

A human fall has a quick acceleration motion of short duration at the beginning until reaching the ground and a slow deceleration motion of long duration toward the end upon lying on the floor. Such a dynamic creates a Doppler radar return that is nonstationary, as in (3). This type of nonstationary signal can be well described and analyzed by joint time-frequency representations that reveal the local behavior of the signal and depict its time-varying Doppler frequency signatures, thereby supporting the radar primary tasks of detection and classification.

A number of methods are available to perform time-frequency analysis of the Doppler signatures [4], [6], [7], [9]. These methods can be generally divided into the linear time-frequency analysis and quadratic time-frequency analysis methods. Short-time Fourier transform (STFT) is a commonly used technique to perform linear time-frequency analysis [16]. Time-scale analysis using WT [17] is also considered an effective linear method to analyze and extract the characteristics of radar fall signals that exhibit nonstationary behaviors [8], [10].

Quadratic time-frequency distributions (QTFDs) involve the data bilinear products and are defined within Cohen's class [18]. QTFDs have been shown to be most suitable in analyzing wideband signals that are instantaneously narrowband. The

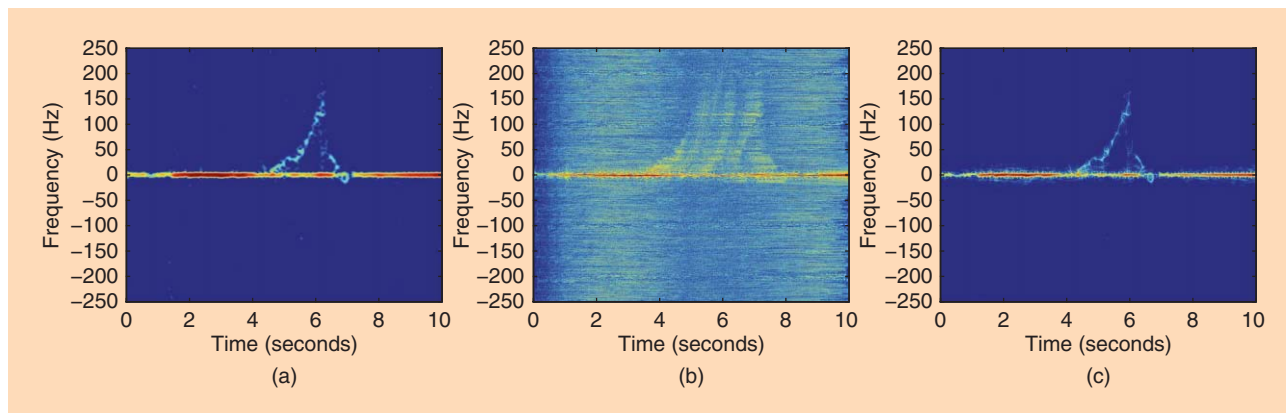


FIGURE 2. Time-frequency distributions of a fall motion: (a) spectrogram, (b) WVD, and (c) EMBD.

spectrogram $S(t, f)$ is a key member of Cohen's class and is obtained at time index t and frequency f by computing the squared magnitude of STFT of the data $x(t)$ with a window $h(t)$. Other members of Cohen's class are obtained by the two-dimensional (2-D) Fourier transform of its kernel ambiguity function, expressed as

$$D(t, f) = \sum_{\theta=-\infty}^{\infty} \sum_{\tau=-\infty}^{\infty} \phi(\theta, \tau) A(\theta, \tau) \exp(j4\pi f\tau - j2\pi\theta t), \quad (4)$$

where

$$A(\theta, \tau) = \sum_{u=-\infty}^{\infty} x(u + \tau) x^*(u - \tau) \exp(-j2\pi\theta u) \quad (5)$$

is the ambiguity function, $\phi(\theta, \tau)$ is the time-frequency kernel, and $(\cdot)^*$ denotes the complex conjugate. Here, θ and τ , respectively, denote the frequency shift (also referred to as *Doppler frequency*) and time lag. The properties of a QTFD are heavily dependent on the applied kernel.

The Wigner-Ville distribution (WVD) is often regarded as the basic or prototype QTFD, since its filtered versions describe Cohen's class. WVD is known to provide the best time-frequency resolution for single-component linear frequency modulated signals, but it yields undesirable cross-terms when the signal frequency law is nonlinear or when a multicomponent signal is analyzed. The kernel function of the WVD is unity across the entire ambiguity function. Various reduced-interference distributions (RIDs) have been developed to reduce the cross-term interference. The majority of signals have autoterms located near the origin in the ambiguity domain, while the signal cross terms are distant from the time-lag and frequency-shift axes. As such, RID kernels

$\phi(\theta, \tau)$ exhibit low-pass filter characteristics to suppress cross terms and preserve autoterms. For example, the Choi-Williams distribution uses a Gaussian kernel in both frequency shift and time lag axes, which is expressed as $\phi(\theta, \tau) = \exp(-\mu(\theta\tau)^2)$, where μ is a constant [19]. Another alternative is the extended modified B-distribution (EMBD), which is a product of a Doppler-domain filter and a lag-domain filter, expressed as [20]

$$\phi(\theta, \tau) = \frac{|\Gamma(\beta + j\pi\theta)|^2}{\Gamma^2(\beta)} \frac{|\Gamma(\alpha + j\pi\tau)|^2}{\Gamma^2(\alpha)}, \quad (6)$$

where $-0.5 \leq \theta \leq 0.5$, $-0.5 \leq \tau \leq 0.5$, $0 \leq \alpha \leq 1$, and $0 \leq \beta \leq 1$. The lengths of the Doppler and lag windows are controlled by separate parameters α and β , respectively. The extra degree of freedom in the formulation of the EMBD allows to independently adjust the lengths of the windows along both lag and Doppler axes.

Driven by a pressing need to detect and attend to a fall, elderly fall detection has become an active area of research and development and is identified as a major innovation opportunity to allow seniors to live independently.

Figure 2 compares different time-frequency representations of the Doppler signature of a human fall from standing in the form of the spectrogram, WVD, and EMBD. A 255-point Hamming window is used for the computation of the spectrogram. All results are depicted on a logarithm scale with a 25 dB dynamic range. It is clear that the spectrogram provides a clean distribution without cross terms, but with a coarse resolution. Due to signal containing multiple irregular components as well as a strong residual clutter, the WVD exhibits a high level of cross-term and sidelobe contamination, thereby rendering QTFD-based motion

classification challenging. The EMBD, on the other hand, provides better contrast and connectivity and reveals a higher level of detail as compared to the spectrogram.

Similar to the STFT, the WT uses the inner products to measure the similarity between a signal and an analyzing function. In STFT, the analyzing functions are windowed complex exponentials, and the STFT coefficients represent the projection of the

signal over a sinusoid in an interval of a specified length. According to the uncertainty principle [18], the product of the time resolution and the frequency resolution is lower bounded, i.e., we cannot achieve a high resolution in both the time domain and the frequency domain at the same time. Therefore, although STFT can observe the time-varying frequency signatures, the question always arises as the optimum window length for the given data for the best tradeoff between spectral and temporal resolutions. In the WT, the analyzing function is a wavelet. The WT implements the multiresolution concept by changing the position and scaling of the mother wavelet function and thereby captures both short-duration, high-frequency components and long-duration, low-frequency components [21]. There are many choices of the wavelet functions, depending on the properties imposed on the wavelets. When the data is in discrete form, the WT can be computed very efficiently by restricting the scales to be dyadic and the positions to be integer. Such a fast computation uses a high-pass filter and a low-pass filter to represent the wavelet function, and successive filtering generates the discrete stationary WT (SWT) [22]. SWT is redundant and it produces the same number of samples as the data at each scale. However, it avoids the shift variant behavior that appears in the nonredundant discrete WT.

It is noted that Mel-frequency cepstrum is another representation of the short-term power spectrum for nonstationary signals and has been used in [4] to represent the Doppler signatures. Empirical mode decomposition (EMD) has also been used to examine human Doppler signatures [23], [24]. EMD is an adaptive technique that decomposes a signal into time-frequency components called *intrinsic mode functions (IMFs)*. Each IMF comprises signal components that belong to a specific oscillatory time scale. The energy as a function of the IMF index provides a unique feature vector with which human motion classification can be achieved. Furthermore, time-frequency representations based on compressed sensing and sparse reconstructions have been successfully employed for high-resolution Doppler signature analysis and radar operation with nonperiodic sub-Nyquist sampling [25], [26].

Feature extraction and classification

Figure 3 shows the data processing blocks for fall detection. The radar data is first transformed to an appropriate domain, followed by a prescreening step that determines whether an important event may have occurred and, if so, its time location. Once an event is detected by the prescreener, a classification process is initiated to detect whether such an event is a fall. More specifically, windowed transformed data around the identified event time location is used to extract pertinent features, which are used by a classifier to perform fall versus nonfall classification. A power burst curve (also referred to as the *energy burst curve*), which represents the signal power within a specific frequency band as a function of time, can be utilized for prescreening [4], [9]. The frequency band chosen for prescreening should be a

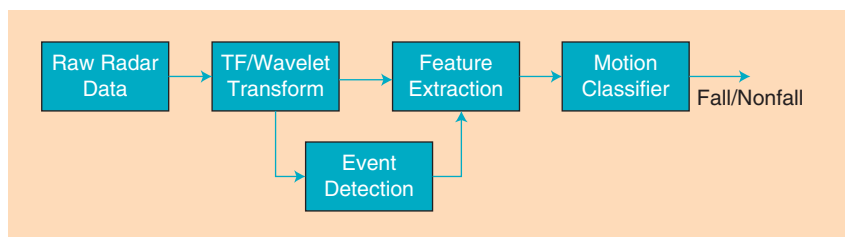


FIGURE 3. Data processing blocks for fall detection.

low-frequency band that excludes the clutter-dominated zero-frequency region but effectively captures human activities. An event is triggered for classification when the signal power in the specified frequency band exceeds a certain level. The coefficients of wavelet decomposition at a given scale have also been used in the prescreening stage to identify the time locations where fall activities may have occurred [10].

Feature definitions

For fall detection based on STFT, pertinent features include extreme frequency magnitude, extreme frequency ratio, and the time span of event [9].

- 1) *Extreme Frequency Magnitude*: The extreme frequency magnitude is defined as $F = \max(f_{+\max}, -f_{-\min})$, where $f_{+\max}$ and $f_{-\min}$, respectively, denote the maximum frequency in the positive frequency range and the minimum frequency in the negative frequency range. Critical falls often exhibit a high extreme frequency magnitude when compared to other types of observed motions.
- 2) *Extreme Frequency Ratio*: The extreme frequency ratio is defined as $R = \max(|f_{+\max}/f_{-\min}|, |f_{-\min}/f_{+\max}|)$. For falls, due to the translational motion of the entire body, a high energy spectrogram is concentrated in either the positive or negative frequencies, resulting in a high extreme frequency ratio. On the other hand, other types of motions, such as sitting and standing, often demonstrate high energy content in both the positive and negative frequency bands because different body parts undergo different motion patterns, thereby corresponding to a low extreme frequency ratio.
- 3) *Time Span of Event*: This feature describes the length of time, in milliseconds, between the start and the end of an event, i.e., $L = t_{\text{extrm}} - t_{\text{begin}}$, where t_{extrm} denotes the time where the extreme frequency occurs and t_{begin} denotes the initiation time of the event. The latter is determined by the time when the magnitude of the frequency content of a signal passes a specific threshold. The different motion patterns being compared in this work generally show distinct time spans.

The aforementioned three features extracted from the spectrogram have been used for fall detection in [9]. Additional features have also been extracted from time-frequency distributions for classification of human activities (see, e.g., [27], [28] and references therein). These include torso Doppler frequency, total bandwidth of the Doppler signal, offset of the total Doppler, normalized standard deviation of the Doppler signal strength, period of the limb motion,

shape of the spectrogram envelope, ratio of torso echoes to other echoes in the spectrogram, and Fourier series coefficients of spectrogram envelope. Nonparametric features derived from subspace representations of the time-frequency distributions have also been proposed. Effective and reliable fall detection often requires the combined use of multiple features. Once a set of features is extracted, a classification algorithm can be applied to determine whether an event is a fall or nonfall activity.

Classifiers

A variety of classifiers have been employed for fall detection [4], [27], with the support vector machine (SVM) being the most commonly used classifier. Different classifiers, including k -nearest neighbor, are used to automatically distinguish falling from activities, such as walking and bending down [4]. The sparse Bayesian learning method based on the relevance vector machine improves fall detection performance over the SVM with fewer relevance vectors, and its effectiveness is demonstrated in [9]. Hidden Markov model-based machine learning is used in [6] to characterize the signal spectrogram for fall detection. However, the choice of employed features has been determined to have a greater impact on the classification performance than the specific classifier applied (see [28] and references therein).

Classification results

A CW radar was set up in the Radar Imaging Lab at Villanova University, Pennsylvania. A vertically polarized horn antenna (BAE Systems, Model H-1479) with an operational frequency range of 1–12.4 GHz and 3-dB beamwidth of 45° was used as a transceiver for the CW radar. The feed point of the antenna was positioned 1 m above the floor. Agilent's E5071B RF network analyzer was used for signal generation and measurement of radar returns. A carrier frequency of 8 GHz was employed and the network analyzer was externally triggered at a 1 kHz sampling rate. Data were collected for eight different motion patterns using two test subjects, with each experiment motion pattern repeated ten times (five times each for two test subjects). Considered motion patterns include 1) forward falling, 2) backward falling, 3) sitting and standing, and 4) bending over and standing up. Two different variations of each motion pattern were measured, one being a standard type of motion, whereas the other demonstrating a high-energy form of the same motion to study the impact of such variations on the classification performance. The recording time for each experiment was 20 seconds [9].

The typical spectrograms of the eight considered motion patterns are shown in Figure 4. The first four patterns are collectively considered falls, whereas the last four patterns are collectively considered nonfall motions. Our objective is to correctly detect fall events from nonfall events. Figure 5

For fall detection based on STFT, pertinent features include extreme frequency magnitude, extreme frequency ratio, and the time span of an event.

depicts the ground truth of three aforementioned STFT-based features, i.e., the extreme frequency magnitude, the extreme frequency ratio, and the time span of the event [9]. Specifically, Figure 5(a) shows the three-dimensional view of the three features, whereas their pairwise 2-D plots are respectively provided in Figure 5(b)–(d), where these features generally provide

a clear distinction between the fall and nonfall events, except one outlier fall event (marked with a circle). Examination of the spectrogram of this outlier fall event shows that the corresponding signal is very weak, yielding low extreme Doppler frequency as well as a short time span of event. The fall events exhibit larger extreme frequency magnitudes, higher extreme frequency ratios, and longer lengths of event time than the nonfall counterparts. These features, however, do not robustly classify the fall and nonfall activities based on a single feature alone.

The SVM classifier is applied by using a Gaussian kernel. Fivefold cross-validation is used on the motion data. The entire sample set is randomly partitioned into five equal-size subsets. Out of the five subsets, a single subset is retained as the validation data for testing the classifier, and the remaining four subsets are used as the training data. The cross-validation process is repeated five times, with each of the five subsets used exactly once as the validation data. The classifier is successfully able to detect fall from nonfall events except for the misclassification of the outlier fall event as described earlier and marked with the circle in Figure 5(a).

Wavelet-based approach

Feature Definition

WT-based features include the smoothed magnitude square of the discrete SWT coefficients of the radar signal at several dyadic scales over a moving window (frame) typically of 0.5 seconds with 50% overlap [10]. The collection of features in 2.5 seconds centered at the event location identified by a prescanner forms the feature vector for classification. The smoothed magnitude square of the SWT coefficients is defined next.

Smoothed Magnitude Square of the SWT Coefficients

Let $\tilde{\xi}_i(k)$ be the sum of the square of the SWT coefficients at dyadic scale 2^i in frame k . There will be nine frames in a total of 2.5 seconds that contain a possible fall event. Normalization of $\tilde{\xi}_i(k)$ by the sum of the nine values is often needed, giving $\xi_i(k)$. The collection of the nine $\xi_i(k)$ s forms the row vector ξ_i . Over the dyadic scales 2^{i_b} to 2^{i_e} , the feature vector for classification is $\mathbf{y} = [\xi_{i_b} \cdots \xi_{i_e}]$.

The study in [4] applied cepstral analysis of the radar signal for fall detection. The MFCCs were extracted over a 4-second data segment that might contain a fall activity and encouraging classification results between falls and nonfalls were observed.

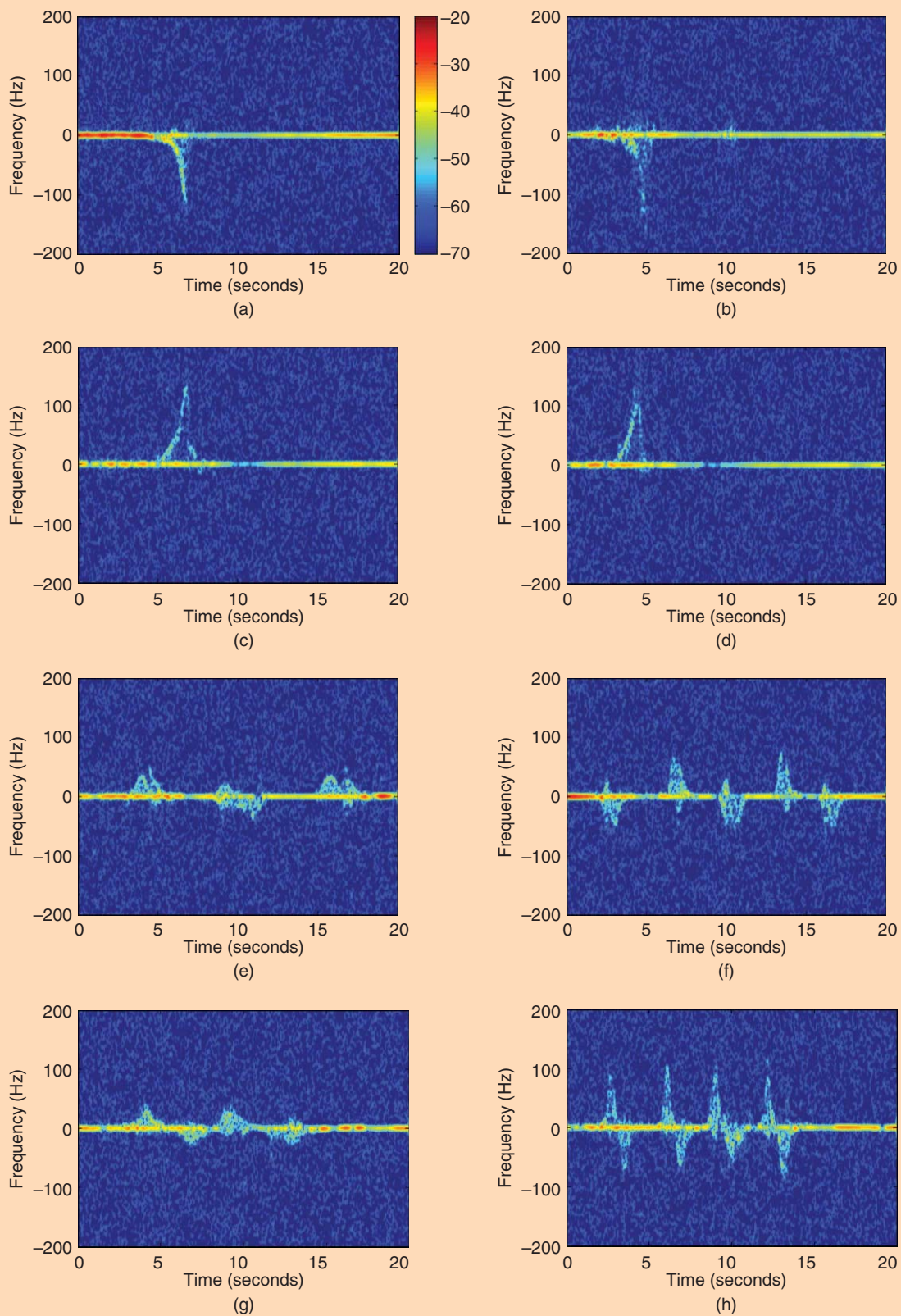


FIGURE 4. Spectrograms of typical motion profiles [9]. (a) Fall backward. (b) Fall backward with arm motion. (c) Fall forward. (d) Fall forward with arm motion. (e) Sit and stand. (f) Fast sit and stand. (g) Bend and stand up. (h) Fast bend and stand up. (Figure reproduced with permission of the Institution of Engineering and Technology.)

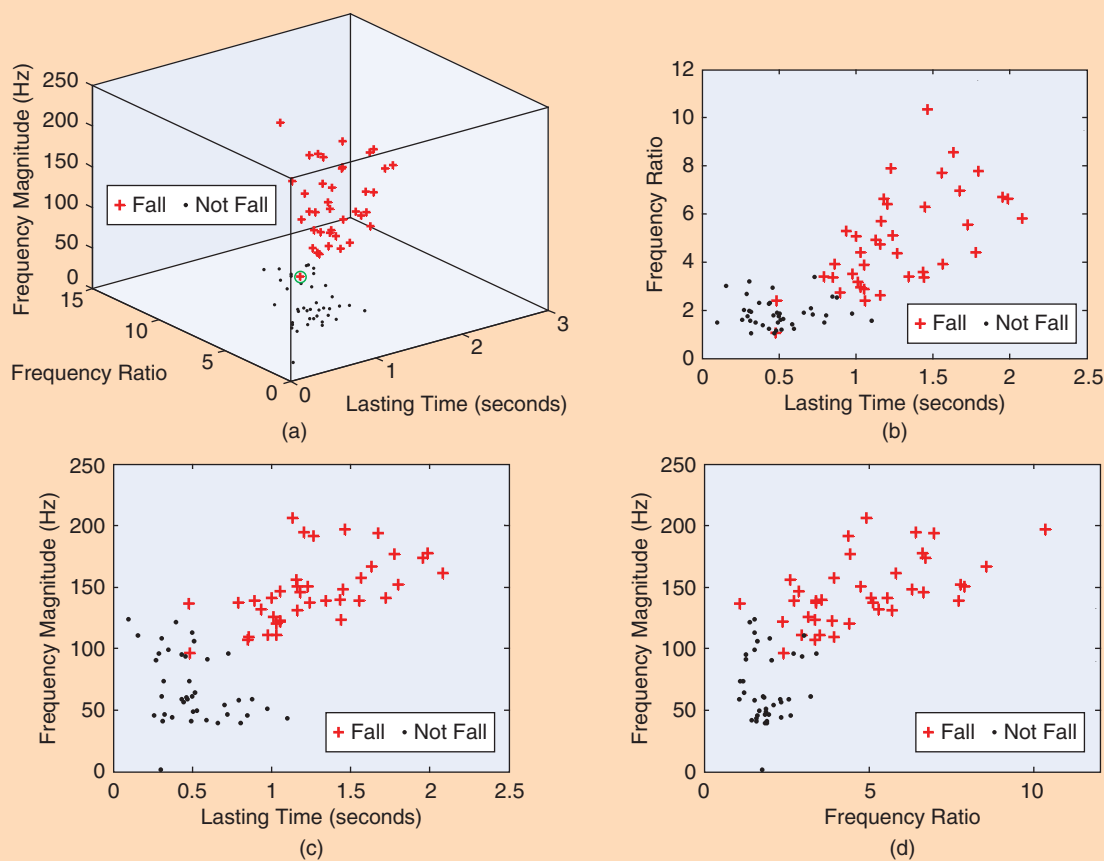


FIGURE 5. Ground truth of motions with 3-D vision and three 2-D visions [9]. (Figure reproduced with permission of the Institution of Engineering and Technology.)

Classification Results

Wavelet-based fall detection results are presented using real data collected in three different bathrooms of senior residence apartments [29]. A bathroom is where falls of elderly people could occur often and yet other sensors, such as video cameras or acoustic sensors, are not suitable due to privacy reasons or strong interferences. The data collection was performed from January to May 2013, where the Doppler radars were mounted above in the attic at the middle of the bathrooms. The data set contains 19 different kinds of falls and 14 various typical nonfalls that were performed by a professionally trained female stunt actor [10]. The fall types and their counts are tabulated in Table 1.

The radar used in the experiment is a commercially available pulse-Doppler range control radar with a price close to that of a webcam. The pulse repetition rate is 10 MHz, the duty cycle is 40%, and the center frequency is 5.8 GHz. The sampling frequency of the radar signal is 960 Hz. Based on the velocity range during a human fall, dyadic scales from two to 64 are used to generate the features, giving the feature vector length of $6(\text{scales}) \times 9(\text{frames}) = 54$. The wavelet function for SWT is the reverse biorthogonal 3.3 wavelet. The window function is Hamming. The classifier is the k -nearest neighbor with $k = 1$ for fall versus nonfall clas-

sification. The data was acquired in a continuous manner as in practice. A prescener based on the SWT coefficient values at scale equal to four gives the potential falls locations for feature extraction and classification. Figure 6 examines the classification performance using the SWT and the MFCC features, using leave-one-out cross-validation between training and testing. The false-alarm rate is the number of false alarms normalized by the total number of events from the prescener. The WT classifier has comparable performance with the MFCC classifier for detection rate below 80% and has much better results otherwise. At a 100% detection rate, the WT classifier reduces the amount of false alarms by more than a factor of four from the prescener.

Open issues and problems

There are many challenges still facing the radar-based fall detection technology. Classifying a fall, once the corresponding event time interval is identified, has been the subject of most work in this area. However, identifying such an interval is still an open question, specifically when a fall is preceded by a high-Doppler gross motor activity. For example, experiments have shown that progressive fall from a rapid walk is not easy to reveal. Fast sitting and slow falling can also be confused

without the effective use of range information. Optimal sensor placement is also an open problem, as the Doppler frequency of a radar return is proportional to the target motion along the radar along the line-of-sight. Placing the radar several feet above the ground can provide clear signals for gait and fall analysis. On the other hand, the fall detection performance may not be as good as when it is mounted in the ceiling due to weaker relative motion that affects the features characterization [30]. Finally, radar fall detection would emerge to be elderly specific. In this respect, it would require 1) tuning the fall detection algorithms to the elderly physical impairments and any awareness of the use of walking aid devices, and 2) making the system dynamic by unsupervised or supervised learning, which can occur by observing the elderly over an extended period of time.

There are limitations of using Doppler radar for fall detection. In fact, it is not straightforward for a Doppler radar to distinguish between a human fall and a pet jumping. Other normal activities, such as sitting on a chair, could also present challenges to a Doppler radar fall detection system. On the other hand, a pet is smaller in size than a human and sitting down does not exhibit the full dynamics of a fall. It is anticipated that, by extracting the reliable features and designing a proper classifier, some of these false alarms could be eliminated. The use of Doppler radar for fall detection is still in its infancy and there are many open issues that need to be addressed and further investigated.

Conclusions

Automatic real-time detection of falls may enable the first responders to provide rapid medical assistance, and, thus, save

Table 1. A description of fall types.

Fall Type	Count
Loose balance-forward	11
Loose balance-backward	9
Loose balance-left	8
Loose balance-right	10
Loss of consciousness-forward	3
Loss of consciousness-backward	3
Loss of consciousness-left	2
Loss of consciousness-right	3
Loss of consciousness-straight down	3
Trip and fall-forward	1
Trip and fall-sideways	2
Slip and fall-forward	4
Slip and fall-sideways	5
Slip and fall-backward	4
Reach-fall (chair)-forward	2
Reach-fall (chair)-left	1
Reach-fall (chair)-right	2
Reach-fall (chair)-sliding forward	4
Reach-fall (chair)-sliding backward	5

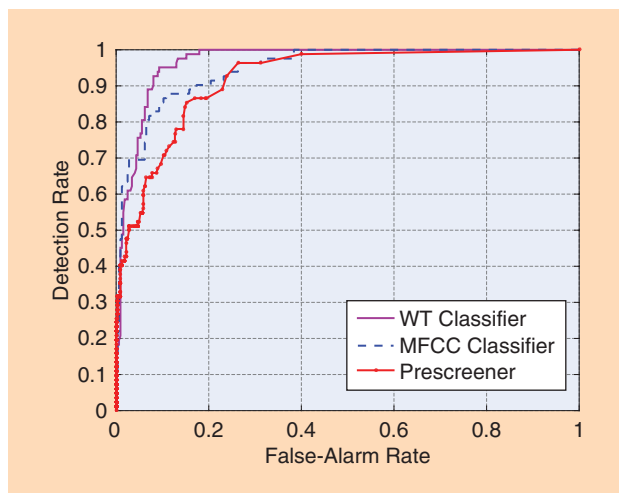


FIGURE 6. Classification performance of WT features.

lives, minimize injury, and reduce the anxiety of the elderly who live alone. Effective use of radar technology for elderly fall detection relies on the signal processing techniques for Doppler signature analysis and motion classifications. In this article, we presented an overview of the the main approaches for revealing pertinent features in the joint-variable time-frequency domain. More specifically, time-frequency analysis in both its linear and bilinear aspects, including WT, was shown to play a fundamental role in fall features determination and human motion classification. The success of feature-based fall detection schemes was demonstrated using real data experiments and challenges facing technology development for fall detection were also discussed. Further developments in this area toward commercialization call for having a large repository of fall data, both real and kinematically modeled, that will provide the means for understanding the nominal features of fall motions, and also for proper training and performance comparison of the different algorithms.

Authors

Moeness G. Amin (moeness.amin@villanova.edu) received his Ph.D. degree in 1984 from the University of Colorado, Boulder. He has been on the faculty of the Department of Electrical and Computer Engineering at Villanova University, Pennsylvania, since 1985, where he is now a professor and the director of the Center for Advanced Communications. He is a recipient of the 2015 IEEE Warren D. White Award for Excellence in Radar Engineering, the 2014 IEEE Signal Processing Society Technical Achievement Award, the 2009 EURASIP Individual Technical Achievement Award, and the IEEE Third Millennium Medal. He was a Distinguished Lecturer of the IEEE Signal Processing Society during 2003–2004. He has authored more than 700 journal and conference publications in the broad area of theory and applications of signal and array processing, including radar. He is a Fellow of the IEEE, EURASIP, SPIE, and IET.

Yimin D. Zhang (ydzhang@temple.edu) received his Ph.D. degree from the University of Tsukuba, Japan, in 1988. He is currently an associate professor in the Department of Electrical and

Computer Engineering, Temple University, Philadelphia, Pennsylvania. He has authored more than 270 publications in the area of array signal processing, time-frequency analysis, compressive sensing, and optimization with applications in radar, communications, and navigation. He is an associate editor of *IEEE Transactions on Signal Processing* and serves on the editorial board of the journal *Signal Processing*. He was an associate editor of *IEEE Signal Processing Letters* during 2006–2010. He is a member of the Sensor Array and Multichannel Technical Committee of the IEEE Signal Processing Society. He is a Senior Member of the IEEE and SPIE.

Fauzia Ahmad (fauzia.ahmad@villanova.edu) received her Ph.D. degree in electrical engineering from the University of Pennsylvania, Philadelphia, in 1997. Since 2002, she has been with the Center for Advanced Communications, Villanova University, Pennsylvania, where she is now a research professor and the director of the Radar Imaging Lab. She has authored more than 170 publications in the areas of radar imaging, radar signal processing, compressive sensing, and array signal processing. She serves on the editorial boards of *IEEE Transactions on Signal Processing*, *IEEE Geoscience and Remote Sensing Letters*, *IET Radar, Sonar, & Navigation Journal*, and *SPIE/IS&T Journal of Electronic Imaging*. She is a member of the Radar Systems Panel of the IEEE Aerospace and Electronic Systems Society and a member of the Sensor Array and Multichannel Technical Committee of the IEEE Signal Processing Society. She is a Senior Member of the IEEE and SPIE.

K.C. (Dominic) Ho (hod@missouri.edu) received his Ph.D. degree in electronic engineering from the Chinese University of Hong Kong, in 1991. Since September 1997, he has been with the University of Missouri, Columbia, where he is currently a professor in the Electrical and Computer Engineering Department. His research interests include sensor array processing; elder care; source localization, detection, and estimation; wireless communications; and the development of efficient signal processing algorithms for various applications. He served as the chair of the Sensor Array and Multichannel Technical Committee of the IEEE Signal Processing Society during 2013–2014. He was an associate editor of *IEEE Transactions on Signal Processing* from 2003 to 2006 and from 2009 to 2013 and *IEEE Signal Processing Letters* from 2004 to 2008. He is a Fellow of the IEEE.

References

- [1] United Nations, Department of Economic and Social Affairs, Population Division. (2011). *World population prospects: The 2010 revision*. [Online]. Available: <http://www.esa.un.org/swpp/>
- [2] AARP. Health Innovation Frontiers: Untapped Market Opportunities for the 50+. [Online]. Available: <http://health50.org/files/2013/05/AARPHHealthInnovationFullReportFINAL.pdf>
- [3] M. G. Amin, Ed., *Through the Wall Radar Imaging*. Boca Raton, FL: CRC Press, 2011.
- [4] L. Liu, M. Popescu, M. Skubic, M. Rantz, T. Yardibi, and P. Cuddihy, "Automatic fall detection based on Doppler radar motion," in *Proc. 5th Int. Conf. Pervasive Computing Technologies for Healthcare*, Dublin, Ireland, May 2011, pp. 222–225.
- [5] S. Tomii and T. Ohtsuki, "Falling detection using multiple Doppler sensors," in *Proc. IEEE Int. Conf. e-Health Networking, Applications and Services*, Beijing, China, Oct. 2012, pp. 196–201.
- [6] M. Wu, X. Dai, Y. D. Zhang, B. Davidson, J. Zhang, and M. G. Amin, "Fall detection based on sequential modeling of radar signal time-frequency features," in *Proc. IEEE Int. Conf. Healthcare Informatics*, Philadelphia, PA, Sept. 2013, pp. 169–174.
- [7] F. Wang, M. Skubic, M. Rantz, and P. E. Cuddihy, "Quantitative gait measurement with pulse-Doppler radar for passive in-home gait assessment," *IEEE Trans. Biomed. Eng.*, vol. 61, no. 9, pp. 2434–2443, Sept. 2014.
- [8] A. Gadde, M. G. Amin, Y. D. Zhang, and F. Ahmad, "Fall detection and classification based on time-scale radar signal characteristics," in *Proc. SPIE*, Baltimore, MD, May 2014, vol. 9077, no. 907712, pp. 1–9.
- [9] Q. Wu, Y. D. Zhang, W. Tao, and M. G. Amin, "Radar-based fall detection based on Doppler time-frequency signatures for assisted living," *IET Radar Sonar Navig.*, vol. 9, no. 2, pp. 164–172, Feb. 2015.
- [10] B. Y. Su, K. C. Ho, M. J. Rantz, and M. Skubic, "Doppler radar fall activity detection using the wavelet transform," *IEEE Trans. Biomed. Eng.*, vol. 62, no. 3, pp. 865–875, Mar. 2015.
- [11] P. Setlur, M. G. Amin, F. Ahmad, and P. D. Zeman, "Experiments on through-the-wall motion detection and ranging," in *Proc. SPIE*, Orlando, FL, Apr. 2007, vol. 6538, no. 653809, pp. 1–10.
- [12] Detecting falling people. [Online]. Available: <http://muscle.ercim.eu/content/view/35/43/>
- [13] J. Sachs and R. Herrmann, "M-sequence based ultra-wideband sensor network for vitality monitoring of elders at home," *IET Radar Sonar and Navig.*, vol. 9, no. 2, pp. 125–137, Feb. 2015.
- [14] P. E. Cuddihy, J. M. Ashe, C.N. Bufi, and S. Genc, "Radar based systems and methods for detecting a fallen person," U.S. Patent 8742935 B2, June 3, 2014.
- [15] Z. A. Cammenga, G. E. Smith, and C. J. Baker, "Combined high range resolution and micro-Doppler analysis of human gait," in *Proc. IEEE Int. Radar Conf.*, Arlington, VA, May 2015, pp. 1038–1043.
- [16] L. B. Almeida, "The fractional Fourier transform and time-frequency representations," *IEEE Trans. Signal Processing*, vol. 42, no. 11, pp. 308–3091, 1994.
- [17] S. Mallat, *A Wavelet Tour of Signal Processing*, 3rd ed. New York: Academic, 2009.
- [18] L. Cohen, *Time-Frequency Analysis*. Englewood Cliffs, NJ: Prentice Hall, 1995.
- [19] H. Choi and W. J. Williams, "Improved time-frequency representation of multi-component signals using exponential kernels," *IEEE Trans. Acoustics Speech Signal Processing*, vol. 37, no. 6, pp. 862–871, June 1989.
- [20] B. Boashash and T. Ben-Jabeur, "Design of a high-resolution separable-kernel quadratic TFD for improving newborn health outcomes using fetal movement detection," in *Proc. Int. Conf. Information Science, Signal Processing and Their Applications*, Montreal, Canada, 2012, pp. 354–359.
- [21] S. Qian, *Introduction to Time-Frequency and Wavelet Transforms*. Englewood Cliffs, NJ: Prentice Hall, 2001.
- [22] G. P. Nason and B. W. Silverman, "The stationary wavelet transform and some statistical applications," *Lect. Notes Stat.*, vol. 103, pp. 281–299, 1995. [23] D. P. Fairchild and R. M. Narayanan, "Classification of human motions using empirical mode decomposition of human micro-Doppler signatures," *IET Radar Sonar Navig.*, vol. 8, no. 5, pp. 425–434, 2014.
- [24] I. Mostafanezhad, O. Boric-Lubecke, V. Lubecke, and D. P. Mandic, "Application of empirical mode decomposition in removing fidgeting interference in Doppler radar life signs monitoring devices," in *Proc. 31st Annu. Int. Conf. IEEE Engineering in Medicine and Biology Society*, Minneapolis, MN, Sept. 2009, pp. 340–343.
- [25] B. Jokanovic, M. G. Amin, Y. D. Zhang, and F. Ahmad, "Multi-window time-frequency signature reconstruction from undersampled continuous wave radar measurements for fall detection," *IET Radar Sonar Navig.*, vol. 9, no. 2, pp. 173–183, Feb. 2015.
- [26] M. G. Amin, B. Jakanovic, Y. D. Zhang, and F. Ahmad, "A sparsity-perspective to quadratic time-frequency distributions," *Digit. Signal Processing*, vol. 46, pp. 175–190, Nov. 2015.
- [27] Y. Kim and H. Ling, "Human activity classification based on micro-Doppler signatures using a support vector machine," *IEEE Trans. Geosci. Remote Sens.*, vol. 47, no. 5, pp. 1328–1337, 2009.
- [28] S. Z. Gurbuz, B. Tekeli, M. Yuksel, C. Karabacak, A. C. Gurbuz, and M. B. Guldogan, "Importance ranking of features for human micro-Doppler classification with a radar network," in *Proc. 16th Int. Conf. Information Fusion*, Istanbul, Turkey, July 2013, pp. 610–616.
- [29] TigerPlace: An assisted living facility in Columbia, MO, USA. [Online]. Available: <http://www.eldertech.missouri.edu/>
- [30] L. Liu, M. Popescu, K. C. Ho, M. Skubic, and M. Rantz, "Doppler radar sensor positioning in a fall detection system," in *Proc. Int. Conf. IEEE Engineering in Medicine and Biology Society*, San Diego, CA, Aug. 2012, pp. 256–259.

Christian Debes, Andreas Merentitis, Sergey Sukhanov,
Maria Niessen, Nicolaos Frangiadakis, and Alexander Bauer

Monitoring Activities of Daily Living in Smart Homes

Understanding human behavior

Monitoring the activities of daily living (ADLs) and detection of deviations from previous patterns is crucial to assessing the ability of an elderly person to live independently in their community and in early detection of upcoming critical situations. “Aging in place” for an elderly person is one key element in ambient assisted living (AAL) technologies.

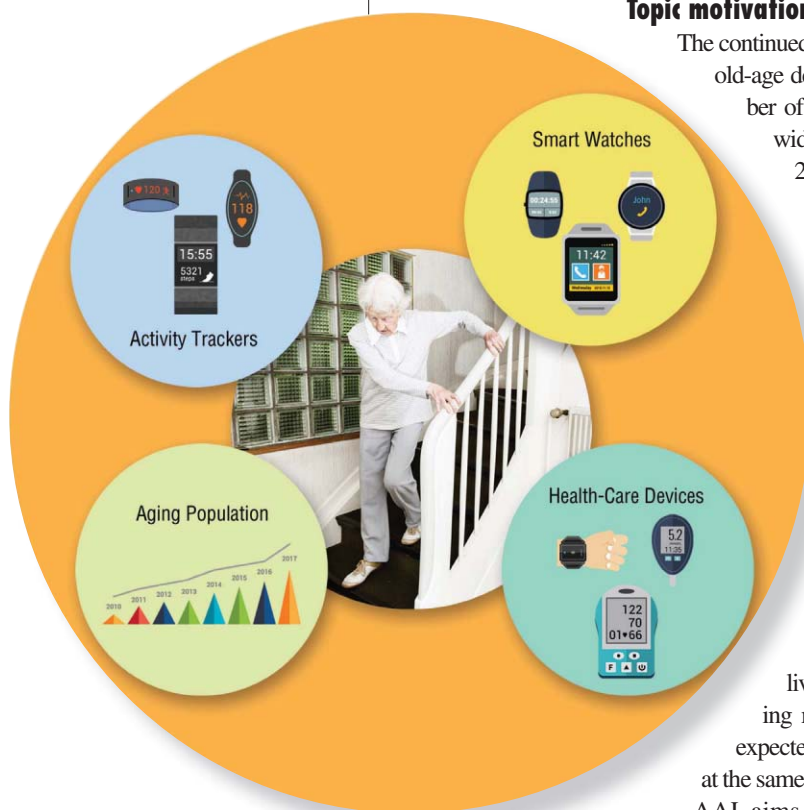
Topic motivation and significance

The continued increase in longevity will yield a steep rise in the old-age dependency ratio, defined as the ratio of the number of elderly people to those of working age. Worldwide, this ratio is expected to double from 11.7% to 25.4% in the next 35 years, with countries like Japan, Germany, Italy, Spain, and Poland exceeding a 50% ratio [1]. In alignment to this development, the number of people aged 80 and over is going to triple in the next 35 years, going from 22 million to 61 million in the European Union [2] with similar developments in the United States [3].

This trend leads to several sociological and economical challenges. On the one hand, several studies show that, at 90%, the vast majority of elderly people have the desire to live as long as possible, independently, in their own home [4]. On the other hand, there is the desire of families and health insurers to have cost-effective alternatives to assisted living and nursing homes. The costs of maintaining retirement living standards due to longevity are expected to roughly double in the next 35 years, while, at the same time, a shortage of caregivers is expected [5], [6]. AAL aims to deal with some of the challenges that develop with longevity. It serves as a framework of solutions ranging

from medication reminder tools to fall detection systems and communication tools. The technology used in these solutions is based on ambient intelligence, a paradigm within information technology that aims to aid people in their everyday lives by learning and adaptively responding to their behavior by integrating technology in their environment. As such, it can also assist elderly people to age in place while still having sufficient security standards in case of emergency [7]–[9].

IMAGE LICENSED BY INGRAM PUBLISHING,
WOMAN—©ISTOCKPHOTO.COM/SILVIAANSEN



Digital Object Identifier 10.1109/MSP.2015.2503881
Date of publication: 7 March 2016

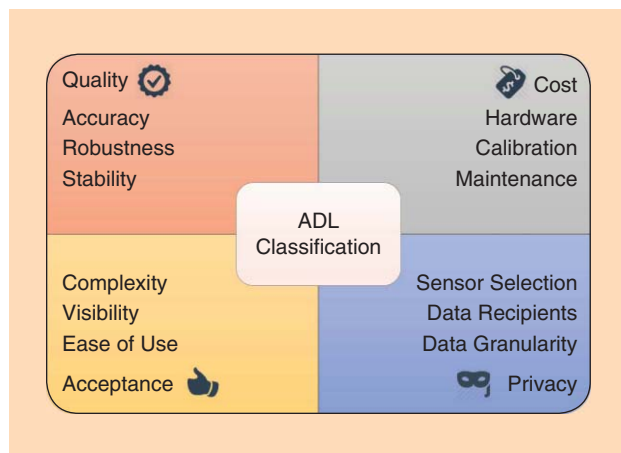


FIGURE 1. The challenges in ADL classification.

One important concept in AAL is the monitoring of ADLs [10]. The concept of ADLs is commonly used in health care, summarizing activities and daily routines, on which the functional status of a person is based, and, ultimately, on which the ability of a person to live independently in a community is assessed. These include six basic ADLs (bathing/showering, dressing, feeding, functional mobility, personal hygiene, and continence) meant to assess physical self-maintenance and a larger number of instrumental ADLs, such as food preparation and housework.

Because the manual assessment of the ADLs of a person is not feasible in a real-life situation, automatic classification and monitoring of ADLs using sensors deployed in households is a crucial technology for AAL. ADL monitoring can allow for early detection of diseases such as Alzheimer's [11], [12] and dementia [13], [14] and can generally reveal a decrease in the ability of a person living independently. ADL monitoring yields several technical and nontechnical issues that need to be addressed. On the technical side, the choice and setup of sensors deployed in households, as well as the signal processing and machine-learning algorithms to be considered for event detection and classification, are important. On the nontechnical side, ease of use and privacy are crucial [15], [16]. The most practically successful and useful system for ADL monitoring is thus one that requires little training or configuration effort and integrates seamlessly in a household. These considerations pose several challenges on the technology side, including:

- **Sensor selection.** Sensors have to be affordable, privacy preserving, and easy to install and configure, ruling out complicated sensors and microphones. This affects the achievable classification accuracy.
- **Household invariance.** Data and ground truth acquisition for each individual household is costly and laborious. ADL classifiers should provide reasonable performance on a variety of household configurations, with additional training data as optional input to boost accuracy.

A primary goal of AAL is to assess the self-maintenance of elderly people still living at home.

Figure 1 summarizes some of the challenges that must be considered in a practically applicable ADL classification system.

State of the art in sensor technology to assess ADLs

Reliable and accurate sensor data is crucial for ADL monitoring and classification tasks. Sensor effectiveness largely depends on the activity type to be recognized. In past works on ADL classification, various types of sensors were deployed in experiments leading to different architectures and performance of the overall systems [17]. Two main categories of sensors can be distinguished: wearable sensors and nonwearable sensors. Wearable sensors are usually attached to a person directly (e.g., bracelet sensors or cardio sensors) or to their clothes (e.g., an accelerometer or a step counter) to measure location, pulse rate, body temperature, blood pressure, and other vitally important metrics as well as motion characteristics. Nonwearable sensors are usually deployed in stationary locations of a house or a room and are able to detect a person and his movements and activities. Nonwearable sensors can specify the operational status of objects, measure water flow,

room temperature, or door/cupboard openings/closings. While wearable sensors allow for higher localization accuracy and can detect body movements and vital health metrics [18], nonwearable sensors are considered less intrusive and do not require any interaction from the user's side. Wearable sensors also may have

harsher power consumption requirements. However, in some cases, the wearable sensors might be part of or make use of devices the user already is familiar with and normally carries with them, such as a wristwatch or a cell phone.

Nonwearable sensors

In Table 1, we summarize and categorize nonwearable sensors that were used for ADL monitoring and classification in previous work.

- Infrared (IR) sensors are the most often used nonwearable sensors in past projects and studies on ADL classification [19]–[24]. They are used to discover human presence in a room, detect motion in a specific area, or to locate a human within a house. In [25], a modified passive IR (PIR) sensor was used to detect stove and oven operation.
- Ultrasonic sensors are usually used for person detection and localization by measuring distances to objects. In [26]–[28], these sensors were deployed together with other sensors to monitor the behavior of a person and to identify ADLs. In other studies, ultrasonic sensors were used to get accurate pacing trajectories and then to find ones that were abnormal [29], [30].
- Photoelectric sensors are devices that detect a light source and output a signal when the light intensity is greater or less than the predefined threshold value. This type of sensor is not extensively used; however, in some projects, they

Table 1. Nonwearable sensors used for ADL classification.

Sensor	Type of Measurement	Task	Usage Example
Passive/Active IR	Motion/Identification	Localization/Presence detection	Detection of person in kitchen
Ultrasonic	Motion/Identification	Localization/Presence detection	Detection of person in kitchen
Photoelectric	Motion/Identification	Localization/Presence detection	Detection of person in kitchen
Video/Thermal	Activity	Localization/Presence detection	Detection of person next to stove
Vibration	Vibration	Presence detection/Object usage	Detection of person in kitchen
Pressure	Pressure on object	Presence/Fall/Steps detection	Fall detection
Magnetic switches	Door/Cupboard opening/Closing	Objects usage/Presence detection	Cupboard opening
Radio-frequency identification (RFID)	Object information	Objects usage/Presence detection	TV usage
Audio	Activity	Objects usage/Presence detection	Shower usage
Wattmeter	Consumption information	Electrical objects usage	Water boiler usage

are used as a presence detection sensor [31], [32] or as gait speed and direction measurer [33].

There are video-based approaches in which a camera is installed in a specific place of a house to detect person movements and/or other general activities. While performing well under laboratory conditions, this type of sensor is unable to provide the same performance in natural conditions because of noise and nonconstant lighting [34]. Moreover, a video-camera-based approach is considered to be strongly privacy-violating. To address privacy concerns, a low-resolution thermal sensor was recently proposed to be used instead of a traditional video camera [35], [36]. This sensor is able to provide almost the same activity information as a video camera while preserving the user's privacy. However, there are no studies that prove high operational performance of such types of sensors in real scenarios.

- Vibration sensors are usually deployed to detect a person falling [25], [37]. Vibration sensors can also be used in identifying interaction with various objects [38], flushing toilets, or detecting water flows [39], [40].
- Pressure sensors are used to detect the presence of a person, steps, and fall events. These sensors are usually deployed in the form of floor mats and smart tiles [25], [31]. In [41], pressure sensors were installed not only in floors but also in furniture to obtain object usage information during activities.
- Magnetic switches are usually used to report whether doors or cupboards are opened or closed. These sensors are also able to provide information on users accessing particular rooms and opening dressers, refrigerators, or trash cans. Details on installation and usage of magnetic switches and other types of door sensors can be found in [24], [31], [42]–[44].
- Audio sensors are usually used to detect sounds in-house and discriminate between different types of sounds. In [27], [45] microphones were installed to classify environmental sounds into classes such as speech, phone ringing, dish clanging, and TV/radio to extract events such as talking, a door closing, a person walking, a phone ringing, an object falling, and TV usage. In [46]

an array of acoustic sensors was installed to detect a person falling.

- A Wattmeter and other sensors that measure electricity consumption of domestic appliances and light are often used in identifying ADLs. Today, this can be one of the major indicator of well-being of a subject [47]. In [48], electricity consumed by room lights and various appliances was used to record electrical activity and then to translate it into the probability of a particular ADL. In [49] domestic energy was monitored along with other sensors to find abnormalities and monitor the person's health and security status.

A smart home is a normal living environment augmented with technology to improve the comfort or security of its residents.

Wearable sensors

In Table 2, we present a summary of wearable sensors that were used for activity recognition and ADL classification. Accelerometers are the most commonly used

sensors for action, movement, and activity recognition [44], [50]. Attached to a specified human body, location accelerometers allow to differentiate between different types of motion (e.g., running, walking, sitting, scrubbing, etc.) [51], [52] or help to identify the posture of a person [53]. Often, accelerometers are also used to detect falls by measuring vibration or acceleration [54]. In some studies, accelerometers are used together with gyroscopes to obtain orientation information and better distinguish various types of motion and movement [55].

Table 2. Wearable sensors used for ADL classification.

Sensor	Task	Usage Example
Accelerometer	Action recognition, types of motion, fall detection	Person running, person falling
Hand-worn sensors	Recognition of gestures, step counter	Person eating, person walking
Smartphone	Recognition of actions, movements, and types of motion	Person sleeping, person riding a bike
RFID	Recognition of actions of a person with objects	Cutlery usage, opening of cupboards, kitchen device usage
Vital monitoring sensors	Monitoring vital body parameters	High blood pressure detection, abnormal heart rate

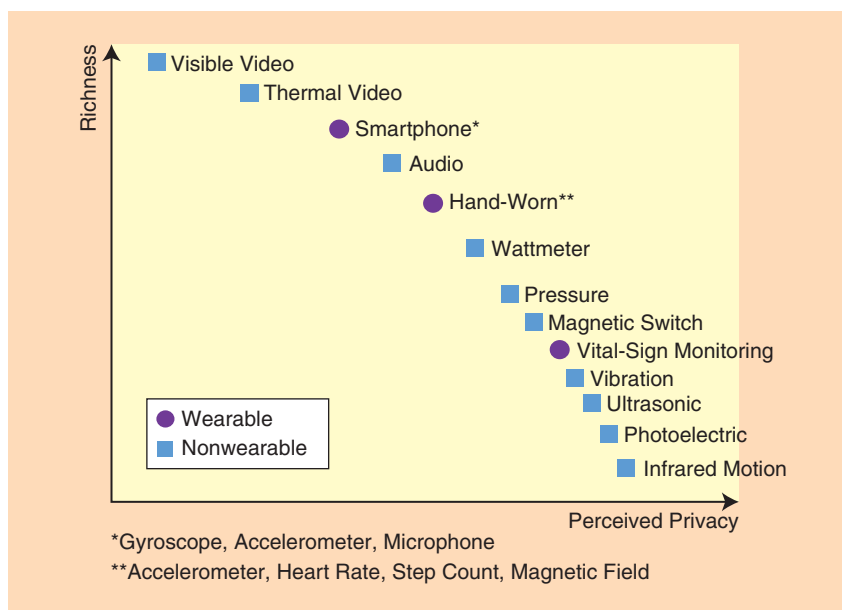


FIGURE 2. The richness of the sensors versus a user's perceived privacy.

Various types of hand-worn sensors are also considered in many activity recognition scenarios. These types of sensors include multifunctional wristwatches, magnetic sensors and other types of bracelets. Accelerometers are often integrated into wristwatches providing hand and arm gesture recognition capabilities [56]. In [57] an wrist-worn activity detector was used to perform sleep/awake activity classification. In [58] inertial sensors, accelerometers, and tilt switches were combined in a wrist-worn sensing unit to model users' rhythms and as a result recognize daily activities. Hand-worn magnetic sensors are able to distinguish between magnetic fields emitted by different electrical devices and recognize the activity of a user [59]. Emergency buttons are often integrated into a wristwatch and used to request help in case of an emergency situation [31]. Also, step counters are often integrated into wristwatches [57].

The modern smartphone offers a wealth of sensors, and can further be used as a communication platform [60]. Usually, accelerometers, gyroscopes, a global positioning system, a magnetometer and a microphone are incorporated into a modern smartphone device, providing all necessary information for movement, action and activity recognition including fall detection [61].

RFID tags are often used to detect the interaction of a person with an object and infer an ADL. In [62], RFID tags were deployed on various kitchen utensils such as bowls, cutlery, dishes, and jars to detect food preparation, eating, and drinking as well as on various cupboards, the TV, and furniture. Similar setups are considered in [63]–[65]. Matic et al. [66] focus specifically on monitoring dressing activity and detecting dressing failures. Often, RFID sensors are used in combination with other sensors such as accelerometers [66].

In addition to these sensors, there is also a large variety of sensors that monitor vital signs such as blood glucose, humidity and temperature, blood pressure, heart rate, pulse oximetry, CO₂ gas, electrocardiography, electroencephalography, electromyography, and electrooculography. These allow for the monitoring of a large set of human vital statistics and support activity recognition and ADL classification tasks [67], [68].

The ability of all of these sensors to provide rich information about people's lives and biometrics can raise severe privacy concerns. Figure 2 illustrates the richness of the sensors versus the perceived privacy of a person using these sensors. It is clear from the figure that sensors that provide rich information about a person are usually not perceived as privacy-preserving. For example, a video camera that allows for the recognition of almost any human activity in its field of view cannot be used in most rooms due to heavy privacy violations. In contrast, magnetic switches can be placed in every room without severely violating privacy, but they do not provide exhaustive information on every human activity. This can be partly improved by installing multiple instances of low-informative sensors (e.g., magnetic switches) so that richer insight into the user's activities can be achieved up to the level of the most informative sensors. However, this comes at the cost of increased installation efforts and complicates the deployment process.

State of the art in ADL experimental setups

A primary goal of AAL is to assess the self-maintenance of elderly people still living at home. Therefore, many studies in ambient intelligence focus on automatically recognizing human activities that correspond to ADLs, such as bathing,

Table 3. A summary of data sets collected in smart home environments, with their name and reference, whether wearable and/or nonwearable sensors were installed, approximately how long the (average) recording time was, and whether it was recorded in a (living) lab or a real home.

Data set	Institution	Sensor Types	Recording Duration	Lab/home
CASAS [70]	Washington State University	Wearable and nonwearable	Up to months	Lab and home
HIS [27]	Grenoble TIMC-IMAG Lab	Wearable and nonwearable	Hours	Lab
[23]	University of Virginia	Nonwearable	Weeks	Home
[24]	University of Amsterdam	Nonwearable	Weeks	Home
TigerPlace [71]	University of Missouri	Nonwearable	Year	Home
[65]	Intel Research Seattle	Wearable	Weeks	Home
[72]	Staffordshire University/Chiang Mai University	Wearable	Days	Lab
[63]	TU Darmstadt/Fraunhofer IGD	Wearable	Hours	Lab

cooking, and eating, to be able to determine any changes in their patterns. The experimental setting in which human activity data can be collected is called a *smart home*. A smart home is a normal living environment augmented with technology to improve the comfort or security of its residents [69]. In the domain of AAL, sensors installed in the smart home can be used to monitor the behavior of people living in the home. For example, a team at Washington State University introduced the Center for Advanced Studies in Adaptive Systems (CASAS) Smart Home to test machine-learning techniques for human activity recognition [70].

Depending on the focus of a study, the experimental scenario and, consequently, the requirements on the smart home environment vary. The smart home can be a real home where sensors are installed, but it may also be a lab in which a smart home is built and where temporary residents can stay for a shorter or longer period of time. In addition, some studies use predefined scenarios to be able to systematically evaluate activity recognition algorithms, while others investigate patterns of normal behavior. Finally, the type of sensors that are installed vary, depending on the focus, e.g., energy efficiency or privacy considerations. Table 3 lists a selection of smart home data sets and properties of the experimental settings.

Related to the two types of sensors described in the “State of the art in sensor technology to assess ADLs” section—wearable and nonwearable—the experimental approaches can be separated in in-situ and ambient approaches. In the in-situ approach, the goal is to correctly identify particular activities, and this is often tested in a laboratory setting for a short period of time according to predefined scenarios. The types of sensors used are mostly low cost and low power, so that many can be installed. These include accelerometers [63], [73], both body-worn and attached to objects; RFIDs [74], [75], also both body-worn and attached to objects; and door contact sensors. Although wearable sensors allow experiments to include activities outside of a home, contrary to the ambient approach, most work in the in-situ approach and are applied indoors and in living labs. The advantage of using low-cost and low-power sensors

is the possibility of running the installation for long uninterrupted periods. However, because these relatively simple sensors require a wide coverage, the initial set up requires more effort. Moreover, wearable sensors may not be easily accepted by elderly users.

The ambient approach is usually applied in experiments of longer duration in real-life settings, either in a smart home where participants live in an apartment (days or weeks, e.g., [70]) or in a real apartment (e.g., [71]). In the controlled environment of a smart home it is easier to gather detailed and balanced data and annotate them, for example, with cameras, making it suitable to gather data to test activity recognition algorithms. On the other hand, data recorded in real environments is more representative of normal behavior and therefore more suited to test algorithms for behavior modeling. For example, in [24], ambient sensors such as door contact sensors, motion sensors, and a float sensor in the toilet were used to recognize patterns of activities. This example was followed in [76] as part of the CASAS project to detect broad activities such as eating breakfast, sleeping, and wandering.

Generative models estimate the joint probability distribution of observation samples, which can be used to predict the most likely class to which a new sample belongs.

ADL classification

The signal processing and machine-learning methods that are referenced in the literature on ADL classification span a broad range of techniques, from simple heuristics to more advanced machine-learning algorithms such as hidden Markov models (HMMs) and conditional random fields (CRFs). Most of the classical machine-learning algorithms such as support vector machines (SVMs) and random forests assume input data that is independent and identically distributed (IID). However, there are certain cases where the independence assumption of each data point does not hold. This is true, for example, in speech recognition (every syllable is dependent on the nearby ones) but also for human behavior modeling and recognition: What someone is doing at a specific point in time is not independent from what he was doing just before. The taxonomy of machine-learning algorithms that are used for structured learning when the IID assumption does not hold is presented in Figure 3.

Two broad categories in machine learning are generative and discriminative models, where the former is modeling the joint probability distribution of the samples and the labels and the latter is modeling the conditional probability of the labels given the samples. The standard HMM is a typical algorithm of the first category, with several of its extensions also falling into the same group. In the discriminative group, the basic models are CRFs and their extensions [for example, latent-dynamic CRFs (LDCRFs) and semi-Markov CRFs (SMCRFs)] as well as certain types of artificial neural networks (ANNs), with the most prominent ones being the recurrent neural networks (RNNs).

Finally, a multitude of hybrid methods, aiming to combine the advantages of discriminative and generative models, are also available. These include, for example, approaches relying on kernel metric distances such as the Fisher kernel and various combinations of HMMs with discriminant models such as random forests and ANNs.

While most work in ADL classification is performed using one of the aforementioned machine-learning techniques, heuristic methods also were successfully applied. Short-term activities and data sets with sufficiently redundant sensor setups (to suppress false alarms) are especially suitable for heuristic methods. One successfully applied heuristic is the circadian activity rhythms [23], [77], which describe the measurement of home rhythmic behavioral activity as the resident engages in the habitat. In some cases, these simple heuristics are either fused together or used as features for a second-level machine-learning algorithm. For example, in [78], simple heuristics measures like means and variances

are used as features for neural network models, while the outcomes of the neural networks are fused under an HMM.

For the data representation in activity recognition and ADL classification scenarios, the bag-of-words (BoW) approach has proven to be convenient and successful. Originating in natural language processing, the BoW approach represents a text (such as a sentence or a document) as the bag (multiset) of its words, disregarding grammar and even word order but preserving multiplicity. An analogous bag-of-visual-words also has been successfully used for general image classification [79] and later for human action recognition and classification in video sequences [80]. Recent studies on human activity recognition show that the BoW representation allows achievement of high-performance action recognition [81], [82].

Generative models

Generative models estimate the joint probability distribution of observation samples, which can be used to predict the most likely class to which a new sample belongs. They are called *generative*, because the model can be used to generate samples given the joint probability distribution. HMMs are a popular generative model that can deal with structured data where the IID assumption does not hold. In the context of traditional HMMs (having a finite number of discrete states), three important questions are asked as part of the model learning and its application on unseen data [83].

- 1) *Likelihood*: Given a model and a sequence of observations, how likely is it that this sequence was generated by the given model? The answer to this problem is given by the forward-backward algorithm.
- 2) *Decoding*: What is the most likely sequence of model states that generated a sequence of observations? The answer to this question is given by the Viterbi algorithm.
- 3) *Learning*: How should transition and emission probabilities be learned from observed sequences? The answer is given by the Baum–Welch algorithm, which can be seen as a special case of the expectation maximization algorithm and tries to optimize the model parameters to best describe the observation sequence, while using also the results of the two previous problems.

Because HMMs are suitable to model sequential data, it is a popular classification method in activity recognition. A variety of HMM-based variants is presented in a comprehensive survey by Turage et al. [84]. Also, the recognition of human motion data can be modeled with HMMs. Li [85] proposed a straightforward and effective motion descriptor based on oriented histograms of optical flow field sequences. Following dimensionality reduction performed by principal component analysis, the method was applied to human action recognition using the HMM approach. Yamato et al., in [86], used HMMs in their simplest form: training a set of HMMs, one for each action and modeling the observation probability function as a discrete distribution, adopting

Because HMMs are suitable to model sequential data, it is a popular classification method in activity recognition.

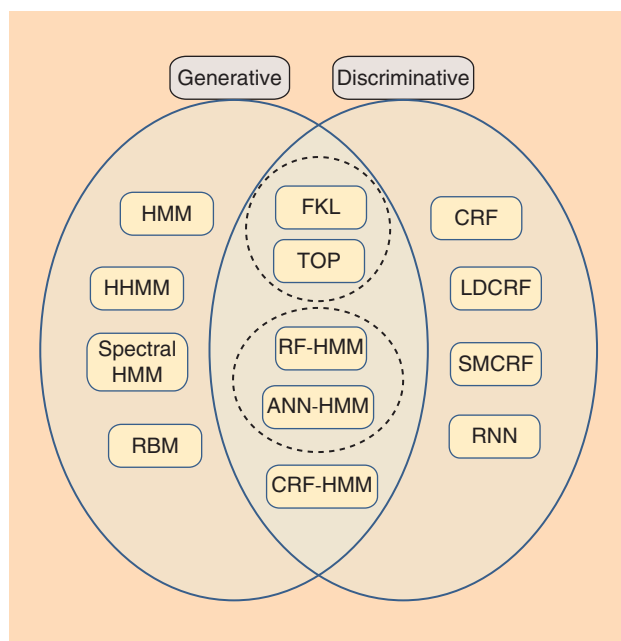


FIGURE 3. The taxonomy of algorithms for structured learning.

a mesh feature that computed frame by frame on the data [87]. Finally, the learning was based on the standard Baum–Welch approach. HMMs also can be applied on more complex data types, as demonstrated in Martinez et al. [88]. They proposed a framework for action recognition based on combining an HMM with a silhouette-based feature set. The proposed solution relies on a two-dimensional modeling of human actions based on motion templates, utilizing motion history images that combine viewpoint (spatial) and movement (temporal) representations.

Besides variations of the standard HMMs such as hierarchical HMMs (HHMMs) (where each class can be an HMM) and spectral HMMs (that can be used to do inference with unknown or continuous state spaces) the second important generative model are restricted Boltzmann machines (RBMs), which are implementing hidden layers in a stochastic neural network. They are often effective in cases where a lot of nonannotated data is available (typically thousands or tens of thousands of samples) but annotated data are scarce.

Discriminative models

While the approaches based on HMMs discussed in the previous section have achieved unquestionable success in numerous applications, one of the drawbacks of HMMs is that they cannot take advantage of powerful discriminative learning techniques that have been developed for the classification of vectorial data, such as kernel machines or metric learning. Contrary to generative models, discriminative models do not try to model the underlying probability distribution, but instead estimate the conditional probability of the labeled sequences given the observations. Among other advantages, discriminative models are typically efficient at dealing with data in high dimensional spaces.

SVMs [89] are considered to be one of the most powerful discriminative classification methods that were applied to various problems including activity recognition and ADL classification [72]. By leveraging the structural risk minimization and the kernel trick concepts [90], SVMs are very effective in discriminating between classes even on very high dimensional vectorial data. SVMs are using only few samples (support vectors) to describe their decision boundaries making them memory efficient and resistant to noise or small class overlaps. The main drawback of SVMs is the high computational complexity of the training procedure that practically limits their applicability. Linear SVMs that are not using kernels are more attractive for large-scale data sets, however, they are not so powerful as SVMs that employ kernels.

Random forest is an ensemble learning method that is using a set of decision trees to solve classification tasks. Introduced by Breiman [91], random forest is famous for its ability to accurately separate data while being able to naturally handle both numerical and categorical features. Random forest requires no

feature scaling procedure and by its intrinsic properties is not prone to overfitting. The employment of random forest in ADL classification scenarios can be found in [92].

CRFs have been proposed as a way to tackle similar structural problems where HMMs are applied, but relaxing certain of their assumptions [76], [93]. CRFs typically require less data to train than HMMs for a given performance level. They allow for the relaxation of the strong independence assumption between predictors and thereby allow for a richer set of features that can be partially overlapping. Their disadvantage is that they are computationally more complex (especially during training time) and, as all discriminative methods, they cannot make explicit estimations regarding the distribution of the observed variables and therefore cannot be used to sample from the learned model.

The standard CRF models the transitions between labels, thus capturing extrinsic dynamics, but lack the ability to represent internal substructure. Several modifications of the standard CRF have been proposed and applied to ADL classification including LDCRFs and semi-CRFs which, however, can be very computationally expensive.

Hybrid models

To address the drawbacks of generative and discriminative models, various studies have proposed to combine them into hybrid ones. Hybrid models allow to leverage the ability to separate structural objects by learning similarity between them and, at the same time, to have access to all tools and advantages of generative models listed above. The Fisher kernel [94] and tangent vector of posterior log-odds (TOP) kernel are cases of such a hybrid method that relies on kernel metric distances. Other hybrid algorithms use a discriminant model such as an ANN or random forest to calculate the frame posterior probabilities and/or additional synthetic features while an HMM is responsible for modeling time dependencies on a metalevel through temporal smoothing on the estimated outcomes of the discriminative methods. Finally, CRF-HMM is another hybrid model often used in natural language processing due to its ability to model non-IID data both at the low as well as the high level of representation, for example to capture relations between letters and words.

Recently, hybrid HMM models have been also proposed for activity recognition. Ellis et al. [95] proposed to first learn low-level code-book representations for each sensor and use a random forest classifier to produce minute-level probabilities for each activity class. Subsequently, a higher-level HMM layer is used to learn patterns of transitions and durations of activities over time to smooth the minute-level predictions. Fisher kernel learning (FKL) is another approach that combines the flexibility of generative methods and the power of discriminative ones [96]. Fisher kernel representations have recently been applied to activity recognition problems [97]. The key intuition behind the Fisher

To address the drawbacks of generative and discriminative models, various studies have proposed to combine them into hybrid ones.

kernel is that similar objects induce similar log-likelihood gradients in the parameters of a generative model allowing effective discrimination of these objects. To construct a Fisher kernel for structured objects, it is required to calculate the log-likelihood gradient for each of the objects in the parameters of a generative model. The Fisher kernel function can then be derived as a weighted inner product between the gradients of two structured objects [96]. The weighting is typically performed using the Fisher information metric; this weighting is necessary because different

types of model parameters have different scales. Jaakkola and Haussler [94] have shown that the Fisher information metric is asymptotically immaterial, which is the theoretical basis for often assuming it to be an identity matrix. In this case, a (normalized) kernel is used that simply embeds objects in an Euclidean space by using the gradients induced by the objects as features [96].

Experimental results

To evaluate different ADL classification methods, we consider the following three data sets:

- *Data set 1:* This data set [24] describes the activities of a 26-year-old man in his apartment where he lived alone. Fourteen state-change sensors were installed at doors, cupboards, the refrigerator, and the toilet flush. Sensors were left unattended, collecting data for 28 days in the apartment, resulting in 2,120 sensor events and 245 activity instances [24]. Seven ADL types were annotated.
- *Data set 2:* The second data set [98] is one of the multiple data sets recorded from the CASAS group of Washington State University. This particular data set was selected because it has the interesting property of capturing the activities of two people in a house, which can occur also in a practical application where one of the residents is a patient while the other is still healthy. The data were recorded over a period of two months using 34 sensors of four types: motion, item, door, and water sensors. Based on the annotations, 124 instances of activities of interest were captured.
- *Data set 3:* Finally, we recorded our own data set in two independent households, each for one week. The sensors installed include contact, motion, acoustic sensors, and power meters. In the first household, there were 7,856 events and in the second household there were 8,618 events, which resulted in 394 and 644 activity instances, respectively, that were annotated as five different ADL types. In the first household, five contact sensors, five motion sensors, three acoustic sensors, and three power meters were distributed over three rooms. In the second household, three contact sensors, five motion sensors, two acoustic sensors, and three power meters were distributed over two rooms. The room layout and sensor positions are shown in Figures 4 and 5.

The following four classifiers are most prominent in the community and are tested on all three data sets: 1) SVM, 2) random forest, 3) HMM, and 4) FKL. Regarding the evaluation of classification accuracy, the time slice accuracy is an established way of evaluating time series and represents the percentage of correctly classified frames, independently of the ADLs. However, since some of the ADLs have significantly larger duration compared to others, we also use the average class accuracy as a second criterion to avoid skewing the performance evaluation exclusively toward the dominant classes. To compute these accuracies, cross-validation is used. However, since the problem is structured learning and the IID assumption does not hold, the cross-validation is done at the event level, that is, without partitioning the samples of the same ADL. For example, of a total of

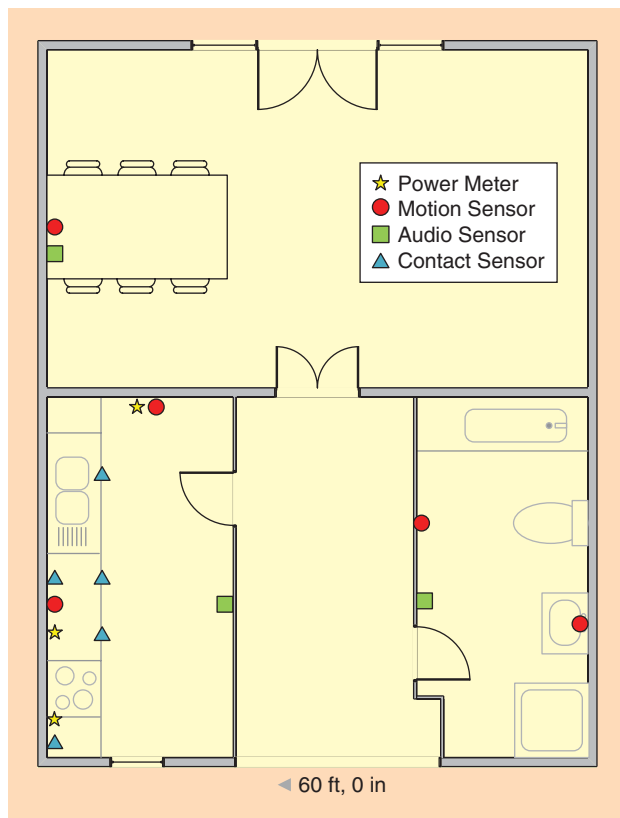


FIGURE 4. The layout and sensor setup of the first household.

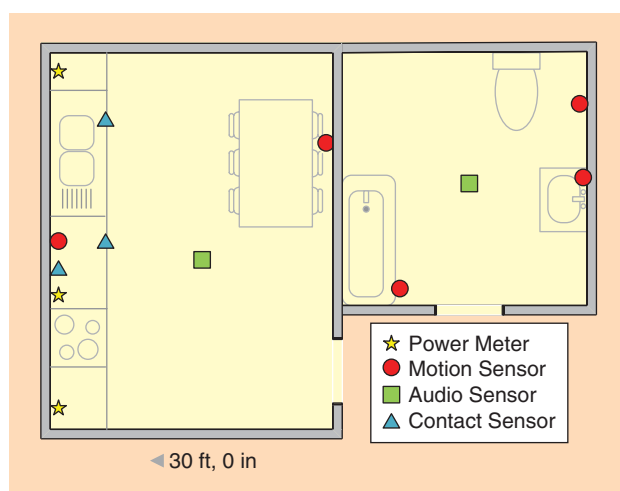


FIGURE 5. The layout and sensor setup of the second household.

Table 4. Time-slice and class-average accuracy for SVM, RF, HMM, and FKL on data set 1.

	SVM	RF	HMM	FKL
Timeslice Accuracy				
Idle	0.82	0.80	0.19	0.67
Toilet	0.58	0.81	0.87	0.77
Shower	0.14	0.10	0.71	0.82
Bed	0.37	0.99	0.96	0.95
Eat	0.28	0.29	0.34	0.61
Drink	0.38	0.13	0.00	0.42
Class-average accuracy	0.43	0.52	0.51	0.71

30 food preparation instances, 20 might end up in the training and the remaining ten in the validation set, both with their full duration (all frames).

Data set 1

The evaluation results on data set 1 are presented in Table 4. Of the different classifiers, FKL performs best on average. SVM has the lowest class-average accuracy since it does not consider time dependencies between data samples. The same holds for random forest, however it is very effective at modeling the variations in the execution of different ADLs and also is a bit less prone to overfit the dominant class (especially given that the annotation of ADLs is to some extent subjective resulting in some noise on the labels). The number of states per class for HMM was taken the same for all classes and this resulted in relatively low accuracy (in other words, this basic type of HMM cannot effectively model sequences that vary significantly in complexity for the different classes). The intrinsic number of states is different for various ADLs and should be determined carefully to obtain better performance. For example, there is a multitude of ways for doing food preparation but fewer ways for drinking. However, this would increase the complexity of HMM, requiring more training data and/or a model that can better capture hierarchy, like an HHMM. A full overview on the confusion between classes for FKL is provided in Figure 6.

Overall, the accuracies of classes Eat and, especially, Drink are substantially lower than those of the other classes because they are confused with each other and Idle. Both activities take place in the same location and involve similar actions such as opening a refrigerator or cupboard. The magnetic contact sensors that comprise the majority of the sensors in this data set are not very efficient for discriminating between events that are so similar that they involve triggering of the exact same sensors.

Data set 2

Because the activities of two residents are recorded in this data set and the classifiers do not allow for overlapping activities, the classifiers are trained and tested on the activities of one of the residents. However, this means the learned activities in the training data as well as the activities in the test set can be



FIGURE 6. The confusion matrix for FKL on data set 1.

Table 5. Time-slice and class-average accuracy for SVM, RF, HMM, and FKL on data set 2.

	SVM	RF	HMM	FKL
Timeslice Acc.				
Personal hygiene	0.56	0.61	0.51	0.64
Sleep	0.43	0.47	0.42	0.52
Work	0.76	0.78	0.80	0.77
Meal preparation	0.84	0.89	0.93	0.84
Watch TV	0.30	0.35	0.00	0.41
Class-average accuracy	0.58	0.62	0.53	0.64

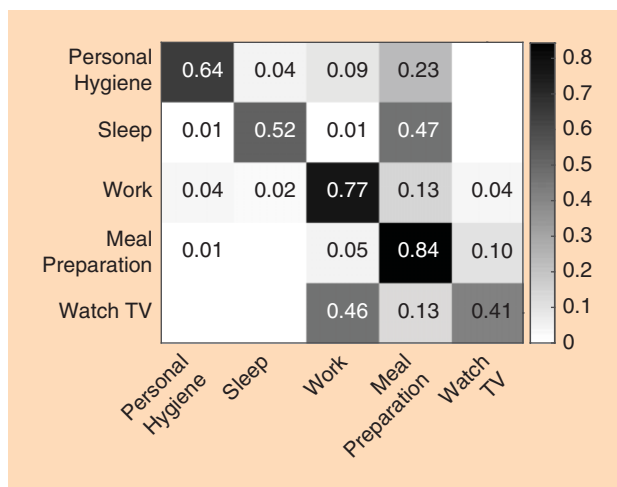


FIGURE 7. The confusion matrix for FKL on data set 2.

contaminated by the second resident. However, the evaluation results in Table 5 show that the classification algorithms can deal with this possible confusion to some extent, except for the Watch TV class. The effect of the contamination will reduce as the number of training examples increases, while the noise on the performance evaluation can be reduced by a bigger test set.

Similar to data set 1 with a one-person household, FKL shows the highest performance in terms of average accuracy. random forest and SVM perform slightly worse than FKL, while HMM provides the worst average accuracy, mostly because of the complete failure on the Watch TV class. A confusion matrix for FKL is provided in Figure 7. The classes Work and Meal Preparation can be discriminated the best among all other ADLs in this data set, while Personal Hygiene and Sleep demonstrate moderate recognition accuracy, and Watch TV performs the worst. Since two people are living in the apartment and can

Automatic classification of ADLs enables automatic monitoring of the ability of an elderly person to live independently in his house and can allow for early detection of diseases such as Alzheimer and dementia.

perform different activities at the same time and at different locations, dissimilar activities such as Sleep and Meal Preparation can be also confused.

Data set 3

For the third data set, we evaluated two scenarios. In the first scenario (one household) training and testing were done only using events coming from a single household. In the second scenario (two households) training and testing were performed on data taken from both

households. All events from both households were shuffled in a way that the event sequence within one ADL is kept to preserve the structure in the data (non-IID assumption). Evaluation results on data set 3 for random forest, SVM, HMM, and FKL on one and two households are provided in Tables 6 and 7, respectively.

Also, for this data set, FKL outperforms the other methods, both for the one household and the two households scenario (see Tables 6 and 7). However, the performance of random forest and HMM are very close to FKL for the two households scenario. The HMM even has an improved performance compared to its performance for the one household scenario, probably because (for this data set) the improvement that it can gain with more data is bigger than the potential loss because of increased variation in the class representation.

The confusion matrices of FKL for the two scenarios are shown in Figures 8 and 9. In the one household scenario, FKL can achieve high performance, with the only noteworthy confusion appearing for very similar activities (see Figure 8). For example, Food Preparation and No ADL (which is defined as an activity that is not described by a formal ADL, e.g., standing in the kitchen, reading at a table, etc.) have an overlap while Continen- ce and Hygiene also are partly difficult to discriminate in the absence of clear signature detections from the sensors on

Table 6. Time-slice and class-average accuracy for SVM, RF, HMM, and FKL on data set 3 for the one household scenario.

	SVM	RF	HMM	FKL
Time-slice Acc.				
No ADL	0.12	0.31	0.17	0.65
Continen- ce	0.39	0.90	0.75	0.70
Hygiene	0.93	0.81	0.63	0.79
Showering	0.89	0.73	0.55	0.94
Food preparation	0.96	0.93	0.98	0.75
Class-average accuracy	0.66	0.74	0.62	0.77

Table 7. Time-slice and class-average accuracy for SVM, RF, HMM, and FKL on data set 3 for the two households scenario.

	SVM	RF	HMM	FKL
Time-slice Acc.				
No ADL	0.31	0.19	0.62	0.63
Continen- ce	0.87	0.91	0.64	0.54
Hygiene	0.72	0.74	0.57	0.78
Showering	0.64	0.44	0.80	0.87
Food preparation	0.88	0.94	0.84	0.74
Class-average accuracy	0.68	0.64	0.69	0.71

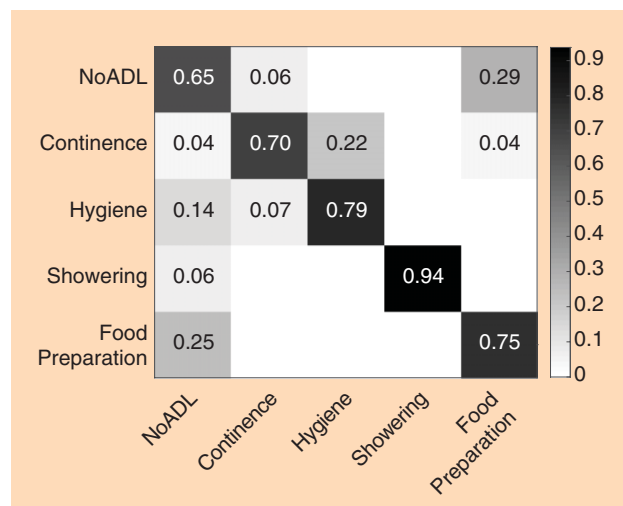


FIGURE 8. The confusion matrix for FKL on data set 3 for one household.

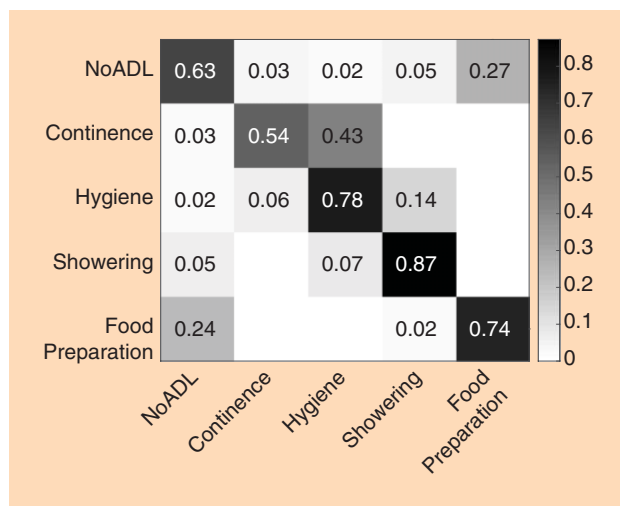


FIGURE 9. The confusion matrix for FKL on data set 3 for two households.

which the events are based (such as water running in the sink, toilet flushing, etc.).

The experiment with two households is more challenging and also more interesting, first of all because the sensor setups between the households are similar but not identical, and a BoW approach is used to map them in a common feature space for learning and inference. Furthermore, the households have different layouts and the persons are doing certain activities in very different ways. For example, in one of the households, cooking always involves opening and closing multiple kitchen cupboards while in the other household this is only done sporadically. Nevertheless, the classification scheme based on Fisher kernel is able to do learning and inference in the joined space, with the only significant overlap between classes appearing between the Contingence and Hygiene, which is to some extent attributable to the different sensor setups and bath layouts.

Conclusions

Automatic classification of ADLs is a crucial part of assisted living technologies. It enables automatic monitoring of the ability of an elderly person to live independently in his or her house and can allow for early detection of diseases such as Alzheimer's and dementia. ADL classification involves the whole chain from a plethora of wearable and nonwearable sensors, deployment options, and signal processing and machine-learning algorithms. Our study concludes that the recent developments in hybrid generative/discriminative methods, relying on kernel metric distances, are superior over traditional generative methods such as HMM and its variants. Specifically, FKL showed the best performance in a variety of data sets covering different activity types, sensors, and setups.

We expect continuing improvements on all aspects of the aforementioned chain ranging from improvement of existing sensor technologies, addition of new sensors, the acceptability of certain technologies up to various algorithmic aspects such as the generalizability and adaptiveness that are briefly detailed next.

Sensor technologies require improvements in several directions including size, accuracy, energy efficiency, and reliability. Establishing a common communication protocol would allow to create an unified framework, providing a significant speed up in infrastructure deployment. Reusability of sensors from smart home applications would be another boosting factor helping to reduce infrastructure and installation costs. Several legal issues related to the data ownership and data security have to be addressed to get acceptance for using ADL monitor systems.

While sensor technology improves, leading to higher-quality measurements and lower costs and maintenance, in practical applications the (elderly) user needs to be taken into account as well (see Figure 1). Specifically, user-centered design and transparency can help to increase the acceptance of users of technology in their home and their perceived privacy [15]. Furthermore, users are more and more exposed to sensor technology in other aspects of their lives, increasing their understanding and, thereby, acceptance.

There is still progress to be made such that research in ADL classification can be reliably applied in a practical solution.

Finally, we note that there is still progress to be made such that research in ADL classification can be reliably applied in a practical solution. This covers the optimization of sensor setups for cost effectiveness, adaptive classification algorithms that allow tracking changing behavior over time and robustness with respect to context changes such as handling of visitors, caregiving personnel, or

pets. One of the biggest challenges from the signal processing and machine-learning side remains the generalizability over households. While training for an individual household is easily possible in a lab setup, this approach is not scalable to a real-world scenario with thousands of households and more. A successful approach for generalizability has to consider environmental/climate parameters, building layout, sensor placement, and the behavior of the elderly.

Authors

Christian Debes (cdebes@agtinternational.com) received B.Sc., M.Sc., and Ph.D. (with highest honors) degrees from Technische Universität Darmstadt, Germany, in 2004, 2006, and 2010, respectively. He currently holds a position as lead data scientist at AGT International and lecturer at Technische Universität Darmstadt, Germany. He is a recipient of the IEEE Geoscience and Remote Sensing Society 2013 Data Fusion Best Classification Award and has authored more than 30 journal and conference papers in target detection, classification, and image processing. He is a member of the editorial board of *Digital Signal Processing* (Elsevier) and area editor of *IEEE Signal Processing Magazine*. He is a Senior Member of the IEEE.

Andreas Merentitis (andreas.merentitis@ieee.org) received B.Sc., M.Sc., and Ph.D. degrees from National Kapodistrian University of Athens in 2003, 2005, and 2010 respectively. In 2011, he joined the research center of AGT International, Darmstadt, Germany, where he is now working as a senior data scientist. He has more than 30 publications related to different aspects of data analysis and machine learning. He was awarded an IEEE Certificate of Appreciation as a core member of the team that won the first place in the Best Classification Challenge of the 2013 IEEE Geoscience and Remote Sensing Society Data Fusion Contest. He is an associate editor of *IEEE Signal Processing Magazine* and a Member of the IEEE.

Sergey Sukhanov (ssukhanov@agtinternational.com) received B.Sc. and M.Sc. degrees from Saint-Petersburg State Electrotechnical University, Russia, and Technische Universität Darmstadt, Germany, respectively. Since 2015, he has been working as a data scientist at AGT International, Darmstadt, Germany. His research interests include data analysis and machine learning. He is a Student Member of the IEEE.

Maria Niessen (mniessen@agtinternational.com) received M.Sc. and Ph.D. degrees from the University of Groningen, The Netherlands. After two years of postdoctoral research at INCAS, she joined AGT International, Darmstadt, Germany, in 2012, where she is currently a senior data scientist. Her research interests include data analysis and acoustics.

Nikolaos Frangiadakis (nfrangiadakis@agtinternational.com) received M.Sc. and Ph.D. degrees from the University of Maryland, College Park. Since 2011, he has been working as a senior researcher at AGT International, Darmstadt, Germany. He is recipient of the IEEE Geoscience and Remote Sensing Society 2013 Data Fusion Best Classification Award, and his research interests include data analysis, mobility modeling, simulation, and prediction. He is a Member of the IEEE.

Alexander Bauer (abauer@agtinternational.com) received the Dipl.-Ing. degree from Karlsruhe Institute of Technology, Germany. He received his Ph.D. degree in computer science from Karlsruhe Institute of Technology, Germany, for his work on recommendation algorithms for satellite image interpretation systems of the German Strategic Intelligence Command. He is a lead data scientist at AGT International, Darmstadt, Germany, with ten years of experience in pattern recognition and machine learning. Since joining AGT in 2011, he designs data analytics components for anomaly detection, behavior analytics, and pattern learning.

References

- [1] M. M. Muszynska and R. Rau, "The old-age healthy dependency ratio in Europe," *J. Popul. Ageing*, vol. 5, no. 3, pp. 151–162, 2012.
- [2] K. Giannakouris, "Ageing characterises the demographic perspectives of the Europe societies," in *Eurostat: Statistics in Focus*, vol. 72. 2008. [Online]. Available: <http://bookshop.europa.eu/en/ageing-characterises-the-demographic-perspectives-of-the-european-societies-pbKSSF08072/>
- [3] G. K. Vincent and V. A. Velkoff, *The Next Four Decades: The Older Population in the United States: 2010 to 2050*, US Department of Commerce, Economics and Statistics Administration, U.S. Census Bureau, 2010.
- [4] N. Farber and D. Shinkle, "Aging in place: A state survey of livability policies and practices," AARP Research Rep., Dec. 2011. [Online]. Available: <https://assets.aarp.org/rgcenter/ppi/liv-com/aging-in-place-2011-full.pdf>
- [5] E. Oppers, K. Chikada, F. Eich, P. Imam, J. Kiff, M. Kisser, M. Soto, and T. Sun, "The financial impact of longevity risk," in *Global Financial Stability Report*. Washington, D.C.: International Monetary Fund, 2012.
- [6] D. Silcock and D. Sinclair, "The cost of our ageing society," Tech. Rep., The International Longevity Centre, 2012. [Online]. Available: http://socialwelfare.bl.uk/subject-areas/services-client-groups/older-adults/ilcuk/141789The_cost_of_our_ageing_society.pdf
- [7] D. J. Cook, J. C. Augusto, and V. R. Jakkula, "Ambient intelligence: Technologies, applications, and opportunities," *Pervasive Mob Comput.*, vol. 5, no. 4, pp. 277–298, 2009.
- [8] P. Rashidi and A. Mihailidis, "A survey on ambient-assisted living tools for older adults," *IEEE J. Biomed. Health Inform.*, vol. 17, no. 3, pp. 579–590, 2013.
- [9] G. Acampora, D. J. Cook, P. Rashidi, and A. V. Vasilakos, "A survey on ambient intelligence in healthcare," *Proc. IEEE*, vol. 101, no. 12, pp. 2470–2494, 2013.
- [10] S. Katz, T. D. Downs, H. R. Cash, and R. C. Grotz, "Progress in development of the index of ADL," *Gerontologist*, vol. 10, no. 1, pp. 20–30, Spring 1970. [Online]. Available: http://gerontologist.oxford-journals.org/content/10/1_Part_1/20.abstract
- [11] L. Nygard, "Instrumental activities of daily living: A stepping-stone towards Alzheimer's disease diagnosis in subjects with mild cognitive impairment?," *Acta Neurol. Scand.*, vol. 107, pp. 42–46, Feb. 2003.
- [12] D. Galasko, D. Bennett, M. Sano, C. Ernesto, R. Thomas, M. Grundman, and S. Ferris, "An inventory to assess activities of daily living for clinical trials in Alzheimer's disease," *Alzheimer Dis. Assoc. Disord.*, vol. 11, no. 2, pp. 33–39, 1997.
- [13] R. S. Bucks, D. L. Ashworth, G. K. Wilcock, and K. Siegfried, "Assessment of activities of daily living in dementia: Development of the Bristol activities of daily living scale," *Age Ageing*, vol. 25, no. 2, pp. 113–120, 1996.
- [14] P. Barberger-Gateau, D. Commenges, M. Gagnon, L. Letenneur, C. Sauvel, and J.F. Dartigues, "Instrumental activities of daily living as a screening tool for cognitive impairment and dementia in elderly community dwellers," *J. Amer. Geriatr. Soc.*, vol. 40, no. 11, pp. 1129–1134, 1992.
- [15] L. Lorenzen-Huber, M. Boutain, L. J. Camp, K. Shankar, and K. H. Connelly, "Privacy, technology, and aging: A proposed framework," *Ageing Int.*, vol. 36, no. 2, pp. 232–252, 2011.
- [16] W. L. Zagler, P. Panek, and M. Rauhala, *Ambient Assisted Living Systems-The Conflicts between Technology, Acceptance, Ethics and Privacy*. Wadern, Germany: Internat. Begegnungs-und Forschungszentrum für Informatik, 2008.
- [17] P. Rashidi, D. J. Cook, L. B. Holder, and M. Schmitter-Edgecombe, "Discovering activities to recognize and track in a smart environment," *IEEE Trans. Knowl. Data Eng.*, vol. 23, no. 4, pp. 527–539, 2011.
- [18] S. Patel, H. Park, P. Bonato, L. Chan, and M. Rodgers, "A review of wearable sensors and systems with application in rehabilitation," *J. Neuroeng. Rehabil.*, vol. 9, no. 12, pp. 1–17, 2012.
- [19] M. Chan, E. Campo, and D. Esteve, "Assessment of activity of elderly people using a home monitoring system," *Int. J. Rehabil. Res.*, vol. 28, no. 1, pp. 69–76, 2005.
- [20] R. Suzuki, S. Otake, T. Izutsu, M. Yoshida, and T. Iwaya, "Rhythm of daily living and detection of atypical days for elderly people living alone as determined with a monitoring system," *J. Telemed. Telecare*, vol. 12, no. 4, pp. 208–214, 2006.
- [21] M. Alwan, J. Leachtenauer, S. Dalal, D. Mack, S. Kell, and B. Turner, "Impact of monitoring technology in assisted living: Outcome pilot," *IEEE Trans. Inform. Technol. Biomed.*, vol. 10, no. 12, pp. 192–198, 2006.
- [22] H. W. Tyrer, M. A. Aud, G. Alexander, M. Skubic, and M. Rantz, "Early detection of health changes in older adults," in *Proc. Engineering in Medicine and Biology Society*, 2007, pp. 4045–4048.
- [23] G. Virone, M. Alwan, S. Dalal, S. W. Kell, B. Turner, J. A. Stankovic, and R. Felder, "Behavioral patterns of older adults in assisted living," *IEEE Trans. Inform. Technol. Biomed.*, vol. 12, no. 3, pp. 387–398, 2008.
- [24] T. L. M. Van Kasteren, A. Noulas, G. Englebienne, and B. J. A. Kröse, "Accurate activity recognition in a home setting," in *Proc. ACM Int. Joint Conf. Pervasive and Ubiquitous Computing*, 2008, pp. 1–9.
- [25] M. Skubic, G. Alexander, M. Popescu, M. Rantz, and J. Keller, "A smart home application to elder care: Current status and lessons learned," *Technol. Health Care*, vol. 17, no. 3, pp. 183–201, 2009.
- [26] J. Biswas, S. D. Kumar, Q. Qui, V. C. Saradhi, and V. T. Pham, "Quality aware elderly people monitoring using ultrasonic sensors," in *Proc. 3rd Int. Conf. Smart Homes and Health Telematics*, 2005, pp. 107–115.
- [27] A. Fleury, M. Vacher, and N. Noury, "SVM-based multimodal classification of activities of daily living in health smart homes: Sensors, algorithms, and first experimental results," *IEEE Trans. Inform. Technol. Biomed.*, vol. 14, no. 2, pp. 274–283, 2010.

- [28] L. Vuegen, B. Van Den Broeck, P. Karsmakers, H. Van Hamme, and B. Vanrumste, "Automatic monitoring of activities of daily living based on real-life acoustic sensor data: A preliminary study," in *Proc. Workshop on Speech and Language Processing for Assistive Technologies*, 2013, vol. 4, pp. 113–118.
- [29] J. Biswas, F. Naumann, and Q. Qiu, "Assessing the completeness of sensor data," in *Proc. Database Systems for Advanced Applications*, 2006, pp. 717–732.
- [30] V. T. Pham, Q. Qiu, A. A. P. Wai, and J. Biswas, "Application of ultrasonic sensors in a smart environment," *Pervasive Mob. Comput.*, vol. 3, no. 2, pp. 180–207, 2007.
- [31] K. Doughty and J. Costa, "Continuous automated telecare assessment of the elderly," *J. Telemed. Telecare*, vol. 3, no. 1, pp. 23–25, 1997.
- [32] K. Z. Haigh, L. M. Kiff, and G. Ho, "The independent lifestyle assistant: Lessons learned," *Assist. Technol.*, vol. 18, no. 1, pp. 87–106, 2006.
- [33] K. Cameron, K. Hughes, and K. Doughty, "Reducing fall incidence in community elders by telecare using predictive systems," in *Proc. 19th Annu. Int. Conf. IEEE Engineering in Medicine and Biology Society*, 1997, vol. 3, pp. 1036–1039.
- [34] E. M. Tapia, S. S. Intille, and K. Larson, "Activity recognition in the home using simple and ubiquitous sensors," *Pervasive Comput.*, vol. 3001, pp. 158–175, Apr. 2004.
- [35] J. Han and B. Bhanu, "Human activity recognition in thermal infrared imagery," in *Proc. IEEE Computer Society Conf. Computer Vision and Pattern Recognition*, 2005, pp. 17–17.
- [36] P. Hevesi, S. Wille, G. Pirkel, N. Wehn, and P. Lukowicz, "Monitoring household activities and user location with a cheap, unobtrusive thermal sensor array," in *Proc. ACM Int. Joint Conf. Pervasive and Ubiquitous Computing*, 2014, pp. 141–145.
- [37] Y. Zigel, D. Litvak, and I. Gannot, "A method for automatic fall detection of elderly people using floor vibrations and sound - proof of concept on human mimicking doll falls," *IEEE Trans. Biomed. Eng.*, vol. 56, no. 12, pp. 2858–2867, 2009.
- [38] S. S. Intille, K. Larson, J. S. Beaudin, J. Nawyn, E. M. Tapia, and P. Kaushik, "A living laboratory for the design and evaluation of ubiquitous computing technologies," in *Proc. CHI'05 Extended Abstracts on Human Factors in Computing Systems*, 2005, pp. 1941–1944.
- [39] T. Tsukiyama, "Ambient sensor system for in-home health monitoring," in *Proc. The 4th Int. Conf. Ambient Computing, Applications, Services and Technologies*, 2014, pp. 47–50.
- [40] L. Hu, Y. Chen, S. Wang, and L. Jia, "A nonintrusive and single-point infrastructure-mediated sensing approach for water-use activity recognition," in *Proc. IEEE Int. Conf. Embedded and Ubiquitous Computing*, 2013, pp. 2120–2126.
- [41] J. H. Lim, H. Jang, J. Jang, and P. Soo-Jun, "Daily activity recognition system for the elderly using pressure sensors," in *Proc. Engineering in Medicine and Biology Society*, 2008, pp. 5188–5191.
- [42] N. Noury, T. Herve, V. Rialle, G. Virone, E. Mercier, G. Morey, A. Moro, and T. Porcheron, "Monitoring behavior in home using a smart fall sensor and position sensors," in *Proc. Int. Conf. Microtechnologies in Medicine and Biology*, 2000, pp. 607–610.
- [43] A. Glascock and D. Kutzik, "Behavioral telemedicine: A new approach to the continuous nonintrusive monitoring of activities of daily living," *Telemed. J.*, vol. 6, no. 1, pp. 33–34, 2004.
- [44] L. Atallah, B. Lo, R. Ali, R. King, and Y. Guang-Zhong, "Real-time activity classification using ambient and wearable sensors," *IEEE Trans. Inform. Technol. Biomed.*, vol. 13, no. 6, pp. 1031–1039, 2009.
- [45] A. Fleury, N. Noury, M. Vacher, H. Glasson, and J. F. Seri, "Sound and speech detection and classification in a health smart home," in *Proc. 30th Annu. Int. Conf. Engineering in Medicine and Biology Society*, 2008, pp. 4644–4647.
- [46] M. Popescu, Y. Li, M. Skubic, and M. Rantz, "An acoustic fall detector system that uses sound height information to reduce the false alarm rate," in *Proc. 30th Annu. Int. Conf. Engineering in Medicine and Biology Society*, 2008, pp. 4628–4631.
- [47] T. D. Hunt, D. Rajendran, M. Nikora, S. Bennett, and A. Fendall, "A minimally intrusive monitoring system that utilizes electricity consumption as a proxy for wellbeing," *J. Appl. Comput. Inform. Technol.*, vol. 18, no. 2, 2014. [Online]. Available: <https://doaj.org/article/30741addf579403387b4bb9d3fb2bfff3>
- [48] G. C. Franco, F. Gallay, M. Berenguer, C. Mourrain, and P. Couturier, "Noninvasive monitoring of the activities of daily living of elderly people at home—A pilot study of the usage of domestic appliances," *J. Telemed. Telecare*, vol. 14, no. 5, pp. 231–235, 2008.
- [49] D. Fei and J.-Y. Xiong, "The investigation of the elder's monitoring system based on life supplying line," in *Proc. IEEE Int. Conf. Industrial Technology*, 2005, pp. 314–318.
- [50] T. Huỳnh, U. Blanke, and B. Schiele, "Scalable recognition of daily activities with wearable sensors," in *Proc. Location-and Context-Awareness*, 2007, pp. 50–67.
- [51] Y. Yang, J. S. Wang, and J. P. Chen, "Using acceleration measurements for activity recognition: An effective learning algorithm for constructing neural classifiers," *Pattern Recognit. Lett.*, vol. 29, no. 16, pp. 2213–2220, 2008.
- [52] A. M. Khan, Y. K. Lee, and S. Y. Lee, "Accelerometer's position free human activity recognition using a hierarchical recognition model," in *Proc. 12th IEEE Int. Conf. e-Health Networking Applications and Services*, 2010, pp. 296–301.
- [53] H. Gjoreski, M. Lustrek, and M. Gams, "Accelerometer placement for posture recognition and fall detection," in *Proc. 7th Int. Conf. Intelligent Environments*, 2011, pp. 47–54.
- [54] M. J. Mathie, A. Coster, N. Lovell, G. Celler, S. Lord, and A. Tiedemann, "A pilot study of long-term monitoring of human movements in the home using accelerometry," *J. Telemed. Telecare*, vol. 10, no. 3, pp. 144–151, 2004.
- [55] Q. Li, J. A. Stankovic, M. A. Hanson, A. T. Barth, J. Lach, and G. Zhou, "Accurate, fast fall detection using gyroscopes and accelerometer-derived posture information," in *Proc. 6th Int. Workshop on Wearable and Implantable Body Sensor Networks*, 2009, pp. 138–143.
- [56] R. Amstutz, O. Amft, B. French, A. Smailagic, D. Siewiorek, and G. Troster, "Performance analysis of an hmm-based gesture recognition using a wristwatch device," in *Proc. Int. Conf. Computational Science and Engineering*, 2009, pp. 303–309.
- [57] J. Merilahti, J. Pärkkä, K. Antila, P. Paavilainen, E. Mattila, E. J. Malm, A. Saarinen, and I. Korhonen, "Compliance and technical feasibility of long-term health monitoring with wearable and ambient technologies," *J. Telemed. Telecare*, vol. 15, no. 6, pp. 302–309, 2009.
- [58] K. Van Laerhoven, D. Kilian, and B. Schiele, "Using rhythm awareness in long-term activity recognition," in *Proc. IEEE Int. Symp. Wearable Computers*, 2008, pp. 63–66.
- [59] T. Maekawa, Y. Kishino, Y. Sakurai, and T. Suyama, "Activity recognition with hand-worn magnetic sensors," *Pers. Ubiquitous Comput.*, vol. 17, no. 6, pp. 1085–1094, 2013.
- [60] J. Lester, T. Choudhury, and G. Borriello, "A practical approach to recognizing physical activities," in *Proc. Pervasive Computing*, 2006, pp. 1–16.
- [61] J. R. Kwapisz, G. M. Weiss, and S. A. Moore, "Activity recognition using cell phone accelerometers," *SIGKDD Explor. Newsl.*, vol. 12, no. 2, pp. 74–82, 2010.

- [62] S. Park and H. Kautz, "Hierarchical recognition of activities of daily living using multi-scale, multi-perspective vision and RFID," in *Proc. IET 4th Int. Conf. Intelligent Environments*, IET, 2008, pp. 1–4.
- [63] M. Stikic, T. Huynh, K. Van Laerhoven, and B. Schiele, "ADL recognition based on the combination of RFID and accelerometer sensing," in *Proc. 2nd Int. Conf. Pervasive Computing Technologies for Healthcare*, 2008, pp. 258–263.
- [64] M. Buettner, R. Prasad, M. Philipose, and D. Wetherall, "Recognizing daily activities with RFID-based sensors," in *Proc. 11th Int. Conf. Ubiquitous Computing*, ACM, 2009, pp. 51–60.
- [65] M. Philipose, K. P. Fishkin, M. Perkowitz, D. J. Patterson, D. Fox, H. Kautz, and D. Hahnel, "Inferring activities from interactions with objects," *IEEE Pervasive Comput.*, vol. 3, no. 4, pp. 50–57, 2004.
- [66] A. Matic, P. Mehta, J. M. Reh, V. Osmani, and O. Mayora, "Monitoring dressing activity failures through RFID and video," *Methods Inform. Med.*, vol. 51, no. 1, pp. 45, 2012.
- [67] S. Junnila, H. Kailanto, J. Merilahti, A.-M. Vainio, A. Vehkaoja, M. Zakrzewski, and J. Hyttinen, "Wireless, multipurpose in-home health monitoring platform: Two case trials," *IEEE Trans. Inform. Technol. Biomed.*, vol. 14, no. 2, pp. 447–455, 2010.
- [68] A. Bulling, J. A. Ward, H. Gellersen, and G. Troster, "Eye movement analysis for activity recognition using electrooculography," *IEEE Trans. Pattern Anal. Mach. Intell.*, vol. 33, no. 4, pp. 741–753, 2011.
- [69] M. Chan, D. Estéve, C. Escriba, and E. Campo, "A review of smart homes—present state and future challenges," *Comput. Methods Programs Biomed.*, vol. 91, no. 1, pp. 55–81, 2008.
- [70] P. Rashidi and D. J. Cook, "Keeping the resident in the loop: Adapting the smart home to the user," *IEEE Trans. Syst. Man Cybern. Part A Syst. Hum.*, vol. 39, no. 5, pp. 949–959, 2009.
- [71] M. J. Rantz, M. Skubic, S. J. Miller, C. Galambos, G. Alexander, J. Keller, and M. Popescu, "Sensor technology to support aging in place," *J. Amer. Med. Dir. Assoc.*, vol. 14, no. 6, pp. 386–391, 2013.
- [72] S. Chernbumroong, S. Cang, A. Atkins, and H. Yu, "Elderly activities recognition and classification for applications in assisted living," *Expert Syst. Appl.*, vol. 40, no. 5, pp. 1662–1674, 2013.
- [73] L. Gao, A. K. Bourke, and J. Nelson, "Evaluation of accelerometer-based multi-sensor versus single-sensor activity recognition systems," *Med. Eng. Phys.*, vol. 36, no. 6, pp. 779–785, June 2014.
- [74] D. J. Patterson, D. Fox, H. Kautz, and M. Philipose, "Fine-grained activity recognition by aggregating abstract object usage," in *Proc. 9th IEEE Int. Symp. Wearable Computers*, 2005, pp. 44–51.
- [75] R. Helaoui, M. Niepert, and H. Stuckenschmidt, "Recognizing interleaved and concurrent activities: A statistical-relational approach," in *Proc. IEEE Int. Conf. Pervasive Computing and Communications (PerCom)*, 2011, pp. 1–9.
- [76] E. Nazerfard, B. Das, L. B. Holder, and D. J. Cook, "Conditional random fields for activity recognition in smart environments," in *Proc. ACM Int. Health Informatics Symp.*, 2010, pp. 282–286.
- [77] G. Virone, N. Noury, and J. Demongeot, "A system for automatic measurement of circadian activity deviations in telemedicine," *IEEE Trans. Biomed. Eng.*, vol. 49, no. 12, pp. 1463–1469, Dec. 2002.
- [78] C. Zhu and W. Sheng, "Motion- and location-based online human daily activity recognition," *Pervasive Mob. Comput.*, vol. 7, no. 2, pp. 256–269, 2011.
- [79] J. Zhang, M. Marszalek, S. Lazebnik, and C. Schmid, "Local features and kernels for classification of texture and object categories: A comprehensive study," *Int. J. Comput. Vis.*, vol. 37, no. 2, pp. 213–238, 2007.
- [80] H. Wang, M. M. Ullah, A. Klser, I. Laptev, and C. Schmid, "Evaluation of local spatiotemporal features for action recognition," in *Proc. British Machine Vision Conf.*, 2009, pp. 124.1–124.11.
- [81] I. Laptev, M. Marszalek, C. Schmid, and B. Rozenfeld, "Learning realistic human actions from movies," in *Proc. IEEE Conf. Computer Vision and Pattern Recognition*, 2008, pp. 1–8.
- [82] P. Bilinski and F. Bremond, "Evaluation of local descriptors for action recognition in videos," *Comput. Vis. Syst. Springer*, vol. 6962, pp. 61–70, 2011. [Online]. Available: http://link.springer.com/chapter/10.1007%2F978-3-642-23968-7_7#page-1
- [83] L. Rabiner and B. H. Juang, "An introduction to hidden Markov models," *IEEE ASSP Mag.*, vol. 3, no. 1, pp. 4–16, Jan. 1986.
- [84] P. Turaga, R. Chellappa, V. S. Subrahmanian, and O. Udrea, "Machine recognition of human activities: A survey," *IEEE Trans. Circuits Syst. Video Technol.*, vol. 18, no. 11, pp. 1473–1488, Nov. 2008.
- [85] X. Li, "HMM-based action recognition using oriented histograms of optical flow field," *Electron. Lett.*, vol. 43, no. 10, pp. 560–561, 2007.
- [86] J. Yamato, J. Ohya, and K. Ishii, "Recognizing human action in time-sequential images using hidden Markov model," in *Proc. IEEE Computer Society Conf. Computer Vision and Pattern Recognition*, June 1992, pp. 379–385.
- [87] C. Yip, *Machine Recognition of Multi-font Printed Chinese Characters*. Pokfulam, Hong Kong: Univ. Hong Kong, 1990.
- [88] F. Martinez-Contreras, C. Orrite-Urunuela, E. Herrero-Jaraba, H. Ragheb, and S. A. Velastin, "Recognizing human actions using silhouette-based HMM," in *Proc. 6th IEEE Int. Conf. Advanced Video and Signal Based Surveillance, 2009 (AVSS'09)*, Sept. 2009, pp. 43–48.
- [89] V. N. Vapnik, *The Nature of Statistical Learning Theory*. New York: Springer-Verlag, 1995.
- [90] B. Scholkopf and A. J. Smola, *Learning with Kernels: Support Vector Machines, Regularization, Optimization, and Beyond*. Cambridge, MA: MIT Press, 2001.
- [91] L. Breiman, "Random forests," *Mach. Learn.*, vol. 45, no. 1, pp. 5–32, 2001.
- [92] P. Urwyler, L. Rampa, R. Stucki, M. Büchler, R. Müri, U. P. Mosimann, and T. Nef, "Recognition of activities of daily living in healthy subjects using two ad-hoc classifiers," *Biomed. Eng. Online*, vol. 14, no. 1, 2015. [Online]. Available: <http://link.springer.com/article/10.1186%2F12938-015-0050-4#page-1>
- [93] K. Bousmalis, S. Zafeiriou, L.-P. Morency, and M. Pantic, "Infinite hidden conditional random fields for human behavior analysis," *IEEE Trans. Neural Netw. Learn. Syst.*, vol. 24, no. 1, pp. 170–177, Jan. 2013.
- [94] T. S. Jaakkola and D. Haussler, "Exploiting generative models in discriminative classifiers," in *Proc. Conf. Advances in Neural Information Processing Systems II*, MIT Press, Cambridge, MA, USA, 1999, pp. 487–493.
- [95] K. Ellis, J. Kerr, S. Godbole, and G. Lanckriet, "Multi-sensor physical activity recognition in free-living," in *Proc. 2014 ACM Int. Joint Conf. Pervasive and Ubiquitous Computing: Adjunct Publication, UbiComp'14 Adjunct*, New York, NY, USA, ACM, 2014, pp. 431–440.
- [96] L. J. P. Van der Maaten, "Learning discriminative fisher kernels," in *Proc. 28th Int. Conf. Machine Learning*, 2011, pp. 217–224.
- [97] I. Alexiou, T. Xiang, and S. Gong, "Learning a joint discriminative-generative model for action recognition," in *Proc. Int. Conf. Systems, Signals and Image Processing*, London, UK, 2015., pp. 1–4. [Online]. Available: <http://ieeexplore.ieee.org/xpl/articleDetails.jsp?reload=true&arnumber=7313922>
- [98] D. J. Cook and M. Schmitter-Edgecombe, "Assessing the quality of activities in a smart environment," *Methods Inform. Med.*, vol. 48, no. 5, pp. 480–485, 2009.

Discovering the Whole by the Coarse

*A topological paradigm
for data analysis*

Hamid Krim, Thanos Gentimis,
and Harish Chintakunta

The increasing interest in big data applications is ushering in a large effort in seeking new, efficient, and adapted data models to reduce complexity, while preserving maximal intrinsic information. Graph-based models have recently been getting a lot of attention on account of their intuitive and direct connection to the data [43]. The cost of these models, however, is to some extent giving up geometric insight as well as algebraic flexibility.

Topology, as an intermediate analysis medium, focuses on coarse structures of an object/signal in general. It affords a formalism of transitioning from a local to a global description of an object, while providing significant information, which respects the local structure of measurements. It may also support a global visualization (e.g., data variation trends) and enhances the understanding of the underlying phenomenon.

Throughout this article, measurements may be considered proximal in various ways, depending on the specific application, and the selected proximity metrics are subsequently used in the construction of a graph structure, thus highlighting various groups of neighboring data. As described later, these groups, often based on proximity criteria, are represented by n -simplices, where $n + 1$ corresponds to the number of points in an associated group. Collectively, they form what is (and will be throughout) referred to as a *simplicial complex*, a special representation of a topological space. The key advantage of computational topology is its inherently algebraic structure on the basic elements of the resulting graph-like structure.

To that end, the goals of this article are to

- introduce the prevalent tools in computational topology (or applied algebraic topology), in an application-friendly context of examples and illustrations; we will try to smooth out an otherwise taxing demand of abstract algebra by using primarily a linear algebra and calculus formalism

Digital Object Identifier 10.1109/MSP.2015.2510703
Date of publication: 7 March 2016

IMAGE LICENSED BY INGRAM PUBLISHING

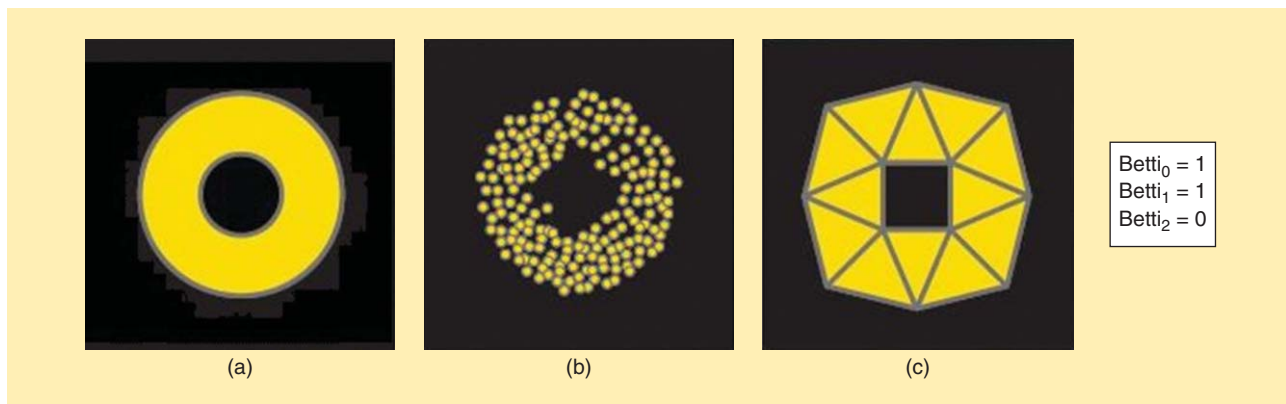


FIGURE 1. The computational topology pipeline: from (a) a continuous manifold with a boundary to (b) its sampled point cloud to (c) a coherent collection of geometric objects. $Betti_i$ refers to the number of i th order topological features. The zeroth order is the connected components, the first order is the number of holes, and the second order is the number of voids.

■ demonstrate that, beyond the technical definitions and jargon, this area offers a framework naturally adapted to many signal processing problems, with familiar tools from linear algebra.

The first natural question one might ask is: Why use topology on data? When topology is preferred over other techniques, it is because of the following two reasons: 1) It studies invariants of continuous deformations of the shape of data; an immediate consequence is that the actual embedding of the data, dictated by the choice of parameters, is not an exceedingly crucial factor in the analysis. 2) It allows coarse measures of shape (clumps, holes, and voids), which are algebraically computed and quantitatively reflected.

The pipeline of the proposed methodology is graphically described in Figure 1. Here, we assume that our data are embedded in a high-dimensional vector space, while in reality, they live in a simpler, smaller manifold. The point cloud thus represents a sampling of that manifold, i.e., an approximation whose invariants approach those of the manifold, thereby allowing one to better understand the process that generated those points. More precise statements about these issues may be found in [4] and [36].

Construction of simplicial complexes

To account for the simultaneous relationship between more than two data points, as is often captured by a graph, and thereby induce an algebraic structure that hypergraphs lack, we will first analyze structures based on elementary blocks. These are combined to yield a “graph” with higher-order relationships among the nodes, which will be referred to as a *simplicial complex* in the remainder of the article. This is a telling name, in that its basic components are simple pieces, called *simplices*; a point is a 0-simplex, an edge with two vertices is a 1-simplex, a filled-in triangle with three edges is a 2-simplex, a tetrahedron is a 3-simplex, and so on.

All closed surfaces (compact manifolds of dimension 2, without boundary) can be approximated by using triangles and identifying some of their edges (for a detailed proof, refer to the appendix “Topology of Cell Complexes” in [24]). The triangle is thus the fundamental building block of two-dimensional (2-D) objects. The process of describing a surface as the union of triangles with some identification is called *triangulation* or *simplicial approximation*, as

illustrated in Figure 2. The triangles are sufficiently simple objects to be described combinatorially through their vertices, and also sufficiently versatile to approximate any such surface.

Simplicial complex: introduction

A simplicial complex is a generalized graph consisting of vertices, edges, triangles, and simplices of higher dimensions that are “glued together,” as depicted in Figure 3. For this gluing operation to yield a concrete algebraic structure, we require that the intersection of any two simplices is either empty or is another simplex.

These simplices can be embedded in a Euclidean space as follows: Given an abstract n -simplex, we describe its corresponding standard n -dimensional simplex as

$$\Delta^n = \{(a_1, \dots, a_{n+1}) \mid \sum_i a_i = 1, a_i \geq 0, \forall i\}.$$

This is the convex hull of the points corresponding to the standard basis, $e_i \in \mathbb{R}^{n+1}$ for $i = 1, \dots, n + 1$. Figure 4 depicts the standard 2-simplex.

From point clouds to simplicial complexes

In this section, we present standard constructions that turn a point cloud, possibly embedded in \mathbb{R}^n , into a combinatorial-topological space, while naturally preserving the proximal properties of the points. The analysis of these spaces yields useful information about the point cloud generating them. We extend these definitions to distance matrices (where the embedding is unknown or is of no interest) to construct a similar approximation. Finally, we demonstrate how a well-known discrete-time technique in dynamical systems theory, i.e., the delay embedding of signals (time series), can be exploited to investigate the topology underlying a signal.

Čech complex

Suppose that we start with a set of points $X = \{x_1, x_2, \dots, x_n\}$ in \mathbb{R}^n . For a given $r > 0$, we construct the balls of radius r around each point of this set. We then consider an abstract collection of

vertices $\{v_1, v_2, \dots, v_n\}$ corresponding to the given points. We connect the vertices v_i, v_j by an edge if the balls $B_r(x_i)$ and $B_r(x_j)$ intersect. If all three of the balls $B_r(x_i), B_r(x_j), B_r(x_k)$ intersect, we add the triangle $[v_i, v_j, v_k]$ and similarly proceed for higher-dimension simplices. The result of this procedure is the Čech complex, which is also often referred to as the *nerve* of the cover of radius r . An example is shown in Figure 5. The nerve theorem states that, under certain conditions, the topological invariants of the union of balls of a cover coincide with those of the Čech complex [16]. This complex is thus an enlargement of the point cloud and can be used to glean its topological properties.

Unfortunately, the information needed to construct a Čech complex is not always available since one needs the actual embedding of these points in some high-dimensional Euclidean space. If, instead, one is just given the distance matrix D of the points X , the following construction may be used to get a simplicial complex with, clearly, less information; nevertheless, it is suitable for further analysis. As a first step, we consider an abstract collection of vertices $\{v_1, v_2, \dots, v_n\}$ corresponding to the given set of data points. We then choose a parameter $r > 0$ and connect the vertices v_i, v_j by an edge if the distance between the point x_i and x_j is less than or equal to $2r$. This will yield the same vertices and edges as the Čech complex defined previously. Since the actual embedding of the points is not given, we cannot proceed with the Čech construction. Instead, we continue by adding a filled-in triangle (2-simplex) $[v_i, v_j, v_k]$, if all three edges $[v_i, v_j], [v_j, v_k], [v_k, v_i]$ exist. We then continue by adding higher-dimensional simplices if all their lower-dimensional faces exist. This is referred to as the *flag complex* construction over the one-dimensional (1-D) skeleton.

It is important to note that this flag complex [Figure 6(c)] is different from the corresponding Čech complex [Figure 6(b)]. It is, in fact, even more of an approximation of the topological space in question, since embedding is not required as in the Čech complex case.

Vietoris–Rips complex

Another construction of a simplicial complex related to a point-cloud $X = \{x_1, x_2, \dots, x_n\}$ in a metric space is the Vietoris–Rips complex. Again, fix a parameter $r > 0$. Then, consider an abstract set of vertices $\{v_1, v_2, \dots, v_n\}$ corresponding to the given set of data points. The simplex $[v_1, v_2, \dots, v_k]$ is added to the simplicial complex if and only if the diameter of the set x_1, x_2, \dots, x_k is less than r . For a big family of metric spaces, the Vietoris–Rips complex thus constructed has the same points and edges as the Čech complex with parameter $r/2$. One advantage of the Vietoris–Rips complex is that it can be determined from only the distances between the points, without having to know their exact embedding. The relationship between the Vietoris–Rips and the Čech complex is as follows [10]:

$$R_r(X) \subset C_r(X) \subset R_r(X), \frac{r}{r'} \geq \sqrt{\frac{2d}{d+1}},$$

where $R_l(X)$ is a Vietoris–Rips complex using proximity parameter l , $C_l(X)$ is the Čech complex theoretically obtained by balls of radius l , and d is the interpoint

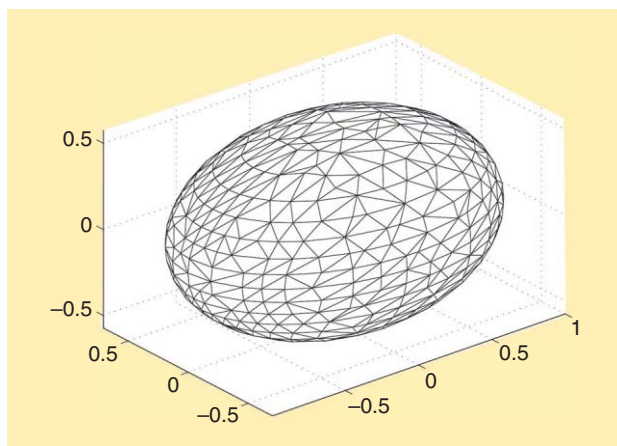


FIGURE 2. A triangulated 2-D ellipsoid.

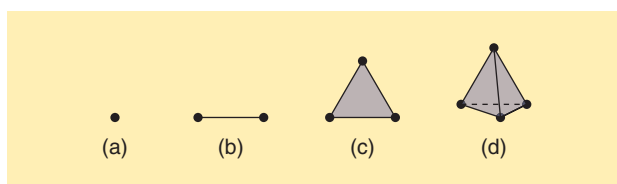


FIGURE 3. Some basic simplices: (a) 0-simplex, (b) 1-simplex, (c) 2-simplex, and (d) 3-simplex.

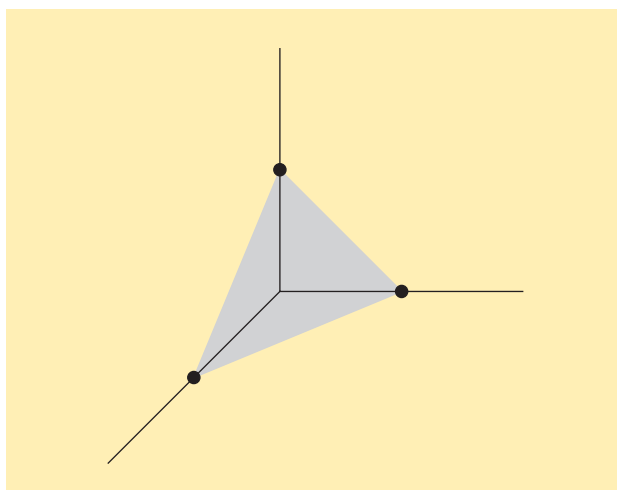


FIGURE 4. The standard 2-simplex embedded in \mathbb{R}^3 .

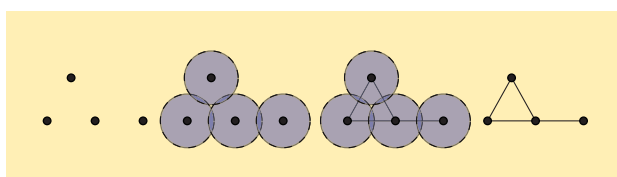


FIGURE 5. The construction of a Čech complex from a set of points.

Euclidean distance. In the following section, we describe how the aforementioned tools can be applied to signals in a meaningful and easy-to-understand way.

Time-delay embedding for signals

In many signal processing applications, time series are the result of a process that can be modeled as a dynamical system. A delay-embedding modeling of the signal is one approach of visualizing the phase space of the associated differential system. The mathematical foundation of the delay-coordinate embedding method is credited to Takens [45], who proposed to embed a scalar time series into an n -dimensional space. The general representation of this delay-coordinate embedding proceeds as follows: Given a discrete time series $x(t)$ [Figure 7(a)] and an embedding dimension n , we consider a vector quantity of n components to be

$$X(t) = (x(t), x(t + \theta_1), x(t + \theta_2), \dots, x(t + \theta_{n-1})),$$

where $\theta_1, \dots, \theta_{n-1}$ are constants representing the different index delays. The delay times and the embedding dimension are essential and problem-specific parameters. Their careful selection is typically a result of some prior knowledge about the signal or, alternatively, a result of experimentation. For the examples presented here, we will be using $n = 2$.

The output of the delay-embedding is a point cloud embedded in the chosen dimension n , as depicted in Figure 7(b). Using the complexes described previously, we can proceed to analyze this point cloud and compute and compare its topological characteristics. We may possibly achieve a reduction in com-

putational complexity by a careful subsampling of this point cloud, while preserving the topological invariants of interest [Figure 7(c)]. As shown later in the “Applications” section, random subsampling is, in some cases, an efficient and effective strategy to recover the topology of the original space.

Homology and higher-order Laplacians

Simplicial homology

In this section, we describe the construction of a topological invariant for the complexes described in the previous section. We start by defining the idea of the homology of a space using an example and explain how that can be computed using higher-order Laplacians, which we first define by building on the well-known notion of the graph Laplacian.

Intuitively, homology identifies topological features of our initial topological space by solving an algebraic problem of matrix reduction and rank identification. We focus our computations on the simplicial complex presented in Figure 8 and point to [24] for a more in-depth description of the relevant theory.

First, consider a vector space $C_0(X)$ whose basis elements are all the vertices of our given simplicial complex. In this example, $C_0(X) = \langle v_1, v_2, v_3, v_4 \rangle$, with coefficients in \mathbb{Z}_2 . (The choice of coefficients plays a role in this construction. For all of our applications, we will confine ourselves to \mathbb{R} coefficients or \mathbb{Z}_2 coefficients; thus, all of our constructions will be vector spaces. By choosing \mathbb{Z}_2 coefficients, we do not have to worry about signs. Again, we point to [8] and [24] for more general and in-depth information.) Similarly, the space of edges will be $C_1(X) = \langle e_1, e_2, e_3, e_4, e_5 \rangle$. Finally, the space of triangles will be $C_2(X) = \langle \sigma_1 \rangle$. We then define a linear “difference” operator, called a *boundary operator* $\partial_1: C_1(X) \rightarrow C_0(X)$, which, when applied to an edge e_1 yields a difference of vertices $\partial_1(e_1) = v_2 - v_1 = v_2 + v_1$. We extend the application of this linear map to all elements of $C_1(X)$, and similarly define a higher-order boundary operator to act on triangles (2-simplices). In our example, $\partial_2(\sigma_1) = e_1 + e_2 + e_3$ for the filled-in triangle σ_1 [or $\partial_2: C_2(X) \rightarrow C_1(X)$]. Such operators can be defined for a structure of any dimension: For

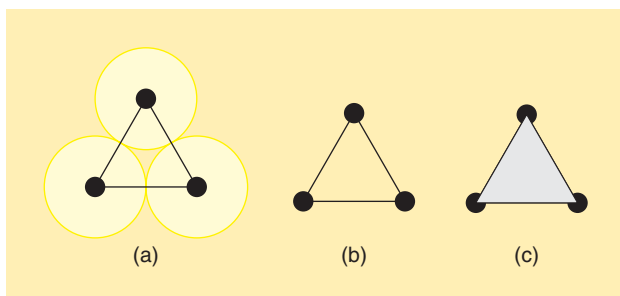


FIGURE 6. The difference between a Čech complex and its flag. (a) Points in \mathbb{R}^2 , (b) the Čech complex, and (c) the Flag complex.

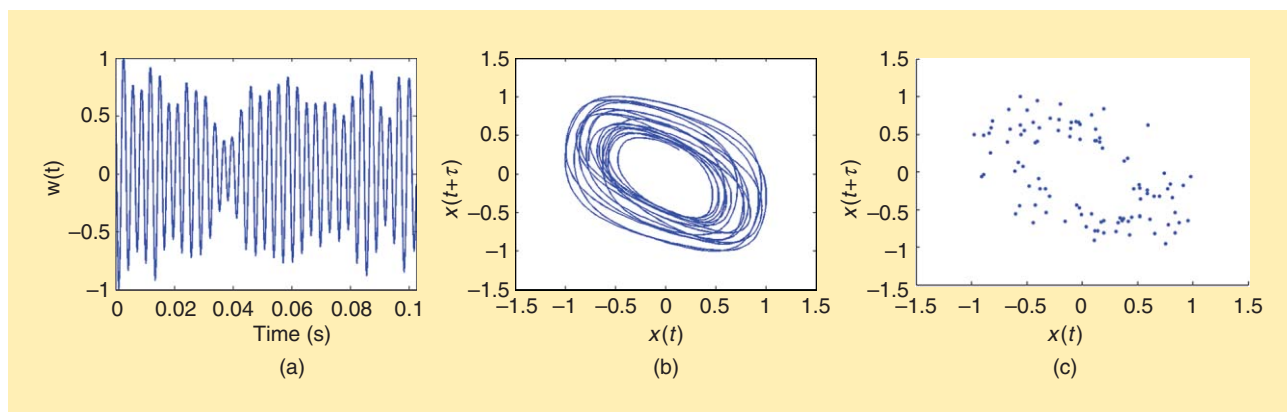


FIGURE 7. From signals to point clouds: (a) time series, (b) 2-D delay, and (c) subsampling.

instance, ∂_3 acts on tetrahedra to yield the sum of its 2-simplex faces (triangles), ∂_4 acts on pentatopes to yield the sum of its 3-simplex faces (tetrahedra), and so on.

A matrix representation of these linear operators is thus obtained, and all of the computations reduce to manipulating tables as shown here:

$$\partial_1 = \begin{matrix} & e_1 & e_2 & e_3 & e_4 & e_5 \\ v_1 & \begin{pmatrix} 1 & 0 & 1 & 1 & 0 \end{pmatrix} \\ v_2 & \begin{pmatrix} 1 & 1 & 0 & 0 & 1 \end{pmatrix} \\ v_3 & \begin{pmatrix} 0 & 1 & 1 & 0 & 0 \end{pmatrix} \\ v_4 & \begin{pmatrix} 0 & 0 & 0 & 1 & 1 \end{pmatrix} \end{matrix}, \quad \partial_2 = \begin{matrix} \sigma_1 \\ e_1 \\ e_2 \\ e_3 \\ e_4 \\ e_5 \end{matrix} \begin{pmatrix} 1 \\ 1 \\ 1 \\ 0 \\ 0 \\ 0 \end{pmatrix},$$

$$\partial_1 \circ \partial_2 = \begin{matrix} \sigma_1 & \sigma_1 \\ v_1 & \begin{pmatrix} 2 \\ 0 \end{pmatrix} \\ v_2 & \begin{pmatrix} 2 \\ 0 \end{pmatrix} \\ v_3 & \begin{pmatrix} 2 \\ 0 \end{pmatrix} \\ v_4 & \begin{pmatrix} 0 \\ 0 \end{pmatrix} \end{matrix}.$$

Formally, the sequential application of these operators on the different spaces may be written as

$$C_2 \xrightarrow{\partial_2} C_1 \xrightarrow{\partial_1} C_0. \tag{1}$$

Note that the element $e_1 + e_2 + e_3$ of C_1 is but a loop that follows the cycle $v_1 \rightarrow v_2 \rightarrow v_3 \rightarrow v_1$. Another loop that is visible in our example is $e_1 + e_5 + e_4$. There is a fundamental difference between these two loops. The first one bounds a filled-in triangle, while the second bounds an empty triangle, or what conceptually can be considered as a true hole. Both of these loops are elements of the vector space $C_1(X)$ and, for both of them, we get $\partial_1(e_1 + e_2 + e_3) = 0 = \partial_1(e_1 + e_5 + e_4)$. Thus, both are in the kernel of ∂_1 defined as $\text{Ker}(\partial_1) = \{x \in C_1(X) : \partial_1(x) = 0\}$.

The element $e_1 + e_2 + e_3$ is obtained as the image of the triangle σ_1 under the map ∂_2 , whereas $e_1 + e_5 + e_4$ is not the image of a triangle. In other words, define $\text{Im}(\partial_2) = \{y \in C_1(X) : \exists x \in C_2(X) \text{ with } \partial_2(x) = y\}$, then $e_1 + e_2 + e_3 \in \text{Im}(\partial_2)$ and $e_1 + e_5 + e_4 \notin \text{Im}(\partial_2)$.

It is also not hard to show that $\partial_1 \circ \partial_2 = 0$ so $\text{Im}(\partial_2) \subseteq \text{Ker}(\partial_1)$. The 1-D homology is obtained by considering the quotient space $H_1(X) = [\text{Ker}(\partial_1) / \text{Im}(\partial_2)]$. The quotient space of a vector space V_1 with respect to $V_2 (V_1/V_2)$ is the space of equivalent sets, where two elements in V_1 are equivalent if their difference is in V_2 . The dimension of V_1/V_2 is equal to $\dim(V_1) - \dim(V_2)$. For more on quotient spaces, we refer the reader to the chapter ‘‘Vector Spaces,’’ Theorem 7 [15]. From the previous discussion, this construction contains information about the holes or cycles bounding areas that are not filled in.

The algebraic structure that is imposed on the basic construction of the spaces makes sequential application of boundary operators possible in any higher dimension. Formally, one defines these quotients as the *homology spaces*

$$H_i(X) = \frac{\text{Ker}(\partial_i)}{\text{Im}(\partial_{i+1})}.$$

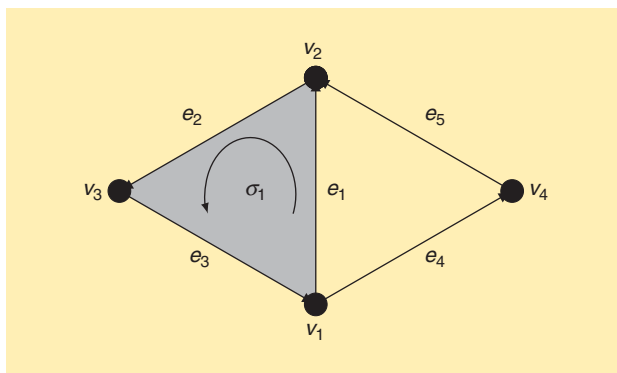


FIGURE 8. An example simplicial complex composed of one 2-simplex σ_1 and two 1-simplices e_4, e_5 .

The dimensions of these spaces, which are called *Betti numbers*, $\beta_i = \dim(H_i)$, can be used to coarsely describe the simplicial complex at hand. Intuitively, β_0 counts the number of connected components, β_1 the number of nonvanishing holes, β_2 the number of voids, etc.

Higher-order Laplacians

A direct computation of the homology spaces as quotient vector spaces is computationally expensive and often unnecessary [5]. Combinatorial Laplacian operators, the matrix representations of which may be viewed as a generalization of the graph Laplacian, are very useful in providing alternative ways to gather information about the homology spaces. These operators are related to combinatorial Hodge theory [25]. The motivation of the graph Laplacian operators on graphs is directly related to probing the structure of graphs by tracking a diffusion (much like heat diffusion in a solid) through it by way of the spectral properties of the operator. A similar strategy can be developed using the boundary operators acting on a simplicial complex.

Given the boundary operators defined previously, a zero-order Laplacian defined as $L_0 = \partial_1 \partial_1^T$, operates on vertices and in fact coincides with the so-called graph Laplacian, which is widely used in numerous applications. It is easy to check that $L_0 = D - A$, where A is the adjacency matrix of the underlying graph of the complex, and D is the diagonal matrix with the degrees of the vertices. It is also well known that the spectrum of a graph Laplacian yields clustering information about a given graph [6]; specifically, the cardinality of the number of 0-eigenvalues equals the number of disjoint connected components of the graph. As we explain below, this property is generalized by higher-order Laplacian operators, providing efficient algebraic tools to assess the higher-order topological properties of any simplicial complex.

In a similar way, we can construct higher-order Laplacian operators, $L_i = \partial_i^T \partial_i + \partial_{i+1} \partial_{i+1}^T$ such that L_1 operates on edges, L_2 operates on triangular faces, and so on. Much like the null-space dimension of a graph Laplacian uncovers the number of connected components in a graph (which can be viewed as zero-cycles), the null space dimension of

the higher-order Laplacians also reflects the number of holes, voids, and higher-dimension analogs—in other words, the rank of the corresponding homology space. Formally, this is expressed as the isomorphism $\text{Ker}(L_i) \simeq H_i$. To see this, note that if $x \in \text{Ker}(L_i)$, then $x \in \text{Ker}(\partial_i)$ and $x \in \text{Ker}(\partial_{i+1}^T)$. Now, $x \in \text{Ker}(\partial_{i+1}^T)$ implies that $x \perp \text{Im}(\partial_{i+1})$, and since $\text{Im}(\partial_{i+1}) \subseteq \text{Ker}(\partial_i)$, we have $\text{Ker}(L_i) \simeq H_i$.

The above isomorphism allows one to take advantage of the properties of the Laplacian operators to either explicitly compute the rank of the homology or to glean pertinent information without having to perform a matrix reduction.

For example, instead of the rank of H_i , one may only wish to find if $H_i \simeq 0$, or equivalently if $\text{Ker}(L_i) = 0$, then the following simple procedure may be followed. First, compute the spectral radius of L_i , say σ , which may easily be accomplished by a power iteration method. Consequently, compute the spectral radius of the matrix $\sigma I - L_i$, say σ' . Since L_i is positive semidefinite, L_i is full rank if and only if $\sigma' < \sigma$. This gives us a simple, low-complexity test for checking if $H_i \simeq 0$. Other properties of the Laplacian operators have also been used in the context of sensor networks to efficiently detect and localize coverage holes [5], [34], [44].

Applications

Biomedical signal analysis: Wheeze detection

Our first example is that of detecting a wheeze in a breathing signal using its global structure. Quoting *Wikipedia*, “A wheeze (formally called *sibilant rhonchi* in medical terminology) is a continuous, coarse, whistling sound produced in the respiratory airways during breathing.” Wheezing is caused by obstructions in the respiratory canal and is often a symptom of certain serious conditions. Therefore, timely detection of wheezing becomes medically very important.

From a signal processing perspective, the obstruction in the respiratory canal gives rise to a quasi-harmonic behavior in the audio signal. Because of this quasi-harmonic nature, time-frequency techniques have difficulty in yielding efficient and consistent real-time algorithms, as shown in [9]. On the other hand, the time-delay embedding as described in the “Time Delay Embedding for Signals” section of a quasi-harmonic signal produces a point cloud where the points accumulate around an ellipse (in two dimensions). This is illustrated in Figure 9(a), where the top row corresponds to normal breathing signals, and bottom two rows correspond to breathing signals containing wheezes of different types. We can efficiently and accurately determine such an elliptical structure in the point cloud using topological methods, as described in the following three steps:

- 1) Convert the time signal into a point cloud using time-delay embedding.
- 2) Clean the resulting point cloud.
- 3) Compute a topological invariant of the resulting point cloud and use it for classification.

From audio signals to point clouds

The eccentricity of the ellipse around which the points lie in the time-delay embedding depends on the delay chosen. The first

step is to obtain a reasonable delay so that the ellipse is not too eccentric, thereby obscuring the real structure in the point cloud.

The following simple heuristic can achieve this: First, we compute the time-varying autocorrelation function of the signal

$$R_{xx}(t) = \sum_k x(k+t)x(k).$$

We then select $t_{c1} < \tau < t_{c2}$, where t_{c1} and t_{c2} are the first and second critical points of $R_{xx}(t)$. The delay time to produce the point clouds in Figure 9(a) was computed this way.

Cleaning the point cloud

First, note that if the points in the given point cloud are organized around an ellipse, then those in a subsample would follow suit. This simple observation enables us to decrease the computational complexity. Our goal here is to highlight that this is a natural consequence of seeking coarse features, as often is the case in topological analysis. In this specific example, our experiments show that we can reliably reduce the size of the point cloud by as much as 92%.

Second, any occasional deviation of the signal from being “almost harmonic” [19] can cause the points to venture into the center [as seen in the first two plots in the second row of Figure 9(a)], thus obscuring the elliptical structure. While this may severely impact the robustness of the procedure, such an occurrence is rare, making the density of points in the center quite low. Such points could easily be pruned off using a density threshold. Figure 9(b) shows an example where the point clouds are shown at various parameters used for density thresholding. In the illustrations shown in Figure 9(b), K is the number of nearest neighbors for each point used to determine the density, and T is the density threshold below which the points will be pruned.

Topological invariants for classification

Once the point cloud is obtained, we proceed to compute the topological invariant that captures the elliptical shape of the point cloud if present. As described in the “Construction of Simplicial Complexes” section, we next construct a simplicial complex from the given point cloud. We could proceed to obtain either a Čech complex or a Vietoris–Rips complex as mentioned there, but since the points here are in two dimensions, we have a better alternative, i.e., 1) compute the Delaunay triangulation [23] of the points and 2) remove all the edges whose length is greater than a certain threshold along with all the triangles adjacent to those edges. Figure 9(c) and (d) illustrates this process. Note that the elliptical structure of the point cloud translates to a hole in the resulting complex, which may then be detected by computing H_1 , the first homology space. We refer the reader to [18] for details on a very efficient method using Euler characteristic [42].

In summary, the presence of a hole indicates an almost harmonic structure, which is shown to characterize wheezes. Note that the null hypothesis is in itself a noteworthy result in that a

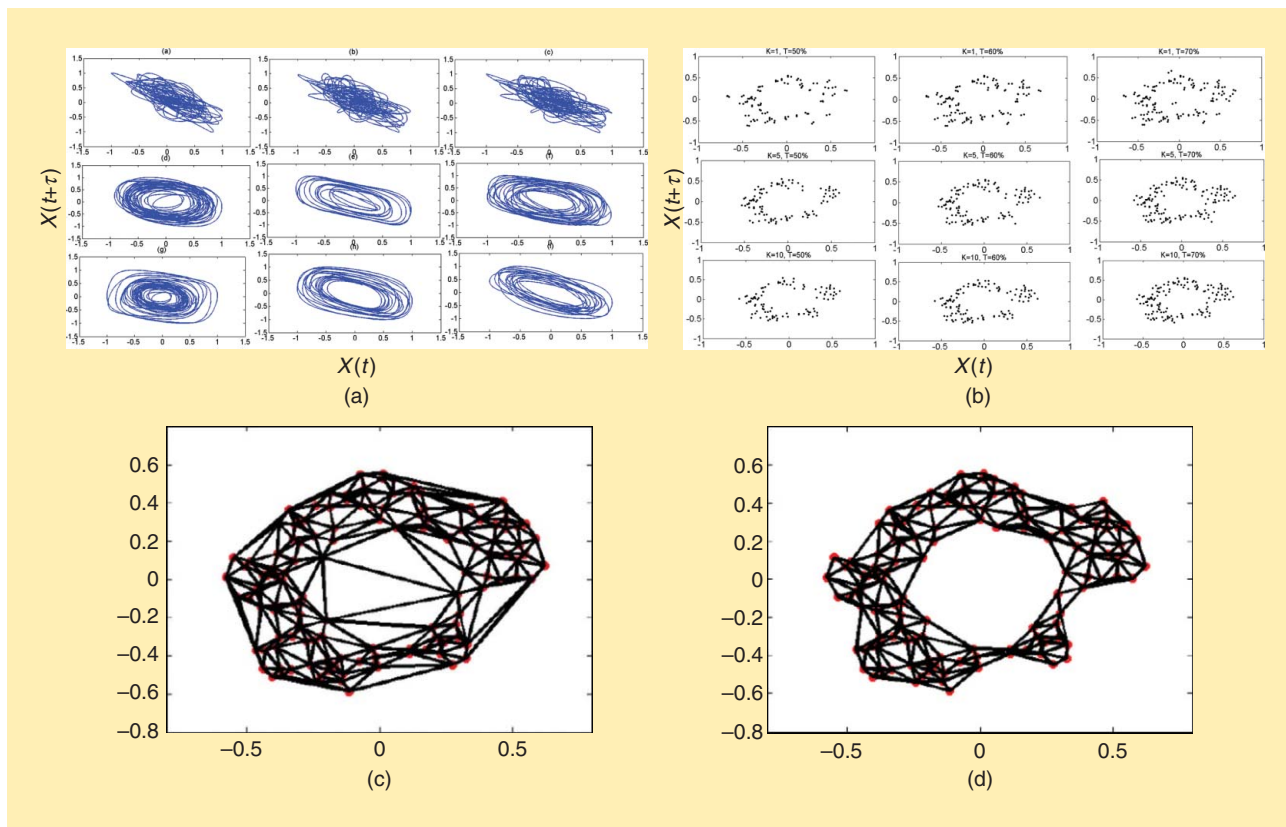


FIGURE 9. The wheeze-detection process. In (a), the top row corresponds to normal signals, while the bottom two rows correspond to wheeze signals. (a) Delay embeddings. (b) Various samplings of a wheeze. (c) A triangulation of a wheeze. (d) A triangulation with large edges removed.

nonwheeze signal appears as chaotic, and its topology is also nicely captured at a minimal computational cost.

Sensor networks

The application of algebraic topology in sensor networks is very illustrative of its utility. Owing to the difficulties of obtaining location information of the sensors in the field and to the need for additional hardware to compute precise distances between pairs of sensors, it may be prohibitively expensive to obtain geometric information. Interestingly,

problems like verifying coverage are purely topological in nature, and, as discussed previously, computational topology provides a coordinate-free solution to quantifying the coverage status as topological information.

Consider a set of sensors randomly deployed in a region to be monitored. Two problems are often of interest:

- verifying if the region being monitored is actually fully covered and accounted for
- discovering uncovered regions and identifying their surrounding nodes.

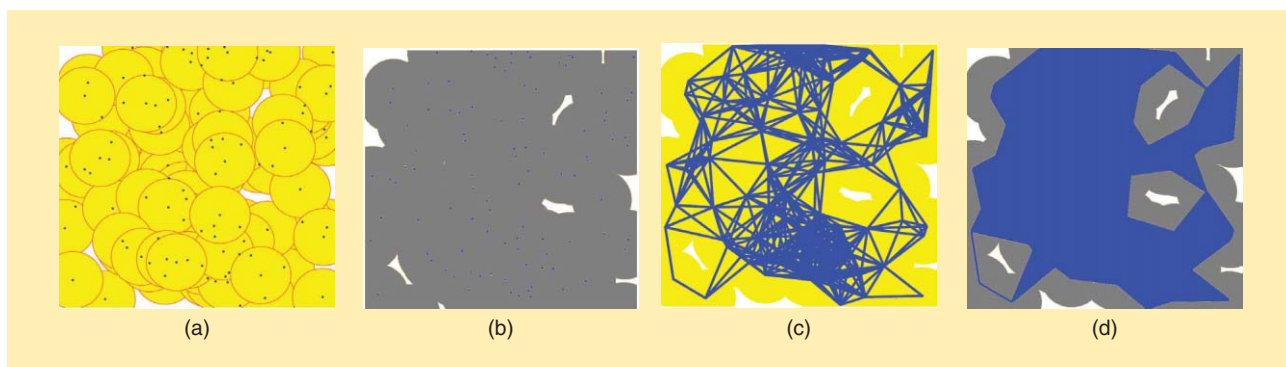


FIGURE 10. A way to approximate the coverage area, shown in (b), in sensor networks using a complex constructed from the communication graph. If the communication radius is twice the individual sensor coverage radius, the Rips shadow is a good topological approximation to the coverage area, as shown in (d). (a) Sensors in a plane. (b) Sensor coverage. (c) The Čech complex. (d) The Rips shadow.

Obtaining an efficient solution that scales with the size of a sensor network is critical and depends on how much information is needed to solve the aforementioned problems. It turns out that each node having a list of “names” of its neighbors in a certain proximity (communication radius) is sufficient to fully address these issues. Figure 10 illustrates this scenario.

To address the first problem, we construct a simplicial complex whose topology is commensurate with that of the total coverage area of sensors [shown in Figure 10(b)]. We subsequently compute the first homology of this complex and check for its triviality. There is good evidence [21] showing that the Vietoris–Rips complex constructed from the communication graph closely represents the coverage area, if the communication radius is twice that of the coverage radius. The first Laplacian operator L_1 , discussed in the “Higher-Order Laplacians” section, may then be used to check for the triviality of the first homology. Note that in using the isomorphism of the null space of L_1 to H_1 , we exploit the sparse structure of the L_1 matrix, with the ij th element being nonzero if and only if the corresponding edges have an edge in common. This property enables us to store and distributively perform iterative computations. Additional implementation details may be found in [5].

One of the earliest applications of topology in sensor networks was presented in [9], where a variant of the coverage problem is considered. Given a set of fence nodes, which surround the intended sensing region, the problem is to determine if the region enclosed by the fence nodes is covered. In [9], a set of sufficient conditions is given to guarantee such coverage.

Intuitively, these conditions specify that there is a disk in the union of coverage areas of individual sensors, whose boundary contains the fence nodes. Finding a small subset of sensors that can form this disk helps minimize the number of sensors required to maintain coverage, thus saving power. The work in [14] presents a distributed algorithm to simultaneously verify the coverage and, if verified, provide such a small subset of sensors.

Another interesting problem that is purely topological in nature is that of target enumeration. In this case, the scenario is that of multiple targets in a sensing field, and each sensor can sense a subset of targets, leading to the challenge of determining the total number of sensors. To solve this problem [2], uses the Euler characteristic.

Social networks

One big-data problem that is of great current interest is that of social networks. We discuss here how one can 1) construct a socioplex, which captures higher-order information among the nodes, and 2) reduce its complexity, in a principled way, to obtain a so-called core network, which contains all of the important nodes and has the same topology as the original one. A topological hole and its higher-dimensional variants may physically be understood as a loss of connectivity or a lack of cooperation.

First, we extend the classical idea of a sociogram [32]—where individuals are represented by vertices, and their pairwise connections are depicted by edges—to that of a socioplex, which takes into account higher-order structures among the individuals.

This socioplex can be obtained from extra information for the specific network. In our example, for instance, we are analyzing the coauthorship Communication and Networks Collaborative Technology Alliance (CNCTA), where a connection between two authors (author~node) is established if and only if they have published a paper together. Similarly, three authors yield a filled-in triangle if all three of them have published a paper together, and so on. The resulting simplicial complex is shown in Figure 11(a). Note that this new network includes all the information in a classical sociogram, as the latter is no more than the 1-D skeleton of the former.

The additional information injected into the socioplex provides, in some sense, sufficient insight to reduce the dimension of the complex by removing simplices through a series of homotopy collapses [26], similar to the one presented in Figure 12. The resulting reduced simplicial complex shown in Figure 11(b) has similar topological invariants (Betti numbers) to the original one, since homotopy collapses respect homology computations.

Whereas the original socioplex contained 516 authors and 980 labels (papers), the final reduced version has 67 authors and 78 labels. Most importantly, the reduced complex contains the important features since, due to the construction of the network, most of the time, the principal investigators are the connecting links between groups and research cliques. Thus, these important nodes are preserved in the collapse, whereas their immediate collaborators (graduate students, postdoctoral researchers, etc.) are collapsed into them. The process presented in [48] takes the redundant labels and appends them to the nodes on the core into which they collapse. There is no relational information loss, as the core preserves the structural entity among the main nodes (or agents) of the original network, with additionally a better visualization potential. Its analysis through homology is also significantly faster since the corresponding Laplacians are of much smaller size.

Conclusions and further reading

This article, meant to be a high-level introduction to the field of topological data analysis, describes a methodology that exploits relations among diverse data for capturing them as a topological complex, which, in turn, allows for further topologically based analysis, including exploration of topology-preserving dimension reduction of a network. We show how computational topology may be effectively applied in the context of failure detection and localization in sensor networks [22] as well as be complementary to computational geometry [12]. The simplicity of the discussed methods led to fast and distributed algorithms [44]. In addition to the examples presented here, other applications have started to appear in various fields of engineering, including computer vision and robotics-related modeling [13], [30], human gait recognition [28], [29], biomedical applications [40], [49], and others.

This article, owing to its intentionally limited scope, skips the practically important and mathematically rigorous concept of persistent homology [3]. The homology spaces described

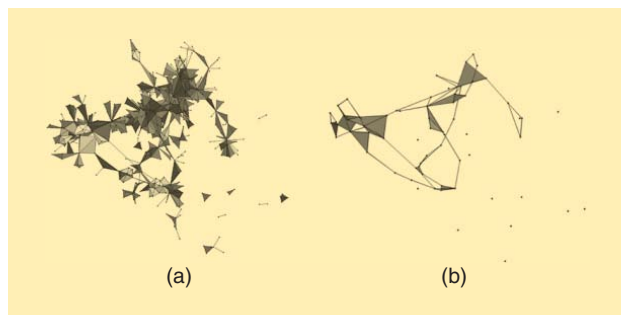


FIGURE 11. Reducing coauthorship networks using topological methods: (a) the coauthorship network CNCTA and (b) the reduced network CNCTA.

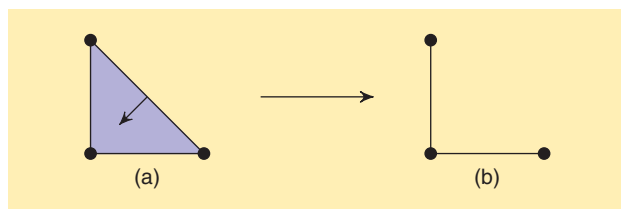


FIGURE 12. A simple homotopy collapse. In (a), the diagonal edges collapse into the paired 2-simplex, resulting in the complex shown in (b). Note that a homotopy collapse preserves topological features.

here may be unstable to disturbances in the data, i.e., it is possible that the generated homological spaces experience a nontrivial change in rank when the data are subjected to an arbitrarily small disturbance in the input data. While the applications chosen here are impervious to this effect, this will not necessarily be true for all applications. Persistent homology offers a stable topological summary of noisy data [7].

The “Simplicial Homology” section presents a view of rank of homology spaces as a generalization of the number of clusters in the data to higher-order features such as nonvanishing holes, voids, etc. Likewise, persistent homology may be viewed as a higher-order analog of hierarchical clustering, which is stable and known to have more interesting properties than hard clustering [27] and has led, in the past few years to many interesting applications in engineering [17]. For example, an excellent application of topology in clinical medicine may be found in [35].

As topological methods provide tools for analysis of various data shapes, there are several application avenues in computer vision and image processing. Some of the examples include graphical representation of gray-scale images [39], deformation-invariant models for digital images [20], [31], shape segmentation [41], and motion analysis [46]. As a further illustration of the scope of this topic, we refer the readers to applications such as comparison of maps [1], graph comparison [11], localization [38], text mining [47], and distributed trees for high-performance computing [33]. Various books have been recently published in this area of research, including a great introduction by Edelsbrunner and Harer [16], a concise book by Zomorodian [50], a more specific book about computational homology by Kaczynski

et al. [26], and a recent book with more engineering flavor by Robinson [37].

This is but a snapshot of the flexible potential of topological analysis, and the afforded robustness together with an amenability to analyze large data sets constitute remarkable capabilities of a topological paradigm in signal analysis, and much awaits to be explored by the signal processing research community, particularly when distributed algorithms, as demonstrated in some of the examples herein, are needed.

Acknowledgments

We profusely thank Vin De Silva first for his inspirational and pioneering work in topological data analysis and also for his encouragement and advice throughout this project, with intuitive graphical examples at times. We would also like to thank the anonymous referees for their excellent contributions that contributed significantly to the final version of this article. This article is the result of research work that was generously supported by DTRA under HDTRA1-08-1-0024.

Authors

Hamid Krim (ahk@ncsu.edu) received his B.S. and M.S. degrees in electrical engineering from Washington University and his Ph.D. degree in electrical and computer engineering from Northeastern University. Following his tenure as a member of technical staff at AT&T Bell Labs, he has worked in the area of telephony and digital communication systems/subsystems. He became a U.S. National Science Foundation (NSF) postdoctoral scholar at Foreign Centers of Excellence (Laboratoire des Signaux et Systèmes Supélec/University of Orsay, Paris, France) in 1991. Subsequently, he was a research scientist at the Laboratory for Information and Decision Systems, Massachusetts Institute of Technology, Cambridge, performing/supervising research in his area of interest, and he later joined the faculty of the Electrical and Computer Engineering Department at North Carolina State University in Raleigh. He is an original contributor and now an affiliate of the Center for Imaging Science sponsored by the U.S. Army. He also is a recipient of the NSF Career Young Investigator Award. He was on the editorial board of *IEEE Transactions on Signal Processing*, *IEEE Transactions on Signal and Information Processing over Networks*, and *IEEE Signal Processing Magazine*, and regularly contributes to the IEEE Signal Processing Society in various ways. He is a member of the Society for Industrial and Applied Mathematics and Sigma Xi. His research interests include statistical signal processing and mathematical modeling, with a keen emphasis on applications. He is a Fellow of the IEEE.

Thanos Gentimis (gentimisth@gmail.com) received his bachelor's and master's degrees in theoretical mathematics from the National and Kapodistrian University of Athens, Greece, in 2002 and 2005, respectively. In 2011, he received his Ph.D. degree in algebraic topology at the University of Florida. He was a postdoctoral researcher at the Electrical and Computer Engineering Department of North Carolina State University, Raleigh. He is an assistant

professor of mathematics and analytics at Florida Polytechnic University.

Harish Chintakunta (Harishkumar.ch@gmail.com) received his M.S. and Ph.D. degrees in electrical engineering from North Carolina State University, Raleigh, in 2008 and 2013, respectively, where he also worked as a postdoctoral researcher. He is an assistant professor of electrical engineering at Florida Polytechnic University. He was previously a postdoctoral researcher at the University of Illinois at Urbana-Champaign.

References

- [1] M. Ahmed, B. T. Fasy, and C. Wenk, "Local persistent homology based distance between maps," in *Proc. 22nd ACM SIGSPATIAL Int. Conf. Advances in Geographic Information Systems*, 2014, pp. 43–52.
- [2] Y. Baryshnikov and R. Ghrist, "Target enumeration via Euler characteristic integrals," *SIAM J. Appl. Math.*, vol. 70, no. 3, pp. 825–844, 2009.
- [3] G. Carlsson, "Topology and data," *Bull. Amer. Math. Soc.*, vol. 46, no. 2, pp. 255–308, Apr. 2009.
- [4] F. Chazal, D. Cohen-Steiner, L. J. Guibas, F. Memoli, and S. Y. Oudot, "Gromov–Hausdorff stable signatures for shapes using persistence," *Comput. Graph. Forum*, vol. 28, no. 5, pp. 1393–1403, 2009.
- [5] H. Chintakunta and H. Krim, "Distributed localization of coverage holes using topological persistence," *IEEE Trans. Signal Processing*, vol. 62, no. 10, pp. 2531–2541, May 2014.
- [6] F. R. K. Chung, *Spectral Graph Theory*. Providence, RI: American Mathematical Society, 1997.
- [7] D. Cohen-Steiner, H. Edelsbrunner, and J. Harer, "Stability of persistence diagrams," *Discrete Comput. Geom.*, vol. 37, no. 1, pp. 103–120, 2007.
- [8] J. F. Davis and P. Kirk, *Lecture Notes in Algebraic Topology*, American Mathematical Society, 2001.
- [9] V. De Silva and R. Ghrist, "Coordinate-free coverage in sensor networks with controlled boundaries via homology," *Int. J. Robot. Res.*, vol. 25, no. 12, pp. 1205–1222, 29 Sept. 2009.
- [10] V. De Silva and R. Ghrist, "Homological sensor networks," *Notices Amer. Math. Soc.*, vol. 54, no. 1, pp. 10–17, 2007.
- [11] T. Dey, D. Shi, and Y. Wang, "Comparing graphs via persistence distortion," in *Proc. 31st Int. Symp. Computational Geometry (SoCG'15)*, Eindhoven, The Netherlands, 22–25 June 2015, pp. 491–506.
- [12] T. K. Dey, H. Edelsbrunner, and S. Guha, "Computational topology," in *Proc. Advances in Discrete and Computational Geometry*, 1999, pp. 109–143.
- [13] A. Dirafzoon and E. Lobaton, "Topological mapping of unknown environments using an unlocalized robotic swarm," in *Proc. IEEE/RSJ Int. Conf. Intelligent Robots and Systems (IROS)*, Nov. 2013, pp. 5545–5551.
- [14] P. Dlotko, R. Ghrist, M. Juda, and M. Mrozek, "Distributed computation of coverage in sensor networks by homological methods," *Appl. Algebra Eng., Commun. Comput.*, vol. 23, no. 1–2, pp. 29–58, 2012.
- [15] D. S. Dummit and R. M. Foote, *Abstract Algebra*, 3rd ed. Hoboken, NJ: Wiley, 2004.
- [16] H. Edelsbrunner and J. L. Harer, *Computational Topology: An Introduction*. Providence, RI: American Mathematical Society, 2010.
- [17] H. Edelsbrunner and D. Morozov, "Persistent homology: Theory and practice," in *Proc. European Congr. Mathematics*, 2014, pp. 31–51.
- [18] S. Emrani, H. Chintakunta, and H. Krim, "Real time detection of harmonic structure: A case of topological signal analysis," in *Proc. Int. Conf. Acoustic Speech and Signal Processing Techniques and Methods*, 4 Nov. 2013, pp. 3445–3449.
- [19] S. Emrani, T. Gentimis, and H. Krim, "Persistent homology of delay embeddings and its application to wheeze detection," *IEEE Signal Processing Lett.*, vol. 21, pp. 459–463, Apr. 2014.
- [20] J. Ernst, M. K. Singh, and V. Ramesh, "Discrete texture traces: Topological representation of geometric context," in *Proc. IEEE Conf. Computer Vision and Pattern Recognition (CVPR)*, 2012, pp. 422–429.
- [21] Y. Feng, P. Martins, and L. Decreusefond, "Accuracy of homology-based approaches for coverage hole detection in wireless sensor networks," in *Proc. IEEE Int. Conf. Communications (ICC)*, 2012, pp. 497–502.
- [22] R. Ghrist and A. Muhammad, "Coverage and hole-detection in sensor networks via homology," in *Proc. Information Processing in Sensor Networks*, 4 Aug. 2005, pp. 254–260.

- [23] L. J. Guibas, D. E. Knuth, and M. Sharir, "Randomized incremental construction of Delaunay and Voronoi diagrams," *Algorithmica*, vol. 7, no. 1–6, pp. 381–413, 1992.
- [24] A. Hatcher, *Algebraic Topology*. Cambridge, U.K.: Cambridge Univ. Press, 2002.
- [25] X. Jiang, L.-H. Lim, Y. Yao, and Y. Ye, "Statistical ranking and combinatorial Hodge theory," *Math. Program.*, vol. 127, no. 1, pp. 203–244, 2011.
- [26] T. Kaczynski, K. Mischaikow, and M. Mrozek, *Computational Homology*. New York: Springer, 2004.
- [27] J. Kleinberg, "An impossibility theorem for clustering," in *Proc. Advances in Neural Information Processing Systems*, 2003, pp. 463–470.
- [28] J. Lamar-Leon, A. Cerri, E. B. G. Reyes, and R. Gonzalez-Diaz, "Gait-based gender classification using persistent homology," in *Proc. Iberoamerican Congr. Pattern Recognition (2)*, 2013, pp. 366–373.
- [29] J. Lamar-Leon, E. B. G. Reyes, and R. Gonzalez-Diaz, "Gait identification using persistent homology," in *Proc. Iberoamerican Congr. Pattern Recognition*, 2012, pp. 244–251.
- [30] E. Lobaton, R. Vasudevan, R. Bajcsy, and S. S. Sastry, "A distributed topological camera network representation for tracking applications," *IEEE Trans. Image Processing*, vol. 19, no. 10, pp. 2516–2529, 2010.
- [31] L. Mazo, N. Passat, M. Couprie, and C. Ronse, "Digital imaging: A unified topological framework," *J. Math. Imaging Vision*, vol. 44, no. 1, pp. 19–37, 2012.
- [32] J. L. Moreno, *Who Shall Survive? A New Approach to the Problem of Human Interrelations* (Nervous and Mental Disease Monograph, vol. 58). Washington, D.C.: Nervous and Mental Disease Publ., 1934.
- [33] D. Morozov and G. Weber, "Distributed merge trees," *ACM SIGPLAN Notices*, vol. 48, no. 8, pp. 93–102, 2013.
- [34] A. Muhammad and A. Jadbabaie, "Dynamic coverage verification in mobile sensor networks via switched higher order Laplacians," in *Proc. Robotics Science and Systems*, 2007. [Online]. Available: <http://www.roboticsproceedings.org/rss03/p39.html>
- [35] M. Nicolau, A. J. Levine, and G. Carlsson, "Topology-based data analysis identifies a subgroup of breast cancers with a unique mutational profile and excellent survival," *Proc. Natl. Acad. Sci.*, vol. 108, no. 17, pp. 7265–7270, 2011.
- [36] P. Niyogi, S. Smale, and S. Weinberger, "Finding the homology of submanifolds with high confidence from samples," *Discrete Comput. Geom.*, vol. 39, no. 1, pp. 419–441, Mar. 2008.
- [37] M. Robinson, "Topological signal processing," in *Mathematical Engineering*. New York: Springer, 2014.
- [38] M. Robinson and R. Ghrist, "Topological localization via signals of opportunity," *IEEE Trans. Signal Processing*, vol. 60, no. 5, pp. 2362–2373, 2012.
- [39] P. Saveliev, "A graph, non-tree representation of the topology of a gray scale image," in *Proc. IS&T/SPIE Electronic Imaging, Int. Society for Optics and Photonics*, 2011, vol. 7870, pp. O1–O19.
- [40] L. Seemann, J. Shulman, and G. H. Gunarante. (2012). A robust topology-based algorithm for gene expression profiling. *Int. Sch. Res. Notices*. [Online]. 2012, pp. 1–11. Available: <http://www.hindawi.com/journals/isrn/2012/381023/>
- [41] P. Skraba, M. Ovsjanikov, F. Chazal, and L. Guibas, "Persistence based segmentation of deformable shapes," in *Proc. IEEE Computer Society Conf. Computer Vision and Pattern Recognition Workshops (CVPRW)*, 2010, pp. 45–52.
- [42] E. H. Spanier, "Algebraic topology," in *Mathematics Subject Classifications*. New York: Springer, 1994.
- [43] *Global SiP Special Symp. Graph Signal Processing*, 2013.
- [44] A. Tahbaz-Salehi and A. Jadbabaie, "Distributed coverage verification in sensor networks without location information," *IEEE Trans. Automat. Contr.*, vol. 55, no. 8, pp. 1837–1849, 2010.
- [45] F. Takens, "Detecting strange attractors in turbulence," *Dyn. Syst. Turbulence*, vol. 898, pp. 366–381, Oct. 1981.
- [46] M. Vejdemo-Johansson, F. T. Pokorny, P. Skraba, and D. Kragic, "Cohomological learning of periodic motion," *Appl. Algebra Eng., Commun. Comput.*, vol. 26, no. 1–2, pp. 5–26, 2015.
- [47] H. Wagner, P. Dlotko, and M. Mrozek, "Computational topology in text mining," in *Proc. Computational Topology in Image Context*, 2012, pp. 68–78.
- [48] A. C. Wilkerson, T. J. Moore, A. Swami, and H. Krim, "Simplifying the homology of networks via strong collapses," in *Proc. Int. Conf. Acoustics, Speech, and Signal Processing*, 2013, pp. 5258–5262.
- [49] Y. Wang, H. Ombao, and M. K. Chung, "Persistence landscape of functional signal and its application to epileptic electroencephalogram data," ENAR Distinguished Student Paper Award, 2014.
- [50] A. J. Zomorodian, "Topology for computing," in *Cambridge Monographs on Applied and Computational Mathematics*, Cambridge, U.K.: Cambridge Univ. Press, 2005.



Lakshmanan Nataraj
and B.S. Manjunath

SPAM: Signal Processing to Analyze Malware

Cyberattacks have risen in recent times. The attack on Sony Pictures by hackers, allegedly from North Korea, received worldwide attention. U.S. President Barack Obama issued a statement and “vowed a U.S. response after North Korea’s alleged cyberattack” [1]. This dangerous malware, termed *wiper*, could overwrite data and stop important execution processes. An analysis by the U.S. Federal Bureau of Investigation showed distinct similarities between this attack and the code used to attack South Korea in 2013, thus confirming that hackers reuse code from already existing malware to create new variants. This attack, along with other recently discovered attacks such as Regin and OpCleave, give one clear message: current cybersecurity defense mechanisms are not sufficient enough to thwart these sophisticated attacks.

Today’s defense mechanisms, such as commercial antivirus (AV) software, is based on scanning systems for suspicious or malicious activity. If such an activity is found, the files under suspect are either quarantined or the vulnerable system is patched with an update. In turn, the AV software is also updated with new signatures to identify such activities in the future. The scanning methods are based on a variety of techniques such as static analysis-, dynamic analysis-, and other heuristics-based techniques, which are often slow to react to new attacks and threats.

Static analysis is based on analyzing an executable without executing

it. These techniques include searching for specific strings, computing cryptographic hashes, and disassembling the executable to extract features. On the other hand, dynamic analysis executes the binary executable and studies its behavioral characteristics in a virtual sandboxed environment. Some of the methods include system-call-level monitoring and memory snapshot comparison. Hackers are familiar with these standard methods and come up with ways to evade the current defense mechanisms. They produce new malware variants that easily evade the detection methods. These variants are created from existing malware using inexpensive, easily available “factory tool kits” in a virtual factory-like setting, which then spread and infect more systems. Once a system is compromised, it either quickly loses control and/or the infection spreads to other networked systems.

While security techniques constantly evolve to keep up with new attacks, hackers too change their ways and continue to evade defense mechanisms. As this never-ending billion dollar “cat and mouse game” continues, it may be useful to look at avenues that can bring in novel alternative and/or orthogonal defense approaches to counter the ongoing threats. The hope is to catch these new attacks using complementary methods that may not be well known to hackers, thus making it more difficult and/or too expensive for them to evade all detection schemes. This article focuses on such orthogonal approaches from signal and image processing that complement standard approaches.

Malware landscape

Malware—malicious software—is any software that is designed to cause damage to a computer, server, network, mobile phones, and other devices. Based on their specific function such as stealing data, spying, keylogging or others, malware are classified into different types such as trojans, backdoors, virus, worm, spyware, adware, and more. Malware are also identified by which platform they belong to, such as Windows, Linux, AndroidOS, and others. While most malware are geared toward the Windows platform, they are also quickly expanding to other platforms such as AndroidOS, Linux, and MAC OS X. Malware are further classified into families, which in turn, have many variants that perform almost the same function (Figure 1). According to the Computer Antivirus Research Organization (CARO) convention for naming malware, a malware is represented by Type:Platform/Family.Variant. For example, PWS:Win32/Zbot.gen denotes a password-stealer malware of the generic Zbot family that attacks 32-bit Windows platforms.

Malware variants are created either by making changes to the malware code or by using executable packers. In the former case, a simple mutation occurs by changing small parts of the code. These are referred to as *unpacked malware variants*. In the latter case, a more complex mutation occurs either by compressing or encrypting (usually with different keys) the main body of the code and appending a decompression/decryption routine, which during

Digital Object Identifier 10.1109/MSP.2015.2507185

Date of publication: 7 March 2016

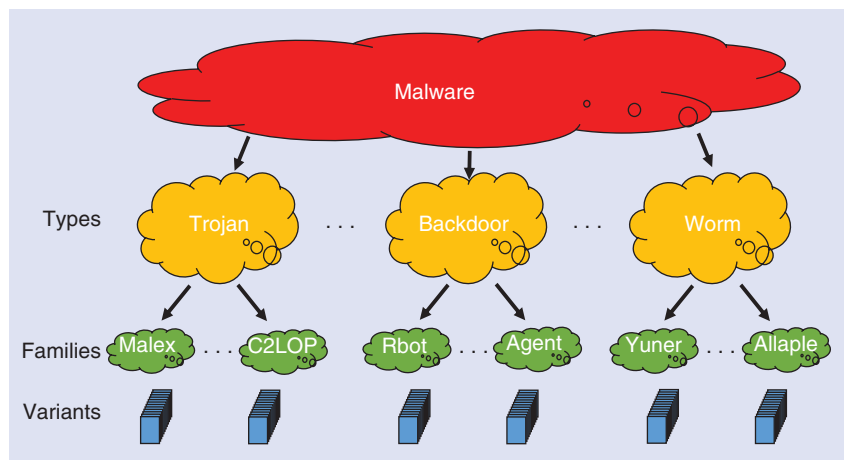


FIGURE 1. The malware landscape: malware are categorized by their type, families, and variants.

runtime decompresses/decrypts the encrypted payload. The new variants are called *packed malware variants*, and they perform the same function as the original malware but their attributes would be so different that AV software, which use traditional signature-based detection, would not be able to detect them. The tools used for obfuscation are called *executable packers*, available both as freeware and commercial tools. There are hundreds of packers that exist today that make it very easy for malware writers to create new variants.

Malware analysis

Malware classification deals with identifying the family of an unknown malware variant from a malware data set that is divided into many families. The level of risk of a particular malware is determined by its function, which is in turn reflected in its family. Hence, identifying the family of an unknown malware is crucial in understanding and stopping new malware. It is usually assumed that an unknown malware variant belongs to a known set of malware families (supervised classification). Having a high classification accuracy (the number of correctly classified families) is desirable. A closely related problem is malware retrieval, where the objective is to retrieve similar malware matches for a given query from a large database of malware. In malware detection, the objective is to determine if an unknown executable is malicious, benign, or unknown. This problem is more challenging than mal-

ware classification, where all samples are known to be malicious. In the following, we will focus on malware classification and malware retrieval.

A common way to defeat static analysis is by using packers on an executable, which compress and/or encrypt the executable code and create a new packed executable that mimics the previous executable in function but reveals the actual code only upon execution runtime. Dynamic analysis is agnostic to packing but is slow and time consuming. Furthermore, today's malware are designed to be virtual machine (VM) aware, which either do not do any malicious activity in the presence of VM or attempts a "suicide" when a VM is detected.

In this context, the challenge is to develop complementary methods that are able to quickly identify malware without the need for disassembly, unpacking, or execution. Alternative representations of malware data as one-dimensional (1-D) or two-dimensional (2-D) signals have patterns that are not captured by standard methods.

Malware images

A common method of viewing and editing malware binaries is by using Hex Editors, which display the bytes of the binaries in hexadecimal representation from "00" to "FF." Effectively, these are 8-bit numbers in the range of 0–255. Grouping these 8-bit numbers results in a 8-bit vector, from which we construct a signal or an image as shown in

Figure 2. For an image, the width is fixed and the height is allowed to vary depending on the file size. To ensure that a small file does not appear horizontally stretched and a large file does not look vertically elongated, we provide some recommended image widths for different file sizes based on empirical observations [6]. Figure 3 shows an example image of a common Windows Trojan downloader, *Dontovo.A*, which downloads and executes arbitrary files. We can see that different sections of this malware exhibit distinctive image patterns. The *.text* section, which contains the executable code, has a fine-grained texture. It is followed by a black block (zeros), indicating zero padding at the end of this section. The *.data* section contains both uninitialized code (black patch) and initialized data (fine-grained texture). The final *.rsrc* section contains all the resources of the module, including the icon of the executable.

Visualizing these malware variants as images, one could make an empirical observation that there is visual similarity among malware variants of the same family (Figure 4). At the same time, the variants are also distinct from those belonging to other families. This is because the variants are created using either simple code mutations or packing. It is easy to identify the variants for unpacked malware since the structure of the variants are very similar. In the case of packed malware, the executable code is compressed and/or encrypted. During runtime, this code is then unpacked and executed. When two unpacked variants belonging to a specific malware family are using a packer to obtain packed variants of the same family, their structure no longer remains the same as that of the unpacked variants. However, the structure within the packed variants are still similar though the actual bytes may vary due to compression and/or encryption. This is because most of the current packers use weak encryption schemes [2]. The visual similarity of malware images motivated us to look at malware classification using techniques from computer vision, where image-based classification has been well studied. We use global image similarity descriptors and obtain compact signatures for these

malware, which are then used to identify their families.

Classification

Once the malware binary is converted to an image, an image similarity descriptor is computed on the image to characterize the malware. The descriptor that we use is the GIST feature [3], which is commonly used in scene classification [3], object recognition [4] and large-scale image search [5]. Every image location is represented by the output of filters tuned to different orientations and scales. A steerable pyramid with four scales and eight orientations is used. The local representation of an image is then given by $V^L(x) = V_k(x)_{k=1..N}$, where $N = 20$ is the number of subbands. To capture the global image properties while retaining some local information, the mean value of the magnitude of the local features is computed and averaged over large spatial regions: $m(x) = \sum_{x'} |V(x')| W(x' - x)$, where $W(x)$ is the averaging window. The resulting representation is downsampled to have a spatial resolution of $M \times M$ pixels (here we use $M = 4$). Thus, the feature vector obtained is of size $M \times M \times N = 320$. For faster processing, the images are usually resized to a smaller size (we use 64×64). Our experiments showed that our initial choice of image width and the width of the resized image does not significantly affect our performance.

To identify malware families, we use the nearest neighbor (NN) classifier, which assigns the family of the nearest malware to an unknown malware. We obtained four data sets: Maling data set (Windows) [8], Malheur data set (Windows) [9], MalGenome data set (Android) [7], and VxShare ELF data set (Linux) [10]. On all four data sets we performed supervised classification with tenfold cross validation and obtained a high-classification accuracy (Table 1). Furthermore the accuracy of this method (95.14%) is comparable to that of the state-of-the-art dynamic analysis (98.12%), but 4,000 times faster [11]. In [12], we extend our approach to separate malware from benign software. To get a richer discrimination between benign and malicious samples, we adopt

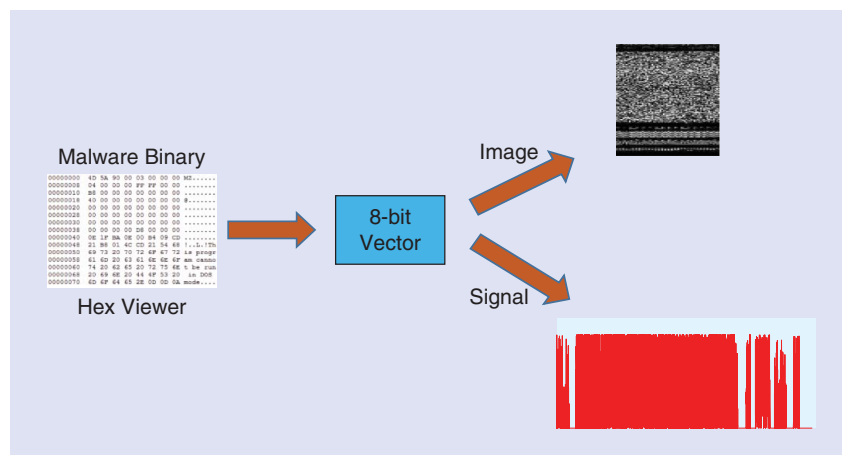


FIGURE 2. Malware can be represented as a 1-D signal or as a 2-D image.

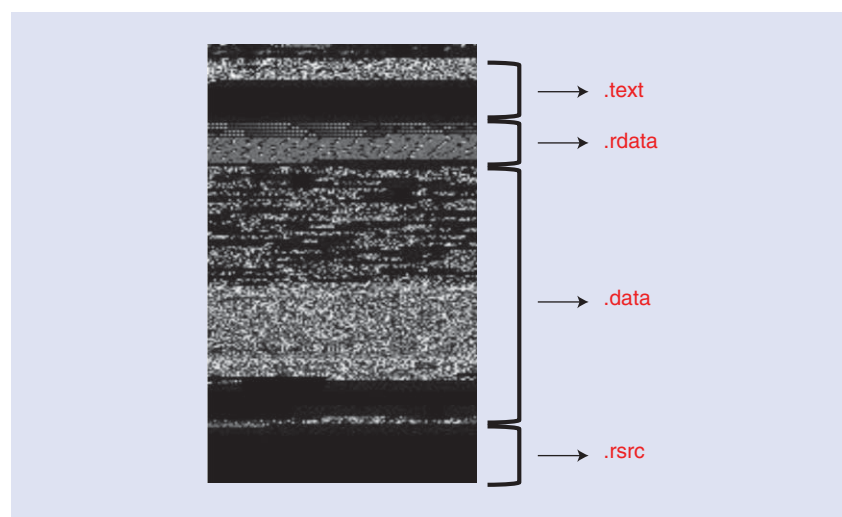


FIGURE 3. Visualizing a malware as a digital image: different sections of the executable are visible in the image.

a section-aware approach and compute GIST descriptors on the entire binary as well as the top two sections of the binary that could contain the code. With more than 99% precision, this approach outperformed other static similarity features.

Search and retrieval

We developed search and retrieval of malware (SARVAM) [13] (<http://sarvam.ece.ucsb.edu>), an online system for large-scale malware search and retrieval (Figure 5). It is one of the few systems available to the public where researchers can upload or search for a sample and retrieve similar malware matches from a large database. As in [6], we use GIST descriptors for content-based search and retrieval of malware. For fast search and retrieval, we use a scalable Balltree-based NN searching technique.

During the initial training phase of building SARVAM, we obtained a large corpus of malware samples from various sources. The image fingerprints for all the samples in the corpus are then computed and stored in a database. Simultaneously, we obtained the AV labels for all the samples from Virustotal [14], an online system that maintains a database of AV labels. These labels act as a ground truth and are later used to describe the nature of a sample, i.e., how malicious or benign a sample is. During the query phase, the fingerprint for the new sample is computed and matched with the existing fingerprints in the database to retrieve the top matches.

The initial database consisted of more than seven million samples comprising mostly malware and a few benign samples. For a new query, SARVAM finds a match in about six seconds. SARVAM

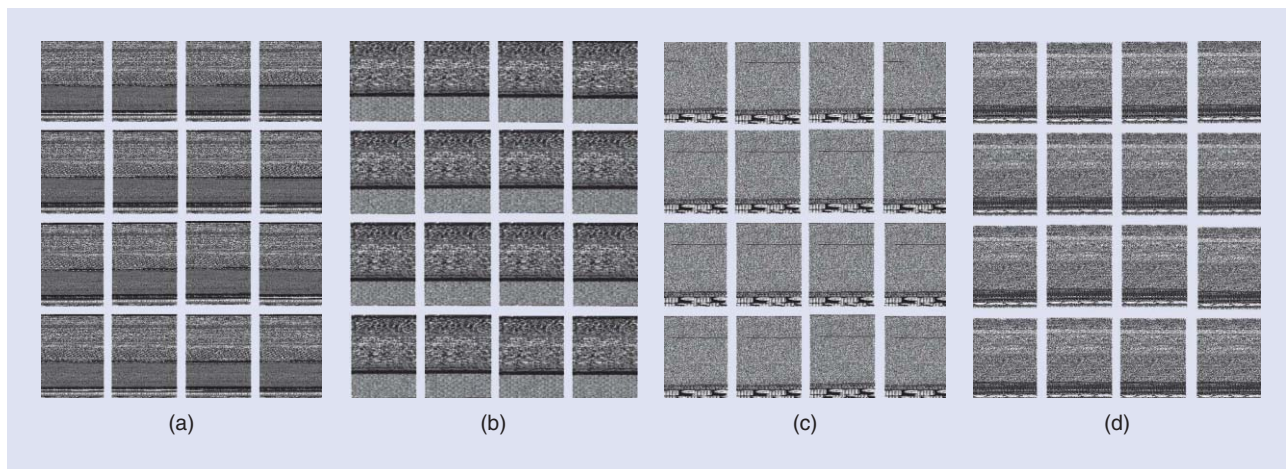


FIGURE 4. Visual similarity among malware variants of four different families. (a) Adialer.C, (b) Dialplatform.B, (c) Fakerean, and (d) Yuner.A.

Table 1. Accuracy on malware data sets from different operating systems: Windows, Linux, and Android.

Data Set	Size	Number of Families	Accuracy
Maling (Win)	9,339	25	97.4
Malheur (Win)	3,131	24	98.37
VxShare (Linux)	568	8	83.27
Malgenome (Android)	1,094	13	84.55

has been operational since May 2012, and we have received more than 440,000 samples since then. Nearly 60% of the samples we received are variants of already existing malware from our database.

Sparsity-based malware analysis

In this section, we explore sparse representation-based classification (SRC) methods to classify malware variants into families. Such methods have been previously applied to problems where samples belonging to a class have small variations in them, such as face recognition [16] and iris recognition [18]. We developed sparsity inspired classification of malware variants (SATTVA) [15], where we model a malware variant belonging to a particular malware family as a linear combination of variants from that family. Since variants of a family have small changes in the overall structure and differ from variants of other families, projections of malware in lower dimensions preserve this “similarity.”

Given a data set of N labeled malware belonging to L different malware families with P malware per family, the task

is to identify the family of an unknown malware \mathbf{u} . We represent a malware as a digital signal \mathbf{x} of range $[0, 255]$, where every entry of \mathbf{x} is a byte value of the malware. Since each malware sample can have a different code-length, we normalize all vectors to a maximum length (M) by zero-padding.

The entire data set can now be represented as an $M \times N$ matrix \mathbf{A} , where every column represents a malware. Further, for every family k ($k = 1, 2, \dots, L$), we define an $M \times P$ matrix $\mathbf{A}_k = [\mathbf{x}_{k1}, \mathbf{x}_{k2}, \dots, \mathbf{x}_{kP}]$ where $\mathbf{x}_{k\{i\}}$ represents a malware sample belonging to family k . Now, \mathbf{A} , can be expressed as a concatenation of block-matrices \mathbf{A}_k

$$\mathbf{A} = [\mathbf{A}_1 \mathbf{A}_2 \dots \mathbf{A}_L] \in \mathbb{R}^{M \times N} \quad (1)$$

Let $\mathbf{u} \in \mathbb{R}^M$ be an unknown malware whose family is to be determined, with the assumption that \mathbf{u} belongs to one of the families in the data set. Then, following [16], we represent \mathbf{u} as a sparse linear combination of the training samples as

$$\mathbf{u} = \sum_{i=1}^L \sum_{j=1}^P \alpha_{ij} \mathbf{x}_{ij} = \mathbf{A}\alpha, \quad (2)$$

where $\alpha = [\alpha_{1,1}, \dots, \alpha_{L,P}]^T$ represents the $N \times 1$ sparse coefficient vector ($N = LP$). α will have nonzero values only for samples that are from the same family as \mathbf{u} . The sparsest solution to (2) can be obtained using basis pursuit [18] by solving an l_1 -norm minimization problem. Estimating the family of \mathbf{u} is done by computing residuals for every family in the training set and then selecting the family that has minimum residue.

Random projections

When a malware binary is represented as a numerical vector by considering every byte, the dimensions of that vector can be very high. For example, a 1-megabyte malware has around 1 million bytes and this could make the calculations computationally expensive. Hence, we project the vectors to lower dimensions using random projections (RPs). This also removes dependency on any particular feature extraction method. Previous works have demonstrated that SRC is effective in lower-dimensional RPs as well; see [16]–[18]. Let $\mathbf{R} \in \mathbb{R}^{D \times M}$ be the matrix that projects \mathbf{u} from signal space M to \mathbf{w} of a lower-dimensional space D ($D \ll M$)

$$\mathbf{w} = \mathbf{R}\mathbf{u} = \mathbf{R}\mathbf{A}\alpha. \quad (3)$$

The entries of \mathbf{R} are drawn from a zero-mean normal distribution. The above system of equations is under-determined and sparse solutions can be obtained by reduced l_1 -norm

minimization. The overall approach is shown in Figure 6.

We test our technique on two public malware data sets: the Maling data set [8] and the Malheur data set [9]. On both data sets, we select equal number of samples to reduce any bias toward a particular family. For comparison, we use GIST descriptors, which we had

previously applied for malware classification. We use the SRC framework to identify the malware family of a test sample and compare it with NN classification that we previously used in [6]. We vary the projected dimensions from 48 to 512, which are consistent for both RP and GIST. In our experiments, we choose 80% of a data set for training and

20% for testing. On both the Maling data set [Figure 7(a)] and the Malheur data set [Figure 7(b)], the best accuracy is obtained for the combination of RPs and the SRC classification framework (92.83% for Maling and 98.55% for Malheur). The projected dimension is 512 from higher dimensions of 840,960 (Maling) and 3,364,864 (Malheur).

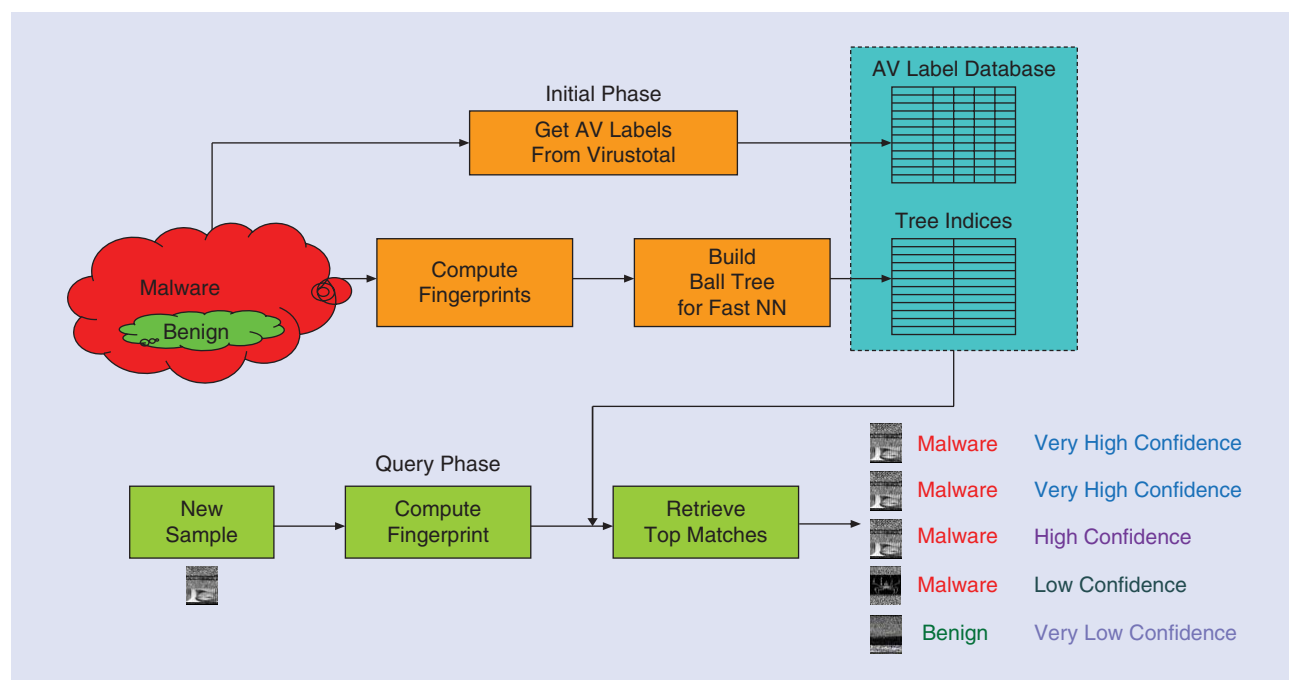


FIGURE 5. The block schematic of SARVAM: In the initial phase, the image similarity descriptors and AV labels are computed and stored in a database. In the query phase, the NNs along with their corresponding AV labels are retrieved.

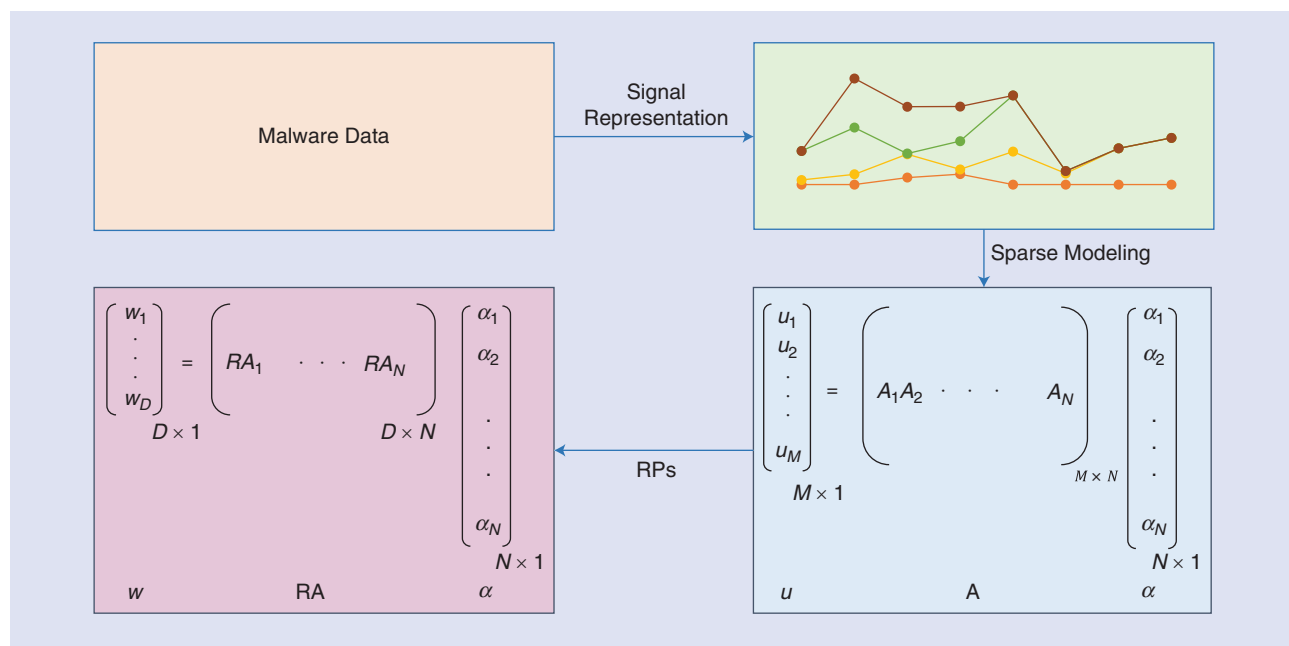


FIGURE 6. The SRC framework for malware classification.

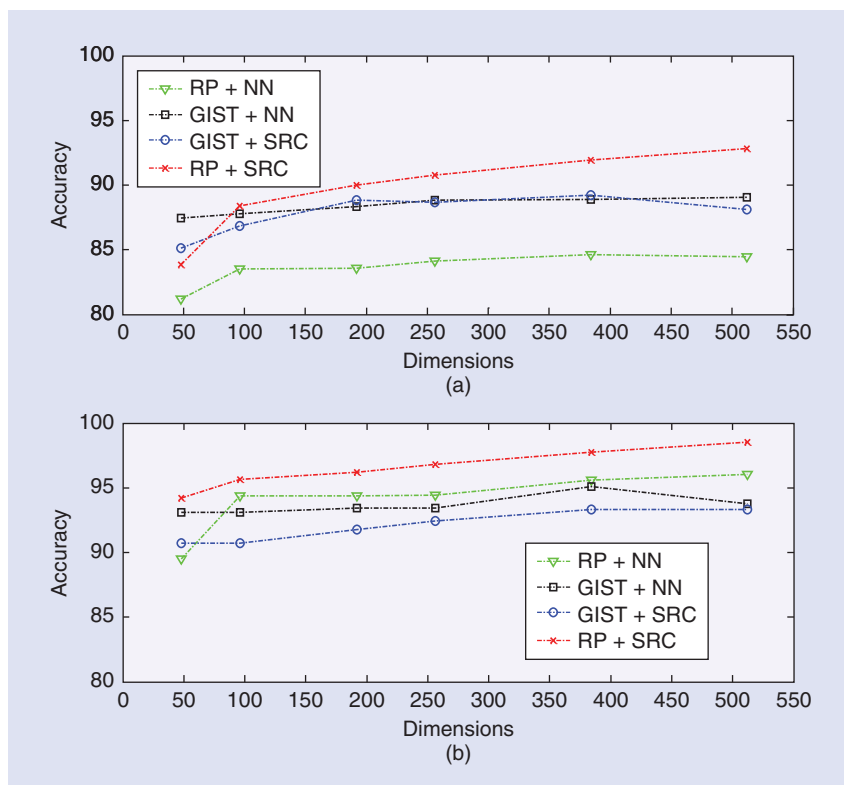


FIGURE 7. Experimental results on (a) Maling data set and (b) Malheur data set with features using RPs and GIST, and classification algorithms using SRC and NN.

The accuracies for GIST for both classifiers are almost the same. In [15], we extend this approach using a simple thresholding scheme to reject potential outliers in a data set.

Future directions

While we explored signal- and image-based analysis of malware data, a natural complement is to treat the malware as audio-like 1-D signals and leverage automated audio descriptors. Another possible approach is computing image similarity descriptors and/or random projections on all the sections and represent a malware as a bag of descriptors, which can then be used for better characterization of malware. Using the error model in the sparse representation-based malware classification framework, we can determine the exact positions in which the malware variant differs from another variant. This approach can also be used to find the exact source from which a malware variant evolves. Patched malware that attaches to benign software can be identified using this method.

Conclusions

In this article, we explored orthogonal methods to analyze malware motivated by signal and image processing. Malware samples are represented as images or signals. Image- and signal-based features are extracted to characterize malware. Our extensive experiments demonstrate the efficacy of our methods on malware classification and retrieval. We believe that our techniques will open the scope of signal- and image-based methods to broader fields in computer security.

Acknowledgments

We would like to thank Prof. Giovanni Vigna and Prof. Christopher Kruegel of UCSB Seclab for providing the malware data and for their valuable suggestions. We are thankful to our colleagues who worked in this project: Dr. Gregoire Jacob, Dr. Dhilung Kirat and Dr. S. Karthikeyan. We would also like to thank Dr. Sukarno Mertoguno of the Office of Naval Research (ONR) for fruitful discussions. This work is supported by grants ONR N00014-11-10111 and ONR N00014-14-1-0027.

Authors

Lakshmanan Nataraj (lakshmanan_nataraj@ece.ucsb.edu) received his Ph.D. degree in electrical and computer engineering from the University of California, Santa Barbara. His research interests include malware analysis, image forensics, and data hiding. He is currently a member of research staff at Mayachitra, Inc.

B.S. Manjunath (manj@ece.ucsb.edu) is a professor in the Department of Electrical and Computer Engineering, University of California, Santa Barbara. His research interests include bioimaging, informatics, media forensics and security, steganography, large-scale image and video sensor networks, and multimedia databases. He is a Fellow of the IEEE.

References

- [1] (2015, Dec.). Sony hack: Obama vows response as FBI blames North Korea. [Online]. Available: <http://www.bbc.com/news/world-us-canada-30555997>
- [2] G. Jacob, P. M. Comparetti, M. Neugschwandtner, C. Kruegel, and G. Vigna, "A static, packer-agnostic filter to detect similar malware samples," in *Proc. 9th Int. Conf. Detection of Intrusions and Malware, and Vulnerability Assessment*, July 2012, pp. 102–122.
- [3] A. Oliva and A. Torralba, "Modeling the shape of the scene: A holistic representation of the spatial envelope," *Int. J. Comput. Vision*, vol. 42, no. 3, pp. 145–175, May 2001.
- [4] A. Torralba, K. P. Murphy, W. T. Freeman, and M. Rubin, "Context-based vision system for place and object recognition," in *Proc. 9th IEEE Int. Conf. Computer Vision*, Oct. 2003, vol. 1, pp. 273–280.
- [5] M. Douze, H. Jgou, H. Sandhawalia, L. Amsaleg, and M. Schmid, "Evaluation of GIST descriptors for Web-scale Image Search," in *Proc. ACM Int. Conf. Image and Video Retrieval*, July 2009, no. 19, pp. 1–8.
- [6] L. Nataraj, S. Karthikeyan, G. Jacob, and B. S. Manjunath, "Malware images: Visualization and automatic classification," in *Proc. 8th Int. Symp. Visualization for Cyber Security*, July 2011, no. 4, pp. 1–7.
- [7] Y. Zhou and X. Jiang, "Dissecting Android malware: Characterization and evolution," in *Proc. IEEE Symp. Security and Privacy*, May 2012, no. 15, pp. 95–109.
- [8] (2015, Dec.). Maling Dataset. [Online]. Available: <http://old.vision.ece.ucsb.edu/spam/maling.shtml>
- [9] K. Rieck, P. Trinius, C. Willems, and T. Holz, "Automatic analysis of malware behavior using machine learning," *J. Comput. Security*, vol. 19, no. 4, pp. 639–668, Dec. 2011.
- [10] (2015, Dec.). VirusShare. [Online]. Available: <http://www.virusshare.com>
- [11] L. Nataraj, V. Yegneswaran, P. Porras, and J. Zhang, "A comparative assessment of malware classification using binary texture analysis and dynamic analysis," in *Proc. 4th ACM Workshop on Security and Artificial Intelligence*, Oct. 2011, pp. 21–30.
- [12] D. Kirat, L. Nataraj, G. Vigna, and B. S. Manjunath, "SigMal: A static signal processing based malware triage," in *Proc. 29th Annu. Computer Security Applications Conf.*, Dec. 2013, pp. 89–98.

(continued on page 117)

Antonio Stanziola, Matthieu Toulemonde, Yesna O. Yildiz, Robert J. Eckersley, and Meng-Xing Tang

Ultrasound Imaging with Microbubbles

Medical ultrasound (US) imaging, also known as *echography*, is one of the most frequently used front-line clinical imaging modalities and is characterized by its safety, affordability, accessibility, and real-time image display. Sound pulses, typically in the megahertz range, are sent into the body and the backscattered echoes are used to create a tomographic image. The contrast of an US image arises from local variations in the physical properties of the tissues, primarily density and elasticity, revealing tissue structures at depth.

The blood flow of a living organism contains essential information related to tissue function and pathology. However, as blood is a fluid composed of plasma and blood cells that are similar to each other acoustically, the scattering of sound from blood is very weak compared to surrounding tissue structures. Consequently, it is difficult to detect vessels that are smaller in size than the pulse length, as the echoes from blood are completely masked by the neighboring tissue response. While for big vessels it is still possible to obtain hemodynamic information due to the weak scattering of blood cells, in general, the signal-to-noise ratio (SNR) is poor and the information content is limited.

To overcome the limitations of conventional US, gas bubbles of micrometer radius can be introduced into a patient's bloodstream as agents for contrast enhanced US imaging (CEUS). Microbubbles (MBs) act as resonant oscillators and scatter US

signals efficiently when excited at the frequencies used in the clinical practice, typically in the range of 1–15 MHz. They are designed to have a diameter ($<7 \mu\text{m}$) capable of passing the pulmonary capillaries (the smallest vessels in the human body) and often include a lipid shell that encapsulates a low solubility gas, so as to increase their longevity in the circulation.

The use of MBs in US imaging generates new and exciting possibilities [1]. It enables real-time imaging of blood flow with unprecedented sensitivity and resolution in both large vessels and microvasculature and provides indicators of the perfusion of organs in, e.g., liver [Figure 1(a) and (b)], kidney [Figure 1(c) and (d)], heart, limbs, brain, breast, and lymphatic systems. The safety of MBs in diagnostic US has been well established. If the MB shell is coated with specific molecules, complementary to those expressed by the vascular walls during specific pathological processes such as the initiation of cancer or atherosclerosis, it is possible to bind MBs to these receptors (targeted MBs) facilitating molecular imaging for early detection and diagnosis [1].

MBs as nonlinear oscillation systems

The equilibrium radius of an MB is a balancing act between the external pressure of the blood, the internal pressure of

The equilibrium radius of an MB is a balancing act between the external pressure of the blood, the internal pressure of the gaseous core, the shell elastic properties, and the surface tension.

the gaseous core, the shell elastic properties, and the surface tension. When an US wave excites an MB, since the bubble diameter (a few μm) is much smaller than the clinical US wavelength (hundreds of μm), it causes a

global change in the external pressure p_0 that results in an oscillation of the MB associated with the emission of sound waves [Figure 2(a) and (b)]. As the gas core is highly compressible, the bubble radius can oscillate significantly around its equilibrium value r_0 if driven at or near its resonance frequency, and this behavior is responsible for the strong scattering of the contrast agents.

MBs are inherently nonlinear oscillation systems. Even with US amplitudes of tens of kilopascal, well below those typically used in clinical imaging, the radius change for an MB is not symmetrical in the compression and expansion phases. This asymmetry is a key source of harmonic generation from MBs.

The MB oscillation and subsequent scattering is highly dependent on the US parameters, including frequency and amplitude. A variety of analytical models have been developed to describe this process, most of them assuming a time-invariant spherical bubble. The simplest is the Rayleigh-Plesset (RP) model, which considers a shell-free bubble of polytropic gas in an

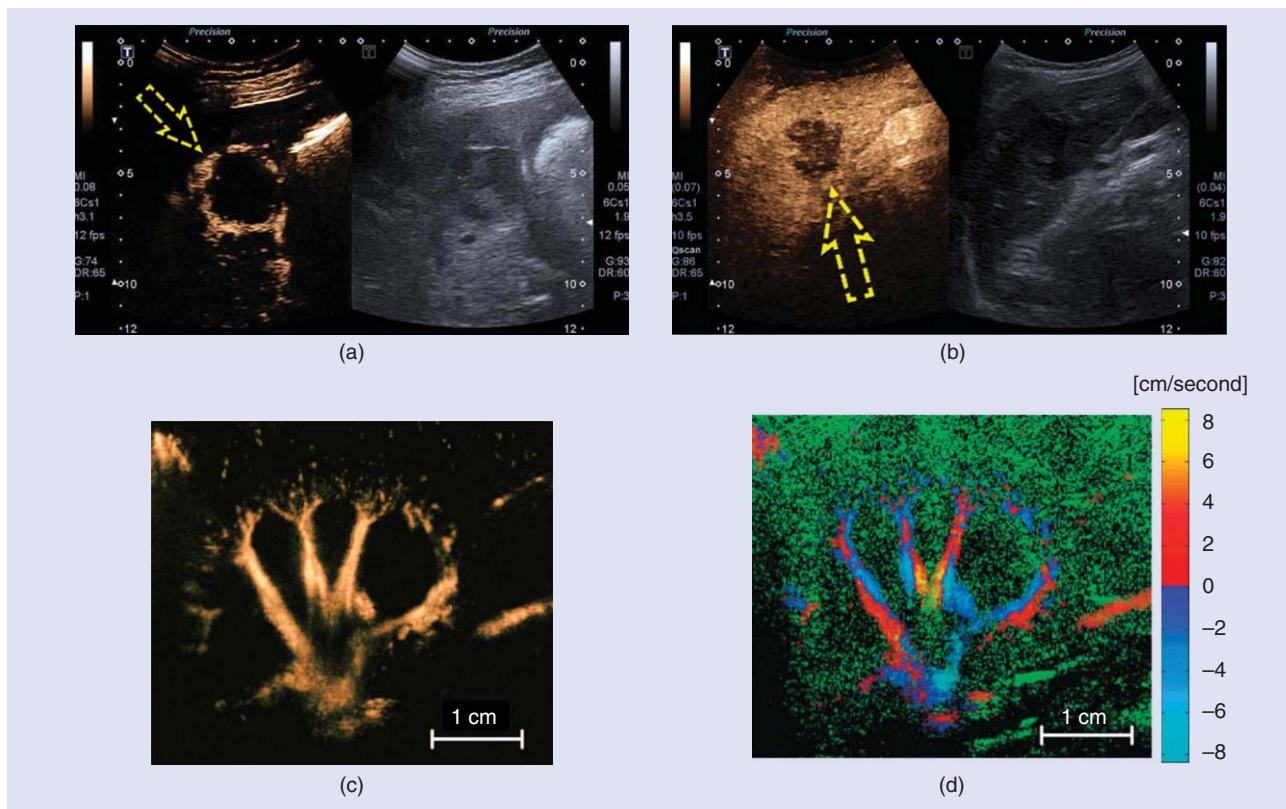


FIGURE 1. The comparison of side by side CEUS contrast specific image (color) versus standard US B-mode image (grayscale) for (a) a liver arterial hemangioma and (b) a liver metastasis. Both lesions are clearly visible in the contrast specific images but not the standard B-mode images. In the contrast specific images, the haemangioma is shown to be surrounded by a ring of contrast enhancement [arrow in (a)], while the metastasis is shown as a dark area [arrow in (b)]. (c) CEUS image and (d) nonlinear Doppler CEUS image of a rabbit kidney vasculature (adapted from [2] with permission). Nonlinear Doppler shows additional information including the direction of flow (blue and red) as well as microcirculation information (green).

inviscid incompressible fluid of density ρ . If p_∞ is the liquid pressure far away from the bubble and $p = p(t)$ the pressure at the bubble interface, the time evolution of the radius r is governed by

$$\ddot{r}r + \frac{3}{2}\dot{r}^2 = \frac{p - p_\infty}{\rho}, \quad (1)$$

where \dot{r} and \ddot{r} are respectively the first and second derivatives of $r(t)$ with respect to time. The nonlinear term on the left-hand side shows that bubble oscillation in response to a pressure wave is nonlinear and, for a sinusoidal excitation, the scattered signal will contain harmonics and subharmonics [Figure 2(c)]. This has been verified experimentally and, since the scattering from existing structures in the body is generally considered to be linear, this is the main characteristic exploited to distinguish between MBs and tissue signals.

The nonlinear behavior of an MB can be further enhanced by the presence of a shell. The RP equation has, therefore,

been refined to include the effects of the shell, the surface tension at the bubble interface, the viscosity of blood, and the finite speed of sound, leading to a number of modified Rayleigh models [3].

Detecting nonlinear scattering signals from MBs

To image the MBs in small vessels, the tissue signals need to be removed to facilitate generation of MB-specific images. While it is possible to use a high-pass filter, with a cut-off frequency between the fundamental and second harmonic (SH) frequencies, to remove the signals reflected by tissues, this approach is fundamentally limited by the transducer bandwidth. In US imaging, a short broadband pulse is required as the spatial resolution is determined by the transmitted pulse length. It is difficult to completely separate the broadband fundamental signal from its harmonics within a limited bandwidth, reducing the contrast between MBs and tissue [Figure 2(h)].

Multipulse acquisition

Multipulse techniques such as pulse inversion (PI) have been developed to elegantly separate the MB signals from tissue without sacrificing spatial resolution. In PI, two identical but phase-inverted pulses, as shown in Figure 2(d), are transmitted into the medium consecutively. While either echo of the two pulses can produce a conventional US image (B-mode image) [Figure 2(g)], the sum of the two echoes is zero for linear scatterers (tissue) while for nonlinear scatterers (MB) the sum is nonzero; see Figure 2(e). In the frequency domain shown in Figure 2(f), for PI, all even harmonics are preserved while the fundamental signal (3 MHz) is suppressed. Standard B-mode, SH-filtered, and PI approaches are compared on a carotid artery phantom in Figure 2(g)–(i), demonstrating PI as a superior technique with almost complete suppression of the tissue and much improved contrast agent-to-tissue ratio.

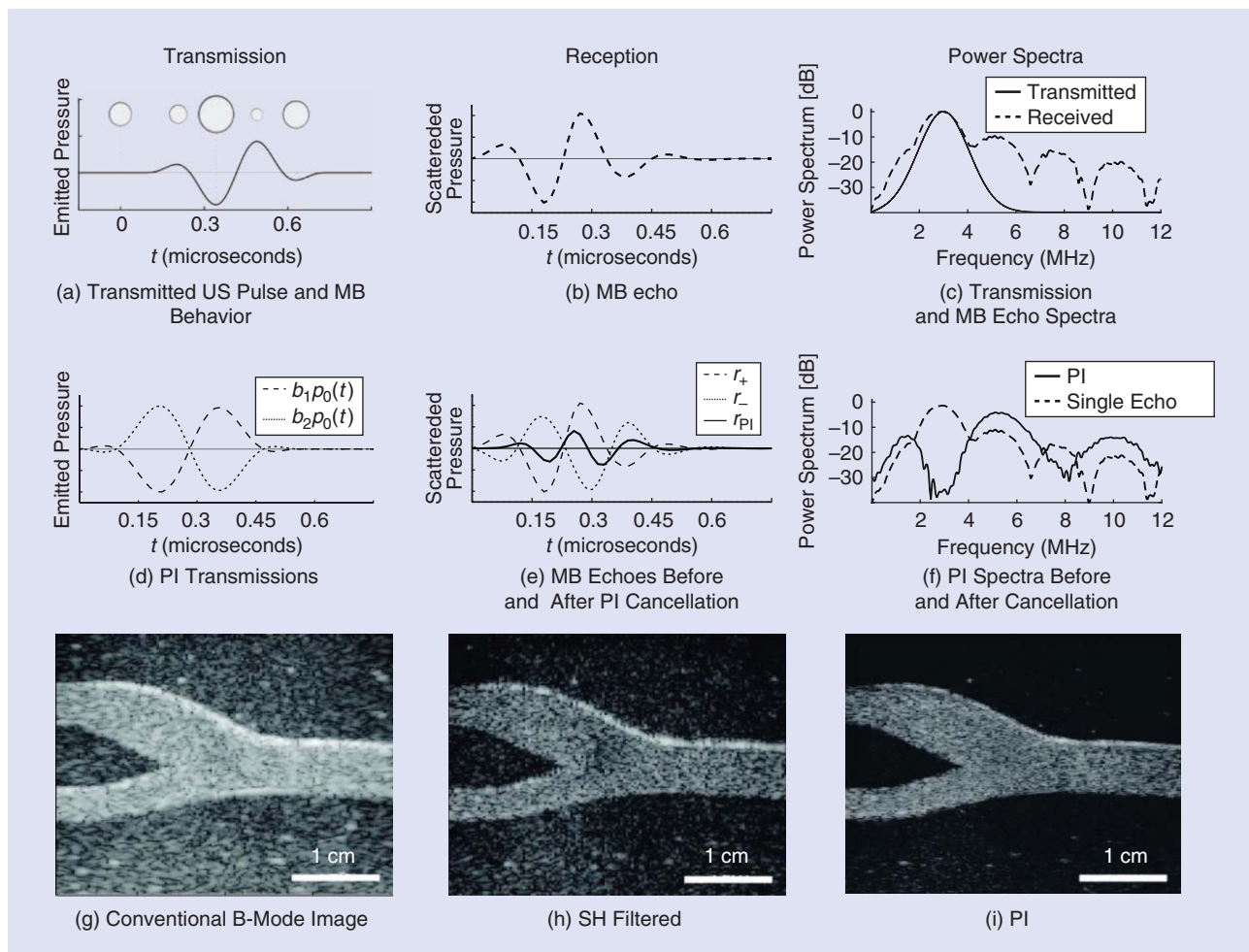


FIGURE 2. Principles of MB detection. (a) MB oscillation in response to an external US pressure field, (b) the scattered US wave, and (c) the frequency response. (d)–(f) illustrates the principle of PI detection: (d) depicts positive and negative transmitted pulses and (e) shows the MB responses to them; the sum of the two responses is shown by the solid line and the frequency spectrum in (f). (i) The PI image has better specificity in imaging MBs than (g) B-mode and (h) SH-filtered images.

There are a number of multipulse techniques related to PI that employ varying pulse phase or amplitude. These can be summarized through a mathematical generalization [4]. If the transmitted US wave is given by

$$b_k p(t) = b_k P_0 e^{j\omega_0 t + \varphi_0}$$

$$b_k = |b_k| e^{j\varphi_k},$$

$$\varphi_k \in [0, 2\pi], k = 1, 2, \dots, K, \quad (2)$$

where $p(t)$ represents the basic pulse, P_0 the amplitude of the wave, ω_0 the US angular frequency, and φ_0 the phase. The changes in amplitude and phase applied to the k th transmitted pulse are indicated by b_k . The k th received wave can then be modeled as a Taylor series

$$r_k(t) = \sum_{n=1}^N a_n [b_k p(t)]^n, \quad (3)$$

where a_n is the weight of the n th nonlinear component and N is the model order. Given a sinusoidal $p(t)$, the n th nonlinear component contains the n th harmonic. After consecutive transmission and reception of K pulses in the medium, the postprocessing to generate contrast specific signals can be done by a weighted sum of the received pulses

$$r_{\text{sum}}(t) = \sum_{k=1}^K \lambda_k r_k(t)$$

$$= \sum_{n=1}^N \left(\sum_{k=1}^K \lambda_k b_k^n \right) a_n p^n(t), \quad (4)$$

where λ_k is a reception coefficient that must be appropriately chosen depending on b_k to cancel linear components. The transmission and reception parameters of PI, amplitude modulation (AM),

and contrast pulse sequence (CPS) are given in Table 1 [4].

While multipulse transmission reduces the imaging frame rate, this can be compensated by the emerging ultrafast imaging techniques with up to tens of thousands of frames/second [5].

Encoded pulses

Even at moderate US amplitudes (tens to hundreds of kilo-Pascals), MBs can be disrupted. This occurs, for example, due to the negative pressure portion in the US pulse can cause the shell to expand until it ruptures. To mitigate this effect, the transmit amplitude needs to be kept low, with a consequent reduction in the SNR. Transmitting longer pulses can increase the signal energy and consequently the SNR, without increasing the peak pressures and the associated risk of

Table 1. Multipulse techniques.

Pulse Sequence	b	λ	$r_{sum}(f)$
PI	$(1, e^{j\pi})$	$(1, 1)$	$\sum_{n=1}^N (1 + e^{jn\pi}) a_n p^n(f)$
AM	$(1, \frac{1}{2})$	$(1, -2)$	$\sum_{n=1}^N (1 - 2^{1-n}) a_n p^n(f)$
CPS	$(1, \frac{1}{2} e^{j\pi}, \frac{1}{2} e^{j\pi})$	$(1, 1, 1)$	$\sum_{n=1}^N (1 + 2^{1-n} e^{jn\pi}) a_n p^n(f)$

MB destruction, but this comes at the cost of a reduced image resolution. Coded transmission techniques, such as frequency encoding (chirp), were developed for radar systems for the conflicting requirements of simultaneous high SNR and high-resolution performance. A long pulse with an embedded code is transmitted. After reception, the signal is cross-correlated with the transmitted pulse to detect and remove the code and restore the spatial resolution in a process called *compression*.

A nonlinear compression filter can be used to selectively extract and

compress the SH from the received echo of MBs [6]. While this combination of harmonic imaging and chirp transmission improves the resolution of the technique, side lobes can appear due to the chirp compression and frequency overlapping. The method can be improved by extracting the chirp SH component in a space between the time and frequency using the fractional Fourier transform [7]. Furthermore, pulse encoding is not limited to frequency encoding (chirp) and other codes, such as Barker and Golay, can also be used.

Detecting bubble motion using nonlinear Doppler processing

The measurement of MB motion can provide insight about the flow conditions (fast versus slow) and is useful for determining whether targeted bubbles are bound or free flowing. Multipulse sequences can be used to both detect the existence of MBs, as previously described, and to provide motion information. The Doppler equation describes the frequency shift given by the relative motion between a sound source and an observer. In US imaging, it can be used to determine movement of objects such as red blood cells or MBs. For the sake of simplicity, we focus only on motion along the US propagation direction. The frequency shift of a linear scatter moving with velocity v is given by

$$\Delta f = \frac{2f_0 v}{c}, \tag{5}$$

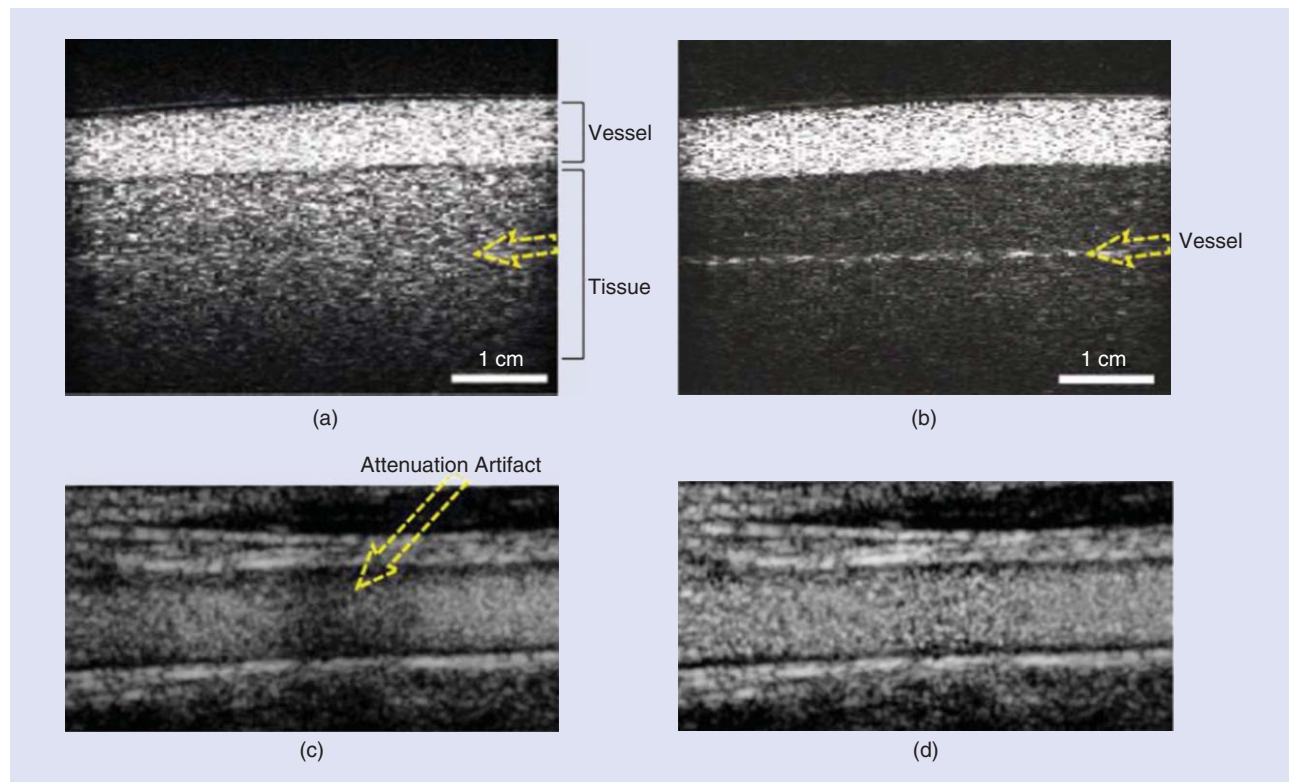


FIGURE 3. Imaging artefact correction: (a) PI and (b) corrected PI images of a flow phantom with two vessels containing diluted suspension of MBs (adapted from [9] with permission), where the yellow arrows point to the small vessel recovered by the artefact correction. An in vivo CEUS image of a carotid artery with (c) attenuation artefact (yellow arrow) and (d) attenuation artefact corrected (adapted from [10] with permission).

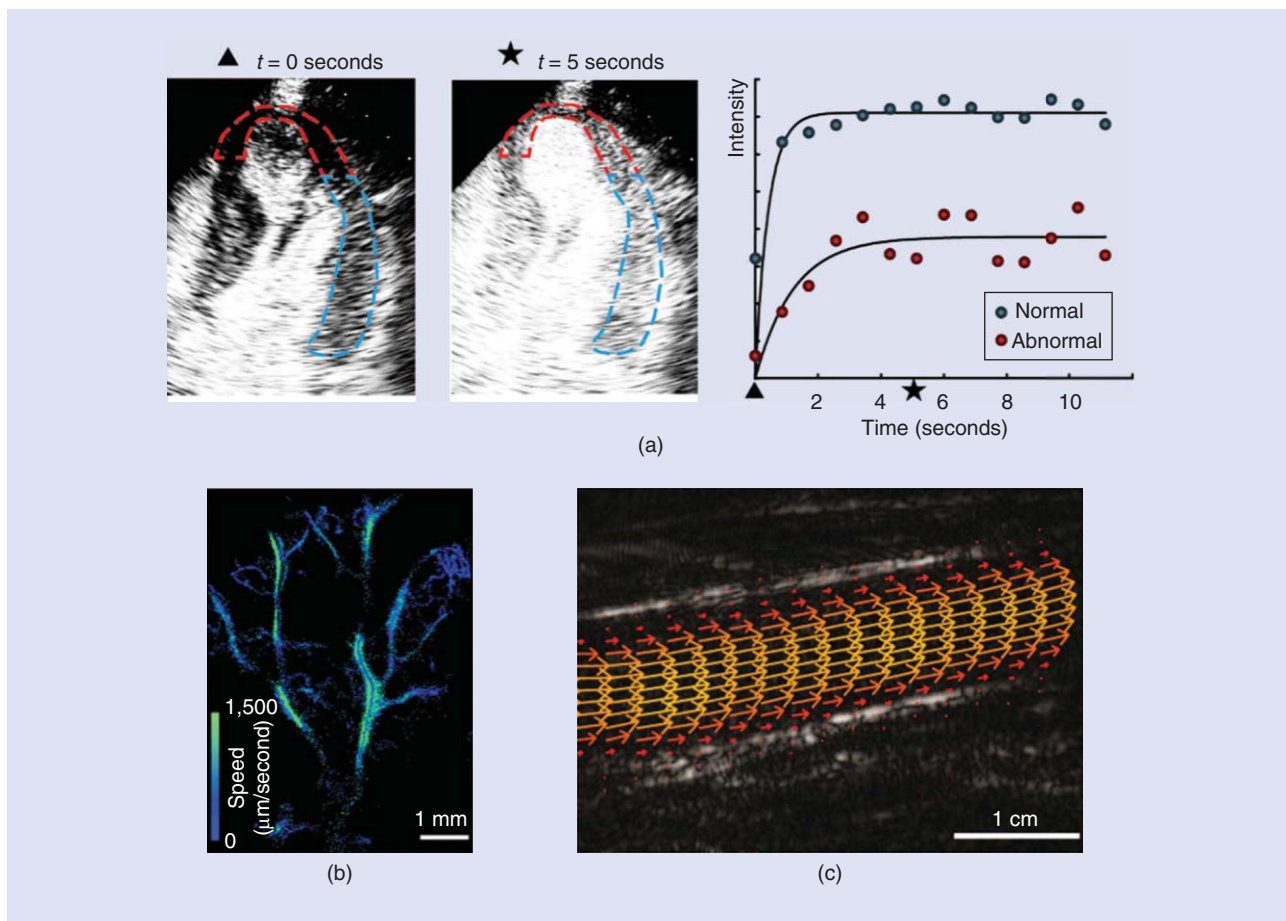


FIGURE 4. Applications of contrast enhanced US imaging: (a) left ventricle myocardium perfusion shown by CEUS at two time points and its quantification, (b) superresolution US imaging (reproduced from [12] with permission) in vivo and (c) blood flow velocity estimation using MB tracking in a rabbit abdominal aorta (adapted from [13] with permission).

where f_0 is the fundamental frequency of the transmitted pulse and c is the speed of sound. Continuous wave Doppler has great velocity resolution but does not offer spatial information. This can be overcome by sending multiple pulses at a frequency f_{PRF} and measuring the relative phase shift of the responses over time $\Delta\phi(t)$, a technique known as *pulsed Doppler*. The Fourier transform of the Doppler signal with phase will return the frequency shift provided that the motion is slow enough to be captured at the given f_{PRF} (Nyquist constraint).

A moving nonlinear scatterer like MBs will generate both fundamental and harmonic Doppler signals of different phase shifts (e.g., SHs have phase shifts that are double that of fundamental signals). This has been used in conjunction with PI to distinguish the movement of MB from tissue [2]. As in PI, the pulses used to generate the Doppler signal are sent with

a phase shift of π between consecutive pulses, so that the phase shift in the consecutive echoes from a moving linear scatterer has an additional π

$$\Delta\phi = 2\pi f_0 \Delta\tau + \pi, \quad (6)$$

where $\Delta\tau = 2v/cf_{PRF}$ is the time shift due to target motion. The additional π due to pulse inversion will shift the spectrum of the Doppler signal for a linear target by a factor of $1/2f_{PRF}$. On the other hand, it does not affect the even harmonics emitted by a nonlinear target, as can be seen through decomposing the nonlinear signals as in (3). The Doppler frequency for the n th harmonic can thus be expressed as

$$f_d = \begin{cases} \frac{2f_0 v}{c} & \text{if } n \text{ is even} \\ \frac{2f_0 v}{c} + \frac{1}{2}f_{PRF} & \text{if } n \text{ is odd.} \end{cases} \quad (7)$$

Using a low-pass filter with cut-off frequency at $1/4f_{PRF}$, it is possible to distinguish between even harmonics emitted by MBs and fundamental signals emitted by tissue, even if they have similar motion. This enables the specific imaging of both fast and slowly moving agents in macro- and microvessels [see Figure 1(d)] or potentially those targeted agents adherent to a vessel.

Artefact reduction for contrast detection

CEUS suffers from various imaging artefacts [8], and signal processing algorithms have been developed to reduce them. One type of common artefact arises from the nonlinear distortion of the transmitted US pulse as it propagates through tissue and MB clouds, generating harmonics. The degree of the nonlinear distortion depends on both the US amplitude and

the medium. These propagation harmonics are subsequently reflected by tissues and then misclassified as MBs. This is commonly referred to as a *nonlinear propagation artefact* and can be observed below the vessel wall in Figure 3(a).

Among the different techniques developed to mitigate such artefacts, the method in [9] uses a signal processing approach, where the nonlinear tissue artefact is estimated based on two simultaneously acquired images: 1) the B-mode image that contains mainly tissue signals and 2) the contrast specific image (such as PI) that contains both MB signals and artefacts. As the artefacts originate from tissue reflection/scattering, removing artefacts means estimating and removing the tissue signals (found in the B-mode image) from the contrast specific image. As the B-mode and the contrast specific images have different point spread functions (PSFs), direct subtraction does not work. In [9], the tissue scatterer distribution (TSD) is first estimated by deconvolving the B-mode image with the measured linear PSF of the system, and the artefact is then estimated by convolving the TSD with the measured nonlinear PSFs. Figure 3(a) and (b) shows the original and corrected PI images in a flow phantom (i.e., an artificial model of human vessels embedded in tissue). The MB signal from a small vessel [indicated by arrows in Figure 3(a) and (b)] buried within tissue artefacts prior to correction has been revealed.

Another common image artefact is due to the attenuation of the US [8], especially from the probe–skin interface and patient-specific, spatially heterogeneous attenuation, which often introduces a vertical shadow in the image [see the arrow in Figure 3(c)]. Correcting this attenuation is crucial for blood flow quantification using CEUS. In [10], an algorithm has been developed to correct attenuation artefacts with the prior knowledge that

US imaging with MBs offers exciting opportunities for revealing the structure and function of the vascular network with unprecedented sensitivity and resolution.

MBs are well mixed and homogeneous throughout the interior of a vessel. The relative attenuation profile in the vessel is estimated by low-pass filtering the image. Then the measured attenua-

tion profile is expanded to adjacent regions of interest such as vessel walls [Figure 3(c) and (d)].

Image processing and analysis

CEUS data encompasses both spatial and temporal information. MB signals in US image sequences can indeed be analyzed over space and time to derive valuable information, e.g., arterial blood flow fields, microvascular morphology, or tissue perfusion indices, in cardiovascular diseases and cancer, for instance.

Perfusion quantification

A unique feature of MBs as contrast agents is that they can be deactivated (destroyed) by using high amplitude (but still safe) US pulses. It enables a well-controlled local input function (step function) and offers the means to study local microflow dynamics through a technique referred to as *destruction reperfusion analysis* [11]. A high-amplitude US destruction pulse is transmitted to wipe out MBs within a region of tissue and subsequent low-amplitude US imaging pulses are then used to observe the replenishment of MB signals. Examples of myocardium reperfusion are shown in Figure 4(a), where the top segment of the myocardium (red line) shows much lower perfusion than the other segment (blue line), indicating a possible stenosis in the coronary artery. Such reperfusion curves [Figure 4(a)] can be fitted to a perfusion model, e.g., $I = A(1 - e^{-\beta t})$, where physiologically relevant quantities such as blood volume (A) and flow rate (β) can be extracted.

Superresolution imaging

MBs provide an opportunity to reveal extra structural information of the vasculature with far more details than what the diffraction limit of US might suggest. As

previously discussed, the nonlinear properties of the MBs facilitate their detection with very high sensitivity so that an individual MB can scatter signals far above the noise floor of the US system. Borrowing ideas from similar approaches in optical superresolution microscopy, it has been shown that by localizing the detected two-dimensional signals from individual MB, using simple spatial filtering tools, vessels $<20 \mu\text{m}$ can be delineated; see Figure 4(b). This is much smaller than the diffraction limited resolution of $\sim 100 \mu\text{m}$ in this example [12].

Bubble tracking

Temporal tracking of MBs offers new opportunities in terms of mapping blood flow and vascular morphology. Combined with the very high frame-rate US currently available (up to 20,000 frames/second), it has been used for mapping rapid arterial flow in US imaging velocimetry (UIV) [also called echo particle image velocimetry (e-PIV)] [13]; see Figure 4(c). Furthermore, tracking individual MBs in perfused tissue can help segment small vessels in the CEUS images and offers a valuable measure of vascular density.

In the reported MB tracking techniques, it is common practice to use cross-correlation. Depending on the prior knowledge of the flow, some applications require an iterative process to refine the size of the spatial window in which the cross-correlation is calculated. There is a significant amount of literature in signal processing on target tracking that could potentially benefit this area and provide more robust and real-time tracking of flow dynamics.

Final remarks

US imaging with MBs offers exciting opportunities for revealing the structure and function of the vascular network with unprecedented sensitivity and resolution. The ongoing demand for more specific detection of MBs, together with the rich data generated in both space and time by CEUS, presents significant opportunities and challenges for the development of signal processing tools and solutions. A notable recent development in US

imaging is the capability of imaging at a frame rate of up to tens of thousands frames/second [5]. While such ultrafast imaging technology offers great opportunities for the improvement of US imaging, especially for fast moving objects such as a beating heart, arterial flow, or a shear wave within the tissue (based on which the tissue elasticity can be quantified), it also raises significant challenges. Techniques to make full use of the GB of data acquired per second are required. There are opportunities to take advantage of the prior knowledge in both the underlying imaging physics and target tissue/organ physiology, and to generate in real-time clinically relevant information that are yet to be fully exploited.

In addition, the complex nonlinear signals generated by MBs provide another avenue for research, as the MB signals can be influenced by many variables related to the in vivo environment, such as blood pressure, proximity to vessel wall, gas saturation, and the mechanical properties of the surrounding tissue. A better understanding of the physics and advanced modeling and signal processing techniques could lead to extracting this clinically relevant information from the MB signals. Additionally, while most clinical US imaging is still in two dimensions, three-dimensional US imaging is arriving and will create further opportunities and challenges for data postprocessing. Finally, molecular imaging using targeted MBs is another exciting area of further development, where more advanced signal processing could help detect and evaluate pathologies at their earliest stage.

Acknowledgments

We would like to thank Dr. Adrian Lim, Prof. David Cosgrove, Prof. Roxy Senior, and Yuanwei Li for providing some of the clinical images used in this article; Dr. Alfred Yu for providing the flow phantom; and the U.K. Engineering and Physical Sciences Research Council for financial support (EP/M011933/1).

Authors

Antonio Stanzola (antonio.stanzola14@ic.ac.uk) is a Ph.D. student with the Ultrasound Laboratory for Imaging and Sensing Group, Imperial College London.

Mathieu Toulemonde (m.toulemonde@ic.ac.uk) is a postdoctoral researcher with the Ultrasound Laboratory for Imaging and Sensing Group, Imperial College London.

Yesna O. Yildiz (y.yildiz11@ic.ac.uk) is a Ph.D. student with the Ultrasound Laboratory for Imaging and Sensing group, Imperial College London.

Robert J. Eckersley (robert.eckersley@kcl.ac.uk) is a senior lecturer at King's College London.

Meng-Xing Tang (mengxing.tang@ic.ac.uk) is a reader (associate professor) of biomedical imaging and the head of the Ultrasound Laboratory for Imaging and Sensing group, Department of Bioengineering, Imperial College London.

References

- [1] J. R. Lindner, "Microbubbles in medical imaging: Current applications and future directions," *Nat. Rev. Drug Discov.*, vol. 3, no. 6, pp. 527–533, 2004.
- [2] C. Tremblay-Darveau, R. Williams, L. Milot, M. Bruce, and P. N. Burns, "Combined perfusion and Doppler imaging using plane-wave nonlinear detection and microbubble contrast agents," *IEEE Trans. Ultrason. Ferroelectr. Freq. Control*, vol. 61, no. 12, pp. 1988–2000, 2014.

- [3] T. Faez, M. Emmer, K. Kooiman, M. Versluis, A. F. W. van der Steen, and N. de Jong, "20 years of ultrasound contrast agent modeling," *IEEE Trans. Ultrason. Ferroelectr. Freq. Control*, vol. 60, no. 1, pp. 7–20, 2013.

- [4] F. Lin, C. Cachard, F. Varray, and O. Basset, "Generalization of multipulse transmission techniques for ultrasound imaging," *Ultrason. Imaging*, vol. 37, no. 4, pp. 294–311, 2015.

- [5] M. Tanter and M. Fink, "Ultrafast imaging in biomedical ultrasound," *IEEE Trans. Ultrason. Ferroelectr. Freq. Control*, vol. 61, no. 1, pp. 102–119, 2014.

- [6] J. M. G. Borsboom, C. T. Chin, A. Bouakaz, M. Versluis, and N. de Jong, "Harmonic chirp imaging method for ultrasound contrast agent," *IEEE Trans. Ultrason. Ferroelectr. Freq. Control*, vol. 52, no. 2, pp. 241–249, 2005.

- [7] S. Harput, J. McLaughlan, D. M. J. Cowell, and S. Freear, "Superharmonic imaging with chirp coded excitation: Filtering spectrally overlapped harmonics," *IEEE Trans. Ultrason. Ferroelectr. Freq. Control*, vol. 61, no. 11, pp. 1802–1814, 2014.

- [8] M.-X. Tang, H. Mulvana, T. Gauthier, A. K. P. Lim, D. O. Cosgrove, R. J. Eckersley, and E. Stride, "Quantitative contrast-enhanced ultrasound imaging: A review of sources of variability," *Interface Focus*, vol. 1, no. 4, pp. 520–539, 2011.

- [9] Y. O. Yildiz, R. J. Eckersley, R. Senior, A. K. P. Lim, D. Cosgrove, and M.-X. Tang, "Correction of non-linear propagation artifact in contrast-enhanced ultrasound imaging of carotid arteries: Methods and in vitro evaluation," *Ultrasound Med. Biol.*, vol. 41, no. 7, pp. 1938–1947, 2015.

- [10] W. K. Cheung, D. M. Gujral, B. N. Shah, N. S. Chahal, S. Bhattacharyya, D. O. Cosgrove, R. J. Eckersley, K. J. Harrington et al., "Attenuation correction and normalisation for quantification of contrast enhancement in ultrasound images of carotid arteries," *Ultrasound Med. Biol.*, vol. 41, no. 7, pp. 1876–1883, 2015.

- [11] K. Wei, A. R. Jayaweera, S. Firoozan, A. Linka, D. M. Skyba, and S. Kaul, "Quantification of myocardial blood flow with ultrasound-induced destruction of microbubbles administered as a constant venous infusion," *Circulation*, vol. 97, no. 5, pp. 473–483, 1998.

- [12] K. Christensen-Jeffries, R. J. Browning, M.-X. Tang, C. Dunsby, and R. J. Eckersley, "In vivo acoustic super-resolution and super-resolved velocity mapping using microbubbles," *IEEE Trans. Med. Imaging*, vol. 34, no. 2, pp. 433–440, 2015.

- [13] C. H. Leow, E. Bazigou, R. J. Eckersley, A. C. H. Yu, P. D. Weinberg, and M.-X. Tang, "Flow velocity mapping using contrast enhanced high-frame-rate plane wave ultrasound and image tracking: Methods and initial in vitro and in vivo evaluation," *Ultrasound Med. Biol.*, vol. 41, no. 11, pp. 2913–2925, 2015.

SP

APPLICATIONS CORNER (continued from page 110)

- [13] L. Nataraj, D. Kirat, B. S. Manjunath, and G. Vigna, "SARVAM: Search And RetrieVAL of Malware," in *Proc. Annu. Computer Security Conf. Workshop on Next Generation Malware Attacks and Defense*, Dec. 2013.

- [14] (2015, Dec.). Virustotal. [Online]. Available: <https://www.virustotal.com/>

- [15] L. Nataraj, S. Karthikeyan, and B. S. Manjunath, "SATTVA: SpArsiTy inspired classification of malware VArants," in *Proc. 3rd ACM*

Workshop on Information Hiding and Multimedia Security, June 2015, pp. 135–140.

- [16] J. Wright, A. Y. Yang, A. Ganesh, S. S. Sastry, and Y. Ma, "Robust face recognition via sparse representation," *IEEE Trans. Pattern Anal. Mach. Intell.*, vol. 31, no. 2, pp. 210–227, Apr. 2008.

- [17] D. Donoho and J. Tanner, "Counting faces of randomly projected polytopes when the projection

radically lowers dimension," *J. Amer. Math. Soc.*, vol. 22, no. 1, pp. 1–53, Jan. 2009.

- [18] J. K. Pillai, V. M. Patel, R. Chellapa, and N. K. Ratha, "Secure and robust iris recognition using random projections and sparse representations," *IEEE Trans. Pattern Anal. Mach. Intell.*, vol. 33, no. 9, pp. 1877–1893, Feb. 2011.

SP

STANDARDS IN A NUTSHELL

Alessandro Artusi, Rafał K. Mantiuk, Thomas Richter, Pavel Korshunov, Philippe Hanhart, Touradj Ebrahimi, and Massimiliano Agostinelli

JPEG XT: A Compression Standard for HDR and WCG Images

High bit depth data acquisition and manipulation have been largely studied at the academic level over the last 15 years and are rapidly attracting interest at the industrial level. An example of the increasing interest for high-dynamic range (HDR) imaging is the use of 32-bit floating point data for video and image acquisition and manipulation that allows a variety of visual effects that closely mimic the real-world visual experience of the end user [1] (see Figure 1). At the industrial level, we are witnessing increasing traction toward supporting HDR and wide color gamut (WCG). WCG leverages HDR for each color channel to display a wider range of colors. Consumer cameras are currently available with a 14- or 16-bit analog-to-digital converter. Rendering devices are also appearing with the capability to display HDR images and video with a peak brightness of up to 4,000 nits and to support WCG (ITU-R Rec. BT.2020 [2]) rather than the historical ITU-R Rec. BT.709 [3]. This trend calls for a widely accepted standard for higher bit depth support that can be seamlessly integrated into existing products and applications.

While standard formats such as the Joint Photographic Experts Group (JPEG) 2000 [5] and JPEG XR [6] offer support for high bit depth image representations, their adoption requires a non-negligible investment that may not always be affordable in existing imaging ecosystems, and induces a difficult transition, as they are not backward-compatible with the popular JPEG image format.

Digital Object Identifier 10.1109/MSP.2015.2506199
Date of publication: 7 March 2016

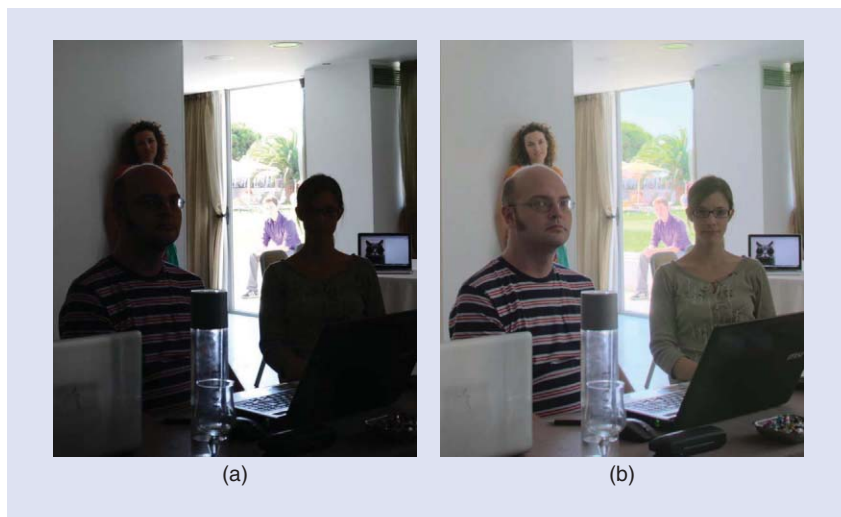


FIGURE 1. (a) A typical LDR image taken with default settings of a Nikon D7100 camera and (b) an HDR image fused from five exposures and tone mapped with drago03 [4] for display.

Instead, most digital camera and mobile phone manufacturers either store images in proprietary RAW formats or, more commonly, offer an HDR mode, which produces a traditional low-dynamic range (LDR) image with improved details. The former solution creates a vendor lock-in problem for consumers, making it difficult to efficiently use images produced by such cameras in practice due to a lack of interoperability between proprietary formats. The latter solution generates an LDR 8-bit JPEG version from the captured high bit depth image. In other words, visual information contained in the original high bit depth digital negative is irremediably lost, which is not optimal for editing, creative enhancements, or even viewing on HDR-capable display devices.

The JPEG XT standard aims to overcome all these drawbacks and lower the entry barriers to the market.

While offering new features such as lossy or lossless representation of WCG and HDR images, JPEG XT remains backward compatible with the legacy JPEG standard. As a result, legacy applications can reconstruct an 8-bit/sample LDR image from any JPEG XT code stream. This LDR version of the image and the original HDR image are related by a tone-mapping process that is not constrained by the standard and can be freely defined by the encoder.

The standards

JPEG, formally known as ISO/IEC JTC1/SC29/WG1, is universally recognized as the leading committee for compressed image formats. The JPEG committee began the standardization of JPEG XT technology in 2012. A call for proposals was issued in June 2012, at its Vienna, Austria, meeting, to which six organizations responded: Dolby, Ecole

Polytechnique Fédérale de Lausanne (EPFL), the University of Stuttgart, Trelis Management, Vrije Universiteit Brussel, and the University of Warwick. As a result, JPEG XT was initiated as a new work item and a set of requirements for its potential applications was identified. The JPEG XT image coding system is organized into nine parts that hierarchically define the baseline coding architecture, known from the legacy JPEG standard, an extensible file format specifying a common syntax for extending the legacy JPEG code stream, and application of this syntax for coding integer or floating point samples between 8- and 16-bit precision. This coding architecture is then further refined to enable lossless and near-lossless coding, and is complemented by an orthogonal extension for representing opacity data, commonly known as *alpha-channels* (see Table 1).

Technology

HDR images require more than the typical 8-bits per sample, e.g., an integer value in [0, 255] for a component of a pixel in the legacy JPEG standard, for faithful image representation. The original JPEG specifications do include a 12-bit mode and the lossless JPEG coding mode supports up to 16-bits per sample. Unfortunately, these two JPEG variants are incompatible with the popular 8-bit mode and, hence, are rarely used in practical applications, such as digital photography.

JPEG XT builds on top of the widely adopted 8-bit mode of JPEG and extends it both in a forward- and backward-compatible way. It is a superset of the 8-bit mode, i.e., JPEG XT reuses existing JPEG technology whenever possible. As a result, legacy JPEG implementations must be able to decode an LDR image from a JPEG XT stream.

Components

Generally, a standard specifies only the decoder side but, for the sake of clarity, we will briefly introduce how the HDR image is preprocessed at the encoder level to take advantage of the existing JPEG 8-bit mode. The input of the encoder is typically a pair of LDR/HDR images. Prior to encoding, the representation of the HDR image is preprocessed using a combination of four elementary operations: 1) scalar nonlinear functions that can be described either by a parameterize curve or a look-up table, 2) 3×3 matrix multiplication, 3) vector addition of three-dimensional vectors, and 4) scalar multiplication of a vector by a scalar number. These operations are applied to each pixel independently, without taking the coding history or the neighborhood of the pixel into account. Preprocessing is therefore straightforward to parallelize. This preprocessing step yields two layers, an LDR image and an extension image, that are both encoded with existing 8-bit mode of JPEG. While JPEG XT defines a unified decoder design that

arranges these components into a workflow, a typical decoder or encoder would not implement all of these components. In real life, a codec is likely to only implement a subset of these operations. As will be detailed later, JPEG XT defines profiles that specify a subset of the full configuration space and, hence, simplify the design of codecs.

As in JPEG, the preprocessed input is then decorrelated with a discrete cosine transform (DCT), quantized, and entropy coded. Since the bit-precision of the legacy 8-bit mode is limited, JPEG XT defines two alternate mechanisms to improve it: refinement coding and residual coding.

Refinement coding extends the coding precision in the DCT domain thanks to a coding mechanism that is closely related to the progressive coding mode of the legacy JPEG standard. It extends the coding precision to 12 bits in the spatial domain. The most significant bits of the quantized DCT coefficients are encoded by a regular JPEG coding mode, forming the code stream that legacy applications can interpret. On the other hand, the least significant bits are encoded with the so-called successive approximation scan, which is part of the progressive coding mode also defined in the legacy JPEG standard. However, the encoded coefficients are not included in the regular code stream. They become part of a side-channel (an extension layer) that is hidden from legacy applications. The transport of this side channel is

Table 1. The description of the JPEG XT standard.

	Title	Description
Part 1	Core Coding System Specification	Definition of the core coding technology, which is the legacy JPEG specifications. Other parts of JPEG XT builds on top of this baseline coding system in a backward-compatible way [7].
Part 2	Extensions for HDR Images	It supplies a legacy syntax for a subset of the tools specified in part 7 [7].
Part 3	Box File Format	Definition of an extensible and flexible container format, called <i>boxes</i> , extending legacy JPEG and the ISO-based media format [7].
Part 4	Conformance Testing and Evaluation	Definition of the methodology to verify that the various parts of the standard are meeting the normative requirements [7].
Part 5	Reference Software Implementation	Reference software for parts 6–9 making use of the file box format specified in part 3 [7].
Part 6	Intermediate Dynamic Range (IDR) Integer Coding	Definition of a scalable coding engine supporting all bit depths between 9 and 16 bits per sample that remains compatible with legacy applications [7].
Part 7	HDR Floating-Point Coding	Definition of a coding engine for images in an HDR representation, e.g., using floating point samples [7].
Part 8	Lossless and Near-Lossless Coding	Definition of a lossless and near-lossless coding engine for IDR and HDR image representations using coding technologies from parts 6 and 7 [7].
Part 9	Encoding of Alpha Channels	Extension of the other parts of the ISO/IEC 18477 standard to support opacity information for LDR, IDR, and HDR images [7].

discussed below in more detail. Refinement coding cannot represent an arbitrary LDR/HDR image pair on its own. The LDR image is indeed implicitly defined by the most significant bits of the HDR stream, making refinement coding alone only suitable for simple applications. The capability to encode an HDR image with an independently defined LDR layer is granted by residual coding that operates entirely in the spatial domain. Using the four elementary operations available at preprocessing, it computes from the LDR/HDR image pair an LDR layer that represents the base code stream that is visible to legacy applications, and an extension layer for the remaining information required to reconstruct the HDR image. The extension layer is also coded by a second regular JPEG mode, and the resulting extension code stream, similarly to the refinement code stream, becomes part of a side channel that is hidden for legacy applications. Both mechanisms, residual and refinement coding, can be combined. For example, the bit-precision of the extension layer from residual coding could be increased by using refinement scans.

Profiles

While preprocessing offers a variety of methods to generate an extension layer

from a given LDR/HDR image pair, we restrict, for the sake of simplicity, the discussion to the three profiles currently defined in the JPEG XT standard, whose decoding workflow is depicted in Figure 2.

Two layers, \mathcal{B} and \mathcal{E} , are used for the reconstruction of the HDR image \mathcal{I} . \mathcal{B} is the base layer, which represent the LDR image as a JPEG image with 8-bits per sample in the ITU BT.601 RGB colorspace. \mathcal{E} is the extension layer, which includes the additional information to reconstruct the HDR image \mathcal{I} starting from the base layer \mathcal{B} . The coding tools of the overall JPEG XT infrastructure used to merge \mathcal{B} and \mathcal{E} together are then profile dependent.

Profile A reconstructs the HDR image \mathcal{I} by multiplying a luminance scale μ with the base image \mathcal{B} after inverse gamma correction using the first base nonlinearity Φ_A

$$\mathcal{I}(x, y) = \mu(\mathcal{E}_0(x, y)) \cdot [C\Phi_A(\mathcal{B}(x, y)) + \nu(SC\Phi_A(\mathcal{B}(x, y))) \cdot R\mathcal{E}^\perp(x, y)], \quad (1)$$

where C and R are 3×3 matrices implementing color transformations, $\mu(\cdot)$ is a scalar function of the luma component of the extension layer \mathcal{E} ,

(postscaling nonlinearity block), and \mathcal{E}^\perp the extension layer projected onto the chroma-subspace, i.e., \mathcal{E} with its luma component set to zero. The matrix C transforms from ITU-R BT.601 to the target colorspace in the extension layer. R is an inverse color decorrelation transformation from YCbCr to RGB in the extension layer to clearly separate the luminance component from the chromaticities (YCbCr) at the encoding level. These matrices are also commonly used in the other two profiles. S is a row-vector transforming color into luminance, and ν is a scalar function taking in input luminance values. Typically, $\nu(x) = x + \epsilon$ where ϵ is a “noise floor” that avoids instability in the encoder for very dark image regions.

Profile B reconstructs the HDR image \mathcal{I} by computing the quotient that can be expressed as a difference in the logarithmic scale:

$$\begin{aligned} \mathcal{I}(x, y)_i &= \sigma \exp(\log([C\Phi_B(\mathcal{B}(x, y))]_i) \\ &\quad - \log(\Psi_B([R\mathcal{E}(x, y)]_i) + \epsilon)) \\ &= \sigma \frac{[C\Phi_B(\mathcal{B}(x, y))]_i}{\Psi_B([R\mathcal{E}(x, y)]_i) + \epsilon} \end{aligned} \quad (2)$$

$(i = 0, 1, 2),$

where i is the index of the RGB color channels. Φ_B and Ψ_B are two inverse

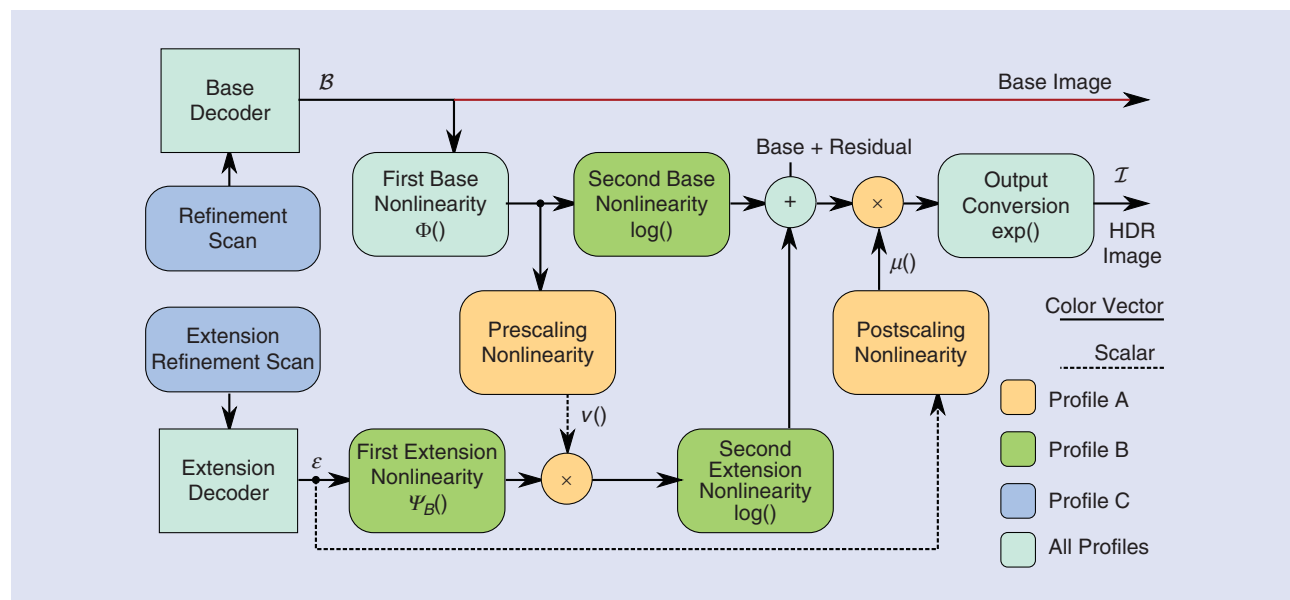


FIGURE 2. A simplified version of the JPEG XT decoder. \mathcal{B} is the base layer and is always represented as a JPEG code stream with 8-bit per sample. \mathcal{E} is the extension layer that used in conjunction with \mathcal{B} allows the reconstruction of the HDR image.

gamma applied to the base and extension layers respectively. Φ_B has the objective to linearize the base layer, while Ψ_B intends to better distribute values closer to zero in the extension layer. The scalar σ is an exposure parameter that scales the luminance of the output image to optimize the split between base and extension layers.

Profile C also employs a sum to merge base and extension images, but here Φ_C not only approximates an inverse gamma transformation, but implements a global inverse tone-mapping procedure that approximates the (possibly local) tone-mapping operator (TMO) that was used to create the LDR image. The extension layer is encoded in the logarithmic domain directly, avoiding an additional transformation. Finally, log and exp are substituted by piecewise linear approximations that are implicitly defined by reinterpreting the bit-pattern of the half-logarithmic IEEE representation of floating-point numbers as integers. It is then easily seen that this simple “casting” between number formats implements two functions $\psi \log$ and $\psi \exp$ that behave approximately like their precise mathematical counterparts, though they provide the additional advantage of being exactly invertible. The reconstruction algorithm for profile C can then be written:

$$I(x, y) = \psi \exp(\hat{\Phi}_C(CB(x, y) + RE(x, y) - 2^{15}(1, 1, 1)^T), (3)$$

where $\hat{\Phi}_C(x) = \psi \log(\Phi_C(x))$, in which Φ_C is the global inverse tone-mapping approximation. 2^{15} is an offset shift to make the extension image symmetric around zero. The code stream never specifies Φ_C directly, but rather includes a representation of $\hat{\Phi}_C$ in the form of a lookup-table, allowing to skip the time-consuming computation of the logarithm.

Lossless coding

An important feature of profile C is that it allows implementations operating entirely with integers until the very last step, where the exponential generates floating-point output. All of these operations, including the exponential mapping, are

exactly invertible. Part 8 of JPEG XT defines now on this basis a lossless coding engine by fully specifying the DCT in the base layer, and by bypassing the DCT entirely in the extension layer. The reader may now verify that the entire operation chain has, indeed, an exact inverse as the coding residual the decoder requires for a given DCT and a given base image is exactly predictable by the encoder, and, hence, can be computed ahead to generate exactly the required sample values.

Transport

Residual coding and refinement coding create additional code streams that need to be incorporated into the legacy JPEG syntax such that current decoders are able to see only the legacy LDR image and skip over the extension layers. A JPEG XT code stream may thus contain up to three side channels for image information: 1) a refinement code stream, 2) a residual code stream, and 3) a residual-refinement code stream. Accounting for the potential presence of an opacity layer, as defined in Part 9 of the standard, up to four additional code streams may be further included: 1) an alpha channel, 2) a residual alpha channel, 3) an alpha channel refinement, and 4) a residual alpha channel refinement. This information is added to the metadata that configures the postprocessing chain of the decoder.

The legacy JPEG syntax already includes a generic extension mechanism by using so-called application-specific (APP) markers JPEG XT reserves one of them. However, APP markers do not carry the data directly. Instead, their payload consists of so-called boxes that yield a better and cleaner structure of its contents. Boxes are not new to JPEG XT; they were previously introduced by the Moving Picture Experts Group (MPEG) and JPEG 2000. The payload data of a box is prefixed by a type and a size such that decoders unaware of a specific box type may simply ignore it. In summary, the JPEG XT file format is a JPEG code stream with APP markers whose contents, when reassembled at the decoder, make up a single box, or a superbox containing multiple other boxes (Figure 3). This is necessary because the capacity of

a single APP marker is limited to 64 Kbytes, whereas a box may be larger and span across several APP markers. Instructions describing how to assemble markers into boxes is included in the first bytes of the marker data itself. Legacy decoders will simply skip over the markers, and will also ignore all boxes and their data.

The payload data of the boxes includes the metadata defining the post-processor in the decoder or the entropy-coded data of refinement and residual code streams. The decoder picks out the data it requires for its operation based on the type signaled in the header of the box.

Testing and performances

The challenge of testing backward-compatible HDR compression is that the compression performance does not depend only on a single quality control parameter, but also on the quality settings for the base layer and on the choice of the TMO, which produces this layer. Therefore, the performance of JPEG XT needs to be evaluated using a comprehensive set of varying parameters and on a data set that covers a large set of standard's use cases.

The JPEG committee has carried out a large number of experiments, using both subjective and objective methodologies, to assess the capability of the JPEG XT. A set of 12 objective quality metrics were tested on 106 HDR images (resolutions range from full HD to 4K) covering a high range of scenes typically captured in HDR images, including indoor, outdoor scenes, architecture, landscapes, portraits, frames from HDR video, and computer-generated images. All images were carefully selected by experts in HDR imaging from these publicly available data sets: Fairchild's HDR Photographic Survey [8] and EPFL's data set of HDR images [9].

Since a TMO can be freely selected for encoding and its selection is not part of JPEG XT specifications, we tested five different commonly used operators: 1) a simple gamma-based operator gamma, 2) a global logarithmic TMO [4] *drago03*, 3) a global version of the photographic operator [10] *reihard02*, 4) an operator optimized for encoding [11]

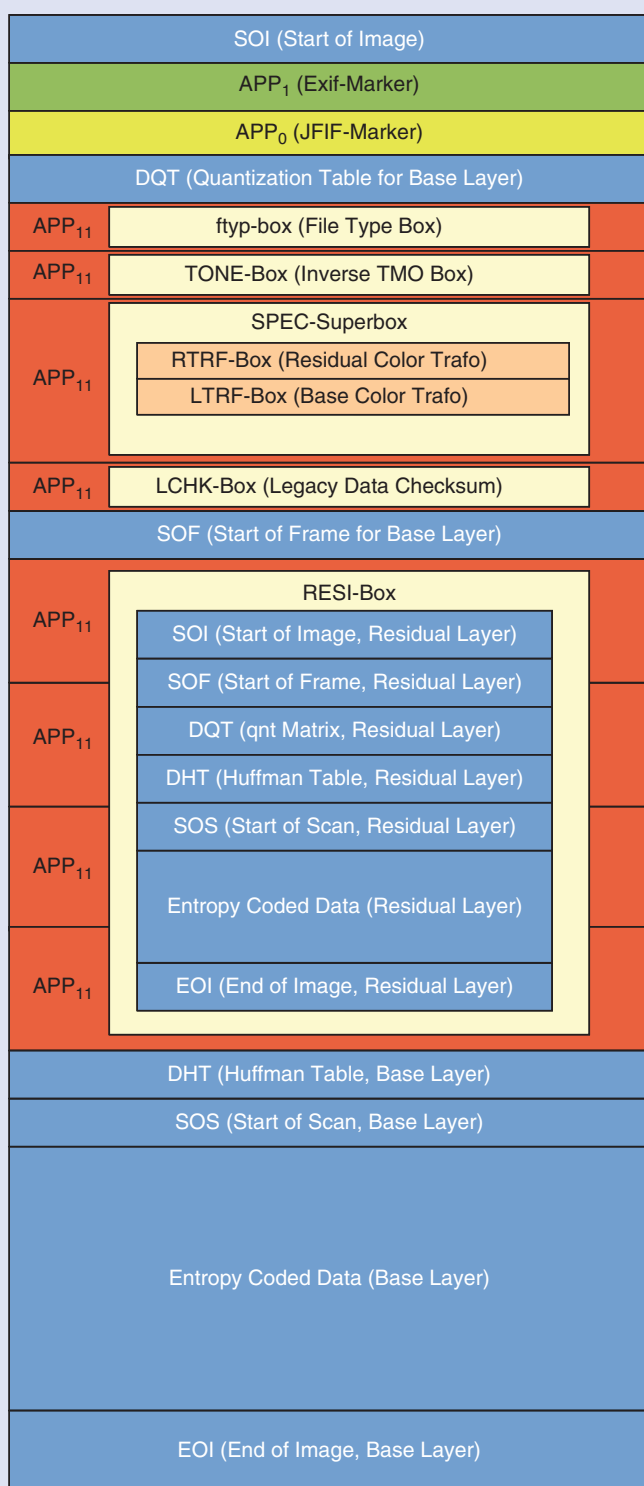


FIGURE 3. The JPEG XT file format: APP markers contain the boxes structure. Blue syntax elements were defined in the legacy JPEG standard, yellow elements were defined in later parts. The green Exif marker is defined outside of JPEG. The red APP₁₁ markers are not part of the legacy JPEG standard and will thus be ignored by legacy JPEG readers. In contrast, JPEG XT readers will be able to interpret the payload data in the boxes that contain relevant JPEG XT information. Since the size of an APP marker is limited to 64 kB, a single box may extend over several markers; the RESI box carrying the residual code stream is a typical example. Otherwise, an APP marker or a series of APP markers contains a single box. This box may be, however, a superbox whose payload again consists of boxes. The SPEC box defining the instructions how to reassemble the HDR image from base and extension image is a typical example.

mail, and 5) a local operator with strong contrast enhancement [12] *man-tiuk06*. To fully understand the implications of the TMOs and JPEG XT parameters, all possible combinations of these parameters were tested. We used the combination of ten base quality levels \times ten extension layer quality levels \times five TMOs \times three profiles, which results in a total of 1,500 conditions for each of the 106 images resulting in 159,000 tests. However, such a large number of conditions clearly cannot be tested in a subjective experiment. Therefore, from the total 106 HDR images, a subset of 20 images was selected by experts for subjective evaluations and these images were adjusted for viewing on an SIM2 HDR monitor; see [13] for more details on the subjective evaluations.

The results of subjective experiments are crucial to select the right image quality metric and to provide ground truth reference. However, a subjective experiment alone cannot cover the entire space of parameters. Due to the tedious nature of those experiments, only a limited number of images can be tested, which makes the findings of such studies difficult to generalize. For that reason, we analyzed compression performances with respect to HDR-VDP-2 [14], the best-performing objective quality metric according to a set of evaluations. The image quality computed for a range of base and extension layer quality settings may result in arbitrary bit rates, making the results difficult to aggregate. Therefore, the predicted quality values were linearly interpolated to find the HDR-VDP-2 Q-scores for each desired bit rate. This step was necessary to determine average performance and confidence intervals for all tested profiles.

In Figure 4, we compare the performance of the three profiles with popular HDR image formats, including lossless OpenEXR, Radiance RGBE, lossy JPEG 2000, and JPEG-XR (floating encoding). OpenEXR and Radiance offer lossless compression, however the loss happens when converting images to their internal pixel formats: 8-bit RGB channels and shared 8-bit mantissa (E) for Radiance RGBE; and 16-bit half-float (sign, 5-bit exponent, 10-bit mantissa) for

OpenEXR. Note that our reference images were stored in 32-bit per-color channel, uncompressed PFM files. JPEG 2000 employs a lossy wavelet-based compression while JPEG-XR uses a two-stage frequency transform, combining the features of both DCT and wavelet transforms. We can notice differences in quality performances between profiles, i.e., C versus A and B; however, these differences are above the predicted mean-opinion-score (MOS) value of 4.6 and are unlikely to be noticeable [15].

HDR-VDP-2 did not detect any degradation in quality for all OpenEXR compression formats (HDRVDP_Q 100 is the highest quality), while small losses in quality were detected for Radiance RGBE. All of those lossless formats preserve very high quality but require at least 27 bits/pixel. JPEG XT performs unexpectedly well when compared with other lossy compression methods. Below 10 bits/pixel, JPEG XT performs better than JPEG XR. Below 6 bits/pixel, the performance of JPEG XT is comparable to JPEG 2000, even though the former encodes an additional tone-mapped image and employs a standard DCT-based JPEG codec, rather than a more advanced compression algorithms found in both JPEG 2000 and JPEG XR, which are newer.

The additional precision of these formats may be needed, however, if the content has to be edited, tone mapped, or further processed. Only profile C offers encoding at precisions matching those offered by OpenEXR format. The bit rate of profile C for the same quality is slightly higher. However, profile C encodes additionally a backward-compatible base layer, which is missing in OpenEXR images.

Conclusions

The lack of an HDR image coding standard has caused the HDR imaging community to rely on specific vendor formats that are unsuitable for the exchange and storage of such images. This has clearly hampered the development of the HDR imaging technology so far. The new upcoming standard—JPEG XT, which is backward-compatible to the popular 8-bit mode of ISO/IEC 10918/ ITU Rec. T.81 (also known as JPEG)—is the response to this situation. In this column, we have

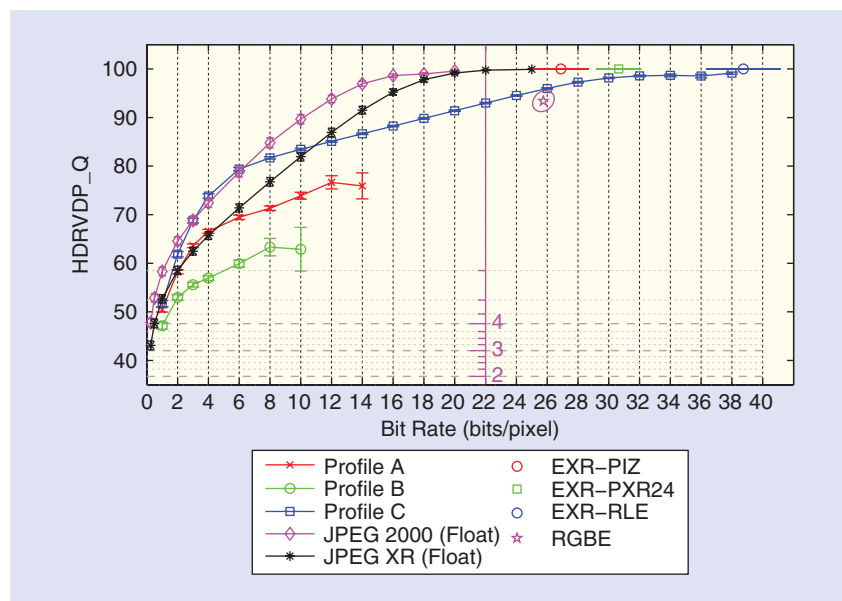


FIGURE 4. The mean compression performance of each profile compared with popular near-lossless HDR image formats: OpenEXR using its three compression algorithms, and Radiance RGBE (.hdr). The base layer quality was fixed at 80. The ellipses denote 95% confidence interval. The magenta scale in the middle of the plot shows MOS values corresponding to HDRVDP_Q predictions.

presented the design philosophy and the technical details of JPEG XT, followed by an extensive evaluation of its performances. Objective evaluation demonstrates the robustness of the upcoming standard to the influence of its parameters: the quality for the base and extension layers and the tone mapping used for the base layer. The comparison to near-lossless and lossless existing formats has shown that the upcoming standard is capable to encode HDR imaging with high MOS of 4.5 already with a bit-rates varying from 1.1 to 1.5 bit/pixels, providing 23 times size reduction.

Interestingly, some of the tools developed for JPEG XT to compress HDR images may also prove useful in other application use cases. In the future, JPEG will explore how to leverage on these new mechanisms in other contexts. For instance, the layered structure of JPEG XT is very appealing to provide images with privacy features. Sensitive parts could be obfuscated, e.g., blurred or pixelated, in the base layer accessible to everyone, whereas the extension material would contain these parts to which only individuals with necessary credentials could have access. Alternately, the layered structure of JPEG XT could also provide a means to record the editing his-

tory of a particular image file. The base layer would contain the latest version of the image, whereas the extension layers would enable the ability to travel back in time and get access to earlier versions of the image. Finally, the box structure of JPEG XT makes it a natural candidate to become part of JPEG 2000 Interactive Protocol, known as *JPIP*, an interactive image browsing protocol similar in essence to the proprietary Google Maps.

Acknowledgments

This work was partially supported by Ministry of Science and Innovation Subprogramme Ramon y Cajal RYC-2011-09372, TIN2013-47276-C6-1-R from the Spanish government, and 2014 SGR 1232 from the Catalan government. The EPFL authors acknowledge the Swiss National Foundation for Scientific Research (FN 200021-143696-1) which supported them in carrying out the work presented in this article. The objective quality evaluation was possible thanks to High-Performance Computing Wales, Wales National Supercomputing Service (hpcwales.co.uk).

Authors

Alessandro Artusi (artusialessandro4@gmail.com) is a Ramon y Cajal fellow at the University of Girona, Spain. He is a

member of the ISO/IEC/JCTC1/SC29/WG1 Committee (also known as JPEG), coeditor of the JPEG XT standard, and recipient of the Emerging Standards Awards from the British Standard Institute. He has contributed to more than 40 papers, books, courses, and patents on the high-dynamic range imaging field.

Rafał K. Mantiuk (rkm38@cam.ac.uk) is a senior lecturer at the Computer Laboratory, University of Cambridge, United Kingdom. He is the author of a popular HDR image quality metric, HDR-VDP-2; the coauthor of pfstools, software for high-dynamic range image processing; and the coauthor of more than 40 papers and book chapters on tone mapping, high dynamic range-quality assessment, and video compression.

Thomas Richter (richter@tik.uni-stuttgart.de) is a researcher at the Computing Center of the University of Stuttgart, Germany. He is one of the editors of the JPEG XT standard and the chair of the test and quality group of JPEG.

Pavel Korshunov (pavel.korshunov@epfl.ch) is a postdoctoral researcher at the Multimedia Signal Processing group at Ecole Polytechnique Fédérale de Lausanne. He has more than 50 research publications and is a coeditor of the JPEG XT standard.

Philippe Hanhart (philippe.hanhart@epfl.ch) is a Ph.D. student working on quality of experience in immersive video technologies at Ecole Polytechnique Fédérale de Lausanne. He is involved in MPEG and JPEG to evaluate new high-dynamic range coding formats.

Touradj Ebrahimi (Touradj.Ebrahimi@epfl.ch) is a professor at Ecole Polytechnique Fédérale de Lausanne heading its Multimedia Signal Processing group. He is also the convener (chair) of the JPEG Standardization Committee.

Massimiliano Agostinelli (max@xdepth.com) is the chief technical officer at XDepth. He is member of the ISO/IEC/JCTC1/SC29/WG1 Committee

(also known as JPEG) and a coeditor of the JPEG XT standard.

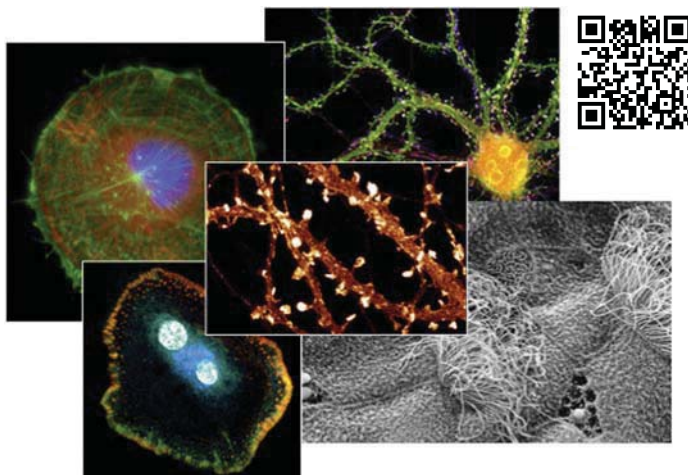
References

- [1] F. Banterle, A. Artusi, K. Debattista, and A. Chalmers, *Advanced High Dynamic Range Imaging: Theory and Practice*. Boca Raton, FL: CRC Press, (AK Peters Ltd.), 2011.
- [2] "ITU-R Recommendation BT.2020: Parameter Values for Ultra-high Definition Television Systems for Production and International Program Exchange," International Telecommunications Union, 2012.
- [3] "ITU-R Recommendation BT.709-5: Parameter Values for the HDTV Standards for Production and for International Programme Exchange," International Telecommunication Union, Geneva, Switzerland, 2002.
- [4] F. Drago, K. Myszkowski, T. Annen, and N. Chiba, "Adaptive logarithmic mapping for displaying high contrast scenes." *Comput. Graph. Forum*, vol. 22, no. 3, pp. 419–426, Sept. 2003.
- [5] ITU, "Recommendation ITU-T Rec. T.800, Information Technology: JPEG 2000 Image Coding System: Core Coding System," International Telecommunications Union, 2002.
- [6] "Recommendation ITU-T Rec. T.832 ISO/IEC 29199-2, Information Technology: JPEG XR Image Coding System Image Coding Specification," International Telecommunications Union, 2012.
- [7] T. Richter, W. Husak, N. Ajit, T. Arkady, P. Korshunov, T. Ebrahimi, A. Artusi, M. Agostinelli et al. (2016). JPEG XT information technology: Scalable compression and coding of continuous-tone still images. [Online]. Available: <http://jpeg.org/jpegxt/index.html>
- [8] M. Fairchild. (2008). Fairchild's HDR photographic survey. [Online]. Available: <http://rit-mcs1.org/fairchild/HDR.html>
- [9] H. Nemoto, P. Korshunov, P. Hanhart, and T. Ebrahimi. (2015). EPFL's dataset of HDR images. [Online]. Available: <http://mmspg.epfl.ch/hdr-eye>
- [10] E. Reinhard, M. Stark, P. Shirley, and J. Ferwerda, "Photographic tone reproduction for digital images," *ACM Trans. Graph.*, vol. 21, no. 3, p. 267, July 2002.
- [11] Z. Mai, H. Mansour, R. Mantiuk, P. Nasiopoulos, R. Ward, and W. Heidrich, "Optimizing a tone curve for backward-compatible high dynamic range image and video compression," *IEEE Trans. Image Processing*, vol. 20, no. 6, pp. 1558–1571, 2011.
- [12] R. Mantiuk, K. Myszkowski, and H. Seidel, "A perceptual framework for contrast processing of high dynamic range images," *ACM Trans. Appl. Percept.*, vol. 3, no. 3, pp. 286–308, 2006.
- [13] P. Korshunov, P. Hanhart, T. Richter, A. Artusi, R. Mantiuk, and T. Ebrahimi, "Subjective quality assessment database of HDR images compressed with JPEG XT," in *Proc. 7th Int. Workshop on Quality of Multimedia Experience (QoMEX)*, 2015, pp. 1–6. [Online]. Available: <http://dx.doi.org/10.1109/QoMEX.2015.7148119>
- [14] M. Narwaria, R. K. Mantiuk, M. P. Da Silva, and P. Le Callet, "HDR-VDP-2.2: A calibrated method for objective quality prediction of high dynamic range and standard images," *J. Electron. Imaging*, vol. 24, no. 1, 2015. [Online]. Available: <http://dx.doi.org/10.1117/1.JEI.24.1.010501>
- [15] A. Artusi, R. Mantiuk, T. Richter, P. Hanhart, P. Korshunov, M. Agostinelli, A. Ten, and T. Ebrahimi, "Overview and evaluation of the JPEG XT HDR image compression standard," *Real-Time Image Processing J.*, pp. 1–16, Dec. 2015.

IEEE Journal of Selected Topics in Signal Processing (JSTSP): Recent Special Issues

- ❖ **March 2016** – Stochastic Simulation and Optimization in Signal Processing
- ❖ **February 2016** – Advanced Signal Processing in Microscopy and Cell Imaging

Scan the QR code to visit IEEE Xplore for more information



Digital Object Identifier 10.1109/MSP.2016.2534198





IEEE TRANSACTIONS ON SIGNAL AND INFORMATION PROCESSING OVER NETWORKS



Now accepting paper submissions

The new *IEEE Transactions on Signal and Information Processing over Networks* publishes high-quality papers that extend the classical notions of processing of signals defined over vector spaces (e.g. time and space) to processing of signals and information (data) defined over networks, potentially dynamically varying. In signal processing over networks, the topology of the network may define structural relationships in the data, or may constrain processing of the data. Topics of interest include, but are not limited to the following:

Adaptation, Detection, Estimation, and Learning

- Distributed detection and estimation
- Distributed adaptation over networks
- Distributed learning over networks
- Distributed target tracking
- Bayesian learning; Bayesian signal processing
- Sequential learning over networks
- Decision making over networks
- Distributed dictionary learning
- Distributed game theoretic strategies
- Distributed information processing
- Graphical and kernel methods
- Consensus over network systems
- Optimization over network systems

Communications, Networking, and Sensing

- Distributed monitoring and sensing
- Signal processing for distributed communications and networking
- Signal processing for cooperative networking
- Signal processing for network security
- Optimal network signal processing and resource allocation

Modeling and Analysis

- Performance and bounds of methods
- Robustness and vulnerability
- Network modeling and identification

Modeling and Analysis (cont.)

- Simulations of networked information processing systems
- Social learning
- Bio-inspired network signal processing
- Epidemics and diffusion in populations

Imaging and Media Applications

- Image and video processing over networks
- Media cloud computing and communication
- Multimedia streaming and transport
- Social media computing and networking
- Signal processing for cyber-physical systems
- Wireless/mobile multimedia

Data Analysis

- Processing, analysis, and visualization of big data
- Signal and information processing for crowd computing
- Signal and information processing for the Internet of Things
- Emergence of behavior

Emerging topics and applications

- Emerging topics
- Applications in life sciences, ecology, energy, social networks, economic networks, finance, social sciences, smart grids, wireless health, robotics, transportation, and other areas of science and engineering

Editor-in-Chief: Petar M. Djurić, Stony Brook University (USA)

To submit a paper, go to: <https://mc.manuscriptcentral.com/tsipn-ieee>



ADVERTISING & SALES



© GRAPHIC STOCK

The Advertisers Index contained in this issue is compiled as a service to our readers and advertisers: the publisher is not liable for errors or omissions although every effort is made to ensure its accuracy. Be sure to let our advertisers know you found them through IEEE Signal Processing Magazine.

CVR 4

Mathworks
www.mathworks.com/ltc
+1 508 647 7040

James A. Vick

Sr. Director, Advertising
Phone: +1 212 419 7767;
Fax: +1 212 419 7589
jv.ieeemedia@ieee.org

Marion Delaney

Advertising Sales Director
Phone: +1 415 863 4717;
Fax: +1 415 863 4717
md.ieeemedia@ieee.org

Mark David

Sr. Manager Advertising & Business Development
Phone: +1 732 465 6473
Fax: +1 732 981 1855
m.david@ieee.org

Mindy Belfer

Advertising Sales Coordinator
Phone: +1 732 562 3937
Fax: +1 732 981 1855
m.belfer@ieee.org

PRODUCT ADVERTISING**MIDATLANTIC**

Lisa Rinaldo
Phone: +1 732 772 0160;
Fax: +1 732 772 0164
lr.ieeemedia@ieee.org
NY, NJ, PA, DE, MD, DC, KY, WV

**NEW ENGLAND/
SOUTH CENTRAL/
EASTERN CANADA**

Jody Estabrook
Phone: +1 774 283 4528;
Fax: +1 774 283 4527
je.ieeemedia@ieee.org
ME, VT, NH, MA, RI, CT, AR, LA, OK, TX
Canada: Quebec, Nova Scotia, Newfoundland, Prince Edward Island, New Brunswick

SOUTHEAST

Cathy Flynn
Phone: +1 770 645 2944;
Fax: +1 770 993 4423
cf.ieeemedia@ieee.org
VA, NC, SC, GA, FL, AL, MS, TN

**MIDWEST/
CENTRAL CANADA**

Dave Jones
Phone: +1 708 442 5633;
Fax: +1 708 442 7620
dj.ieeemedia@ieee.org
IL, IA, KS, MN, MO, NE, ND, SD, WI, OH
Canada: Manitoba, Saskatchewan, Alberta

**MIDWEST/
ONTARIO, CANADA**

Will Hamilton
Phone: +1 269 381 2156;
Fax: +1 269 381 2556
wh.ieeemedia@ieee.org
IN, MI, Canada: Ontario

**WEST COAST/
MOUNTAIN STATES/
WESTERN CANADA**

Marshall Rubin
Phone: +1 818 888 2407;
Fax: +1 818 888 4907
mr.ieeemedia@ieee.org
AZ, CO, HI, NM, NV, UT, AK, ID, MT, WY, OR, WA, CA. Canada: British Columbia

**EUROPE/AFRICA/
MIDDLE EAST**

**ASIA/FAR EAST/
PACIFIC RIM**
Louise Smith
Phone: +44 1875 825 700;
Fax: +44 1875 825 701
les.ieeemedia@ieee.org
Europe, Africa, Middle East
Asia, Far East, Pacific Rim, Australia, New Zealand

**RECRUITMENT
ADVERTISING****MIDATLANTIC**

Lisa Rinaldo
Phone: +1 732 772 0160;
Fax: +1 732 772 0164
lr.ieeemedia@ieee.org
NY, NJ, CT, PA, DE, MD, DC, KY, WV

**NEW ENGLAND/
EASTERN CANADA**

Liza Reich
Phone: +1 212 419 7578;
Fax: +1 212 419 7589
e.reich@ieee.org
ME, VT, NH, MA, RI, Canada: Quebec, Nova Scotia, Prince Edward Island, Newfoundland, New Brunswick

SOUTHEAST

Cathy Flynn
Phone: +1 770 645 2944;
Fax: +1 770 993 4423
cf.ieeemedia@ieee.org
VA, NC, SC, GA, FL, AL, MS, TN

**MIDWEST/
SOUTH CENTRAL/
CENTRAL CANADA**

Darcy Giovino
Phone: +224 616 3034;
Fax: +1 847 729 4269
dg.ieeemedia@ieee.org
AR, IL, IN, IA, KS, LA, MI, MN, MO, NE, ND, SD, OH, OK, TX, WI. Canada: Ontario, Manitoba, Saskatchewan, Alberta

**WEST COAST/
SOUTHWEST/
MOUNTAIN STATES/ASIA**

Tim Matteson
Phone: +1 310 836 4064;
Fax: +1 310 836 4067
tm.ieeemedia@ieee.org
AZ, CO, HI, NV, NM, UT, CA, AK, ID, MT, WY, OR, WA. Canada: British Columbia

**EUROPE/AFRICA/
MIDDLE EAST**

Louise Smith
Phone: +44 1875 825 700;
Fax: +44 1875 825 701
les.ieeemedia@ieee.org
Europe, Africa, Middle East

SP

Digital Object Identifier 10.1109/MSP.2016.2529378

NEW!

IEEE TRANSACTIONS ON COMPUTATIONAL IMAGING

**Editor-in-Chief**

W. Clem Karl
Boston University

Technical Committee

Charles Bouman
Eric Miller
Peter Corcoran
Jong Chul Ye
Dave Brady
William Freeman

The IEEE Transactions on Computational Imaging publishes research results where computation plays an integral role in the image formation process. All areas of computational imaging are appropriate, ranging from the principles and theory of computational imaging, to modeling paradigms for computational imaging, to image formation methods, to the latest innovative computational imaging system designs. Topics of interest include, but are not limited to the following:

Computational Imaging Methods and Model

- Coded imaging sensing
- Compressed sensing
- Sparse and low-rank models
- Learning-based models, dictionary methods
- Graphical image models
- Perceptual models

Computational Image Formation

- Sparsity-based reconstruction
- Statistically-based inversion methods
- Multi-image and sensor fusion
- Optimization-based methods; proximal iterative methods, ADMM

Computational Photography

- Non-classical image capture
- Generalized illumination
- Time-of-flight imaging
- High dynamic range imaging
- Plenoptic imaging

Computational Consumer Model

- Mobile imaging, cell phone imaging
- Camera-array systems
- Depth cameras, multi-focus imaging
- Pervasive imaging, camera networks

Computational Acoustic Imaging

- Multi-static ultrasound imaging
- Photo-acoustic imaging
- Acoustic tomography

Computational Microscopy

- Holographic microscopy
- Quantitative phase imaging
- Multi-illumination microscopy
- Lensless microscopy
- Light field microscopy

Imaging Hardware and Software

- Embedded Computing Systems
- Big data computational imaging
- Integrated hardware/digital design

Tomographic Imaging

- X-ray CT
- PET
- SPECT

Magnetic Resonance Imaging

- Diffusion tensor imaging
- Fast acquisition

Radar Imaging

- Synthetic aperture imaging
- Inverse synthetic imaging
- Terahertz imaging

Geophysical Imaging

- Multi-spectral imaging
- Ground penetrating radar
- Seismic tomography

Multi-spectral Imaging

- Multi-spectral imaging
- Hyper-spectral imaging
- Spectroscopic imaging

For more information on the IEEE Transactions on Computational Imaging see
<http://www.signalprocessing.org/publications/periodicals/tci/>

**No Page
Charges in
2016 and Fast
Turn Around!**



Digital Object Identifier 10.1109/MSP.2016.2534498



DATES AHEAD

Please send calendar submissions to:
Dates Ahead, Attn: Jessica Barragué
E-mail: j.barrague@ieee.org

2016

MARCH

41st IEEE International Conference on Acoustics, Speech, and Signal Processing (ICASSP)

21–25 March, Shanghai, China.
General Chairs: Zhi Ding, Zhi-Quan Luo, and Wenjun Zhang
URL: <http://icassp2016.org>

Data Compression Conference (DCC)

29 March–1 April, Snowbird, Utah, USA.
URL: <http://www.cs.brandeis.edu/~dcc/>

APRIL

15th ACM/IEEE International Conference on Information Processing in Sensor Networks (IPSN)

11–14 April, Vienna, Austria.
General Chair: Guoliang Xing
URL: <http://ipsn.acm.org/2016/>

IEEE International Symposium on Biomedical Imaging (ISBI)

13–16 April, Prague, Czech Republic.
General Chairs: Jan Kybic and Milan Sonka
URL: <http://biomedicalimaging.org/2016/>

IEEE SPS Forum on Signal and Data Science (SIDAS)

24–26 April, Wuhan, China.
General Chairs: Shiguang Shan, Zixiang Xiong, and Jingdong Chen
URL: <http://mclab.eic.hust.edu.cn/sidas2016/>

JUNE

IEEE Workshop on Statistical Signal Processing (SSP)

26–29 June, Palma de Mallorca, Spain.
General Chairs: Antonio Artés-Rodríguez and Joaquín Míguez
URL: <http://ssp2016.tsc.uc3m.es/>

Digital Object Identifier 10.1109/MSP.2015.2510291
Date of publication: 7 March 2016



Shanghai International Convention Center
ICASSP 2016

JULY

IEEE Ninth IEEE Sensor Array and Multichannel Signal Processing Workshop (SAM)

10–13 July, Rio de Janeiro, Brazil.
General Chairs: Rodrigo C. de Lamare and Martin Haardt
URL: <http://delamare.cetuc.puc-rio.br/sam2016/index.html>

IEEE 12th Image, Video, and Multidimensional Signal Processing Workshop (IVMSP)

11–12 July, Bordeaux, France.
General Chairs: Yannick Berthoumieu
URL: <http://ivmsp2016.org/>

IEEE International Conference on Multimedia and Expo (ICME)

11–15 July, Seattle, Washington, USA.
General Chairs: Tsuhan Chen, Ming-Ting Sun, and Cha Zhang
URL: <http://www.icme2016.org/>

AUGUST

IEEE 13th IEEE International Conference on Advanced Video and Signal Based Surveillance (AVSS)

23–26 August, Colorado Springs, Colorado, USA.
General Cochairs: Terry Boult and Ram Nevatia
URL: <http://avss2016.org/>

IEEE 24th European Signal Processing Conference (EUSIPCO)

29 August–2 September, Budapest, Hungary.
General Chair: Lajos Hanzo
URL: <http://www.eusipco2016.org/>

SEPTEMBER

IEEE International Workshop on Machine Learning for Signal Processing (MLSP)

13–16 September, Salerno, Italy.

IEEE International 18th International Workshop on Multimedia Signal Processing (MMSP)

20–23 September, Montreal, Quebec, Canada.

Sensor Signal Processing for Defence (SSPD)

22–23 September, Edinburgh, Great Britain.
URL: <http://www.sspd.eng.ed.ac.uk>

IEEE International Conference on Image Processing (ICIP)

25–28 September, Phoenix, Arizona, USA.
General Chair: Lina Karam
URL: <http://www.ieeeicip2016.org>

DECEMBER

8th IEEE International Workshop on Information Forensics and Security (WIFS)

5–7 December, Abu Dhabi, United Arab Emirates
General Chairs: Ernesto Damiani and Nasir Memon
URL: <http://wifs2016.mdabaie.com/>

IEEE Global Conference on Signal and Information Processing (GlobalSIP)

7–9 December, Greater Washington, D.C., USA.
General Chairs: Zhi Tian and Brian Sadler
URL: <http://2016.ieeeglobalsip.org>

IEEE Spoken Language Technology Workshop (SLT)

13–16 December, San Juan, Puerto Rico.

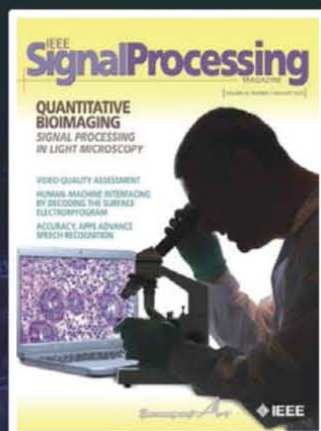
2017

MARCH

2017 IEEE International Conference on Acoustics, Speech, and Signal Processing (ICASSP)

5–9 March, New Orleans, Louisiana, USA.

January 2015
Quantitative Bioimaging



March 2015
Assistive Listening



May 2015
Feature Article Collection



Publish with IEEE Signal Processing Magazine

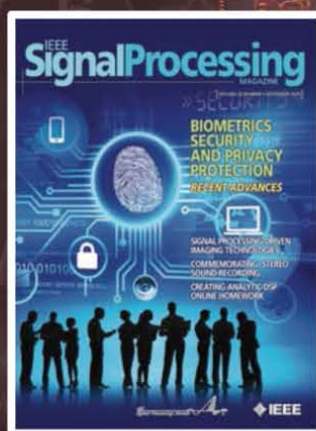
HIGH IMPACT among all electrical engineering publications

REACH a broad signal processing audience worldwide

WELCOME proposals for Special Issues and Feature Articles, and contributions to Columns



July 2015
Art Investigation



September 2015
Biometrics Security & Privacy



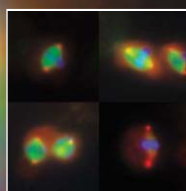
November 2015
Feature Article Collection

Digital Object Identifier 10.1109/MSP.2016.2534419



あなたは MATLAB を話しますか?

Over one million people around the world speak MATLAB. Engineers and scientists in every field from aerospace and semiconductors to biotech, financial services, and earth and ocean sciences use it to express their ideas. Do you speak MATLAB?



*Cells in mitosis:
high-throughput microscopy
for image-based screens.
Provided by Roy Wollman,
Univ. California, Davis.*

Article available at
mathworks.com/ltc

MATLAB®

The language of technical computing

IEEE SIGNAL PROCESSING SOCIETY

Content Gazette

MARCH 2016

ISSN 2167-5023

**IEEE Journal of Selected Topics in Signal Processing**<http://www.signalprocessingsociety.org/publications/periodicals/jstsp/>**IEEE Signal Processing Letters**<http://www.signalprocessingsociety.org/publications/periodicals/letters/>**IEEE Signal Processing Magazine**<http://www.signalprocessingsociety.org/publications/periodicals/spm/>**IEEE/ACM Transactions on Audio, Speech, and Language Processing-
IEEE Transactions on Signal Processing**<http://www.signalprocessingsociety.org/publications/periodicals/taslp/>**IEEE Transactions on Image Processing**<http://www.signalprocessingsociety.org/publications/periodicals/image-processing/>**IEEE Transactions on Information Forensics and Security**<http://www.signalprocessingsociety.org/publications/periodicals/forensics/>**IEEE Transactions on Signal Processing**<http://www.signalprocessingsociety.org/publications/periodicals/tsp/>**IEEE Transactions on Multimedia**<http://www.signalprocessingsociety.org/tmm/>

MLSP2016

IEEE International Workshop on
MACHINE LEARNING FOR SIGNAL PROCESSING

SEPTEMBER 13-16, 2016 VIETRI SUL MARE, SALERNO, ITALY
MLSP2016.CONWIZ.DK

Organizing committee

General Chair	Francesco A. N. Palmieri <i>Seconda Università di Napoli, Italy</i>
Program Chairs	Aurelio Uncini <i>Università di Roma La Sapienza, Italy</i> Kostas Diamantaras, TEI <i>of Thessaloniki, Greece</i>
Finance Chair	Ferdinando Mancini <i>Università di Salerno and IIASS "E. R. Caianiello"</i>
Data Competition Chair	Catherine Huang <i>Intel Corporation, USA</i>
Publicity Chair	Marc van Hulle <i>KU Leuven</i>
Publication Chair	Jan Larsen <i>Technical University of Denmark, Denmark</i>
Program Advisory Committee	Eros Pasero <i>Politecnico di Torino, Italy</i> Tülay Adalı <i>University of Maryland, Baltimore County, USA</i> Vince Calhoun <i>University of New Mexico, USA</i>



CALL FOR PAPERS

The 26th MLSP workshop in the series of workshops organized by the IEEE Signal Processing Society MLSP Technical Committee will present the most recent and exciting advances in machine learning for signal processing through keynote talks, tutorials, as well as special and regular single-track sessions. Prospective authors are invited to submit papers on relevant algorithms and applications including, but not limited to:

- Bayesian learning and signal processing
- Cognitive information processing
- Deep learning techniques
- Dictionary learning
- Graphical and kernel methods
- Independent component analysis
- Information-theoretic learning
- Learning theory and algorithms
- Pattern recognition and classification
- Bounds on performance
- Subspace and manifold learning
- Sequential learning and decision methods
- Source separation
- Applications including: speech, audio & music, image & video, biomedical signals & images, communications, bioinformatics, biometrics, systems biology, computational intelligence, genomic signals & sequences, social networks, games, smart grid, security & privacy

Important Dates and Deadlines

Special session proposals	April 3, 2016
Paper submissions	May 1, 2016
Decision notifications	June 5, 2016
Camera-ready papers and advance author registration	July 31, 2016

Sponsored by



Supported by



Istituto Internazionale Alti Studi
Scientifici "E. Caianiello"



Società Italiana RETi Neuroniche



Seconda Università di Napoli



Università di Salerno

Data Analysis and Signal Processing Competition is organized in conjunction with the workshop. The goal of the competition is to advance the current state-of-the-art in theoretical and practical aspects of signal processing domains.

MLSP 2016 seeks proposals for **Special Sessions** that will address research in emerging or interdisciplinary areas of particular interest, not covered already by traditional MLSP sessions.

The **MLSP Best Student Paper Award** will be granted to the best paper for which a student is the principal author and presenter.

Prospective authors are invited to submit a double column paper of up to six pages using the electronic submission procedure at <http://mlsp2016.conwiz.dk>. Accepted papers will be published on a password-protected website that will be available during the workshop. The presented papers will be published in and indexed by IEEE Xplore.

IEEE TRANSACTIONS ON SIGNAL PROCESSING

A PUBLICATION OF THE IEEE SIGNAL PROCESSING SOCIETY



www.signalprocessingsociety.org

Indexed in PubMed® and MEDLINE®, products of the United States National Library of Medicine



FEBRUARY 1, 2016

VOLUME 64

NUMBER 3

ITPRED

(ISSN 1053-587X)

REGULAR PAPERS

Stability and Continuity of Centrality Measures in Weighted Graphs http://dx.doi.org/10.1109/TSP.2015.2486740	543
..... <i>S. Segarra and A. Ribeiro</i>	
Decentralized and Collaborative Subspace Pursuit: A Communication-Efficient Algorithm for Joint Sparsity Pattern Recovery With Sensor Networks http://dx.doi.org/10.1109/TSP.2015.2483482	556
..... <i>G. Li, T. Wimalajeewa, and P. K. Varshney</i>	
Binary Sparse Coding of Convolutional Mixtures for Sound Localization and Separation via Spatialization http://dx.doi.org/10.1109/TSP.2015.2488598	567
..... <i>A. Asaei, M. J. Taghizadeh, S. Haghghatshoar, B. Raj, H. Bourslard, and V. Cevher</i>	
Empirically Estimable Classification Bounds Based on a Nonparametric Divergence Measure http://dx.doi.org/10.1109/TSP.2015.2477805 ..	580
..... <i>V. Berisha, A. Wisler, A. O. Hero, and A. Spanias</i>	
Correlation Based Online Dictionary Learning Algorithm http://dx.doi.org/10.1109/TSP.2015.2486743	592
..... <i>Y. Naderahmadian, S. Beheshti, and M. A. Tinati</i>	



On Digital Post-Distortion Techniques http://dx.doi.org/10.1109/TSP.2015.2477806	<i>Z. Alina and O. Amrani</i>	603
Metrics in the Space of High Order Networks http://dx.doi.org/10.1109/TSP.2015.2481864	<i>W. Huang and A. Ribeiro</i>	615
Joint Delay and Doppler Estimation for Passive Sensing With Direct-Path Interference http://dx.doi.org/10.1109/TSP.2015.2488584	<i>X. Zhang, H. Li, J. Liu, and B. Himed</i>	630
Probability Density Function Estimation Using the EEF With Application to Subset/Feature Selection http://dx.doi.org/10.1109/TSP.2015.2488591	<i>S. Kay, Q. Ding, B. Tang, and H. He</i>	641
Coexisting Linear and Widely Linear Transceivers in the MIMO Interference Channel http://dx.doi.org/10.1109/TSP.2015.2489604	<i>S. Lagen, A. Agustin, and J. Vidal</i>	652
A Signal Decomposition Model-Based Bayesian Framework for ECG Components Separation http://dx.doi.org/10.1109/TSP.2015.2489598	<i>E. Kheirati Roonizi and R. Sassi</i>	665
Symbol-Decision Successive Cancellation List Decoder for Polar Codes http://dx.doi.org/10.1109/TSP.2015.2486750	<i>C. Xiong, J. Lin, and Z. Yan</i>	675
Online Distributed Sparsity-Aware Canonical Correlation Analysis http://dx.doi.org/10.1109/TSP.2015.2481861	<i>J. Chen and I. D. Schizas</i>	688
Minimum Proper Loss Estimators for Parametric Models http://dx.doi.org/10.1109/TSP.2015.2489608	<i>M. J. Holland and K. Ikeda</i>	704
Modified Rao Test for Multichannel Adaptive Signal Detection http://dx.doi.org/10.1109/TSP.2015.2491892	<i>J. Liu, W. Liu, B. Chen, H. Liu, H. Li, and C. Hao</i>	714
Multimedia Transmission Over Cognitive Radio Channels Under Sensing Uncertainty http://dx.doi.org/10.1109/TSP.2015.2478747	<i>C. Ye, G. Ozcan, M. C. Gursoy, and S. Velipasalar</i>	726
Distributed Inference for Relay-Assisted Sensor Networks With Intermittent Measurements Over Fading Channels http://dx.doi.org/10.1109/TSP.2015.2489606	<i>S. Zhu, Y. C. Soh, and L. Xie</i>	742
Robust Turbo Analog Error Correcting Codes Based on Analog CRC Verification http://dx.doi.org/10.1109/TSP.2015.2491879	<i>A. Zanko, A. Leshem, and E. Zehavi</i>	757
Parameter Estimation of Multicomponent 2D Polynomial-Phase Signals Using the 2D PHAF-Based Approach http://dx.doi.org/10.1109/TSP.2015.2491887	<i>M. Simeunović and I. Djurović</i>	771
Distributed Variational Bayesian Algorithms Over Sensor Networks http://dx.doi.org/10.1109/TSP.2015.2493979	<i>J. Hua and C. Li</i>	783
Performance Study of a Near Maximum Likelihood Code-Aided Timing Recovery Technique http://dx.doi.org/10.1109/TSP.2015.2489602 ..	<i>I. Nasr, B. Geller, L. N. Atallah, and S. Cherif</i>	799

IEEE TRANSACTIONS ON SIGNAL PROCESSING

A PUBLICATION OF THE IEEE SIGNAL PROCESSING SOCIETY



www.signalprocessingsociety.org

Indexed in PubMed® and MEDLINE®, products of the United States National Library of Medicine



FEBRUARY 15, 2016

VOLUME 64

NUMBER 4

ITPRED

(ISSN 1053-587X)

REGULAR PAPERS

Steady-State Performance of Spline Adaptive Filters http://dx.doi.org/10.1109/TSP.2015.2493986	816
..... <i>M. Scarpiniti, D. Comminiello, G. Scarano, R. Parisi, and A. Uncini</i>	
Fault-Tolerant Associative Memories Based on <i>c</i> -Partite Graphs http://dx.doi.org/10.1109/TSP.2015.2489600	829
..... <i>F. Leduc-Primeau, V. Gripon, M. G. Rabbat, and W. J. Gross</i>	
Energy Efficiency Optimization for MISO SWIPT Systems With Zero-Forcing Beamforming http://dx.doi.org/10.1109/TSP.2015.2489603 ..	842
..... <i>Q. Shi, C. Peng, W. Xu, M. Hong, and Y. Cai</i>	
Fast Discrete Linear Canonical Transform Based on CM-CC-CM Decomposition and FFT http://dx.doi.org/10.1109/TSP.2015.2491891	855
..... <i>S.-C. Pei and S.-G. Huang</i>	
Probabilistic Power Allocation for Cognitive Radio Networks With Outage Constraints and One-Bit Side Information http://dx.doi.org/10.1109/TSP.2015.2494852	867
..... <i>W.-H. Chen, W.-R. Lin, H.-C. Tsao, and C. Lin</i>	
Distributed Energy Spectral Efficiency Optimization for Partial/Full Interference Alignment in Multi-user Multi-relay Multi-cell MIMO Systems http://dx.doi.org/10.1109/TSP.2015.2488579	882
..... <i>K. T. K. Cheung, S. Yang, and L. Hanzo</i>	



Asymptotically Optimal CFAR Detectors http://dx.doi.org/10.1109/TSP.2015.2500181	897
..... <i>A. Ghobadzadeh, S. Gazor, M. Naderpour, and A. A. Tadaion</i>	
Multi-Wideband Waveform Design for Distance-Adaptive Wireless Communications in the Terahertz Band http://dx.doi.org/10.1109/TSP.2015.2498133	910
..... <i>C. Han, A. O. Bicen, and I. F. Akyildiz</i>	
A Bayesian Technique for Real and Integer Parameters Estimation in Linear Models and Its Application to GNSS High Precision Positioning http://dx.doi.org/10.1109/TSP.2015.2500195	923
..... <i>J. G. Garcia, P. A. Roncagliolo, and C. H. Muravchik</i>	
Comparing Multivariate Complex Random Signals: Algorithm, Performance Analysis and Application http://dx.doi.org/10.1109/TSP.2015.2498128	934
..... <i>J. K. Tugnait</i>	
The Accurate Continuous-Discrete Extended Kalman Filter for Radar Tracking http://dx.doi.org/10.1109/TSP.2015.2493985	948
..... <i>G. Y. Kulikov and M. V. Kulikova</i>	
Predicting Grades http://dx.doi.org/10.1109/TSP.2015.2496278	959
..... <i>Y. Meier, J. Xu, O. Atan, and M. van der Schaar</i>	
Fast and Accurate Rank Selection Methods for Multistage Wiener Filter http://dx.doi.org/10.1109/TSP.2015.2493990	973
..... <i>M. Zhang, A. Zhang, and J. Li</i>	
Mean-Square Deviation Analysis of Multiband-Structured Subband Adaptive Filter Algorithm http://dx.doi.org/10.1109/TSP.2015.2498136	985
..... <i>J. J. Jeong, S. H. Kim, G. Koo, and S. W. Kim</i>	
Enhancing Sparsity and Resolution via Reweighted Atomic Norm Minimization http://dx.doi.org/10.1109/TSP.2015.2493987	995
..... <i>Z. Yang and L. Xie</i>	
Robust, Scalable, and Fast Bootstrap Method for Analyzing Large Scale Data http://dx.doi.org/10.1109/TSP.2015.2498121	1007
..... <i>S. Basiri, E. Ollila, and V. Koivunen</i>	
Self-Localization of Ad-Hoc Arrays Using Time Difference of Arrivals http://dx.doi.org/10.1109/TSP.2015.2498130	1018
..... <i>L. Wang, T.-K. Hon, J. D. Reiss, and A. Cavallaro</i>	
Energy Efficiency of Distributed Signal Processing in Wireless Networks: A Cross-Layer Analysis http://dx.doi.org/10.1109/TSP.2015.2494865	1034
..... <i>G. Geraci, M. Wildemeersch, and T. Q. S. Quek</i>	
Convergence and Fluctuations of Regularized Tyler Estimators http://dx.doi.org/10.1109/TSP.2015.2494858	1048
..... <i>A. Kammoun, R. Couillet, F. Pascal, and M.-S. Alouini</i>	
FIR Filter Design via Extended Optimal Factoring http://dx.doi.org/10.1109/TSP.2015.2494846	1061
..... <i>A. Mehrnia and A. N. Willson</i>	
Recovery of Sparse Signals via Generalized Orthogonal Matching Pursuit: A New Analysis http://dx.doi.org/10.1109/TSP.2015.2498132 ..	1076
..... <i>J. Wang, S. Kwon, P. Li, and B. Shim</i>	
<hr/>	
EDICS—Editors' Information Classification Scheme http://dx.doi.org/10.1109/TSP.2016.2523078	1090
Information for Authors http://dx.doi.org/10.1109/TSP.2016.2523079	1091



IEEE TRANSACTIONS ON

SIGNAL AND INFORMATION PROCESSING OVER NETWORKS



Now accepting paper submissions

The new *IEEE Transactions on Signal and Information Processing over Networks* publishes high-quality papers that extend the classical notions of processing of signals defined over vector spaces (e.g. time and space) to processing of signals and information (data) defined over networks, potentially dynamically varying. In signal processing over networks, the topology of the network may define structural relationships in the data, or may constrain processing of the data. Topics of interest include, but are not limited to the following:

Adaptation, Detection, Estimation, and Learning

- Distributed detection and estimation
- Distributed adaptation over networks
- Distributed learning over networks
- Distributed target tracking
- Bayesian learning; Bayesian signal processing
- Sequential learning over networks
- Decision making over networks
- Distributed dictionary learning
- Distributed game theoretic strategies
- Distributed information processing
- Graphical and kernel methods
- Consensus over network systems
- Optimization over network systems

Communications, Networking, and Sensing

- Distributed monitoring and sensing
- Signal processing for distributed communications and networking
- Signal processing for cooperative networking
- Signal processing for network security
- Optimal network signal processing and resource allocation

Modeling and Analysis

- Performance and bounds of methods
- Robustness and vulnerability
- Network modeling and identification

Modeling and Analysis (cont.)

- Simulations of networked information processing systems
- Social learning
- Bio-inspired network signal processing
- Epidemics and diffusion in populations

Imaging and Media Applications

- Image and video processing over networks
- Media cloud computing and communication
- Multimedia streaming and transport
- Social media computing and networking
- Signal processing for cyber-physical systems
- Wireless/mobile multimedia

Data Analysis

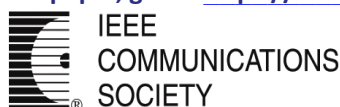
- Processing, analysis, and visualization of big data
- Signal and information processing for crowd computing
- Signal and information processing for the Internet of Things
- Emergence of behavior

Emerging topics and applications

- Emerging topics
- Applications in life sciences, ecology, energy, social networks, economic networks, finance, social sciences, smart grids, wireless health, robotics, transportation, and other areas of science and engineering

Editor-in-Chief: Petar M. Djurić, Stony Brook University (USA)

To submit a paper, go to: <https://mc.manuscriptcentral.com/tsipn-ieee>



Call for Papers
IEEE Signal Processing Society
IEEE Transactions on Signal and Information Processing over Networks

Special Issue on Distributed Information Processing in Social Networks

Over the past few decades, online social networks such as *Facebook* and *Twitter* have significantly changed the way people communicate and share information with each other. The opinion and behavior of each individual are heavily influenced through interacting with others. These local interactions lead to many interesting collective phenomena such as herding, consensus, and rumor spreading. At the same time, there is always the danger of mob mentality of following crowds, celebrities, or gurus who might provide misleading or even malicious information. Many efforts have been devoted to investigating the collective behavior in the context of various network topologies and the robustness of social networks in the presence of malicious threats. On the other hand, activities in social networks (clicks, searches, transactions, posts, and tweets) generate a massive amount of decentralized data, which is not only big in size but also complex in terms of its structure. Processing these data requires significant advances in accurate mathematical modeling and computationally efficient algorithm design.

Many modern technological systems such as wireless sensor and robot networks are virtually the same as social networks in the sense that the nodes in both networks carry disparate information and communicate with constraints. Thus, investigating social networks will bring insightful principles on the system and algorithmic designs of many engineering networks. An example of such is the implementation of consensus algorithms for coordination and control in robot networks. Additionally, more and more research projects nowadays are data-driven. Social networks are natural sources of massive and diverse big data, which present unique opportunities and challenges to further develop theoretical data processing toolsets and investigate novel applications. This special issue aims to focus on addressing distributed information (signal, data, etc.) processing problems in social networks and also invites submissions from all other related disciplines to present comprehensive and diverse perspectives.

Topics of interest include, but are not limited to:

- Dynamic social networks: time varying network topology, edge weights, etc.
- Social learning, distributed decision-making, estimation, and filtering
- Consensus and coordination in multi-agent networks
- Modeling and inference for information diffusion and rumor spreading
- Multi-layered social networks where social interactions take place at different scales or modalities
- Resource allocation, optimization, and control in multi-agent networks
- Modeling and strategic considerations for malicious behavior in networks
- Social media computing and networking
- Data mining, machine learning, and statistical inference frameworks and algorithms for handling big data from social networks
- Data-driven applications: attribution models for marketing and advertising, trend prediction, recommendation systems, crowdsourcing, etc.
- Other topics associated with social networks: graphical modeling, trust, privacy, engineering applications, etc.

Important Dates:

- Manuscript submission due: September 15, 2016
- First review completed: November 1, 2016
- Revised manuscript due: December 15, 2016
- Second review completed: February 1, 2017
- Final manuscript due: March 15, 2017
- Publication: June 1, 2017

Guest Editors:

- Zhenliang Zhang, Qualcomm Corporate R&D (zhenlian@qti.qualcomm.com)
- Wee Peng Tay, Nanyang Technological University (wptay@ntu.edu.sg)
- Moez Draief, Imperial College London (m.draief@imperial.ac.uk)
- Xiaodong Wang, Columbia University (xw2008@columbia.edu)
- Edwin K. P. Chong, Colorado State University (edwin.chong@colostate.edu)
- Alfred O. Hero III, University of Michigan (hero@eecs.umich.edu)

IEEE/ACM TRANSACTIONS ON AUDIO, SPEECH, AND LANGUAGE PROCESSING

A PUBLICATION OF THE IEEE SIGNAL PROCESSING SOCIETY



www.signalprocessingsociety.org

Indexed in PubMed® and MEDLINE®, products of the United States National Library of Medicine



FEBRUARY 2016

VOLUME 24

NUMBER 2

ITASFA

(ISSN 2329-9290)

REGULAR PAPERS

Regularization Approaches for Synthesizing HRTF Directivity Patterns http://dx.doi.org/10.1109/TASLP.2015.2504874	215
..... <i>E. Rasumow, M. Hansen, S. van de Par, D. Püschel, V. Mellert, S. Doclo, and M. Blau</i>	
Design of Directivity Patterns with a Unique Null of Maximum Multiplicity http://dx.doi.org/10.1109/TASLP.2015.2504866	226
..... <i>C. Pan, J. Benesty, and J. Chen</i>	
Robust Speech Recognition via Enhancing the Complex-Valued Acoustic Spectrum in Modulation Domain http://dx.doi.org/10.1109/TASLP.2015.2504781	236
..... <i>J.-W. Hung, H.-J. Hsieh, and B. Chen</i>	
Boosting Contextual Information for Deep Neural Network Based Voice Activity Detection http://dx.doi.org/10.1109/TASLP.2015.2505415 ..	252
..... <i>X.-L. Zhang and D. Wang</i>	
Source and Filter Estimation for Throat-Microphone Speech Enhancement http://dx.doi.org/10.1109/TASLP.2015.2499040	265
..... <i>M. A. T. Turan and E. Erzin</i>	



Speech Dereverberation Using Non-Negative Convolutional Transfer Function and Spectro-Temporal Modeling http://dx.doi.org/10.1109/TASLP.2015.2501724	<i>N. Mohammadiha and S. Doclo</i>	276
Two-Stage Supervised Learning-Based Method to Detect Screams and Cries in Urban Environments http://dx.doi.org/10.1109/TASLP.2015.2506264	<i>A. Sharma and S. Kaul</i>	290
Directivity Factors of the First-Order Steerable Differential Array With Microphone Mismatches: Deterministic and Worst-Case Analysis http://dx.doi.org/10.1109/TASLP.2015.2506269	<i>X. Wu and H. Chen</i>	300
A Fast Method for High-Resolution Voiced/Unvoiced Detection and Glottal Closure/Opening Instant Estimation of Speech http://dx.doi.org/10.1109/TASLP.2015.2506263	<i>A. I. Koutrouvelis, G. P. Kafentzis, N. D. Gaubitch, and R. Heusdens</i>	316
Real-Time Audio-to-Score Alignment of Music Performances Containing Errors and Arbitrary Repeats and Skips http://dx.doi.org/10.1109/TASLP.2015.2507862	<i>T. Nakamura, E. Nakamura, and S. Sagayama</i>	329
Optimizing the Similarity of Loudspeaker–Room Responses in Multiple Listening Positions http://dx.doi.org/10.1109/TASLP.2015.2496156 ..	<i>A. Bahne and A. Ahlén</i>	340
The Hearing-Aid Audio Quality Index (HAAQI) http://dx.doi.org/10.1109/TASLP.2015.2507858	<i>J. M. Kates and K. H. Arehart</i>	354
A Semidefinite Programming Approach to Min-max Estimation of the Common Part of Acoustic Feedback Paths in Hearing Aids http://dx.doi.org/10.1109/TASLP.2015.2507940	<i>H. Schepker and S. Doclo</i>	366
Packet Loss Concealment Based on Deep Neural Networks for Digital Speech Transmission http://dx.doi.org/10.1109/TASLP.2015.2509780 ..	<i>B.-K. Lee and J.-H. Chang</i>	378
On the Evaluation of Adaptive Machine Translation for Human Post-Editing http://dx.doi.org/10.1109/TASLP.2015.2509241	<i>L. Bentivogli, N. Bertoldi, M. Cettolo, M. Federico, M. Negri, and M. Turchi</i>	388

EDICS—Editor’s Information Classification Scheme http://dx.doi.org/10.1109/TASLP.2016.2519640		400
Information for Authors http://dx.doi.org/10.1109/TASLP.2016.2519641		402

ANNOUNCEMENT

Call for Papers—Special Issue on Sound Scene and Event Analysis http://dx.doi.org/10.1109/TASLP.2016.2519219		404
--	--	-----

CALL FOR PAPERS

IEEE/ACM Transactions on Audio, Speech and Language Processing
Special issue on **Sound Scene and Event Analysis**

It is still difficult for a machine listening system to demonstrate the same capabilities as human listeners in the analysis of realistic acoustic scenes. Besides speech and music, the analysis of other types of sounds, generally referred to as environmental sounds, is the subject of growing interest from the community and is targeting an ever increasing set of audio categories. In realistic environments, multiple sources are often present simultaneously, and in reverberant conditions, which makes the computational scene analysis challenging.

Typical tasks on audio scene analysis are audio-based scene classification and audio event detection and recognition targeting categories such as “door knocks”, “gunshots”, “crowds”, “car engine noise”, as well as marine mammal and bird species, etc. The wide heterogeneity of possible sounds means that novel types of signal processing and machine learning methods should be developed including novel concepts for audio source segmentation and separation. Beyond recognizing sound scenes and sources of interest, a key task of complex audio scene analysis is sound-source localization.

Further, most of the methods developed until now are probably not tractable on big data so there is also a need for new approaches that are, by design, efficient on large scale problems. Acquiring large scale labelled databases is still problematic and such datasets are most likely collected on heterogeneous sets of acoustic conditions (mobile phone recordings, urban/domestic audio,...) most of which are usually offering a degraded version of the signal of interest with potential variable annotation strategies. Therefore methods to tackle large scale problems also have to be robust against signal degradation, acoustic variability, and annotation variability.

We invite papers on various topics on Sound Scene and Event Analysis, including but not limited to :

- * Audio scene classification;
- * Sound event detection and classification
- * Large-scale environmental audio data sets;
- * Acoustic features for environmental sound analysis;
- * Source localization methods for environmental audio scene analysis
- * Source separation for environmental audio scene analysis
- * Big data in environmental audio;
- * Environmental sound recognition;
- * Computational auditory scene analysis;

The authors are required to follow the Author's Guide for manuscript submission to the IEEE /ACM Transactions on Audio, Speech, and Language Processing at <http://www.signalprocessingsociety.org/publications/periodicals/taslp/>

Important Dates:

Manuscript submission due: July 1st, 2016
First review completed: Sept. 30th 2016
Revised manuscript due: October 20th, 2016
Second review completed: Dec. 1st, 2016
Final manuscript due: Dec. 31st, 2016
Publication date: February 2017

Guest Editors:

Gaël Richard, Télécom ParisTech, France (lead guest editor)
Tuomas Virtanen, Tampere University of Technology, Finland
Juan Pablo Bello, New York University, USA
Nobutaka Ono, National Institute of Informatics, Japan

IEEE TRANSACTIONS ON IMAGE PROCESSING

A PUBLICATION OF THE IEEE SIGNAL PROCESSING SOCIETY



www.signalprocessingsociety.org

Indexed in PubMed® and MEDLINE®, products of the United States National Library of Medicine



FEBRUARY 2016

VOLUME 25

NUMBER 2

IIPRE4

(ISSN 1057-7149)

PAPERS

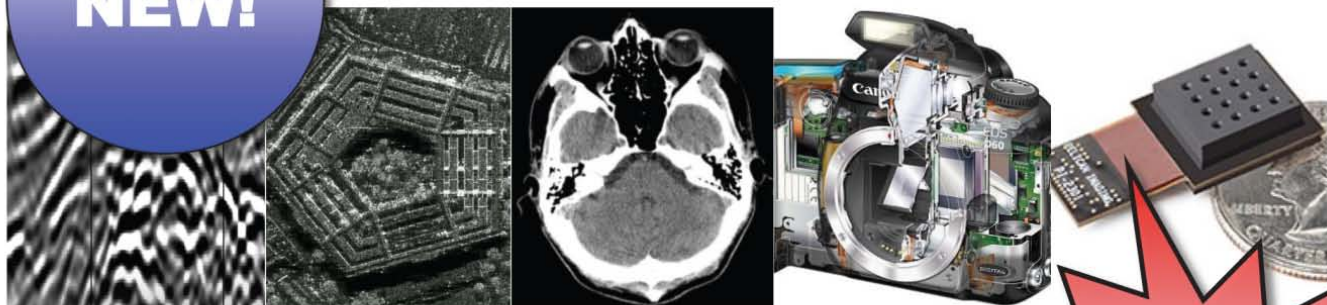
Fast Appearance Modeling for Automatic Primary Video Object Segmentation http://dx.doi.org/10.1109/TIP.2015.2500820	503
..... <i>J. Yang, B. Price, X. Shen, Z. Lin, and J. Yuan</i>	
Sub-Markov Random Walk for Image Segmentation http://dx.doi.org/10.1109/TIP.2015.2505184	516
..... <i>X. Dong, J. Shen, L. Shao, and L. Van Gool</i>	
GMM Estimation of 2D-RCA Models With Applications to Texture Image Classification http://dx.doi.org/10.1109/TIP.2015.2494740	528
..... <i>A. Boulemdjel, F. Hachouf, and S. Kharfouchi</i>	
Removal of Vesicle Structures From Transmission Electron Microscope Images http://dx.doi.org/10.1109/TIP.2015.2504901	540
..... <i>K. H. Jensen, F. J. Sigworth, and S. S. Brandt</i>	
Detecting Densely Distributed Graph Patterns for Fine-Grained Image Categorization http://dx.doi.org/10.1109/TIP.2015.2502147	553
..... <i>L. Zhang, Y. Yang, M. Wang, R. Hong, L. Nie, and X. Li</i>	
Quaternionic Local Ranking Binary Pattern: A Local Descriptor of Color Images http://dx.doi.org/10.1109/TIP.2015.2507404	566
..... <i>R. Lan, Y. Zhou, and Y. Y. Tang</i>	
An Automatic 3D Facial Landmarking Algorithm Using 2D Gabor Wavelets http://dx.doi.org/10.1109/TIP.2015.2496183	580
..... <i>M. A. de Jong, A. Wollstein, C. Ruff, D. Dunaway, P. Hysi, T. Spector, F. Liu, W. Niessen, M. J. Koudstaal, M. Kayser, E. B. Wolvius, and S. Böhringer</i>	
Bayesian Depth-From-Defocus With Shading Constraints http://dx.doi.org/10.1109/TIP.2015.2507403	589
..... <i>C. Li, S. Su, Y. Matsushita, K. Zhou, and S. Lin</i>	
Halftone Blending Between Smooth and Detail Screens to Improve Print Quality With Electrophotographic Printers http://dx.doi.org/10.1109/TIP.2015.2500035	601
..... <i>S. J. Park, M. Q. Shaw, G. Kerby, T. Nelson, D.-Y. Tzeng, K. R. Bengtson, and J. P. Allebach</i>	
Stereoscopic 3D Visual Discomfort Prediction: A Dynamic Accommodation and Vergence Interaction Model http://dx.doi.org/10.1109/TIP.2015.2506340	615
..... <i>H. Oh, S. Lee, and A. C. Bovik</i>	
Learning of Multimodal Representations With Random Walks on the Click Graph http://dx.doi.org/10.1109/TIP.2015.2507401	630
..... <i>F. Wu, X. Lu, J. Song, S. Yan, Z. Zhang, Y. Rui, and Y. Zhuang</i>	
Design of Steerable Wavelets to Detect Multifold Junctions http://dx.doi.org/10.1109/TIP.2015.2507981	643
..... <i>Z. Püspöki, V. Uhlmann, C. Vonesch, and M. Unser</i>	



A Novel Multi-Purpose Matching Representation of Local 3D Surfaces: A Rotationally Invariant, Efficient, and Highly Discriminative Approach With an Adjustable Sensitivity http://dx.doi.org/10.1109/TIP.2015.2492826	<i>F. R. Al-Osaimi</i>	658
Contrast Enhancement by Nonlinear Diffusion Filtering http://dx.doi.org/10.1109/TIP.2015.2507405	<i>Z. Liang, W. Liu, and R. Yao</i>	673
Robust Texture Image Representation by Scale Selective Local Binary Patterns http://dx.doi.org/10.1109/TIP.2015.2507408	<i>Z. Guo, X. Wang, J. Zhou, and J. You</i>	687
Dual Sparse Constrained Cascade Regression for Robust Face Alignment http://dx.doi.org/10.1109/TIP.2015.2502485	<i>Q. Liu, J. Deng, and D. Tao</i>	700
Generalization of SPIHT: Set Partition Coding System http://dx.doi.org/10.1109/TIP.2015.2509253	<i>Q. Li, D. Chen, W. Jiang, B. Liu, and J. Gong</i>	713
Depth Estimation Using a Sliding Camera http://dx.doi.org/10.1109/TIP.2015.2507984	<i>K. Ge, H. Hu, J. Feng, and J. Zhou</i>	726
Surveillance Video Synopsis via Scaling Down Objects http://dx.doi.org/10.1109/TIP.2015.2507942	<i>X. Li, Z. Wang, and X. Lu</i>	740
Compressive Sequential Learning for Action Similarity Labeling http://dx.doi.org/10.1109/TIP.2015.2508600	<i>J. Qin, L. Liu, Z. Zhang, Y. Wang, and L. Shao</i>	756
On Counting Metamers http://dx.doi.org/10.1109/TIP.2015.2504900	<i>A. D. Logvinenko and E. Demidenko</i>	770
Articulated and Generalized Gaussian Kernel Correlation for Human Pose Estimation http://dx.doi.org/10.1109/TIP.2015.2507445	<i>M. Ding and G. Fan</i>	776
Recognition of Images Degraded by Gaussian Blur http://dx.doi.org/10.1109/TIP.2015.2512108	<i>J. Flusser, S. Farokhi, C. Höschl IV, T. Suk, B. Zitová, and M. Pedone</i>	790
Variational Phase Imaging Using the Transport-of-Intensity Equation http://dx.doi.org/10.1109/TIP.2015.2509249	<i>E. Bostan, E. Froustey, M. Nilchian, D. Sage, and M. Unser</i>	807
Focus Profile Modeling http://dx.doi.org/10.1109/TIP.2015.2509427	<i>D.-C. Tsai and H. H. Chen</i>	818
Nonconvex Nonsmooth Low Rank Minimization via Iteratively Reweighted Nuclear Norm http://dx.doi.org/10.1109/TIP.2015.2511584	<i>C. Lu, J. Tang, S. Yan, and Z. Lin</i>	829
Sparse Hashing Tracking http://dx.doi.org/10.1109/TIP.2015.2509244	<i>L. Zhang, H. Lu, D. Du, and L. Liu</i>	840
Discriminative Transfer Subspace Learning via Low-Rank and Sparse Representation http://dx.doi.org/10.1109/TIP.2015.2510498	<i>Y. Xu, X. Fang, J. Wu, X. Li, and D. Zhang</i>	850
Detail-Preserving and Content-Aware Variational Multi-View Stereo Reconstruction http://dx.doi.org/10.1109/TIP.2015.2507400	<i>Z. Li, K. Wang, W. Zuo, D. Meng, and L. Zhang</i>	864
Fused One-vs-All Features With Semantic Alignments for Fine-Grained Visual Categorization http://dx.doi.org/10.1109/TIP.2015.2509425	<i>X. Zhang, H. Xiong, W. Zhou, and Q. Tian</i>	878
Robust w-Estimators for Cryo-EM Class Means http://dx.doi.org/10.1109/TIP.2015.2512384	<i>C. Huang and H. D. Tagare</i>	893
Query-Adaptive Reciprocal Hash Tables for Nearest Neighbor Search http://dx.doi.org/10.1109/TIP.2015.2505180	<i>X. Liu, C. Deng, B. Lang, D. Tao, and X. Li</i>	907
The Radon Cumulative Distribution Transform and Its Application to Image Classification http://dx.doi.org/10.1109/TIP.2015.2509419	<i>S. Kolouri, S. R. Park, and G. K. Rohde</i>	920
Single-Image Super-Resolution Using Active-Sampling Gaussian Process Regression http://dx.doi.org/10.1109/TIP.2015.2512104	<i>H. Wang, X. Gao, K. Zhang, and J. Li</i>	935
Simple to Complex Transfer Learning for Action Recognition http://dx.doi.org/10.1109/TIP.2015.2512107	<i>F. Liu, X. Xu, S. Qiu, C. Qing, and D. Tao</i>	949
Coupled Learning for Facial Deblur http://dx.doi.org/10.1109/TIP.2015.2509418	<i>D. Tian and D. Tao</i>	961
Multinomial Latent Logistic Regression for Image Understanding http://dx.doi.org/10.1109/TIP.2015.2509422	<i>Z. Xu, Z. Hong, Y. Zhang, J. Wu, A. C. Tsoi, and D. Tao</i>	973
Curve-Like Structure Extraction Using Minimal Path Propagation With Backtracking http://dx.doi.org/10.1109/TIP.2015.2496279	<i>Y. Chen, Y. Zhang, J. Yang, Q. Cao, G. Yang, J. Chen, H. Shu, L. Luo, J.-L. Coatrieux, and Q. Feng</i>	988
<hr/>		
EDICS-Editor's Information Classification Scheme http://dx.doi.org/10.1109/TIP.2016.2516200		1004
Information for Authors http://dx.doi.org/10.1109/TIP.2016.2516199		1005



IEEE TRANSACTIONS ON COMPUTATIONAL IMAGING



Editor-in-Chief

W. Clem Karl
Boston University

Technical Committee

Charles Bouman
Eric Miller
Peter Corcoran
Jong Chul Ye
Dave Brady
William Freeman

The IEEE Transactions on Computational Imaging publishes research results where computation plays an integral role in the image formation process. All areas of computational imaging are appropriate, ranging from the principles and theory of computational imaging, to modeling paradigms for computational imaging, to image formation methods, to the latest innovative computational imaging system designs. Topics of interest include, but are not limited to the following:

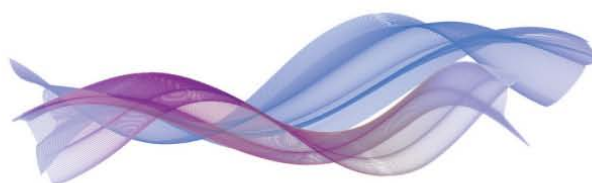
**30% FASTER
TURN AROUND
THAN TIP!**

<p>Computational Imaging Methods and Models</p> <ul style="list-style-type: none"> • Coded image sensing • Compressed sensing • Sparse and low-rank models • Learning-based models, dictionary methods • Graphical image models • Perceptual models <p>Computational Image Formation</p> <ul style="list-style-type: none"> • Sparsity-based reconstruction • Statistically-based inversion methods • Multi-image and sensor fusion • Optimization-based methods; proximal iterative methods, ADMM <p>Computational Photography</p> <ul style="list-style-type: none"> • Non-classical image capture • Generalized illumination • Time-of-flight imaging • High dynamic range imaging • Plenoptic imaging 	<p>Computational Consumer Imaging</p> <ul style="list-style-type: none"> • Mobile imaging, cell phone imaging • Camera-array systems • Depth cameras, multi-focus imaging • Pervasive imaging, camera networks <p>Computational Acoustic Imaging</p> <ul style="list-style-type: none"> • Multi-static ultrasound imaging • Photo-acoustic imaging • Acoustic tomography <p>Computational Microscopy</p> <ul style="list-style-type: none"> • Holographic microscopy • Quantitative phase imaging • Multi-illumination microscopy • Lensless microscopy • Light field microscopy <p>Imaging Hardware and Software</p> <ul style="list-style-type: none"> • Embedded computing systems • Big data computational imaging • Integrated hardware/digital design 	<p>Tomographic Imaging</p> <ul style="list-style-type: none"> • X-ray CT • PET • SPECT <p>Magnetic Resonance Imaging</p> <ul style="list-style-type: none"> • Diffusion tensor imaging • Fast acquisition <p>Radar Imaging</p> <ul style="list-style-type: none"> • Synthetic aperture imaging • Inverse synthetic aperture imaging <p>Geophysical Imaging</p> <ul style="list-style-type: none"> • Multi-spectral imaging • Ground penetrating radar • Seismic tomography <p>Multi-spectral Imaging</p> <ul style="list-style-type: none"> • Multi-spectral imaging • Hyper-spectral imaging • Spectroscopic imaging
---	--	---

For more information on the IEEE Transactions on Computational Imaging see <http://www.signalprocessingsociety.org/publications/periodicals/tci/>

**NOW WITH
NO PAGE
CHARGES!**





CAMSAP 2017

Call for Papers

The Seventh IEEE International Workshop on Computational Advances in Multi-Sensor Adaptive Processing

Curaçao, Dutch Antilles

December 10-13, 2017

<http://www.cs.huji.ac.il/conferences/CAMSAP17>



Following the success of the first six editions of the IEEE workshop on Computational Advances in Multi-Sensor Adaptive Processing, we are pleased to announce the seventh workshop in this series. IEEE CAMSAP 2017 will be held in Curaçao, Dutch Antilles, and will feature a number of plenary talks from the world's leading researchers in the area, special focus sessions, and contributed papers. All papers will undergo peer review in order to provide feedback to the authors and ensure a high-quality program.

Topics and applications of interest for the workshop include, but are not limited to, the following.

TOPICS OF INTEREST

- Array processing, waveform diversity, space-time adaptive processing
- Convex optimization and relaxation
- Computational linear & multi-linear algebra
- Computer-intensive methods in signal processing (bootstrap, MCMC, EM, particle filtering, etc.)
- Signal and information processing over networks
- Sparse signal processing

APPLICATIONS

- Big data
- Biomedical signal processing
- Communication systems
- Computational imaging
- Radar
- Sensor networks
- Smart grids
- Sonar

Submission of Papers: Prospective authors are invited to submit original full-length papers, with up to four pages for technical content including figures and references, using the formatting guidelines on the website for reviewing purposes. All accepted papers must be presented at the workshop to appear in the proceedings. Best student paper awards, selected by a CAMSAP committee, will also be presented at the workshop.

Special Session Proposals: In addition to contributed sessions, the workshop will also have a number of special sessions. Prospective organizers of special sessions are invited to submit a proposal form, available on the workshop website, by e-mail to the Special Sessions Chair.

IMPORTANT DEADLINES

Submission of proposals for special sessions	March, 2017
Notification of special session acceptance	March 15, 2015
Submission of papers	July, 2017
Notification of paper acceptance	September, 2017
Final paper submission	



General Chairs

André L. F. de Almeida
andre@gtel.ufc.br
Federal University of Ceará,
Brazil

Martin Haardt
martin.haardt@tu-ilmenau.de
Ilmenau University of Technology,
Germany

Technical Program Chairs

Xiaoli Ma
xiaoli@gatech.edu
Georgia Institute of Technology,
USA

Shahram ShahbazPanahi
shahram.shahbazpanahi@uoit.ca
University of Ontario Institute of
Technology,
Canada

Finance Chair

Cihan Tepedelenlioglu
cihan@asu.edu
Arizona State University,
USA

Publicity and Publications Chair

Ami Wiesel
ami.wiesel@huji.ac.il
Hebrew University of Jerusalem,
Israel

Local Arrangements Chair

Geert Leus
g.j.t.leus@tudelft.nl
Delft University of Technology,
The Netherlands

Robert W. Heath Jr.
rheath@utexas.edu
University of Texas at Austin,
USA



Join Twitter Conversation
#CAMSAP2017



IEEE TRANSACTIONS ON INFORMATION FORENSICS AND SECURITY

A PUBLICATION OF THE IEEE SIGNAL PROCESSING SOCIETY



www.signalprocessingsociety.org

MARCH 2016

VOLUME 11

NUMBER 3

(ISSN 1556-6013)

OVERVIEW ARTICLE

- What Else Does Your Biometric Data Reveal? A Survey on Soft Biometrics <http://dx.doi.org/10.1109/TIFS.2015.2480381> *A. Dantcheva, P. Elia, and A. Ross* 441
-

REGULAR PAPERS

- Condition Factorization: A Technique for Building Fast and Compact Packet Matching Automata <http://dx.doi.org/10.1109/TIFS.2015.2489182> *A. Tongaonkar and R. Sekar* 468
- Fine-Grained Two-Factor Access Control for Web-Based Cloud Computing Services <http://dx.doi.org/10.1109/TIFS.2015.2493983> *J. K. Liu, M. H. Au, X. Huang, R. Lu, and J. Li* 484
- Performance Analysis of Touch-Interaction Behavior for Active Smartphone Authentication <http://dx.doi.org/10.1109/TIFS.2015.2503258> .. *C. Shen, Y. Zhang, X. Guan, and R. A. Maxion* 498
- Detection of Superpoints Using a Vector Bloom Filter <http://dx.doi.org/10.1109/TIFS.2015.2503269> *W. Liu, W. Qu, J. Gong, and K. Li* 514
- Fast Detection of Transformed Data Leaks <http://dx.doi.org/10.1109/TIFS.2015.2503271> *X. Shu, J. Zhang, D. Yao, and W.-C. Feng* 528
- A Security-Enhanced Alignment-Free Fuzzy Vault-Based Fingerprint Cryptosystem Using Pair-Polar Minutiae Structures <http://dx.doi.org/10.1109/TIFS.2015.2505630> *C. Li and J. Hu* 543
- A Game Theoretical Approach to Defend Against Co-Resident Attacks in Cloud Computing: Preventing Co-Residence Using Semi-Supervised Learning <http://dx.doi.org/10.1109/TIFS.2015.2505680> *Y. Han, T. Alpcan, J. Chan, C. Leckie, and B. I. P. Rubinstein* 556
- Two-Level QR Code for Private Message Sharing and Document Authentication <http://dx.doi.org/10.1109/TIFS.2015.2506546> *I. Tkachenko, W. Puech, C. Destruel, O. Strauss, J.-M. Gaudin, and C. Guichard* 571
- On 802.11 Access Point Locatability and Named Entity Recognition in Service Set Identifiers <http://dx.doi.org/10.1109/TIFS.2015.2507542> .. *M. Chernyshev, C. Valli, and P. Hannay* 584
-

Iterative Distributed Minimum Total MSE Approach for Secure Communications in MIMO Interference Channels http://dx.doi.org/10.1109/TIFS.2015.2493888	<i>Z. Kong, S. Yang, F. Wu, S. Peng, L. Zhong, and L. Hanzo</i>	594
Interference Improves PHY Security for Cognitive Radio Networks http://dx.doi.org/10.1109/TIFS.2015.2500184	<i>H. Zhang, T. Wang, L. Song, and Z. Han</i>	609
Oculomotor Plant Characteristics: The Effects of Environment and Stimulus http://dx.doi.org/10.1109/TIFS.2015.2503263	<i>O. Komogortsev, A. Karpov, and C. Holland</i>	621
Suspecting Less and Doing Better: New Insights on Palmprint Identification for Faster and More Accurate Matching http://dx.doi.org/10.1109/TIFS.2015.2503265	<i>Q. Zheng, A. Kumar, and G. Pan</i>	633
Piecewise Function Approximation With Private Data http://dx.doi.org/10.1109/TIFS.2015.2503268	<i>R. Lazzaretti, T. Pignata, and M. Barni</i>	642

COMMENTS AND CORRECTIONS

Comments on “Public Integrity Auditing for Dynamic Data Sharing With Multiuser Modification” http://dx.doi.org/10.1109/TIFS.2015.2501728	<i>Y. Yu, Y. Li, J. Ni, G. Yang, Y. Mu, and W. Susilo</i>	658
---	---	-----



The 2016 IEEE Image, Video, and Multidimensional Signal Processing (IVMSP) Workshop is the 12th of a series of unique meetings that bring together researchers in academia and industry to share the most recent and exciting advances in image, video, and multidimensional signal processing and analysis. The main theme of the 2016 IVMSP Workshop is **low-dimensional models for image and video processing and analysis**.

General chair

Yannick Berthoumieu
Univ. of Bordeaux, France

Technical program co-chairs

Christine Guillemot, INRIA, France

Mujdat Cetin, Sabanci Univ., Turkey

Plenary and invited session chairs

Béatrice Pesquet-Popescu, Telecom-paristech, France

Pascal Frossard, EPFL, Switzerland

Financial chair

Christian Germain, Univ. of Bordeaux, France

Publication co-chairs

Marc Donias, Univ. of Bordeaux, France

Nelly Pustelnik, ENS Lyon, France

Local arrangement co-chairs

Nathalie Toulon, Univ. of Bordeaux, France

Jean-Pierre Da Costa, Univ. of Bordeaux, France

The scientific program of IVMSP 2016 will include plenary talks, invited sessions, as well as regular sessions with contributed research papers. Papers are solicited in (but not limited to) the following topics:

- Image and video modeling on manifolds
- Manifold learning for classification and recognition
- Manifold sparse coding
- Graph-based manifold ranking
- Information geometry on probabilistic manifolds
- Low dimensional models and low rank methods
- Sparse and low-rank models in learning and pattern recognition
- Graphical models for image and video analysis
- Other related topics

PAPER SUBMISSION

Papers cannot be longer than 5 pages (double-column IEEE conference format), including all text, figures, and references. The 5th page cannot contain any text other than references. See the website for additional information regarding the submission process: www.ivmsp2016.org.

BEST STUDENT PAPER AWARDS

The IVMSP Best Student Paper Awards will be granted to the first, second, and third best contributed papers in the regular sessions for which a student is the principal author and presenter. The selection will be based on the technical quality, originality, and clarity of the submission.

IMPORTANT DATES

- | | |
|---------------------------------|----------------|
| • Submission of full papers | March 10, 2016 |
| • Notification of acceptance | May 10, 2016 |
| • Author advance registration | June 1, 2016 |
| • Camera-ready paper submission | June 1, 2016 |

IEEE
Signal Processing Society  ®

IEEE TRANSACTIONS ON *MULTIMEDIA*

A PUBLICATION OF
THE IEEE CIRCUITS AND SYSTEMS SOCIETY
THE IEEE SIGNAL PROCESSING SOCIETY
THE IEEE COMMUNICATIONS SOCIETY
THE IEEE COMPUTER SOCIETY



<http://www.signalprocessingsociety.org/tmm/>

FEBRUARY 2016

VOLUME 18

NUMBER 2

ITMUF8

(ISSN 1520-9210)

PAPERS

3D Audio Signal Processing

Effective Active Skeleton Representation for Low Latency Human Action Recognition <http://dx.doi.org/10.1109/TMM.2015.2505089> X. Cai, W. Zhou, L. Wu, J. Luo, and H. Li 141

3D Video Signal Processing

Content-Based Guided Image Filtering, Weighted Semi-Global Optimization, and Efficient Disparity Refinement for Fast and Accurate Disparity Estimation <http://dx.doi.org/10.1109/TMM.2015.2505905> G. A. Kordelas, D. S. Alexiadis, P. Daras, and E. Izquierdo 155

Compression and Coding

HEMS: Hierarchical Exemplar-Based Matching-Synthesis for Object-Aware Image Reconstruction <http://dx.doi.org/10.1109/TMM.2015.2496246> Y. Sun, X. Tao, Y. Li, L. Dong, and J. Lu 171

Probabilistic Approach for Predicting the Size of Coding Units in the Quad-Tree Structure of the Quality and Spatial Scalable HEVC <http://dx.doi.org/10.1109/TMM.2015.2510332> H. R. Tohidpour, M. T. Pourazad, and P. Nasiopoulos 182

Watermarking, Encryption, and Data Hiding

Multiplicative Watermark Decoder in Contourlet Domain Using the Normal Inverse Gaussian Distribution <http://dx.doi.org/10.1109/TMM.2015.2508147> H. Sadreazami, M. O. Ahmad, and M. N. S. Swamy 196

Joint Processing of Heterogeneous Data

Discriminative Dictionary Learning With Common Label Alignment for Cross-Modal Retrieval <http://dx.doi.org/10.1109/TMM.2015.2508146> C. Deng, X. Tang, J. Yan, W. Liu, and X. Gao 208



Subjective and Objective Quality Assessment, and User Experience

Guided Image Contrast Enhancement Based on Retrieved Images in Cloud <http://dx.doi.org/10.1109/TMM.2015.2510326> S. Wang, K. Gu, S. Ma, W. Lin, X. Liu, and W. Gao 219

Knowledge and Semantics Modeling for Multimedia Databases

Multi-Modal Event Topic Model for Social Event Analysis <http://dx.doi.org/10.1109/TMM.2015.2510329> S. Qian, T. Zhang, C. Xu, and J. Shao 233

Visual Understanding via Multi-Feature Shared Learning With Global Consistency <http://dx.doi.org/10.1109/TMM.2015.2510509> L. Zhang and D. Zhang 247

Multimedia Search and Retrieval

Zero-Shot Person Re-identification via Cross-View Consistency <http://dx.doi.org/10.1109/TMM.2015.2505083> Z. Wang, R. Hu, C. Liang, Y. Yu, J. Jiang, M. Ye, J. Chen, and Q. Leng 260

Multimedia Algorithms, Systems, and Interfaces

A Computational Model for Object-Based Visual Saliency: Spreading Attention Along Gestalt Cues <http://dx.doi.org/10.1109/TMM.2015.2505908> J.-G. Yu, G.-S. Xia, C. Gao, and A. Samal 273

Multimedia Social Networks

Social Friend Recommendation Based on Multiple Network Correlation <http://dx.doi.org/10.1109/TMM.2015.2510333> S. Huang, J. Zhang, L. Wang, and X.-S. Hua 287

Multimedia for Personal Applications (Mobile, Wearables, Interactive)

Exploiting Perceptual Anchoring for Color Image Enhancement <http://dx.doi.org/10.1109/TMM.2015.2503918> K.-T. Shih and H. H. Chen 300

Information for Authors <http://dx.doi.org/10.1109/TMM.2016.2517438> 311

IEEE JOURNAL OF SELECTED TOPICS IN SIGNAL PROCESSING



www.ieee.org/sp/index.html

FEBRUARY 2016

VOLUME 10

NUMBER 1

IJSTGY

(ISSN 1932-4553)

EDITORIAL

Introduction to the Issue on Advanced Signal Processing in Microscopy and Cell Imaging <http://dx.doi.org/10.1109/JSTSP.2015.2511299> ...
..... *C. Kervrann, S. T. Acton, J.-C. Olivo-Marin, C. O. S. Sorzano, and M. Unser* 3

OVERVIEW ARTICLE

A Guided Tour of Selected Image Processing and Analysis Methods for Fluorescence and Electron Microscopy
<http://dx.doi.org/10.1109/JSTSP.2015.2505402> *C. Kervrann, C. O. S. Sorzano, S. T. Acton, J.-C. Olivo-Marin, and M. Unser* 6

PAPERS

Reconstruction Algorithms in Undersampled AFM Imaging <http://dx.doi.org/10.1109/JSTSP.2015.2500363>
..... *T. Arildsen, C. S. Oxvig, P. S. Pedersen, J. Østergaard, and T. Larsen* 31

Tomographic Reconstruction and Alignment Using Matrix Norm Minimization <http://dx.doi.org/10.1109/JSTSP.2015.2510163>
..... *K. Song and M. Horowitz* 47

Reconstruction From Multiple Poses in Fluorescence Imaging: Proof of Concept <http://dx.doi.org/10.1109/JSTSP.2015.2493884>
..... *D. Fortun, P. Guichard, N. Chu, and M. Unser* 61

Image Restoration Using Gradient Iteration and Constraints for Band Extrapolation <http://dx.doi.org/10.1109/JSTSP.2015.2493978>
..... *M. Ponti, E. S. Helou, P. J. S. G. Ferreira, and N. D. A. Mascarenhas* 71

Phase and TV Based Convex Sets for Blind Deconvolution of Microscopic Images <http://dx.doi.org/10.1109/JSTSP.2015.2502541>
..... *M. Tofghi, O. Yorulmaz, K. Köse, D. C. Yıldırım, R. Çetin-Atalay, and A. E. Çetin* 81

Generalized Pareto Distributions—Application to Autofocus in Automated Microscopy <http://dx.doi.org/10.1109/JSTSP.2015.2482949>
..... *R. Lenz* 92



A Natural-Scene Gradient Distribution Prior and its Application in Light-Microscopy Image Processing http://dx.doi.org/10.1109/JSTSP.2015.2506122	<i>Y. Gong and I. F. Sbalzarini</i>	99
Unsupervised Profiling of Microglial Arbor Morphologies and Distribution Using a Nonparametric Bayesian Approach http://dx.doi.org/10.1109/JSTSP.2015.2505660	<i>Y. Xu, M. Meghani, K. Trett, W. Shain, B. Roysam, and Z. Han</i>	115
Maximum Margin Learning of t-SPNs for Cell Classification With Filtered Input http://dx.doi.org/10.1109/JSTSP.2015.2502542	<i>H. Kang, C. D. Yoo, and Y. Na</i>	130
Segmentation of Nuclei From 3D Microscopy Images of Tissue via Graphcut Optimization http://dx.doi.org/10.1109/JSTSP.2015.2505148 ..	<i>K. Nandy, R. Chellappa, A. Kumar, and S. J. Lockett</i>	140
A Unified Geometric Model for Virtual Slide Image Processing and Classification http://dx.doi.org/10.1109/JSTSP.2015.2482941	<i>M. Toutain, A. Elmoataz, X. Desquesnes, and J.-H. Pruvot</i>	151
Coarse-Graining of Volumes for Modeling of Structure and Dynamics in Electron Microscopy: Algorithm to Automatically Control Accuracy of Approximation http://dx.doi.org/10.1109/JSTSP.2015.2489186	<i>S. Jonić and C. O. S. Sorzano</i>	161
Segmentation and Track-Analysis in Time-Lapse Imaging of Bacteria http://dx.doi.org/10.1109/JSTSP.2015.2491304	<i>S. K. Sadanandan, O. Baltekin, K. E. G. Magnusson, A. Boucharin, P. Ranefall, J. Jaldén, J. Elf, and C. Wählby</i>	174
A Probabilistic Relaxation Labeling (PRL) Based Method for <i>C. elegans</i> Cell Tracking in Microscopic Image Sequences http://dx.doi.org/10.1109/JSTSP.2015.2503924	<i>L. Chen, Z. Zhao, and H. Yan</i>	185
Marker-Less Stage Drift Correction in Super-Resolution Microscopy Using the Single-Cluster PHD Filter http://dx.doi.org/10.1109/JSTSP.2015.2506402	<i>I. Schlangen, J. Franco, J. Houssineau, W. T. E. Pitkeathly, D. Clark, I. Smal, and C. Rickman</i>	193
Counting-Based Particle Flux Estimation for Traffic Analysis in Live Cell Imaging http://dx.doi.org/10.1109/JSTSP.2015.2482460	<i>T. Pécot, C. Kervrann, J. Salamero, and J. Boulanger</i>	203

CALL FOR PAPERS*IEEE Signal Processing Society***IEEE Journal of Selected Topics in Signal processing***Special Issue on Advances in Time/Frequency Modulated Array Signal Processing***Aims and Scope**

In recent years, time/frequency modulated array techniques have developed beyond the focus of antenna design to address promising applications in radar, navigation, communications, microwave imaging, and biomedical engineering. Specifically, a time modulated array (TMA), by connecting and disconnecting the elements from the feed network, can create a beampattern with low sidelobes. Two typical frequency modulated arrays are the frequency diverse array (FDA) and multiple-input multiple-output (MIMO). The former produces a range-dependent pattern, whereas the latter provides increased degrees-of-freedom.

There are still many technical challenges for time/frequency modulated arrays, which include: (a) optimization of array parameters involving waveform design is required to further assess their effects on performance; (b) although linear array geometry is predominantly considered in the literature, theoretical analysis and applications of time/frequency modulated arrays should expose possible benefits of alternative geometries, and direct further studies toward advanced concepts for novel array structures; and (c) optimal time/frequency modulated array signal processing algorithms should be devised to address the issues of range, time, angle, and frequency dependent responses for target localization and dimensionality reduction. There is thus a huge demand for developing innovative, effective and efficient signal processing algorithms for time/frequency modulated array techniques and systems.

This special issue will touch on a wide variety of signal processing topics for optimal time/frequency modulated array design and their potential applications. It aims to compile relevant research contributions from various disciplines including signal processing, radar, wireless communications, antenna array design, geophysics, biomedical engineering, and applied mathematics to foster future research in this emerging area.

Topics of Interest include (but not limited to):

Signal Processing for Optimal Array Design	Potential Applications
– Space, time / range and frequency signal processing	– Cognitive radar / communications
– Dimensionality reduction algorithms	– Physical security communications
– Range-coupled adaptive signal processing	– Low probability of identification (LPI) radar
– Biomimetic spatial processing	– Adaptive interference/clutter suppression
– Array manifold analysis	– Ground moving target indication
– Low-sidelobe beampattern synthesis	– Microwave imaging
– Array parameter optimization and design	– Source detection and estimation
– Multidimensional waveform design / optimization	– Target localization and tracking
– Information fusion and knowledge extraction	– MIMO / hybrid array / stealth radar
– Array calibration and diagnosis	– Biomedical engineering

Important Dates:

Manuscript submission due: 1 April 2016
First review completed: 30 June 2016
Revised manuscript due: 15 August 2016
Second review completed: 1 October 2016
Final manuscript due: 15 November 2016
Publication: March 2017

Prospective authors should visit <http://www.signalprocessingsociety.org/publications/periodicals/jstsp/> for information on paper submission. Manuscripts should be submitted at <http://mc.manuscriptcentral.com/jstsp-ieee>.

Guest Editors:

Hing Cheung So, City University of Hong Kong, Hong Kong, email: hcs0@ee.cityu.edu.hk

Moeness G. Amin, Villanova University, USA, email: moeness.amin@villanova.edu

Shannon Blunt, University of Kansas, USA, email: sdblunt@ittc.ku.edu

Fulvio Gini, University of Pisa, Italy, email: f.gini@ing.unipi.it

Wen-Qin Wang, University of Electronic Science and Technology of China, China, email: wqwang@uestc.edu.cn

IEEE

SIGNAL PROCESSING LETTERS

A PUBLICATION OF THE IEEE SIGNAL PROCESSING SOCIETY


www.ieee.org/sp/index.html

JANUARY 2016

VOLUME 23

NUMBER 1

ISPLEM

(ISSN 1070-9908)

 Dear *Signal Processing Letters* Readers <http://dx.doi.org/10.1109/LSP.2015.2511258> *P. Willett* 5

LETTERS

Speech Enhancement with Nonstationary Acoustic Noise Detection in Time Domain http://dx.doi.org/10.1109/LSP.2015.2495102	<i>R. Tavares and R. Coelho</i>	6
An Effective Video Synopsis Approach with Seam Carving http://dx.doi.org/10.1109/LSP.2015.2496558	<i>K. Li, B. Yan, W. Wang, and H. Gharavi</i>	11
An Optimal Dimensionality Sampling Scheme on the Sphere with Accurate and Efficient Spherical Harmonic Transform for Diffusion MRI http://dx.doi.org/10.1109/LSP.2015.2498162	<i>A. P. Bates, Z. Khalid, and R. A. Kennedy</i>	15
Channel Capacity Analysis of the Multiple Orthogonal Sequence Spread Spectrum Watermarking in Audio Signals http://dx.doi.org/10.1109/LSP.2015.2497460	<i>Z. Xu, C. Ao, and B. Huang</i>	20
Consistent Basis Pursuit for Signal and Matrix Estimates in Quantized Compressed Sensing http://dx.doi.org/10.1109/LSP.2015.2497543 ..	<i>A. Moshtaghpour, L. Jacques, V. Cambareli, K. Degraux, and C. De Vleeschouwer</i>	25
An Improved Soft-Input Soft-Output Detector for Generalized Spatial Modulation http://dx.doi.org/10.1109/LSP.2015.2498147	<i>L. Xiao, P. Yang, Y. Xiao, J. Liu, S. Fan, B. Dong, and S. Li</i>	30
Importance Sampling-Based Maximum Likelihood Estimation for Multidimensional Harmonic Retrieval http://dx.doi.org/10.1109/LSP.2015.2498195	<i>W.-H. Fang, Y.-C. Lee, and Y.-T. Chen</i>	35
Patch-based Scale Calculation for Real-time Visual Tracking http://dx.doi.org/10.1109/LSP.2015.2479360	<i>Y. Xu, J. Wang, H. Li, Y. Li, Z. Miao, and Y. Zhang</i>	40
Detection of Moving Objects Using Fuzzy Color Difference Histogram Based Background Subtraction http://dx.doi.org/10.1109/LSP.2015.2498839	<i>D. K. Panda and S. Meher</i>	45

Wireless Networks with Energy Harvesting and Power Transfer: Joint Power and Time Allocation http://dx.doi.org/10.1109/LSP.2015.2500340	<i>Z. Hadzi-Velkov, I. Nikoloska, G. K. Karagiannidis, and T. Q. Duong</i>	50
Affine-Transformation Parameters Regression for Face Alignment http://dx.doi.org/10.1109/LSP.2015.2499778	<i>X. Li, Y. Xu, Q. Lv, and Y. Dou</i>	55
Robustness Analysis of Structured Matrix Factorization via Self-Dictionary Mixed-Norm Optimization http://dx.doi.org/10.1109/LSP.2015.2498523	<i>X. Fu and W.-K. Ma</i>	60
Decision Fusion for Image Quality Assessment using an Optimization Approach http://dx.doi.org/10.1109/LSP.2015.2500819	<i>M. Oszust</i>	65
Integer 2-D Discrete Fourier Transform Pairs and Eigenvectors using Ramanujan's Sum http://dx.doi.org/10.1109/LSP.2015.2501421	<i>S.-C. Pei and K.-W. Chang</i>	70
Fast Matrix Inversion Updates for Massive MIMO Detection and Precoding http://dx.doi.org/10.1109/LSP.2015.2500682	<i>F. Rosário, F. A. Monteiro, and A. Rodrigues</i>	75
On the Properties of Cubic Metric for OFDM Signals http://dx.doi.org/10.1109/LSP.2015.2502261	<i>K.-H. Kim, J.-S. No, and D.-J. Shin</i>	80
Similarity Learning with Top-heavy Ranking Loss for Person Re-identification http://dx.doi.org/10.1109/LSP.2015.2502271	<i>J. Wang, N. Sang, Z. Wang, and C. Gao</i>	84
A Path-following Algorithm for Robust Point Matching http://dx.doi.org/10.1109/LSP.2015.2501546	<i>W. Lian</i>	89
Multichannel Double-Talk Detector based on Fundamental Frequency Estimation http://dx.doi.org/10.1109/LSP.2015.2502761	<i>S. Cecchi, L. Romoli, and F. Piazza</i>	94
Regularized Kernel Least Mean Square Algorithm with Multiple-delay Feedback http://dx.doi.org/10.1109/LSP.2015.2503000	<i>S. Wang, Y. Zheng, and C. Ling</i>	98
Joint Learning of Multiple Regressors for Single Image Super-Resolution http://dx.doi.org/10.1109/LSP.2015.2504121	<i>K. Zhang, B. Wang, W. Zuo, H. Zhang, and L. Zhang</i>	102
A Full-Duplex Bob in the MIMO Gaussian Wiretap Channel: Scheme and Performance http://dx.doi.org/10.1109/LSP.2015.2504396	<i>L. Li, Z. Chen, D. Zhang, and J. Fang</i>	107
Joint Robust Transmit/Receive Adaptive Beamforming for MIMO Radar Using Probability-Constrained Optimization http://dx.doi.org/10.1109/LSP.2015.2504386	<i>W. Zhang and S. A. Vorobyov</i>	112
Adaptive Overhearing in Two-Way Multi-Antenna Relay Channels http://dx.doi.org/10.1109/LSP.2015.2504559	<i>C. Li, H. J. Yang, F. Sun, J. M. Cioffi, and L. Yang</i>	117
Interference-plus-Noise Covariance Matrix Reconstruction via Spatial Power Spectrum Sampling for Robust Adaptive Beamforming http://dx.doi.org/10.1109/LSP.2015.2504954	<i>Z. Zhang, W. Liu, W. Leng, A. Wang, and H. Shi</i>	121
Probabilistic Kernels for Improved Text-to-Speech Alignment in Long Audio Tracks http://dx.doi.org/10.1109/LSP.2015.2505140	<i>G. Bordel, M. Penagarikano, L. J. Rodríguez-Fuentes, A. Álvarez, and A. Varona</i>	126
Adaptive Reversible Data Hiding by Extending the Generalized Integer Transformation http://dx.doi.org/10.1109/LSP.2015.2504464	<i>Y. Qiu, Z. Qian, and L. Yu</i>	130
Complex Exponential Pseudomodes of LTI Operators Over Finite Intervals http://dx.doi.org/10.1109/LSP.2015.2504877	<i>P. A. Kelly and S. Kibria</i>	135
Iterative Time-Frequency Filtering of Sinusoidal Signals With Updated Frequency Estimation http://dx.doi.org/10.1109/LSP.2015.2504565 ..	<i>H. Zhang, L. Yu, and G.-S. Xia</i>	139
A Simple and Accurate TDOA-AOA Localization Method Using Two Stations http://dx.doi.org/10.1109/LSP.2015.2505138	<i>J. Yin, Q. Wan, S. Yang, and K. C. Ho</i>	144
Covariance-Assisted Matching Pursuit http://dx.doi.org/10.1109/LSP.2015.2506684	<i>A. Adler</i>	149
Human Body Part Selection by Group Lasso of Motion for Model-Free Gait Recognition http://dx.doi.org/10.1109/LSP.2015.2507200	<i>I. Rida, X. Jiang, and G. L. Marcialis</i>	154
Analysis of Additional Stable Gain by Frequency Shifting for Acoustic Feedback Suppression using Statistical Room Acoustics http://dx.doi.org/10.1109/LSP.2015.2507205	<i>C. Zheng, C. Hofmann, X. Li, and W. Kellermann</i>	159
On The Exact Recovery Condition of Simultaneous Orthogonal Matching Pursuit http://dx.doi.org/10.1109/LSP.2015.2506989	<i>J.-F. Determe, J. Louveaux, L. Jacques, and F. Horlin</i>	164
Improved Tampering Localization in Digital Image Forensics Based on Maximal Entropy Random Walk http://dx.doi.org/10.1109/LSP.2015.2507598	<i>P. Korus and J. Huang</i>	169
Compressive Parameter Estimation for Correlated Frames in MIMO Visible Light Communications http://dx.doi.org/10.1109/LSP.2015.2506683	<i>J. Perez-Ramirez and D. K. Borah</i>	174
A Simple Sampler for the Horseshoe Estimator http://dx.doi.org/10.1109/LSP.2015.2503725	<i>E. Makalic and D. F. Schmidt</i>	179

IEEE SignalProcessing

MAGAZINE

[VOLUME 33 NUMBER 1 JANUARY 2016]

TAKING SPS TO NEW HEIGHTS

**BAYESIAN MACHINE LEARNING
FOR EEG/MEG**

DECISION LEARNING

**BLOCK-STRUCTURED OPTIMIZATION
FOR BIG DATA**

COMPRESSIVE COVARIANCE SENSING

GAME THEORY FOR NETWORKS

COMBINATIONS OF ADAPTIVE FILTER

IEEE
Signal Processing Society

IEEE

[CONTENTS]

[VOLUME 33 NUMBER 1]

[FEATURES]

[LEARNING]

14 BAYESIAN MACHINE LEARNING

Wei Wu, Srikantan Nagarajan,
and Zhe Chen

37 DECISION LEARNING

Yan Chen, Chunxiao Jiang,
Chih-Yu Wang, Yang Gao,
and K.J. Ray Liu

[BIG DATA]

57 A UNIFIED ALGORITHMIC FRAMEWORK FOR BLOCK-STRUCTURED OPTIMIZATION INVOLVING BIG DATA

Mingyi Hong, Meisam Razaviyayn,
Zhi-Quan Luo, and Jong-Shi Pang

[THEORY AND METHODS]

78 COMPRESSIVE COVARIANCE SENSING

Daniel Romero, Dyonisius Dony Ariananda,
Zhi Tian, and Geert Leus

94 GAME THEORY FOR NETWORKS

Giacomo Bacci, Samson Lasaulce,
Walid Saad, and Luca Sanguinetti

120 COMBINATIONS OF ADAPTIVE FILTERS

Jerónimo Arenas-García,
Luis A. Azpicueta-Ruiz,
Magno T.M. Silva, Vítor H. Nascimento,
and Ali H. Sayed

[COLUMNS]

4 FROM THE EDITOR

Women in Science, Engineering,
and Signal Processing
Min Wu

6 PRESIDENT'S MESSAGE

We Need Your Help to Take
the Society to New Heights
Alex Acero

11 SPECIAL REPORTS

Signal Processing Research
Resonates with
Hearing Loss Sufferers
John Edwards

141 REFLECTIONS

James L. Flanagan: A Scholar
and a True Gentleman
Lawrence Rabiner

144 LECTURE NOTES

Polyphase Channelizer Demystified
P. Murali Krishna
and T.P. Sameer Babu

151 SP TIPS&TRICKS

Cascading Tricks for Designing
Composite Filters with Sharp
Transition Bands
David Shiung, Ya-Yin Yang,
and Chu-Sing Yang

158 STANDARDS IN A NUTSHELL

Next-Generation Broadcast
Television: ATSC 3.0
Richard Chernock
and Jerry C. Whitaker

163 BOOK REVIEWS

Foundations of Signal Processing
Andres Kwasinski

*Handbook of Digital Forensics
of Multimedia Data and Devices*
Luisa Verdoliva

166 BOOK DIGEST

[DEPARTMENTS]

7 SOCIETY NEWS

2016 Class of Distinguished
Lecturers

IEEE Signal Processing Society
Young Professionals Meet
During ICIP 2015

168 DATES AHEAD

Digital Object Identifier 10.1109/MSP.2015.2479476

CALL FOR PAPERS AND PROPOSALS
2016 IEEE 3rd World Forum on Internet of Things (WF-IoT)
12-14 December 2016 — Reston, USA
<http://sites.ieee.org/wf-iot-2016/>

IoT: Smart Innovation for Vibrant Ecosystems

The 2016 IEEE 3rd World Forum on Internet of Things (WF-IoT) seeks contributions on how to nurture and cultivate IoT technologies and applications for the benefit of society. Original papers are solicited in, but are not limited to, the following topics:

IoT Enabling Technologies

- 5G Networks and IoT
- Software Defined Network (SDN) and IoT
- Sensor and Actuator Networks
- Ultra-low power IoT Technologies and Embedded Systems Architectures
- Wearables, Body Sensor Networks, Smart Portable Devices
- Design Space Exploration Techniques for IoT Devices and Systems
- Heterogeneous Networks, Web of Things, Web of Everything
- IoT Protocols (IPv6, 6LoWPAN, RPL, 6TiSCH, W3C)
- Internet of Nano Things
- Sensors Data Management, IoT Mining and Analytics
- Adaptive Systems and Models at Runtime
- Distributed Storage, Data Fusion
- Routing and Control Protocols
- Resource Management, Access Control
- Mobility, Localization and Management Aspects
- Identity Management and Object Recognition
- Localization Technologies
- Edge Computing, Fog Computing and IoT
- Machine to Machine (M2M)/Devices-to-Devices communications and IoT
- Industrial IoT and Factory of Things and Internet of Things

IoT Application and Services

- Cyber-physical systems, Context Awareness, Situation Awareness, Ambient Intelligence
- Collaborative Applications and Systems
- Service Experiences and Analysis
- Smart Cities, Smart Public Places, Smart Home/Building Automation
- e-Health, e-Wellness, Automotive, Intelligent Transport
- Smart Grid, Energy Management
- Consumer Electronics, Assisted Living, Rural Services and Production
- Industrial IoT Service Creation and Management Aspects
- Crowd-sensing, human centric sensing
- Big data and IoT Data Analytics
- Internet Applications Naming and Identifiers
- Semantic Technologies, Collective Intelligence
- Cognitive and Reasoning about Things and Smart Objects
- Mobile Cloud Computing (MCC) and IoT
- IoT Multimedia

IoT Societal Impacts

- Human Role in the IoT, Social Aspects and Services
- Value Chain Analysis and Evolution Aspects
- New Human-Device Interactions for IoT, Do-It-Yourself
- Social Models and Networks
- Green IoT: Sustainable Design and Technologies
- Urban Dynamics and crowdsourcing services
- Metrics, Measurements, and Evaluation of IoT Sustainability and ROI

2016 IEEE Workshop on Multimedia Signal Processing

Sept. 21-23, 2016
Montréal, Canada

<http://www.mmsp2016.org/>

General Co-Chairs

Christine GUILLEMOT, *INRIA, France*
Douglas O'SHAUGHNESSY, *INRS-EMT, Canada*

Technical Program Co-Chairs

Ricardo DE QUEIROZ, *Universidade de Brasilia, Brazil*;
Tiago H. FALK, *INRS-EMT, Canada*
Shrikanth NARAYANAN, *University of Southern California, USA*

Plenary and Panel Co-Chairs

Zhou WANG, *University of Waterloo, Canada*
Dong XU, *Nanyang Technological University, Singapore*

Local Arrangements Chair:

Jean-Charles GRÉGOIRE, *INRS-EMT, Canada*

Finance Chair

Fabrice LABEAU, *McGill University, Canada*

Publicity Chair

Alexandros POTAMIANOS, *National Technical University of Athens, Greece*

Publications Chair

Xiaokang YANG, *Shanghai Jiao Tong University, China*

Special Sessions Co-Chairs:

Alain APRIL *École de Technologie Supérieure (ETS), Canada*
Mohamed CHÉRIET, *École de Technologie Supérieure (ETS), Canada*

Demo/industry Co-Chairs

Stéphane COULOMBE, *École de Technologie Supérieure (ETS), Canada*
Sebastian MÖLLER, *TU Berlin, Germany*

Europe Liaison

Benoit MACQ, *Université catholique de Louvain, Belgium*

MMSp 2016 is the 18th International Workshop on Multimedia Signal Processing. The workshop is organized by the Multimedia Signal Processing Technical Committee of the IEEE Signal Processing Society. This year's event has a theme of 'Enhancing the Multimedia Experience in the 21st Century.'

The multimedia communications industry is going through a phase of rapid development and new services are emerging continuously, such as multimedia telepresence, augmented and virtual reality, immersive gaming, multimedia human-computer interfaces, and novel sensory interfaces, to name a few. Moreover, traditional multimedia content (e.g., audio, video, images) is increasingly being delivered over heterogeneous networks and consumed in a wide variety of formats, bit and compression rates, and display sizes. Ultimately, the success or failure of an emerging multimedia service will rely on the end-user's perception of quality and quality-of-experience. As such, in order to remain competitive, service providers have to ensure that end-users are delivered media content that is fulfilling, engaging, and, of course, of high quality. This is not a simple task and requires insights from multiple disciplines, such as engineering, computer science, psychology, and cognitive science, to name a few. The goal of the 2016 International Workshop on Multimedia Signal Processing will be to bring experts from such interdisciplinary domains to discuss ways of *Enhancing the Multimedia Experience in the 21st Century*.

Papers are solicited in (but not limited to) the following areas, covering not only the workshop's theme, but also the general scope of multimedia signal processing:

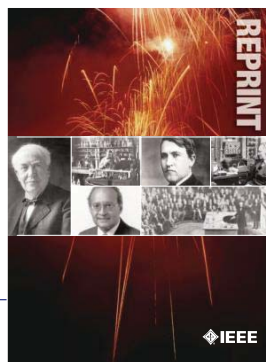
1. Augmented, mixed and virtual reality
2. Multiple sensorial media (multimedia) and multimedia environments
3. Multimedia signal processing in immersive gaming
4. Multimedia enhancement
5. Human-centric multimedia signal processing
6. Affective computing and cross-media sentiment analysis
7. Media algorithm optimization and complexity analysis
8. Multimedia applications in the humanities (finance, business analytics), health, and consumer domains
9. Image/video coding and processing
10. Speech/audio coding and processing
11. Multimedia traffic, communications and heterogeneous interactions

Important Dates

Proposals for Special Sessions: March 15, 2016
Submission of Papers: **May 15, 2016**
Notification of Acceptance: June 30, 2016
Camera Ready Deadline: July 10, 2016
Conference Dates: September 21-23, 2016



IEEE
Signal Processing Society



IEEE ORDER FORM FOR REPRINTS

Purchasing IEEE Papers in Print is easy, cost-effective and quick.

Complete this form, send via our secure fax (24 hours a day) to 732-981-8062 or mail it back to us.

PLEASE FILL OUT THE FOLLOWING

Author: _____

Publication Title: _____

Paper Title: _____

RETURN THIS FORM TO:
 IEEE Publishing Services
 445 Hoes Lane
 Piscataway, NJ 08855-1331

Email the Reprint Department at
reprints@ieee.org **for questions regarding**
this form

PLEASE SEND ME

- 50 100 200 300 400 500 or _____ (in multiples of 50) reprints.
- YES NO Self-covering/title page required. COVER PRICE: \$74 per 100, \$39 per 50.
- \$58.00 Air Freight must be added for all orders being shipped outside the U.S.
- \$21.50 must be added for all USA shipments to cover the cost of UPS shipping and handling.

PAYMENT

- Check enclosed. Payable on a bank in the USA.
- Charge my: Visa Mastercard Amex Diners Club

Account # _____ Exp. date _____

Cardholder's Name (please print): _____

Bill me (you must attach a purchase order) Purchase Order Number _____

Send Reprints to: _____ Bill to address, if different: _____

Because information and papers are gathered from various sources, there may be a delay in receiving your reprint request. This is especially true with postconference publications. Please provide us with contact information if you would like notification of a delay of more than 12 weeks.

Telephone: _____ Fax: _____ Email Address: _____

2012 REPRINT PRICES (without covers)

Number of Text Pages

	1-4	5-8	9-12	13-16	17-20	21-24	25-28	29-32	33-36	37-40	41-44	45-48
50	\$129	\$213	\$245	\$248	\$288	\$340	\$371	\$408	\$440	\$477	\$510	\$543
100	\$245	\$425	\$479	\$495	\$573	\$680	\$742	\$817	\$885	\$953	\$1021	\$1088

Larger quantities can be ordered. Email reprints@ieee.org with specific details.

Tax Applies on shipments of regular reprints to CA, DC, FL, MI, NJ, NY, OH and Canada (GST Registration no. 12534188).
 Prices are based on black & white printing. Please call us for full color price quote, if applicable.

Authorized Signature: _____ Date: _____



2016 IEEE MEMBERSHIP APPLICATION

(students and graduate students must apply online)

Start your membership immediately: Join online www.ieee.org/join

Please complete both sides of this form, typing or **printing in capital letters**. Use only English characters and abbreviate only if more than 40 characters and spaces per line. We regret that incomplete applications cannot be processed.

1 Name & Contact Information

Please PRINT your name as you want it to appear on your membership card and IEEE correspondence. As a key identifier for the IEEE database, circle your last/surname.

Male Female Date of birth (Day/Month/Year) ____/____/____

Title First/Given Name Middle Last/Family Surname

▼ **Primary Address** Home Business (All IEEE mail sent here)

Street Address

City State/Province

Postal Code Country

Primary Phone

Primary E-mail

▼ **Secondary Address** Home Business

Company Name Department/Division

Street Address City State/Province

Postal Code Country

Secondary Phone

Secondary E-mail

To better serve our members and supplement member dues, your postal mailing address is made available to carefully selected organizations to provide you with information on technical services, continuing education, and conferences. Your e-mail address is **not** rented by IEEE. Please check box **only** if you do not want to receive these postal mailings to the selected address.

2 Attestation

I have graduated from a three- to five-year academic program with a university-level degree.

Yes No

This program is in one of the following fields of study:

- Engineering
- Computer Sciences and Information Technologies
- Physical Sciences
- Biological and Medical Sciences
- Mathematics
- Technical Communications, Education, Management, Law and Policy
- Other (please specify): _____

This academic institution or program is accredited in the country where the institution is located. Yes No Do not know

I have _____ years of professional experience in teaching, creating, developing, practicing, or managing within the following field:

- Engineering
- Computer Sciences and Information Technologies
- Physical Sciences
- Biological and Medical Sciences
- Mathematics
- Technical Communications, Education, Management, Law and Policy
- Other (please specify): _____

3 Please Tell Us About Yourself

Select the numbered option that best describes yourself. This information is used by IEEE magazines to verify their annual circulation. Please enter numbered selections in the boxes provided.

A. Primary line of business _____ →

1. Computers
2. Computer peripheral equipment
3. Software
4. Office and business machines
5. Test, measurement and instrumentation equipment
6. Communications systems and equipment
7. Navigation and guidance systems and equipment
8. Consumer electronics/appliances
9. Industrial equipment, controls and systems
10. ICs and microprocessors
11. Semiconductors, components, sub-assemblies, materials and supplies
12. Aircraft, missiles, space and ground support equipment
13. Oceanography and support equipment
14. Medical electronic equipment
15. OEM incorporating electronics in their end product (not elsewhere classified)
16. Independent and university research, test and design laboratories and consultants (not connected with a mfg. co.)
17. Government agencies and armed forces
18. Companies using and/or incorporating any electronic products in their manufacturing, processing, research or development activities
19. Telecommunications services, telephone (including cellular)
20. Broadcast services (TV, cable, radio)
21. Transportation services (airline, railroad, etc.)
22. Computer and communications and data processing services
23. Power production, generation, transmission and distribution
24. Other commercial users of electrical, electronic equipment and services (not elsewhere classified)
25. Distributor (reseller, wholesaler, retailer)
26. University, college/other educational institutions, libraries
27. Retired
28. Other _____

B. Principal job function _____ →

- | | |
|--|--|
| 1. General and corporate management | 9. Design/development engineering—digital |
| 2. Engineering management | 10. Hardware engineering |
| 3. Project engineering management | 11. Software design/development management |
| 4. Research and development management | 12. Computer science |
| 5. Design engineering management—analogue | 13. Science/physics/mathematics |
| 6. Design engineering management—digital | 14. Engineering (not elsewhere specified) |
| 7. Research and development engineering | 15. Marketing/sales/purchasing |
| 8. Design/development engineering—analogue | 16. Consulting |
| | 17. Education/teaching |
| | 18. Retired |
| | 19. Other _____ |

C. Principal responsibility _____ →

- | | |
|--|-----------------------|
| 1. Engineering and scientific management | 6. Education/teaching |
| 2. Management other than engineering | 7. Consulting |
| 3. Engineering design | 8. Retired |
| 4. Engineering | 9. Other _____ |
| 5. Software: science/mngmnt/engineering | |

D. Title _____ →

- | | |
|--|--------------------------------|
| 1. Chairman of the Board/President/CEO | 10. Design Engineering Manager |
| 2. Owner/Partner | 11. Design Engineer |
| 3. General Manager | 12. Hardware Engineer |
| 4. VP Operations | 13. Software Engineer |
| 5. VP Engineering/Dir. Engineering | 14. Computer Scientist |
| 6. Chief Engineer/Chief Scientist | 15. Dean/Professor/Instructor |
| 7. Engineering Management | 16. Consultant |
| 8. Scientific Management | 17. Retired |
| 9. Member of Technical Staff | 18. Other _____ |

Are you now or were you ever a member of IEEE?
 Yes No If yes, provide, if known:

Membership Number _____ Grade _____ Year Expired _____

4 Please Sign Your Application

I hereby apply for IEEE membership and agree to be governed by the IEEE Constitution, Bylaws, and Code of Ethics. I understand that IEEE will communicate with me regarding my individual membership and all related benefits. **Application must be signed.**

Signature _____ Date _____ *Over Please*

(continued on next page)

5 Add IEEE Society Memberships (Optional)

The 39 IEEE Societies support your technical and professional interests. Many society memberships include a personal subscription to the core journal, magazine, or newsletter of that society. **For a complete list of everything included with your IEEE Society membership, visit www.ieee.org/join.** All prices are quoted in US dollars.

Please check the appropriate box.

		BETWEEN 16 AUG 2015- 28 FEB 2016 PAY	BETWEEN 1 MAR 2016- 15 AUG 2016 PAY
IEEE Aerospace and Electronic Systems	AES010	25.00 <input type="checkbox"/>	12.50 <input type="checkbox"/>
IEEE Antennas and Propagation	AP003	15.00 <input type="checkbox"/>	7.50 <input type="checkbox"/>
IEEE Broadcast Technology	BT002	15.00 <input type="checkbox"/>	7.50 <input type="checkbox"/>
IEEE Circuits and Systems	CAS004	22.00 <input type="checkbox"/>	11.00 <input type="checkbox"/>
IEEE Communications	COM019	30.00 <input type="checkbox"/>	15.00 <input type="checkbox"/>
IEEE Components, Packaging, & Manu. Tech.	CPMT021	15.00 <input type="checkbox"/>	7.50 <input type="checkbox"/>
IEEE Computational Intelligence	CIS011	29.00 <input type="checkbox"/>	14.50 <input type="checkbox"/>
IEEE Computer	CO16	56.00 <input type="checkbox"/>	28.00 <input type="checkbox"/>
IEEE Consumer Electronics	CE008	20.00 <input type="checkbox"/>	10.00 <input type="checkbox"/>
IEEE Control Systems	CS023	25.00 <input type="checkbox"/>	12.50 <input type="checkbox"/>
IEEE Dielectrics and Electrical Insulation	DEI032	26.00 <input type="checkbox"/>	13.00 <input type="checkbox"/>
IEEE Education	EO25	20.00 <input type="checkbox"/>	10.00 <input type="checkbox"/>
IEEE Electromagnetic Compatibility	EMC027	31.00 <input type="checkbox"/>	15.50 <input type="checkbox"/>
IEEE Electron Devices	ED015	18.00 <input type="checkbox"/>	9.00 <input type="checkbox"/>
IEEE Engineering in Medicine and Biology	EMB018	40.00 <input type="checkbox"/>	20.00 <input type="checkbox"/>
IEEE Geoscience and Remote Sensing	GRS029	19.00 <input type="checkbox"/>	9.50 <input type="checkbox"/>
IEEE Industrial Electronics	IE013	9.00 <input type="checkbox"/>	4.50 <input type="checkbox"/>
IEEE Industry Applications	IA034	20.00 <input type="checkbox"/>	10.00 <input type="checkbox"/>
IEEE Information Theory	IT012	30.00 <input type="checkbox"/>	15.00 <input type="checkbox"/>
IEEE Instrumentation and Measurement	IM009	29.00 <input type="checkbox"/>	14.50 <input type="checkbox"/>
IEEE Intelligent Transportation Systems	ITSS038	35.00 <input type="checkbox"/>	17.50 <input type="checkbox"/>
IEEE Magnetics	MAG033	26.00 <input type="checkbox"/>	13.00 <input type="checkbox"/>
IEEE Microwave Theory and Techniques	MIT017	17.00 <input type="checkbox"/>	8.50 <input type="checkbox"/>
IEEE Nuclear and Plasma Sciences	NPS005	35.00 <input type="checkbox"/>	17.50 <input type="checkbox"/>
IEEE Oceanic Engineering	OE022	19.00 <input type="checkbox"/>	9.50 <input type="checkbox"/>
IEEE Photonics	PHO036	34.00 <input type="checkbox"/>	17.00 <input type="checkbox"/>
IEEE Power Electronics	PEL035	25.00 <input type="checkbox"/>	12.50 <input type="checkbox"/>
IEEE Power & Energy	PE031	35.00 <input type="checkbox"/>	17.50 <input type="checkbox"/>
IEEE Product Safety Engineering	PSE043	35.00 <input type="checkbox"/>	17.50 <input type="checkbox"/>
IEEE Professional Communication	PC026	31.00 <input type="checkbox"/>	15.50 <input type="checkbox"/>
IEEE Reliability	RL007	35.00 <input type="checkbox"/>	17.50 <input type="checkbox"/>
IEEE Robotics and Automation	RA024	9.00 <input type="checkbox"/>	4.50 <input type="checkbox"/>
IEEE Signal Processing	SP001	22.00 <input type="checkbox"/>	11.00 <input type="checkbox"/>
IEEE Social Implications of Technology	SIT030	33.00 <input type="checkbox"/>	16.50 <input type="checkbox"/>
IEEE Solid-State Circuits	SSC037	22.00 <input type="checkbox"/>	11.00 <input type="checkbox"/>
IEEE Systems, Man, & Cybernetics	SMC028	12.00 <input type="checkbox"/>	6.00 <input type="checkbox"/>
IEEE Technology & Engineering Management	TEM014	35.00 <input type="checkbox"/>	17.50 <input type="checkbox"/>
IEEE Ultrasonics, Ferroelectrics, & Frequency Control	UFFC020	20.00 <input type="checkbox"/>	10.00 <input type="checkbox"/>
IEEE Vehicular Technology	VT006	18.00 <input type="checkbox"/>	9.00 <input type="checkbox"/>

Legend—Society membership includes:

- One or more Society publications
- Society newsletter
- Online access to publication
- CD-ROM of selected society publications

Complete both sides of this form, sign, and return to:

IEEE MEMBERSHIP APPLICATION PROCESSING
445 HOES LN, PISCATAWAY, NJ 08854-4141 USA
or fax to +1 732 981 0225
or join online at www.ieee.org/join

Please reprint your full name here

6 2016 IEEE Membership Rates
(student rates available online)

IEEE member dues and regional assessments are based on where you live and when you apply. Membership is based on the calendar year from 1 January through 31 December. All prices are quoted in US dollars.

Please check the appropriate box.

RESIDENCE	BETWEEN 16 AUG 2015- 28 FEB 2016 PAY	BETWEEN 1 MAR 2016- 15 AUG 2016 PAY
United States.....	\$197.00 <input type="checkbox"/>	\$98.50 <input type="checkbox"/>
Canada (GST)*.....	\$173.35 <input type="checkbox"/>	\$86.68 <input type="checkbox"/>
Canada (NB, NF and ON HST)*.....	\$185.11 <input type="checkbox"/>	\$92.56 <input type="checkbox"/>
Canada (Nova Scotia HST)*.....	\$188.05 <input type="checkbox"/>	\$94.03 <input type="checkbox"/>
Canada (PEI HST)*.....	\$186.58 <input type="checkbox"/>	\$93.29 <input type="checkbox"/>
Canada (GST and QST Quebec).....	\$188.01 <input type="checkbox"/>	\$94.01 <input type="checkbox"/>
Africa, Europe, Middle East.....	\$160.00 <input type="checkbox"/>	\$80.00 <input type="checkbox"/>
Latin America.....	\$151.00 <input type="checkbox"/>	\$75.50 <input type="checkbox"/>
Asia, Pacific.....	\$152.00 <input type="checkbox"/>	\$76.00 <input type="checkbox"/>

*IEEE Canada Business No. 125634188

Minimum Income or Unemployed Provision

Applicants who certify that their prior year income did not exceed US\$14,700 (or equivalent) or were not employed are granted 50% reduction in: full-year dues, regional assessment and fees for one IEEE Membership plus one Society Membership. If applicable, please check appropriate box and adjust payment accordingly. Student members are not eligible.

- I certify I earned less than US\$14,700 in 2015
- I certify that I was unemployed in 2015

7 More Recommended Options

- Proceedings of the IEEE..... print \$47.00 or online \$41.00
- Proceedings of the IEEE (print/online combination).....\$57.00
- IEEE Standards Association (IEEE-SA).....\$53.00
- IEEE Women in Engineering (WIE).....\$25.00

8 Payment Amount

Please total the Membership dues, Society dues, and other amounts from this page:

- IEEE Membership dues\$
- IEEE Society dues (optional)\$
- IEEE-SA/WIE dues (optional)\$
- Proceedings of the IEEE (optional)\$
- Canadian residents pay 5% GST or appropriate HST (BC—12%; NB, NF, ON—13%;NS—15%) on Society payments & publications only.....TAX \$

AMOUNT PAID **TOTAL \$**

Payment Method

All prices are quoted in US dollars. You may pay for IEEE membership by credit card (see below), check, or money order payable to IEEE, drawn on a US bank.

Check

Credit Card Number

MONTH YEAR CARDHOLDER'S 5-DIGIT ZIP/PCODE (BILLING STATEMENT ADDRESS) USA ONLY

Name as it appears on card

Signature

- Auto Renew my Memberships and Subscriptions (available when paying by credit card).
- I agree to the Terms and Conditions located at www.ieee.org/autorenew

9 Were You Referred to IEEE?

- Yes No If yes, provide the following:
- Member Recruiter Name
- IEEE Recruiter's Member Number (Required)

CAMPAIGN CODE PROMO CODE

Information for Authors

(Updated/Effective January 2015)

For Transactions and Journals:

Authors are encouraged to submit manuscripts of Regular papers (papers which provide a complete disclosure of a technical premise), or Comment Correspondences (brief items that provide comment on a paper previously published in these TRANSACTIONS).

Submissions/resubmissions must be previously unpublished and may not be under consideration elsewhere.

Every manuscript must:

- i. provide a clear statement of the problem and what the contribution of the work is to the relevant research community;
- ii. state why this contribution is significant (what impact it will have);
- iii. provide citation of the published literature most closely related to the manuscript; and
- iv. state what is distinctive and new about the current manuscript relative to these previously published works.

By submission of your manuscript to these TRANSACTIONS, all listed authors have agreed to the authorship list and all the contents and confirm that the work is original and that figures, tables and other reported results accurately reflect the experimental work. In addition, the authors all acknowledge that they accept the rules established for publication of manuscripts, including agreement to pay all overlength page charges, color charges, and any other charges and fees associated with publication of the manuscript. Such charges are not negotiable and cannot be suspended. The corresponding author is responsible for obtaining consent from all co-authors and, if needed, from sponsors before submission.

In order to be considered for review, a paper must be within the scope of the journal and represent a novel contribution. A paper is a candidate for an Immediate Rejection if it is of limited novelty, e.g. a straightforward combination of theories and algorithms that are well established and are repeated on a known scenario. Experimental contributions will be rejected without review if there is insufficient experimental data. These TRANSACTIONS are published in English. Papers that have a large number of typographical and/or grammatical errors will also be rejected without review.

In addition to presenting a novel contribution, acceptable manuscripts must describe and cite related work in the field to put the contribution in context. Do not give theoretical derivations or algorithm descriptions that are easily found in the literature; merely cite the reference.

New and revised manuscripts should be prepared following the "Manuscript Submission" guidelines below, and submitted to the online manuscript system, ScholarOne Manuscripts. Do not send original submissions or revisions directly to the Editor-in-Chief or Associate Editors; they will access your manuscript electronically via the ScholarOne Manuscript system.

Manuscript Submission. Please follow the next steps.

1. *Account in ScholarOne Manuscripts.* If necessary, create an account in the on-line submission system ScholarOne Manuscripts. Please check first if you already have an existing account which is based on your e-mail address and may have been created for you when you reviewed or authored a previous paper.
2. *Electronic Manuscript.* Prepare a PDF file containing your manuscript in double-column, single-spaced format using a font size of 10 points or larger, having a margin of at least 1 inch on all sides. Upload this version of the manuscript as a PDF file "double.pdf" to the ScholarOne-Manuscripts site. Since many reviewers prefer a larger font, you are strongly encouraged to also submit a single-column, double-spaced version (11 point font or larger), which is easy to create with the templates provided **IEEE Author Digital Toolbox** (http://www.ieee.org/publications_standards/publications/authors/authors_journals.html). Page length restrictions will be determined by the double-column

version. Proofread your submission, confirming that all figures and equations are visible in your document before you "SUBMIT" your manuscript. Proofreading is critical; once you submit your manuscript, the manuscript cannot be changed in any way. You may also submit your manuscript as a .PDF or MS Word file. The system has the capability of converting your files to PDF, however it is your responsibility to confirm that the conversion is correct and there are no font or graphics issues prior to completing the submission process.

3. *EDICS (Not applicable to Journal of Selected Topics in Signal Processing).* All submissions must be classified by the author with an EDICS (Editors' Information Classification Scheme) selected from the list of EDICS published online at the at the publication's EDICS webpage (*please see the list below). Upon submission of a new manuscript, please choose the EDICS categories that best suit your manuscript. Failure to do so will likely result in a delay of the peer review process.
4. *Additional Documents for Review.* Please upload pdf versions of all items in the reference list that are not publicly available, such as unpublished (submitted) papers. Graphical abstracts and supplemental materials intended to appear with the final paper (see below) must also be uploaded for review at the time of the initial submission for consideration in the review process. Use short filenames without spaces or special characters. When the upload of each file is completed, you will be asked to provide a description of that file.
5. *Supplemental Materials.* IEEE Xplore can publish multimedia files (audio, images, video), datasets, and software (e.g. Matlab code) along with your paper. Alternatively, you can provide the links to such files in a README file that appears on Xplore along with your paper. For details, please see IEEE Author Digital Toolbox under "Multimedia." To make your work reproducible by others, these TRANSACTIONS encourages you to submit all files that can recreate the figures in your paper.
6. *Submission.* After uploading all files and proofreading them, submit your manuscript by clicking "Submit." A confirmation of the successful submission will open on screen containing the manuscript tracking number and will be followed with an e-mail confirmation to the corresponding and all contributing authors. Once you click "Submit," your manuscript cannot be changed in any way.
7. *Copyright Form and Consent Form.* By policy, IEEE owns the copyright to the technical contributions it publishes on behalf of the interests of the IEEE, its authors, and their employers; and to facilitate the appropriate reuse of this material by others. To comply with the IEEE copyright policies, authors are required to sign and submit a completed "IEEE Copyright and Consent Form" prior to publication by the IEEE. The IEEE recommends authors to use an effective electronic copyright form (eCF) tool within the ScholarOne Manuscripts system. You will be redirected to the "IEEE Electronic Copyright Form" wizard at the end of your original submission; please simply sign the eCF by typing your name at the proper location and click on the "Submit" button.

Comment Correspondence. Comment Correspondences provide brief comments on material previously published in these TRANSACTIONS. These items may not exceed 2 pages in double-column, single spaced format, using 9 point type, with margins of 1 inch minimum on all sides, and including: title, names and contact information for authors, abstract, text, references, and an appropriate number of illustrations and/or tables. Correspondence items are submitted in the same way as regular manuscripts (see "Manuscript Submission" above for instructions). Authors may also submit manuscripts of overview articles, but note that these include an additional white paper approval process <http://www.signalprocessingsociety.org/publications/overview-articles/>. [This does not apply to the Journal of Selected Topics in Signal Processing. Please contact the Editor-in-Chief.]

Digital Object Identifier

Manuscript Length. For the initial submission of a regular paper, the manuscript may not exceed 13 double-column pages (10 point font), including title; names of authors and their complete contact information; abstract; text; all images, figures and tables, appendices and proofs; and all references. Supplemental materials and graphical abstracts are not included in the page count. For regular papers, the revised manuscript may not exceed 16 double-column pages (10 point font), including title; names of authors and their complete contact information; abstract; text; all images, figures and tables, appendices and proofs; and all references. For Overview Papers, the maximum length is double that for regular submissions at each stage (please reference <http://www.signalprocessingsociety.org/publications/overview-articles/> for more information).

Note that any paper in excess of 10 pages will be subject to mandatory overlength page charges. Since changes recommended as a result of peer review may require additions to the manuscript, it is strongly recommended that you practice economy in preparing original submissions. Note: Papers submitted to the TRANSACTIONS ON MULTIMEDIA in excess of 8 pages will be subject to mandatory overlength page charges.

Exceptions to manuscript length requirements may, under extraordinary circumstances, be granted by the Editor-in-Chief. However, such exception does not obviate your requirement to pay any and all overlength or additional charges that attach to the manuscript.

Resubmission of Previously Rejected Manuscripts. Authors of manuscripts rejected from any journal are allowed to resubmit their manuscripts only once. At the time of submission, you will be asked whether your manuscript is a new submission or a resubmission of an earlier rejected manuscript. If it is a resubmission of a manuscript previously rejected by any journal, you are expected to submit supporting documents identifying the previous submission and detailing how your new version addresses all of the reviewers' comments. Papers that do not disclose connection to a previously rejected paper or that do not provide documentation as to changes made may be immediately rejected.

Author Misconduct. Author misconduct includes plagiarism, self-plagiarism, and research misconduct, including falsification or misrepresentation of results. All forms of misconduct are unacceptable and may result in sanctions and/or other corrective actions. Plagiarism includes copying someone else's work without appropriate credit, using someone else's work without clear delineation of citation, and the uncited reuse of an author's previously published work that also involves other authors. Self-plagiarism involves the verbatim copying or reuse of an authors own prior work without appropriate citation, including duplicate submission of a single journal manuscript to two different journals, and submission of two different journal manuscripts which overlap substantially in language or technical contribution. For more information on the definitions, investigation process, and corrective actions related to author misconduct, see the Signal Processing Society Policies and Procedures Manual, Section 6.1. <http://www.signalprocessingsociety.org/about-sps/governance/policy-procedure/part-2>. Author misconduct may also be actionable by the IEEE under the rules of Member Conduct.

Extensions of the Author's Prior Work. It is acceptable for conference papers to be used as the basis for a more fully developed journal submission. Still, authors are required to cite their related prior work; the papers cannot be identical; and the journal publication must include substantively novel aspects such as new experimental results and analysis or added theoretical work. The journal publication should clearly specify how the journal paper offers novel contributions when citing the prior work. Limited overlap with prior journal publications with a common author is allowed only if it is necessary for the readability of the paper, and the prior work must be cited as the primary source.

Submission Format. Authors are required to prepare manuscripts employing the on-line style files developed by IEEE, which include guidelines for abbreviations, mathematics, and graphics. All manuscripts accepted for publication will require the authors to make final submission employing these style files. The style files are available on the web at the **IEEE Author Digital Toolbox** under "Template for all TRANSACTIONS." (LaTeX and MS Word). Please note the following requirements about the abstract:

- The abstract must be a concise yet comprehensive reflection of what is in your article.
- The abstract must be self-contained, without abbreviations, footnotes, displayed equations, or references.

- The abstract must be between 150-250 words.
- The abstract should include a few keywords or phrases, as this will help readers to find it. Avoid over-repetition of such phrases as this can result in a page being rejected by search engines.

In addition to written abstracts, papers may include a graphical abstract; see http://www.ieee.org/publications_standards/publications/authors/authors_journals.html for options and format requirements.

IEEE supports the publication of author names in the native language alongside the English versions of the names in the author list of an article. For more information, see "Author names in native languages" (http://www.ieee.org/publications_standards/publications/authors/auth_names_native_lang.pdf) on the IEEE Author Digital Toolbox page.

Open Access. The publication is a hybrid journal, allowing either Traditional manuscript submission or Open Access (author-pays OA) manuscript submission. Upon submission, if you choose to have your manuscript be an Open Access article, you commit to pay the discounted \$1,750 OA fee if your manuscript is accepted for publication in order to enable unrestricted public access. Any other application charges (such as overlength page charge and/or charge for the use of color in the print format) will be billed separately once the manuscript formatting is complete but prior to the publication. If you would like your manuscript to be a Traditional submission, your article will be available to qualified subscribers and purchasers via IEEE Xplore. No OA payment is required for Traditional submission.

Page Charges.

Voluntary Page Charges. Upon acceptance of a manuscript for publication, the author(s) or his/her/their company or institution will be asked to pay a charge of \$110 per page to cover part of the cost of publication of the first ten pages that comprise the standard length (two pages, in the case of Correspondences).

Mandatory Page Charges The author(s) or his/her/their company or institution will be billed \$220 per each page in excess of the first ten published pages for regular papers and six published pages for correspondence items. (**NOTE: Papers accepted to IEEE TRANSACTIONS ON MULTIMEDIA in excess of 8 pages will be subject to mandatory overlength page charges.) These are mandatory page charges and the author(s) will be held responsible for them. They are not negotiable or voluntary. The author(s) signifies his willingness to pay these charges simply by submitting his/her/their manuscript to the TRANSACTIONS. The Publisher holds the right to withhold publication under any circumstance, as well as publication of the current or future submissions of authors who have outstanding mandatory page charge debt. No mandatory overlength page charges will be applied to overview articles in the Society's journals.

Color Charges. Color figures which appear in color only in the electronic (Xplore) version can be used free of charge. In this case, the figure will be printed in the hardcopy version in grayscale, and the author is responsible that the corresponding grayscale figure is intelligible. Color reproduction charges for print are the responsibility of the author. Details of the associated charges can be found on the IEEE Publications page.

Payment of fees on color reproduction is not negotiable or voluntary, and the author's agreement to publish the manuscript in these TRANSACTIONS is considered acceptance of this requirement.

*EDICS Webpages:

IEEE TRANSACTIONS ON SIGNAL PROCESSING:

<http://www.signalprocessingsociety.org/publications/periodicals/tsp/TSP-EDICS/>

IEEE TRANSACTIONS ON IMAGE PROCESSING:

<http://www.signalprocessingsociety.org/publications/periodicals/image-processing/tip-edics/>

IEEE/ACM TRANSACTIONS ON AUDIO, SPEECH, AND LANGUAGE / ACM:

<http://www.signalprocessingsociety.org/publications/periodicals/taslp/taslp-edics/>

IEEE TRANSACTIONS ON INFORMATION, FORENSICS AND SECURITY:

<http://www.signalprocessingsociety.org/publications/periodicals/forensics/forensics-edics/>

IEEE TRANSACTIONS ON MULTIMEDIA:

<http://www.signalprocessingsociety.org/tmm/tmm-edics/>

IEEE TRANSACTIONS ON COMPUTATIONAL IMAGING:

<http://www.signalprocessingsociety.org/publications/periodicals/tci/tci-edics/>

IEEE TRANSACTIONS ON SIGNAL AND INFORMATION PROCESSING OVER NETWORKS:

<http://www.signalprocessingsociety.org/publications/periodicals/tsipn/tsipn-edics/>

2016 IEEE SIGNAL PROCESSING SOCIETY MEMBERSHIP APPLICATION

Mail to: IEEE OPERATIONS CENTER, ATTN: Matthew Plotner, Member and Geographic Activities, 445 Hoes Lane, Piscataway, New Jersey 08854 USA
or Fax to (732) 981-0225 (credit card payments only.)

For info call (732) 981-0060 or 1 (800) 678-IEEE or E-mail: new.membership@ieee.org



1. PERSONAL INFORMATION

NAME AS IT SHOULD APPEAR ON IEEE MAILINGS: SEND MAIL TO: Home Address OR Business/School Address
If not indicated, mail will be sent to home address. Note: Enter your name as you wish it to appear on membership card and all correspondence.
PLEASE PRINT Do not exceed 40 characters or spaces per line. Abbreviate as needed. Please circle your last/surname as a key identifier for the IEEE database.

TITLE	FIRST OR GIVEN NAME	MIDDLE NAME	SURNAME/LAST NAME
HOME ADDRESS			
CITY		STATE/PROVINCE	POSTAL CODE
COUNTRY			

2. Are you now or were you ever a member of IEEE? Yes No
If yes, please provide, if known:

MEMBERSHIP NUMBER _____

Grade _____ Year Membership Expired: _____

3. BUSINESS/PROFESSIONAL INFORMATION

Company Name _____

Department/Division _____

Title/Position _____ Years in Current Position _____

Years in the Profession Since Graduation _____ PE State/Province _____

Street Address _____

City _____ State/Province _____ Postal Code _____ Country _____

4. EDUCATION

A baccalaureate degree from an IEEE recognized educational program assures assignment of "Member" grade. For others, additional information and references may be necessary for grade assignment.

A. Baccalaureate Degree Received _____ Program/Course of Study _____

College/University _____ Campus _____

State/Province _____ Country _____ Mo./Yr. Degree Received _____

B. Highest Technical Degree Received _____ Program/Course of Study _____

College/University _____ Campus _____

State/Province _____ Country _____ Mo./Yr. Degree Received _____

5. Full signature of applicant _____

6. DEMOGRAPHIC INFORMATION – ALL APPLICANTS -

Date Of Birth _____ Male Female

Day _____ Month _____ Year _____

7. CONTACT INFORMATION

Office Phone/Office Fax _____ Home Phone/Home Fax _____

Office E-Mail _____ Home E-Mail _____

8. 2016 IEEE MEMBER RATES

IEEE DUES	16 Aug -14-28 Feb 15	1 Mar -15 Aug 15
Residence	Pay Full Year	Pay Half Year**
United States	\$197.00 <input type="checkbox"/>	\$98.50 <input type="checkbox"/>
Canada (incl. GST)	\$173.35 <input type="checkbox"/>	\$86.68 <input type="checkbox"/>
Canada (incl. HST for PEI)	\$186.58 <input type="checkbox"/>	\$93.29 <input type="checkbox"/>
Canada (incl. HST for Nova Scotia)	\$188.05 <input type="checkbox"/>	\$94.03 <input type="checkbox"/>
Canada (incl. HST for NB, NF and ON)	\$185.11 <input type="checkbox"/>	\$92.56 <input type="checkbox"/>
Canada (incl. GST and QST Quebec)	\$188.01 <input type="checkbox"/>	\$94.01 <input type="checkbox"/>
Africa, Europe, Middle East	\$160.00 <input type="checkbox"/>	\$80.00 <input type="checkbox"/>
Latin America	\$151.00 <input type="checkbox"/>	\$75.50 <input type="checkbox"/>
Asia, Pacific	\$152.00 <input type="checkbox"/>	\$76.00 <input type="checkbox"/>

Canadian Taxes (GST/HST): All supplies, which include dues, Society membership fees, online products and publications (except CD-ROM and DVD media), shipped to locations within Canada are subject to the GST of 5% or the HST of 12%, 13% or 15%, depending on the Province to which the materials are shipped. GST and HST do not apply to Regional Assessments. (IEEE Canadian Business Number 12563 4188 RT0001)

Value Added Tax (VAT) in the European Union: In accordance with the European Union Council Directives 2002/38/EC and 77/388/EEC amended by Council Regulation (EC)792/2002, IEEE is required to charge and collect VAT on electronic/digitized products sold to private consumers that reside in the European Union. The VAT rate applied is the EU member country standard rate where the consumer is resident. (IEEE's VAT registration number is EU826000051)

U.S. Sales Taxes: Please add applicable state and local sales and use tax on orders shipped to Alabama, Arizona, California, Colorado, District of Columbia, Florida, Georgia, Illinois, Indiana, Kentucky, Massachusetts, Maryland, Michigan, Minnesota, Missouri, New Jersey, New Mexico, New York, North Carolina, Ohio, Oklahoma, West Virginia, Wisconsin. Customers claiming a tax exemption must include an appropriate and properly completed tax-exemption certificate with their first order.



2016 SPS MEMBER RATES

16 Aug-28 Feb 1 Mar-15 Aug
Pay Full Year Pay Half Year

Signal Processing Society Membership Fee* \$ 22.00 \$ 11.00
 Fee includes: IEEE Signal Processing Magazine (electronic and digital), Inside Signal Proc. eNewsletter (electronic) and IEEE Signal Processing Society Content Gazette (electronic).

Add \$17 to enhance SPS Membership and also receive: \$17.00 \$ 8.50
 IEEE Signal Processing Magazine (print) and SPS Digital Library: online access to Signal Processing Magazine, Signal Processing Letters, Journal of Selected Topics in Signal Processing, Trans. on Audio, Speech, and Language Processing, Trans. on Image Processing, Trans. on Information Forensics and Security and Trans. on Signal Processing.

Publications available only with SPS membership:

Signal Processing, IEEE Transactions on:	Print	\$209.00 <input type="checkbox"/>	\$104.50 <input type="checkbox"/>
Audio, Speech, and Lang. Proc., IEEE/ACM Trans. on:	Print	\$160.00 <input type="checkbox"/>	\$ 80.00 <input type="checkbox"/>
Image Processing, IEEE Transactions on:	Print	\$207.00 <input type="checkbox"/>	\$103.50 <input type="checkbox"/>
Information Forensics and Security, IEEE Trans. on:	Print	\$179.00 <input type="checkbox"/>	\$ 89.50 <input type="checkbox"/>
IEEE Journal of Selected Topics in Signal Processing:	Print	\$176.00 <input type="checkbox"/>	\$ 88.00 <input type="checkbox"/>
Affective Computing, IEEE Transactions on:	Electronic	\$ 36.00 <input type="checkbox"/>	\$ 18.00 <input type="checkbox"/>
Biomedical and Health Informatics, IEEE Journal of:	Print	\$ 55.00 <input type="checkbox"/>	\$ 27.50 <input type="checkbox"/>
	Electronic	\$ 40.00 <input type="checkbox"/>	\$ 20.00 <input type="checkbox"/>
	Print & Electronic	\$ 65.00 <input type="checkbox"/>	\$ 32.50 <input type="checkbox"/>
IEEE Cloud Computing	Electronic and Digital	\$ 39.00 <input type="checkbox"/>	\$ 19.50 <input type="checkbox"/>
IEEE Trans. on Cognitive Comm. & Networking	Electronic	\$ 27.00 <input type="checkbox"/>	\$ 13.50 <input type="checkbox"/>
IEEE Trans. on Computational Imaging	Electronic	\$ 28.00 <input type="checkbox"/>	\$ 14.00 <input type="checkbox"/>
IEEE Trans. on Big Data	Electronic	\$ 26.00 <input type="checkbox"/>	\$ 13.00 <input type="checkbox"/>
IEEE Trans. on Molecular, Biological, & Multi-scale Communications	Electronic	\$ 25.00 <input type="checkbox"/>	\$ 12.50 <input type="checkbox"/>
IEEE Internet of Things Journal	Electronic	\$ 26.00 <input type="checkbox"/>	\$ 13.00 <input type="checkbox"/>
IEEE Trans. on Cloud Computing	Electronic	\$ 43.00 <input type="checkbox"/>	\$ 21.50 <input type="checkbox"/>
IEEE Trans. on Computational Social Systems	Electronic	\$ 30.00 <input type="checkbox"/>	\$ 15.00 <input type="checkbox"/>
IEEE Trans. on Signal & Info Proc. Over Networks	Electronic	\$ 28.00 <input type="checkbox"/>	\$ 14.00 <input type="checkbox"/>
IEEE Biometrics Compendium:	Online	\$ 30.00 <input type="checkbox"/>	\$ 15.00 <input type="checkbox"/>
Computing in Science & Engrg. Mag.:	Electronic and Digital	\$ 39.00 <input type="checkbox"/>	\$ 19.50 <input type="checkbox"/>
	Print	\$ 69.00 <input type="checkbox"/>	\$ 34.50 <input type="checkbox"/>
Medical Imaging, IEEE Transactions on:	Print	\$ 74.00 <input type="checkbox"/>	\$ 37.00 <input type="checkbox"/>
	Electronic	\$ 63.00 <input type="checkbox"/>	\$ 26.50 <input type="checkbox"/>
	Print & Electronic	\$ 89.00 <input type="checkbox"/>	\$ 44.50 <input type="checkbox"/>

Mobile Computing, IEEE Transactions on:	ELE/Print Abstract/CD-ROM	\$ 41.00 <input type="checkbox"/>	\$ 20.50 <input type="checkbox"/>
Multimedia, IEEE Transactions on:	Electronic	\$ 43.00 <input type="checkbox"/>	\$ 21.50 <input type="checkbox"/>
IEEE Multimedia Magazine:	Electronic and Digital	\$ 39.00 <input type="checkbox"/>	\$ 19.50 <input type="checkbox"/>
	Print	\$ 69.00 <input type="checkbox"/>	\$ 34.50 <input type="checkbox"/>
Network Science and Engrg., IEEE Trans. on:	Electronic	\$ 34.00 <input type="checkbox"/>	\$ 17.00 <input type="checkbox"/>
IEEE Reviews in Biomedical Engineering:	Print	\$ 25.00 <input type="checkbox"/>	\$ 12.50 <input type="checkbox"/>
	Print & Electronic	\$ 40.00 <input type="checkbox"/>	\$ 20.00 <input type="checkbox"/>
IEEE Security and Privacy Magazine:	Electronic and Digital	\$ 39.00 <input type="checkbox"/>	\$ 19.50 <input type="checkbox"/>
	Print	\$ 69.00 <input type="checkbox"/>	\$ 34.50 <input type="checkbox"/>
IEEE Sensors Journal:	Electronic	\$ 40.00 <input type="checkbox"/>	\$ 20.00 <input type="checkbox"/>
Smart Grid, IEEE Transactions on:	Print	\$100.00 <input type="checkbox"/>	\$ 50.00 <input type="checkbox"/>
	Electronic	\$ 40.00 <input type="checkbox"/>	\$ 20.00 <input type="checkbox"/>
	Print & Electronic	\$120.00 <input type="checkbox"/>	\$ 60.00 <input type="checkbox"/>

Wireless Communications, IEEE Transactions on:	Print	\$127.00 <input type="checkbox"/>	\$ 63.50 <input type="checkbox"/>
	Electronic	\$ 49.00 <input type="checkbox"/>	\$ 24.50 <input type="checkbox"/>
	Print & Electronic	\$127.00 <input type="checkbox"/>	\$ 63.50 <input type="checkbox"/>
IEEE Wireless Communications Letters:	Electronic	\$ 19.00 <input type="checkbox"/>	\$ 9.50 <input type="checkbox"/>

*IEEE membership required or requested
 Affiliate application to join SP Society only. Amount Paid \$ _____

9. IEEE Membership Affiliate Fee (See pricing in Section 8) \$ _____

Signal Processing Society Fees \$ _____

Canadian residents pay 5% GST or 13% HST
 Reg. No. 125634188 on Society payment(s) & pubs only Tax \$ _____

AMOUNT PAID WITH APPLICATION TOTAL \$ _____

Prices subject to change without notice.

Check or money order enclosed Payable to IEEE on a U.S. Bank
 American Express VISA MasterCard
 Diners Club

Exp. Date/ Mo./Yr.	_____	_____	_____	_____	_____	_____	_____
Cardholder Zip Code Billing Statement Address/USA Only	_____	_____	_____	_____	_____	_____	_____

Full signature of applicant using credit card _____ Date _____

10. WERE YOU REFERRED?

Yes No If yes, please provide the follow information:
 Member Recruiter Name: _____
 IEEE Recruiter's Member Number (Required): _____

2016 IEEE SIGNAL PROCESSING SOCIETY STUDENT MEMBERSHIP APPLICATION

(Current and reinstating IEEE members joining SPS complete areas 1, 2, 8, 9.)

Mail to: IEEE OPERATIONS CENTER, ATTN: Matthew Plotner, Member and Geographic Activities, 445 Hoes Lane, Piscataway, New Jersey 08854 USA
or Fax to (732) 981-0225 (credit card payments only.)

For info call (732) 981-0060 or 1 (800) 678-IEEE or E-mail: new.membership@ieee.org



1. PERSONAL INFORMATION

NAME AS IT SHOULD APPEAR ON IEEE MAILINGS: SEND MAIL TO: Home Address OR Business/School Address
If not indicated, mail will be sent to home address. Note: Enter your name as you wish it to appear on membership card and all correspondence.
PLEASE PRINT Do not exceed 40 characters or spaces per line. Abbreviate as needed. Please circle your last/surname as a key identifier for the IEEE database.

TITLE	FIRST OR GIVEN NAME	MIDDLE NAME	SURNAME/LAST NAME
HOME ADDRESS			
CITY	STATE/PROVINCE	POSTAL CODE	COUNTRY

2. Are you now or were you ever a member of IEEE? Yes No
If yes, please provide, if known:

MEMBERSHIP NUMBER _____

Grade _____ Year Membership Expired: _____

2016 SPS STUDENT MEMBER RATES	16 Aug-28 Feb Pay Full Year	1 Mar-15 Aug Pay Half Year
Signal Processing Society Membership Fee*	\$11.00 <input type="checkbox"/>	\$ 5.50 <input type="checkbox"/>

Fee includes: IEEE Signal Processing Magazine (electronic and digital), Inside Signal Processing eNewsletter (electronic) and IEEE Signal Processing Society Content Gazette (electronic).

3. BUSINESS/PROFESSIONAL INFORMATION

Company Name _____

Department/Division _____

Title/Position _____ Years in Current Position _____

Years in the Profession Since Graduation _____ PE State/Province _____

Street Address _____

City _____ State/Province _____ Postal Code _____ Country _____

Add \$8 to enhance SPS Membership and also receive: \$ 9.00 \$ 4.50

IEEE Signal Processing Society Magazine (print) and SPS Digital Library: online access to Signal Processing Magazine, Signal Processing Letters, Journal of Selected Topics in Signal Processing, Trans. on Audio, Speech, and Language Processing, Trans. on Image Processing, Trans. on Information Forensics and Security and Trans. on Signal Processing.

Publications available only with SPS membership:

Signal Processing, IEEE Transactions on:	Print	\$105.00 <input type="checkbox"/>	\$ 52.50 <input type="checkbox"/>
Audio, Speech, and Lang. Proc., IEEE/ACM Trans. on:	Print	\$ 80.00 <input type="checkbox"/>	\$ 40.00 <input type="checkbox"/>
Image Processing, IEEE Transactions on:	Print	\$104.00 <input type="checkbox"/>	\$ 52.00 <input type="checkbox"/>
Information Forensics and Security, IEEE Trans. on:	Print	\$ 90.00 <input type="checkbox"/>	\$ 45.00 <input type="checkbox"/>
IEEE Journal of Selected Topics in Signal Processing:	Print	\$ 88.00 <input type="checkbox"/>	\$ 44.00 <input type="checkbox"/>
Affective Computing, IEEE Transactions on:	Electronic	\$ 18.00 <input type="checkbox"/>	\$ 9.00 <input type="checkbox"/>
Biomedical and Health Informatics, IEEE Journal of:	Print	\$ 28.00 <input type="checkbox"/>	\$ 14.00 <input type="checkbox"/>
	Electronic	\$ 20.00 <input type="checkbox"/>	\$ 10.00 <input type="checkbox"/>
	Print & Electronic	\$ 33.00 <input type="checkbox"/>	\$ 16.50 <input type="checkbox"/>
IEEE Cloud Computing	Electronic and Digital	\$ 20.00 <input type="checkbox"/>	\$ 10.00 <input type="checkbox"/>
IEEE Trans. on Cognitive Comm. & Networking	Electronic	\$ 14.00 <input type="checkbox"/>	\$ 7.00 <input type="checkbox"/>
IEEE Trans. on Computational Imaging	Electronic	\$ 14.00 <input type="checkbox"/>	\$ 7.00 <input type="checkbox"/>
IEEE Trans. on Big Data	Electronic	\$ 13.00 <input type="checkbox"/>	\$ 6.50 <input type="checkbox"/>
IEEE Trans. on Molecular, Biological, & Multi-Scale Communications	Electronic	\$ 13.00 <input type="checkbox"/>	\$ 6.50 <input type="checkbox"/>
IEEE Internet of Things Journal	Electronic	\$ 13.00 <input type="checkbox"/>	\$ 6.50 <input type="checkbox"/>
IEEE Trans. on Cloud Computing	Electronic	\$ 22.00 <input type="checkbox"/>	\$ 11.00 <input type="checkbox"/>
IEEE Trans. on Computational Social Systems	Electronic	\$ 15.00 <input type="checkbox"/>	\$ 7.50 <input type="checkbox"/>
IEEE Trans. on Signal & Info Proc. Over Networks	Electronic	\$ 14.00 <input type="checkbox"/>	\$ 7.00 <input type="checkbox"/>
IEEE Biometrics Compendium:	Online	\$ 15.00 <input type="checkbox"/>	\$ 7.50 <input type="checkbox"/>
Computing in Science & Engrg. Mag.:	Electronic and Digital	\$ 20.00 <input type="checkbox"/>	\$ 10.00 <input type="checkbox"/>
	Print	\$ 35.00 <input type="checkbox"/>	\$ 17.50 <input type="checkbox"/>
Medical Imaging, IEEE Transactions on:	Print	\$ 37.00 <input type="checkbox"/>	\$ 18.50 <input type="checkbox"/>
	Electronic	\$ 27.00 <input type="checkbox"/>	\$ 13.50 <input type="checkbox"/>
	Print & Electronic	\$ 45.00 <input type="checkbox"/>	\$ 22.50 <input type="checkbox"/>
Mobile Computing, IEEE Transactions on:	ELE/Print Abstract/CD-ROM	\$ 21.00 <input type="checkbox"/>	\$ 10.50 <input type="checkbox"/>
Multimedia, IEEE Transactions on:	Electronic	\$ 22.00 <input type="checkbox"/>	\$ 11.00 <input type="checkbox"/>
IEEE MultiMedia Magazine:	Electronic and Digital	\$ 20.00 <input type="checkbox"/>	\$ 10.00 <input type="checkbox"/>
	Print	\$ 35.00 <input type="checkbox"/>	\$ 17.50 <input type="checkbox"/>
Network Science and Engrg., IEEE Trans. on:	Electronic	\$ 17.00 <input type="checkbox"/>	\$ 8.50 <input type="checkbox"/>
IEEE Reviews in Biomedical Engineering:	Print	\$ 13.00 <input type="checkbox"/>	\$ 6.50 <input type="checkbox"/>
IEEE Security and Privacy Magazine:	Print & Electronic	\$ 20.00 <input type="checkbox"/>	\$ 10.00 <input type="checkbox"/>
	Electronic and Digital	\$ 20.00 <input type="checkbox"/>	\$ 10.00 <input type="checkbox"/>
	Print	\$ 35.00 <input type="checkbox"/>	\$ 17.50 <input type="checkbox"/>
IEEE Sensors Journal:	Electronic	\$ 20.00 <input type="checkbox"/>	\$ 10.00 <input type="checkbox"/>
Smart Grid, IEEE Transactions on:	Print	\$ 50.00 <input type="checkbox"/>	\$ 25.00 <input type="checkbox"/>
	Electronic	\$ 20.00 <input type="checkbox"/>	\$ 10.00 <input type="checkbox"/>
	Print & Electronic	\$ 60.00 <input type="checkbox"/>	\$ 30.00 <input type="checkbox"/>
Wireless Communications, IEEE Transactions on:	Print	\$ 64.00 <input type="checkbox"/>	\$ 32.00 <input type="checkbox"/>
	Electronic	\$ 25.00 <input type="checkbox"/>	\$ 12.50 <input type="checkbox"/>
	Print & Electronic	\$ 64.00 <input type="checkbox"/>	\$ 32.00 <input type="checkbox"/>
IEEE Wireless Communications Letters:	Electronic	\$ 10.00 <input type="checkbox"/>	\$ 5.00 <input type="checkbox"/>

4. EDUCATION

A baccalaureate degree from an IEEE recognized educational program assures assignment of "Member" grade. For others, additional information and references may be necessary for grade assignment.

A. Baccalaureate Degree Received _____ Program/Course of Study _____

College/University _____ Campus _____

State/Province _____ Country _____ Mo./Yr. Degree Received _____

B. Highest Technical Degree Received _____ Program/Course of Study _____

College/University _____ Campus _____

State/Province _____ Country _____ Mo./Yr. Degree Received _____

5. Full signature of applicant

6. DEMOGRAPHIC INFORMATION – ALL APPLICANTS -

Date Of Birth _____ Male Female
Day Month Year

7. CONTACT INFORMATION

Office Phone/Office Fax _____ Home Phone/Home Fax _____

Office E-Mail _____ Home E-Mail _____

2016 IEEE STUDENT MEMBER RATES			
IEEE DUES	16 Aug-14-28 Feb 15	1 Mar-15 Aug 15	
Residence	Pay Full Year	Pay Half Year**	
United States	\$32.00 <input type="checkbox"/>	\$16.00 <input type="checkbox"/>	
Canada (incl. GST)	\$33.60 <input type="checkbox"/>	\$16.80 <input type="checkbox"/>	
Canada (incl. HST for NB, NF, and ON)	\$36.16 <input type="checkbox"/>	\$18.08 <input type="checkbox"/>	
Canada (incl. HST for Nova Scotia)	\$36.80 <input type="checkbox"/>	\$18.40 <input type="checkbox"/>	
Canada (incl. HST for PEI)	\$36.48 <input type="checkbox"/>	\$18.24 <input type="checkbox"/>	
Canada (incl. GST and QST Quebec)	\$36.79 <input type="checkbox"/>	\$18.40 <input type="checkbox"/>	
Africa, Europe, Middle East, Latin America, Asia, Pacific	\$27.00 <input type="checkbox"/>	\$13.50 <input type="checkbox"/>	

9. IEEE Membership Fee (See pricing in Section 8) \$ _____

Signal Processing Society Fees \$ _____

Canadian residents pay 5% GST or 13% HST
Reg. No. 125634188 on Society payment(s) & pubs only Tax \$ _____

AMOUNT PAID WITH APPLICATION TOTAL \$ _____

Prices subject to change without notice.

Check or money order enclosed Payable to IEEE on a U.S. Bank

American Express VISA MasterCard Diners Club

Exp. Date/ Mo./Yr.	Cardholder Zip Code Billing Statement Address/USA Only
--------------------	--

Full signature of applicant using credit card _____ Date _____

10. WERE YOU REFERRED?

Yes No If yes, please provide the follow information:
Member Recruiter Name: _____
IEEE Recruiter's Member Number (Required): _____

Canadian Taxes (GST/HST): All supplies, which include dues, Society membership fees, online products and publications (except CD-ROM and DVD media), shipped to locations within Canada are subject to the GST of 5% or the HST of 12%, 13% or 15%, depending on the Province to which the materials are shipped. GST and HST do not apply to Regional Assessments. (IEEE Canadian Business Number 12563 4188 RT0001)

Value Added Tax (VAT) in the European Union: In accordance with the European Union Council Directives 2002/38/EC and 77/388/EEC amended by Council Regulation (EC)792/2002, IEEE is required to charge and collect VAT on electronic/digitized products sold to private consumers that reside in the European Union. The VAT rate applied is the EU member country standard rate where the consumer is resident. (IEEE's VAT registration number is EU826000081)

U.S. Sales Taxes: Please add applicable state and local sales and use tax on orders shipped to Alabama, Arizona, California, Colorado, District of Columbia, Florida, Georgia, Illinois, Indiana, Kentucky, Massachusetts, Maryland, Michigan, Minnesota, Missouri, New Jersey, New Mexico, New York, North Carolina, Ohio, Oklahoma, West Virginia, Wisconsin. Customers claiming a tax exemption must include an appropriate and properly completed tax-exemption certificate with their first order.



2016 IEEE SIGNAL PROCESSING SOCIETY AFFILIATE MEMBERSHIP APPLICATION

Mail to: IEEE OPERATIONS CENTER, ATTN: Matthew Plotner, Member and Geographic Activities, 445 Hoes Lane, Piscataway, New Jersey 08854 USA or Fax to (732) 981-0225 (credit card payments only.)

For info call (732) 981-0060 or 1 (800) 678-IEEE or E-mail: new.membership@ieee.org



1. PERSONAL INFORMATION

NAME AS IT SHOULD APPEAR ON IEEE MAILINGS: SEND MAIL TO: Home Address OR Business/School Address. PLEASE PRINT Do not exceed 40 characters or spaces per line. Abbreviate as needed. Please circle your last/surname as a key identifier for the IEEE database.

2. Are you now or were you ever a member of IEEE? Yes No. If yes, please provide, if known: MEMBERSHIP NUMBER Grade Year Membership Expired:

2016 SPS MEMBER RATES. Table with columns for membership type (Signal Processing Society, eNewsletter, Add \$17 to enhance SPS Membership), payment options (Pay Full Year, Pay Half Year), and rates for 16 Aug-28 Feb and 1 Mar-15 Aug.

3. BUSINESS/PROFESSIONAL INFORMATION

Company Name, Department/Division, Title/Position, Years in Current Position, Years in the Profession Since Graduation, Street Address, City, State/Province, Postal Code, Country.

Publications available only with SPS membership: Signal Processing, IEEE Transactions on: Audio, Speech, and Lang. Proc., IEEE/ACM Trans. on: Image Processing, IEEE Transactions on: Information Forensics and Security, IEEE Trans. on: IEEE Journal of Selected Topics in Signal Processing: Affective Computing, IEEE Transactions on: Biomedical and Health Informatics, IEEE Journal of: IEEE Cloud Computing, IEEE Trans. on Cognitive Comm. & Networking, IEEE Trans. on Computational Imaging, IEEE Trans. on Big Data, IEEE Trans. on Molecular, Biological, & Multi-scale Communications, IEEE Internet of Things Journal, IEEE Trans. on Cloud Computing, IEEE Trans. on Computational Social Systems, IEEE Trans. on Signal & Info Proc. Over Networks, IEEE Biometrics Compendium: Computing in Science & Engrg. Mag.: Medical Imaging, IEEE Transactions on: Mobile Computing, IEEE Transactions on: Multimedia, IEEE Transactions on: IEEE MultiMedia Magazine: Network Science and Engrg., IEEE Trans. on: IEEE Reviews in Biomedical Engineering: IEEE Security and Privacy Magazine: IEEE Sensors Journal: Smart Grid, IEEE Transactions on: Wireless Communications, IEEE Transactions on: IEEE Wireless Communications Letters:

4. EDUCATION A baccalaureate degree from an IEEE recognized educational program assures assignment of "Member" grade. For others, additional information and references may be necessary for grade assignment.

A. Baccalaureate Degree Received, College/University, State/Province, Country, Mo./Yr. Degree Received. B. Highest Technical Degree Received, College/University, State/Province, Country, Mo./Yr. Degree Received.

5. Full signature of applicant

6. DEMOGRAPHIC INFORMATION - ALL APPLICANTS -

Date of Birth, Male Female

7. CONTACT INFORMATION

Office Phone/Office Fax, Home Phone/Home Fax, Office E-Mail, Home E-Mail

8. 2016 IEEE AFFILIATE RATES

Table with columns for IEEE DUES, Residence (United States, Canada, Africa, Latin America, Asia, Pacific), and rates for 16 Aug-14-28 Feb 15 and 1 Mar-15 Aug 15.

Canadian Taxes (GST/HST): All supplies, which include dues, Society membership fees, online products and publications (except CD-ROM and DVD media), shipped to locations within Canada are subject to the GST of 5% or the HST of 13%, 14% or 15%, depending on the Province to which the materials are shipped. GST and HST do not apply to Regional Assessments. (IEEE Canadian Business Number 12563 4188 RT0001)

Value Added Tax (VAT) in the European Union: In accordance with the European Union Council Directives 2002/38/EC and 77/388/EEC amended by Council Regulation (EC)792/2002, IEEE is required to charge and collect VAT on electronic/digitized products sold to private consumers that reside in the European Union. The VAT rate applied is the EU member country standard rate where the consumer is resident. (IEEE's VAT registration number is EU826000081)

U.S. Sales Taxes: Please add applicable state and local sales and use tax on orders shipped to Alabama, Arizona, California, Colorado, District of Columbia, Florida, Georgia, Illinois, Indiana, Kentucky, Massachusetts, Maryland, Michigan, Minnesota, Missouri, New Jersey, New Mexico, New York, North Carolina, Ohio, Oklahoma, West Virginia, Wisconsin. Customers claiming a tax exemption must include an appropriate and properly completed tax-exemption certificate with their first order.



9. IEEE Membership Affiliate Fee (See pricing in Section 8) \$

Signal Processing Society Fees \$

Canadian residents pay 5% GST or 13% HST. Reg. No. 125634188 on Society payment(s) & pubs only Tax \$

AMOUNT PAID WITH APPLICATION TOTAL \$

Prices subject to change without notice

Check or money order enclosed Payable to IEEE on a U.S. Bank

American Express VISA MasterCard

Diners Club

Exp. Date/ Mo./Yr., Cardholder Zip Code Billing Statement Address/USA Only

Full signature of applicant using credit card Date

10. WERE YOU REFERRED?

Yes No If yes, please provide the follow information:

Member Recruiter Name:

IEEE Recruiter's Member Number (Required):

